



Doctoral Thesis

**Study on Influence of Tunnel Quality Defects on
Lining Structure and its Reinforcement Design**

July 2022

**Graduate School of Engineering
Nagasaki University**

Wei HAN

Acknowledgements

The three years of studying at Nagasaki University are meaningful to my life. I would like to express my sincere gratitude to those who helped me during my study at Nagasaki University.

First and foremost, I would like to express my deep respect to my supervisor, Professor **Yujing Jiang**, for his great support in my study. From the topic selection to the completion of this thesis, he provided me with valuable advice and constant support. His rigorous work style and approachable personality also deeply influenced me, which will benefit me greatly in my whole life.

I would like to express my sincere gratitude to Professor **Kiyoshi Omine**, Associate Professor **Satoshi Sugimoto** at Nagasaki University for their kind help and continuous support during my research and daily life. I am especially grateful to Dr. **Chuanzheng Liu** at Southwest University of Science and Technology, for his valuable suggestions and fruitful discussions. Meanwhile, I would like to thank Professor **Gang Wang**, Dr. **Hengjie Luan**, Dr. **Xuepeng Zhang**, Dr. **Changsheng Wang**, Dr. **Bin Gong**, Dr. **Jiankang Liu**, Mr. **Yiteng Du**, and Dr. **Xinshuai Shi** in Shandong University of Science and Technology, Associate Professor **Xuezhen Wu** in Fuzhou University, for their great support for my research and daily life.

I wish to express my gratitude to my friends in Nagasaki, Mr. **Hongbin Chen**, Mr. **Qiwei Lin**, Mr. **Xun Li**, Mr. **Wenzheng Cao**, Mr. **Xuesen Zhang**, Mr. **Jing Wang**, Mr. **Yang Zheng**, Mr. **Zichen Zhang**, Mr. **Bin Wang**, Mr. **Peng Yan**, and all others who helped me in Japan.

Finally, I would like to express my sincere gratitude to my parents for their unconditional love, great advice, and endless support.

Wei HAN

Nagasaki, July 2022

Abstract

With the development of underground transportation, more and more tunnels have been constructed. As the main support structure of the tunnel, the lining is essential for the safe operation of the tunnel. However, typical tunnel quality defects such as voids and lining insufficient thickness can commonly occur, seriously threatening the durability and safety of lining structures. Unfortunately, with the long-term operation of the tunnel, the aging phenomenon of the lining is also inevitable. Consequently, it is crucial to clarify the influence of quality defects on the lining structure and identify effective reinforcement schemes. The main research contents of this thesis can be summarized as follows:

At first, the health inspection and formation cause for typical tunnel quality defects of void and lining insufficient thickness were systematically reviewed. The health inspection was summarized, including the inspection methods and defect distribution characteristics. The formation causes of void and insufficient thickness were discussed with the hierarchical structure model. In addition, the avoidable formation causes were marked, which can be applied as the main guidance for defect prevention.

Secondly, the fracture characteristics and cracking mechanism of the lining structure containing combined defects were explored with the finite element method (FEM)-cohesive zone model (CZM) method. Additionally, the cracking characteristics under the fiber-reinforced plastic (FRP)-polymer cement mortar (PCM) reinforcement method were evaluated. The main results indicated that the crack pattern and crack statistics are affected by the defect type and defect range. The cracking degree corresponding to the void zone is larger than that of the insufficient thickness zone. The cracking distribution of tensile ring cracks zone (TRCZ), shear ring cracks zone (SRCZ), shear longitudinal cracks zone (SLCZ), mixed-failure longitudinal cracks zone (MLCZ), and mixed-failure cross cracks zone (MCCZ) is determined. Furthermore, the FRP-PCM method presents a significant inhibition on the cracking of the lining inner surface.

Thirdly, the mechanical properties and failure mechanism of degraded linings with void quality defects that significantly affect the lining were investigated. The reinforcement effect of the FRP-PCM method on degraded linings with void quality defects was evaluated. The main results indicated that void layout and void distance significantly affect the mechanical properties. Especially, an obvious three-dimensional bending outwards phenomenon within the void-affected zone is observed. The lining deterioration

degree and the void distribution exhibit an apparent influence on the failure characteristics. The FRP-PCM method can effectively reduce the plastic failure rate of the lining.

Then, the failure and time-dependent characteristics of linings with compound quality defect were investigated. Subsequently, the reinforcement effect under the FRP-PCM method was evaluated. Further, the impact of defect range and defect location on time-dependent characteristics of lining structures with compound defects were explored. The main results indicated that the failure and mechanical characteristics are significantly affected by defect location, defect range, lining degradation degree, and grade of the ground class. The FRP-PCM method can effectively improve the safety state and reduce the plastic rate of the lining, the reinforcement effect is closely related to the grade of FRP grids and lining deterioration degree. In addition, the mechanical properties, deformation, and failure rate of the lining structure exhibit a significant relation with time.

Further, the dynamic response of tunnel structures with void defects and lining defects was investigated. The effect of defect parameters on the distribution of mechanical and physical properties was investigated. Then, the effect of dynamic level, defect type, defect range, and reinforcement types on the variation of the acceleration and velocity dynamic response was analyzed by the standard spectral ratio (SSR). The main results indicated that the physical properties of peak acceleration and peak velocity are significantly affected by the defect type, defect range, and defect location. In addition, the distribution of acceleration SSR or velocity SSR is significantly influenced by the defect type, void range, and dynamic level. Moreover, the reinforcement type significantly affects the dynamic response of the lining structure.

Finally, the reinforcement design of the lining structure was discussed. As a prerequisite, an evaluation model of the influence degree of typical defects and disease on the health state of lining structures was constructed based on the fuzzy comprehensive evaluation (FCE) method. As an illustration, the application of the established FCE model was conducted. To conduct the reasonable reinforcement design, commonly applied reinforcement methods for defective lining structures were reviewed. Subsequently, the reinforcement design for the defective and diseased lining structure was suggested based on the FCE method. Further, the flowchart of reinforcement designs for lining structures was summarized.

Keywords: Tunnel quality defects; Void; Lining insufficient thickness; Degraded linings; Failure characteristic; Time-dependent characteristic; FRP-PCM method; Cracking mechanism; Dynamic response; Reinforcement design

Contents

Acknowledgements	I
Abstract	II
Contents	IV
1 Introduction.....	1
1.1 Background and objectives	1
1.2 Thesis structure.....	4
References	6
2 Review of health inspection and formation causes for typical tunnel quality defects.....	9
2.1 Inspection of tunnel quality defects.....	9
2.1.1 Ground-penetrating radar.....	10
2.1.2 Microtremor method.....	12
2.1.3 Technology of three-dimensional laser scanning in borehole.....	12
2.1.4 Other common inspection techniques.....	13
2.2 Distribution characteristics of tunnel quality defects	14
2.3 Formation causes of typical tunnel quality defects	16
2.3.1 Void quality defects.....	16
2.3.2 Insufficient lining thickness.....	19
2.4 Conclusions	21
References	21
3 Fracture characteristics and cracking mechanism of linings containing typical quality defects with the FEM-CZM method	29
3.1 Introduction	29
3.2 FEM-CZM method.....	32
3.2.1 Constitutive model.....	32
3.2.2 Embedding process of cohesive elements.....	33
3.3 Model establishment.....	34
3.4 Numerical results.....	36
3.4.1 Mechanical properties.....	36
3.4.2 Characteristics of cracking distribution	37
3.4.3 Statistics of cracks	43
3.4.4 Cracking mechanism.....	47
3.4.5 Discussion of fracture characteristics	51

3.5 Cracking characteristics of the reinforced lining structure.....	51
3.6 Conclusions	53
References	55
4 Mechanical properties and failure mechanism of degraded linings with void quality defects	61
4.1 Introduction	61
4.2 Model establishment.....	63
4.3 Mechanical properties and failure characteristics	66
4.3.1 Distribution of inner force	67
4.3.2 Distribution of principal stress.....	73
4.3.3 Distribution of failure zone.....	74
4.4 Reinforcement characteristics of the FRP-PCM method.....	76
4.5 Discussion	79
4.6 Conclusions	80
References	81
5 Failure and time-dependent characteristics of linings with compound quality defects.....	85
5.1 Introduction	85
5.2 Model establishment.....	87
5.3 Numerical results.....	89
5.3.1 Mechanical characteristics	89
5.3.2 Distribution of failure zone.....	91
5.3.3 Reinforcement effect of the FRP-PCM method.....	94
5.4 Time-dependent characteristics	96
5.4.1 Model overview	96
5.4.2 Numerical results	97
5.5 Conclusions	105
References	105
6 Dynamic response of tunnel structures with quality defects of void and lining defect	109
6.1 Introduction	109
6.2 Numerical model	111
6.2.1 Model establishment	111
6.2.2 Calculation conditions	112
6.2.3 Input motion.....	113
6.3 Mechanical and physical properties	114
6.3.1 Characteristics of principal stress	114
6.3.2 Characteristics of maximum shear stress.....	115
6.3.3 Distribution of peak acceleration.....	116

6.3.4 Distribution of peak velocity	118
6.4 Distribution of spectrum characteristic analysis.....	122
6.4.1 Characteristics of acceleration SSR.....	122
6.4.2 Characteristics of velocity SSR	127
6.4.3 Characteristics of SSR under the reinforcement	132
6.5 Discussion	138
6.6 Conclusions	142
References	142
7 Reinforcement design of lining structure with typical quality defects and disease.....	147
7.1 Introduction	147
7.2 Hierarchical model establishment	148
7.2.1 Index analysis	148
7.2.2 Weight calculation method.....	150
7.2.3 Weight analysis	152
7.3 Establishment of the FCE model.....	156
7.3.1 Principle of the FCE method.....	156
7.3.2 Establishment of evaluation model.....	157
7.4 Application of the established evaluation model.....	163
7.5 Review of reinforcement methods of tunnel linings	164
7.5.1 Traditional methods	164
7.5.2 FRP reinforcement method.....	168
7.6 Reinforcement design of lining structures.....	169
7.7 Conclusions	173
References	174
8 Summaries and prospects.....	181
8.1 Summaries.....	181
8.2 Prospects.....	183

1 Introduction

1.1 Background and objectives

With the development of transportation, more and more tunnels have been constructed globally, significantly improving convenience. However, with the continued and long-term operation of tunnels, the aging and degradation will generate, which will bring hidden dangers to safe operation (Jiang et al. 2017; Jiang et al. 2019; Higashi et al. 2014). As for China, more than 30%-40% of road tunnels are in a sub-health or even diseased state (Jiang and Zhang 2021). It is noted that the aging and diseased tunnels have occupied a considerable proportion. If the countermeasures are not handled properly, the corresponding ratio will further increase, seriously affecting the safe operation.

As the main support structure of tunnels, the lining plays an essential role in ensuring the safety of people's lives and property. However, with the long-term operation of tunnels, safety accidents caused by the partial failure of the lining frequently occur. Tunnel diseases and aging factors can be considered typical incentives of the local or overall failure of the lining structure. The lining structures can be divided into the intact lining, defective lining, and diseased lining (Ministry of Railways of the PRC 2004; Zhang 2012). As a distinction, voids and insufficient lining thickness can be referred to as tunnel quality defects, while lining cracks, water leakage, and spalling can be called tunnel diseases (Ministry of Railways of the PRC 2004; Zhang 2012). To clarify the influence of tunnel quality defects and diseases on linings, it is necessary to conduct systematic investigations on typical lining safety accidents.

In Japan, many tunnels in service are facing deterioration, and engineering accidents caused by tunnel diseases have become a severe issue. According to the investigation of tunnel accidents in Japan (Asakura and Kojima 2003), the safety accidents of concrete spalling happened in the Fukuoka Tunnel on June 27, 1999, where spalling concrete was identified on the shoulder, resulting in car damage. On November 28, 1999, a train derailment accident occurred in Rebunhama Tunnel, and the reason for the safety accident is that a number of concrete blocks appeared on the track, which was caused by spalling of concrete (Asakura and Kojima 2003). In October 2004, the Uonuma Tunnel suffered

severe damage under the Niigataken-Chuetsu Earthquake, and the largest lining block dropped onto the track was close to 2m^3 (Yashiro et al. 2007). The 2008 Wenchuan earthquake led to the collapse of the Longxi Tunnel, and the void behind the lining is considered a cause that could not be ignored (Nie et al. 2015). A variety of lining diseases occurred in the Wushaoling Tunnel in Gansu Province, and road traffic accidents often occur (Jiang and Zhang 2021). The Longmen Tunnel in Fujian Province, China, was affected by the goaf area of a coal seam, resulting in secondary lining cracking, water seepage, and other diseases, and even block dropping (Huang 2001). Zhang (2020) indicated that lining spalling is the dominant accident type. Overall, it is noted that tunnel quality defects and diseases present a significantly negative impact on the safe operation of tunnels. In addition, due to the inevitable aging phenomenon of tunnel structures during long-term operation, safe operation faces considerable threats. Therefore, identifying the effective reinforcement and repair countermeasures for degraded tunnel structures is crucial.

Maintenance and management standards for tunnel structures have been developed in various countries to guide the reinforcement of tunnels, for example, in China (Ministry of Railways of the PRC 2004). Meanwhile, some classic methods have been applied to the reinforcement and repair of defective and diseased linings, such as the backfill method (Liu et al. 2021; Zhang et al. 2021; Jiang et al. 2017; Wang et al. 2021), the reinforcement method of the inner surface (Liu et al. 2020; Liu et al. 2021). With the increase in experience in dealing with damaged tunnels, advanced materials are gradually applied to the maintenance and reinforcement of tunnel damage, among which fiber-reinforced plastic (FRP) material is representative (Department of China Journal of Highway and Transport 2015). The FRP materials have the advantages of high strength, lightweight, easy construction, fatigue, and corrosion resistance (Higashi et al. 2014). Regarding the type of FRP material, it mainly includes Carbon FRP (CFRP), Glass FRP (GFRP), aramid FRP (AFRP), et al. (Günaslan et al. 2014), in the forms of sheets, bars, cables, et al. (Wu et al. 2007). Especially, in recent years, a new type of FRP composite material, FRP grid, has been utilized for concrete structural reinforcement (FRP Grid Method Association of Japan). The FRP grid is connected to the concrete surface by rivets, and the adhesion performance under wet and low temperatures is better than that of the FRP sheet (Guo et al. 2018). Some materials have been recently applied as the protection substance, for

example, polymer cement mortar (PCM) (FRP Grid Method Association of Japan; Yamaguchi et al. 2014; Guo et al. 2018). PCM is a new type of composite material, which has the advantages of low permeability, high strength, better resistance to drying shrinkage cracking, and excellent adhesion to concrete (Guo et al. 2018; Cai and Tang 2007). Consequently, the reinforcement method of the FRP-PCM was developed, which can give full play to their respective properties (FRP Grid Method Association of Japan; Yamaguchi et al. 2014; Guo et al. 2018). Concerning the reinforcement behavior of the FRP-PCM method, Guo et al. (2019) evaluated the strengthening effect of concrete beams reinforced with the FRP-PCM method and indicated that the shear reinforcement effect for RC beams is adequate. Further, Guo et al. (2020) investigated the flexural reinforcement effect of beams strengthened by the FRP-PCM method and found that the flexural strengthening effect is obvious. Liu et al. (2022) experimental explored the cracking characteristics of linings under bias pressure strengthened by the FRP-PCM method and indicated that the method could be applied as the control method for tensile cracks. In addition, the reinforcement effect of the FRP-PCM method on the degraded lining was also explored (Higashi et al. 2014; Jiang et al. 2017).

From the above research background, it can be observed that tunnel accidents caused by tunnel diseases and defects are common, resulting in many casualties and economic losses, and bringing a considerable challenge to the safe operation of tunnels. If the tunnel quality defects and diseases are not handled properly, the service life of the tunnel will be greatly reduced and the safe operation of the tunnel will be seriously threatened. To better repair and reinforce the diseased and defective tunnel, it is necessary to clarify the formation causes and damage mechanism. In addition, the lining at the quality defect can be regarded as a weak part, which will induce tunnel diseases such as cracking, water seepage, and collapse under certain conditions (Zhang 2012). Therefore, it is significant to systematically clarify the influence of typical quality defects on the mechanical properties and failure mechanism of the lining. In addition, the FRP-PCM method has been widely applied as an advanced method in the reinforcement of tunnels. It is of great significance to systematically clarify the reinforcement effect of the FRP-PCM method on degraded tunnels.

1.2 Thesis structure

With the research background given above, the overall object of this thesis is to systematically reveal the mechanical properties and failure characteristics of degraded tunnel linings with typical quality defects. Meanwhile, the reinforcement design of the defective and diseased lining structure is also carried out. The outline of this thesis can be presented in Fig. 1.1. The research contents of each chapter are as follows:

In Chapter 1, the research background, an overview of accident disasters, and reinforcement of the diseased and defective tunnel are introduced. Meanwhile, the objectives and the thesis structure are also determined.

In Chapter 2, the health inspection and formation cause of typical quality defects of voids and lining insufficient thickness are reviewed and summarized, respectively. The health inspection, including the inspection methods and defect distribution characteristics, is summarized. The formation causes of voids and lining insufficient thickness are discussed with the hierarchical structure model. In addition, the formation causes that can be effectively avoided are marked, which can be applied as the main guidance for defect prevention. These contents are the basis of the following research content and have an important relationship with the following research content.

In Chapter 3, the fracture characteristics and cracking mechanism of linings with combined tunnel quality defects under gradual load are investigated using the FEM-CZM method. The stress distribution, cracking characteristics, and crack statistics are investigated, respectively. Further, the cracking mechanism and morphological characteristics are discussed. Finally, the reinforcement effect of the FRP-PCM method on lining cracking is evaluated. In this chapter, the type of defect that has a greater impact on the lining structure is identified.

In Chapter 4, the void quality defect identified in chapter 3, which has a significant impact on the tunnel, is used as the object to explore the effect on the mechanical properties and failure mechanism of degraded linings. First, the effect of void distribution and void distance on the three-dimensional distribution of inner force is explored. Then, the plastic failure behavior of linings with different deterioration degrees is explored. Subsequently, the reinforcement effect of the FRP-PCM method is focused on. Finally, the distribution of potential cracking zone is discussed.

In Chapter 5, based on the study of void defects, the compound defect of void and insufficient lining thickness, that is, the type of lining defect is further considered as the object. The mechanical properties, safety state, and failure characteristics of degraded tunnels with compound quality defects are systematically investigated. At first, the three-dimensional distribution of mechanical properties and the plastic failure characteristics are explored. Subsequently, the potential cracking zone of a deep-buried tunnel structure with compound quality defects is determined. Then, the safety state and the failure rate of tunnel lining with the reinforcement of the FRP-PCM method are evaluated. Moreover, the time-dependent characteristics of linings with compound quality defects are also discussed.

In Chapter 6, the dynamic response of tunnel structures with the void defect and lining defect is investigated. At first, the mechanical and physical properties are studied considering the effect of defect type, range, and location. Then, the variation of the acceleration and velocity dynamic response of the defective tunnel structure is analyzed by the standard spectral ratio (SSR). Subsequently, the influences of reinforcement methods on the distribution of SSR are explored. To more intuitively explore the effect of defect properties and reinforcement methods on the dynamic response, the degree of influence is discussed.

In Chapter 7, the reinforcement design of the lining structure is carried out. At first, the influence degree of typical defects and diseases on lining health is determined with the FCE method. Subsequently, the application of the established model is discussed. To conduct a reasonable reinforcement design, the research status of reinforcement methods for tunnel structures, especially the FRP-PCM method, is reviewed. Then, the reinforcement design of the defective and diseased lining structure is suggested with the established FCE model. Finally, the typical process of reinforcement design for the defective and diseased lining structure is summarized.

In Chapter 8, the major conclusions of this thesis are summarized. Meanwhile, the prospects are also indicated.

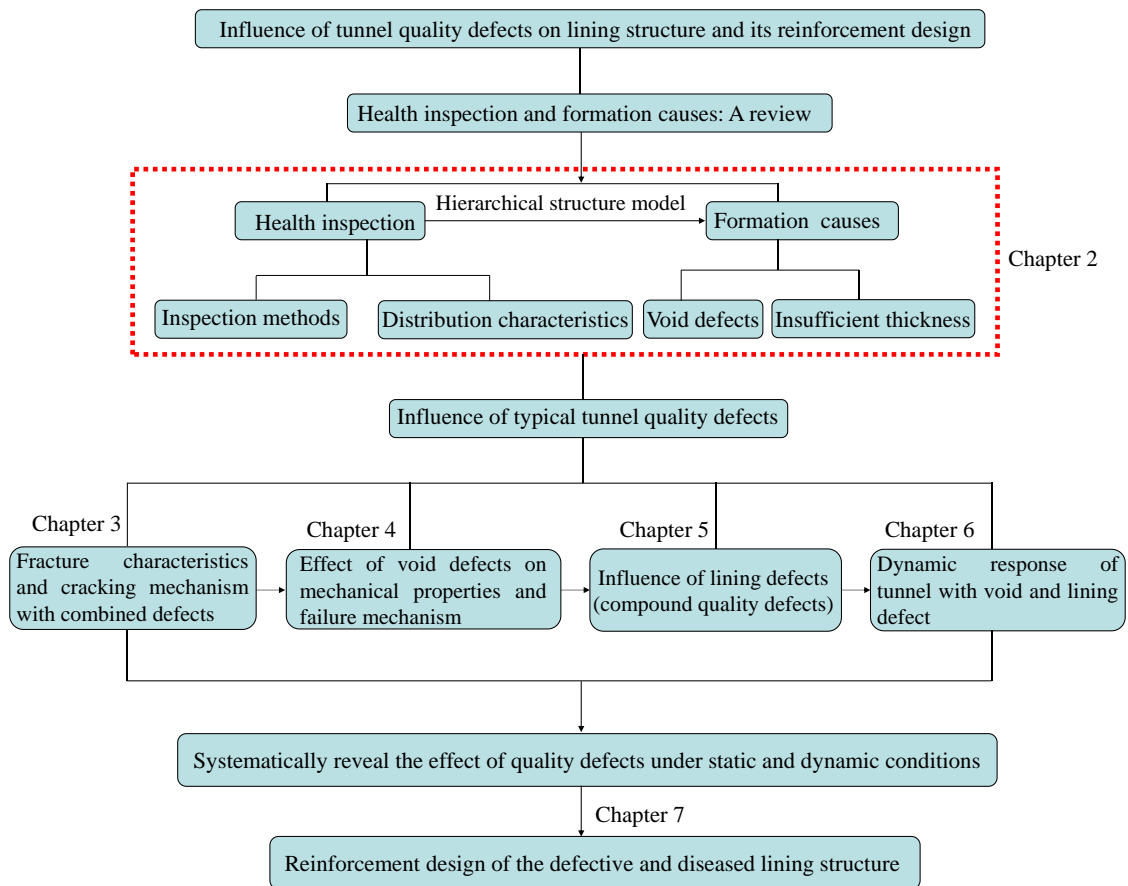


Fig. 1.1 Thesis structure.

References

- Asakura T, Kojima Y. Tunnel maintenance in Japan. *Tunnelling and Underground Space Technology*, 2003, 18(2-3), 161-169.
[https://doi.org/10.1016/S0886-7798\(03\)00024-5](https://doi.org/10.1016/S0886-7798(03)00024-5)
- Cai SH, Tang LF. Study on Polymer Cement Mortar in Concrete Patching. *Journal of Yangtze River Scientific Research Institute*, 2007, 24(1), 44-46.
- Department of China Journal of Highway and Transport. Review of China's Tunnel Engineering Research:2015. *China Journal of Highway and Transport*, 2015, 28(5), 1-65.
- FRP Grid Method Association of Japan. Design and construction manual of the Repair & reinforcement method for RC structures by FRP grid [O/L],
<http://www.frp-grid.com/01.html>

- Günaşlan SE, Karaşin A, Öncü ME. Properties of FRP Materials for Strengthening. *International Journal of Innovative Science, Engineering & Technology*, 2014, 1(9), 656-660.
- Guo R, Cai L, Hino S, Wang B. Experimental Study on Shear Strengthening of RC Beams with an FRP Grid-PCM Reinforcement Layer. *Applied Sciences*, 2019, 9(15), 2984. <https://doi.org/10.3390/app9152984>
- Guo R, Hu WH, Li MQ, Wang B. Study on the flexural strengthening effect of RC beams reinforced by FRP grid with PCM shotcrete. *Composite Structures*, 2020, 239, 112000. <https://doi.org/10.1016/j.compstruct.2020.112000>
- Guo R, Pan Y, Cai L, Hino S. Study on design formula of shear capacity of RC beams reinforced by CFRP grid with PCM shotcrete method. *Engineering Structures*, 2018, 166, 427-440. <https://doi.org/10.1016/j.engstruct.2018.03.095>
- Higashi Y, Li B, Jiang YJ. Analytical Evaluation of Tunnel Reinforcement Effect by PCM Shotcrete Method Using FRP Grid. *Journal of Society of Materials Science, Japan*, 2014, 63(6), 451-458. <https://doi.org/10.2472/jmsms.63.451>
- Huang B. Longmen Tunnel Reinforcement Measures and Its Assessment. *Journal of Highway and Transportation Research and Development*, 2001, 18(5), 39-45.
- Jiang YJ, Wang XS, Li B, Higashi Y, Taniguchi K, Ishida K. Estimation of reinforcing effects of FRP-PCM method on degraded tunnel linings. *Soils and Foundations*, 2017, 57(3), 327-340. <https://doi.org/10.1016/j.sandf.2017.05.002>
- Jiang YJ, Zhang XP. Research on Automatic Detection and Health Assessment of Tunnel Lining. *Tunnel Construction*, 2021, 41(3), 341.
- Jiang YJ, Zhang XP, Taniguchi T. Quantitative condition inspection and assessment of tunnel lining. *Automation in Construction*, 2019, 102, 258-269. <https://doi.org/10.1016/j.autcon.2019.03.001>
- Liu C, Zhang DL, Zhang SL. Characteristics and treatment measures of lining damage: A case study on a mountain tunnel. *Engineering Failure Analysis*, 2021, 128, 105595. <https://doi.org/10.1016/j.engfailanal.2021.105595>
- Liu DJ, Shang Q, Li M, Zuo JP, Gao Y, Xu F. Cracking behaviour of tunnel lining under bias pressure strengthened using FRP Grid-PCM method. *Tunnelling and Underground Space Technology*, 2022, 123, 104436. <https://doi.org/10.1016/j.tust.2022.104436>
- Liu SH, Shi Y, Sun R, Yang JS. Damage behavior and maintenance design of tunnel lining based on numerical evaluation. *Engineering Failure Analysis*, 2020, 109, 104209.

- <https://doi.org/10.1016/j.engfailanal.2019.104209>
- Ministry of Railways of the People's Republic of China (Ministry of Railways of the PRC). Provisional Regulations on the Evaluation of Safety Classification for Railway Operation Tunnel Lining, 2004. (in Chinese)
- Nie ZY, Zhang CL, Li FX. Effect of void behind lining on seismic performance of tunnel. *China Earthquake Engineering Journal*, 2015, 37(1), 138-143.
- Wang XS, Wei L, Wang ZQ, Jiang YJ, Zhang LM, Meng FZ, Cong Y. Study on the Reinforcing Effects of the FRP-PCM Method on Tunnel Linings for Dynamic Strengthening. *Geofluids*, 2021, 2021, 8926423.
<https://doi.org/10.1155/2021/8926423>
- Wu G, Wu ZS, Jiang JB, Luo YB. A New Technology of Strengthening Concrete Structures with FRP Grids and Its Application. *Construction Technology*, 2007, 36(12), 98-102.
- Yamaguchi K, Guo R, Hino S, Miyano N. Shearing capacity and adhesive characteristic of reinforced interface for RC beam with haunch retrofitted by CFRP covering PCM shotcrete. *Proc Jpn Concr Inst*, 2014, 36(2), 1261-1266.
- Yashiro K, Kojima Y, Shimizu M. Historical Earthquake Damage to Tunnels in Japan and Case Studies of Railway Tunnels in the 2004 Niigataken-Chuetsu Earthquake. *QR of RTRI*, 2007, 48(3), 136-141.
- Zhang S. Study on Influence mechanism of lining Defects and Bearing Capacity of Highway Tunnel Lining. Ph.D. Thesis, Lanzhou University, Lanzhou, 2020.
- Zhang SL. Study on Health Diagnosis and Technical Condition Assessment for Tunnel Lining Structure. Ph.D. Thesis, Beijing Jiaotong University, Beijing, 2012.
- Zhang Y, Yuan M, Liu C, Zhang X, Yang B, Yang J. Repairing Damaged Tunnel Lining with Small-Size Cavity in Surrounding Rocks. *Journal of Performance of Constructed Facilities*, 2021, 35(4), 06021002.
[https://doi.org/10.1061/\(ASCE\)CF.1943-5509.0001597](https://doi.org/10.1061/(ASCE)CF.1943-5509.0001597)

2 Review of health inspection and formation causes for typical tunnel quality defects

2.1 Inspection of tunnel quality defects

The safe operation of tunnels is vital to the safety of people's lives and property. However, tunnel damage such as cracking, spalling, and falling blocks appeared, seriously affecting the bearing capacity and durability of the tunnel structure (Liu et al. 2019). Therefore, the accurate detection of tunnel diseases and the determination of effective tunnel reinforcement schemes have received extensive attention.

According to corresponding statistics, tunnel accidents caused by tunnel diseases are quite common (Asakura and Kojima 2003; Yashiro et al. 2007). In addition to the long-term operation of tunnels that can lead to tunnel diseases, the tunnel quality defects such as voids and insufficient lining thickness can also be considered typical incentives for tunnel diseases (Ding et al. 2020; Han et al. 2021a; Bian et al. 2016; Ding et al. 2019; Zhang et al. 2021; Han et al. 2021b; Zhang 2012; Liu et al. 2020; Zhang 2020). If countermeasures are not handled properly, it will lead to the continuous development of tunnel diseases and gradually have a serious impact on the tunnel, thereby causing tunnel disasters. Based on the background, the typical induction process of tunnel accidents caused by tunnel quality defects can be presented in Fig. 2.1. Therefore, tunnel quality defects exhibit a non-negligible negative effect on the safe operation of tunnels. Concealment, as a typical feature of tunnel quality defects, further increases the difficulty of detection (Zhang 2020; Ye et al. 2021). However, through the effective repair and reinforcement of tunnel quality defects, tunnel diseases caused by defects can be effectively avoided. Therefore, the effective prevention and control of tunnel quality defects are essential to resist tunnel diseases and ensure safe tunnel operation. However, it is a prerequisite to accurately determine the distribution and formation causes of tunnel quality defects. Consequently, this chapter systematically reviewed and discussed the inspection methods, distribution characteristics, and formation causes of typical tunnel

quality defects, which are crucial for the effective prevention and control of tunnel quality defects.

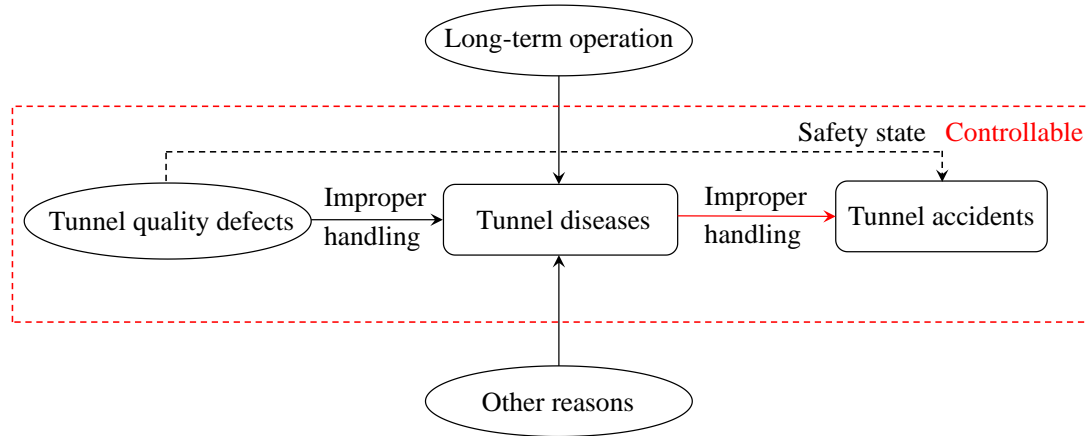


Fig. 2.1 Typical induction process of tunnel accidents caused by tunnel quality defects.

2.1.1 Ground-penetrating radar

The premise of a reinforcement design is to carry out a health inspection and diagnosis of the tunnel structure. Meanwhile, accurate defect distribution characteristics and geometric parameters are the basis for an effective reinforcement design. Regarding the inspection methods of tunnel quality defects, there are two categories of destructive testing and non-destructive testing methods (Gao et al. 2014). It is noted that nondestructive testing methods dominate the detection of tunnel quality defects as they cause no damage to structures (Zhang 2020). Therefore, this section will mainly review nondestructive testing methods for the detection of tunnel quality defects. As a typical nondestructive testing method, ground-penetrating radar (GPR) has been widely applied due to its advantages of nondestructive and high-resolution (Liu et al. 2005). According to the corresponding references, the application of GPR to the health inspection of tunnel structures was reviewed from the three perspectives of tunnel information, subject of inspection, major findings or remarks, as summarized in Table 2.1. It is noted that the GPR technique can effectively identify typical tunnel quality defects such as void behind the lining and insufficient lining thickness. It is noted that void parameters such as void position and void range can be well determined by GPR (He et al. 2021). Liu et al. (2021a) applied a geological radar to conduct the health inspection of linings, and the parameters

of void height and void length were concerned. The combined method of GPR and finite-difference time-domain can significantly improve efficiency (Xiang et al. 2013). The parameters of the center frequency of GPR significantly affect the inspection effect (Qin et al. 2020). Furthermore, some problems that are often encountered during the application of GPR were also indicated by Deng et al. (2015).

Table 2.1 Review of the GPR application on the health inspection of tunnels.

References	Tunnel information	Subject of inspection	Major findings or Remarks
Xiang et al. (2013)	Damaoshan tunnel	The thickness of the second lining and damage distribution	The combination of GPR and finite-difference time-domain is efficient; The average qualified rate of lining thickness is 79.87%.
Xie et al. (2013)	Road tunnel	Lining thickness and grouting of the void behind the lining	The GPR is a useful technique to monitor the grout patterns, and antennae of 500 MHz are recommended.
Prego et al. (2016)	High-speed railway tunnel during the construction	The thickness of the gunite layer and voids	The potential of the GPR method was concerned when applied during the early stages of construction.
Ye and Zhang (2020)	Railway tunnel	Void behind the lining and lining thickness	The location of the loosened contact state can be well identified by the GPR image.
Qin et al. (2020)	Experimental model	Void inside and behind tunnel lining	The centre frequency GPR affects the detection effect of different void types.
Li et al. (2011)	Long Hai tunnel	Lining thickness	Information such as the lining average thicknesses and qualification rates of lining thickness can be obtained by automatic recognition.
Deng et al. (2015)	Highway tunnel	Void behind the lining and lining thickness	The tunnel quality defect can be efficiently determined by the GPR. Meanwhile, some problems encountered during the application were indicated.
He et al. (2021)	Highway tunnel	Void behind the tunnel lining	The position and range of voids were determined with the GPR.
Liu et al. (2021a)	Mountain tunnel	Void behind the lining	The distribution of void height and length was concerned.

In addition, Lalagüe et al. (2016) applied the GRP to detect the rockfall on a lining structure. Peng et al. (2021) reviewed the application of GPR on tunnel linings from the frequency, survey line direction, location, tunnel type, and detection object, and the advances in the GRP detection of grouting defects were concerned. Overall, it can be observed that the GPR technique is popular and has broad application prospects in tunnel health inspection.

2.1.2 *Microtremor method*

Recently, microtremor has attracted wide attention in the study of dynamic characteristics of concrete structures (Gao et al. 2014; Tuladhar et al. 2004). As early as 1989, the microtremor method was applied to investigate the dynamic response of soil and rock ground (Nakamura 1989). Subsequently, the microtremor method was popularized for structural analysis in some studies (Chatelain et al. 2000; Ikeda et al. 2010). Gao et al. (2014) applied the average normalized power spectrum density of microtremor to determine the peak frequencies of concrete and the contact state between the tunnel lining and the rock mass. Further, Gao et al. (2016) applied the normalized ratio of vibration intensity of microtremor in different orientations to detect void defects. Overall, it can be observed that the microtremor method can be applied to detect tunnel quality defects.

2.1.3 *Technology of three-dimensional laser scanning in borehole*

Non-contact, high accuracy, and time-saving scanning can be regarded as the typical advantages of the three-dimensional laser scanning technology (Li et al. 2015). Gong et al. (2016) indicated that the radial dimension of void defects could not be detected with the GPR, so they applied the technology of three-dimensional laser scanning in borehole to realize the accurate measurement of void defects. In addition, Fan et al. (2020) applied the method of GPR and the technology of three-dimensional laser scanning in borehole to detect the distribution of void defects, and 23 voids were observed at the crown. Overall, it can be observed that the technology of three-dimensional laser scanning in borehole can be applied to detect the three-dimensional properties of void defects.

2.1.4 Other common inspection techniques

To clarify the research status of inspection methods of tunnel quality defects, it is necessary to review the other common methods. According to the corresponding references, other common inspection methods were reviewed from the three aspects, type of inspection method, subject of detection, and major findings or remarks, respectively, as summarized in Table 2.2.

Table 2.2 Review of other common inspection methods for tunnel quality defects.

References	Inspection methods	Subject of detection	Major findings or Remarks
Cao et al. (2019)	Impact-echo method	Void quality defect	The vibration energy can be applied for void evaluation, and the void position can be well identified by the dynamic stiffness method.
Zhang et al. (2019)	Time-energy density analysis based on wavelet transform method	Lining thickness	The thickness of concrete can be well identified by this method, and the relative error is no more than 5%.
Konishi et al. (2016)	Inspection method with infrared thermometry	Void in subway tunnel lining	The voids can be determined by infrared thermometry, and the accuracy of infrared thermometry in the detection of voids is influenced by the temperature.
Liu et al. (2021b)	Combined method of impact elastic wave technology and machine learning algorithms	Void quality defect	The average accuracy for void detection is 90.83%, and the application potential in void detection is great.
Geng et al. (2022)	Transient electromagnetic radar (TER) method	Voids behind the lining	The void defect can be well detected by the TER method, and the image of the results is more intuitive than GPR.
Tang et al. (2019)	Acoustic spectrum analysis method	Void quality defect	The existence of a void and its size and location can be detected by this method.
Ye et al. (2020)	TER method	Lining insufficient thickness; Voids behind the lining	The image of the boundary is clear, and the void and lining thickness can be identified by the TER method.

As presented in Table 2.2, the listed typical methods include the impact-echo (IE) method (Cao et al. 2019), time-energy density analysis based on the wavelet transform method (Zhang et al. 2019), inspection method with infrared thermometry (Konishi et al.

2016), combined method of impact elastic wave technology and machine learning algorithms (Liu et al. 2021b), acoustic spectrum analysis method (Tang et al. 2019), and transient electromagnetic radar (TER) method (Geng et al. 2022; Ye et al. 2020). It is noted that the relative error of identifying the thickness of concrete with time-energy density analysis based on the wavelet transform method is no more than 5% (Zhang et al. 2019). The average accuracy for the detection of void defects of the combined method of impact elastic wave technique and machine learning algorithms is 90.83% (Liu et al. 2021b). In addition, the application conditions and precautions were also clarified in Table 2.2, which can provide the basis for choosing a suitable inspection method. Furthermore, the engineering background should also be considered to determine suitable inspection techniques.

2.2 Distribution characteristics of tunnel quality defects

In the health inspection of tunnels, the distribution of tunnel quality defects can be effectively identified with non-destructive testing techniques. In this section, the void location and void size were mainly discussed regarding the distribution of void defects. The statistics of void location can be presented in Fig. 2.2 (data sources are from Zhang et al. 2020, Wu 2021, Liu 2018, and Zhang 2020). The above statistical analysis shows that the proportions of void defects at the crown and shoulder are more significant than that of the sidewall. Therefore, special attention should be paid to the influence of voids at the crown and shoulder. In addition, since void defects are more likely to occur at the crown and shoulder, attention needs to be paid to the effect of multiple defects. Regarding the statistics of void size, the focus of this section is on the void height and void longitudinal length. For the distribution of void height, Liu et al. (2021a) analyzed the characteristics of the detected voids and indicated that the void height is primarily concentrated in the range of 0.2m-0.6m. Zhang (2020) statistically analyzed the data of 961 voids behind the lining and found that the number of voids with a height of 10cm-50cm is the largest. Zhang et al. (2020) indicated that the void height is mainly distributed in the range of 0-25cm. Liu (2018) analyzed the characteristics of the 1117 detected voids and indicated that the void height is mostly concentrated in the range of 0-35cm. Furthermore, Wu (2021) indicated that the void height is primarily concentrated in the

range of 40cm-50cm behind the primary lining, while 10cm-20cm behind the secondary lining. Concerning the distribution of void longitudinal length, Liu et al. (2021a) indicated that the void number in different length intervals is significantly different, and when the void length is in the interval of 4m-6m, the number is the largest. Zhang (2020) indicated that the number of voids with a longitudinal length of 2m-8m is the largest, accounting for more than 60%. In addition, Zhang et al. (2020) indicated that the void longitudinal length is mainly distributed in the range of 0-20m. Wu (2021) pointed out that the proportion of void length in the range of 5m-10m is the largest, accounting for 45% for the primarily lining, while 42% for the secondary lining. Liu (2018) indicated that the proportion of void length in the range of 0-5m is about 60%. The statistical characteristic of the void length is quite different, which is mainly due to the differences in the geological environment and operating conditions of the tunnel structure. By analyzing the characteristics of void distribution, it is helpful to provide essential guidance for designing a numerical model.

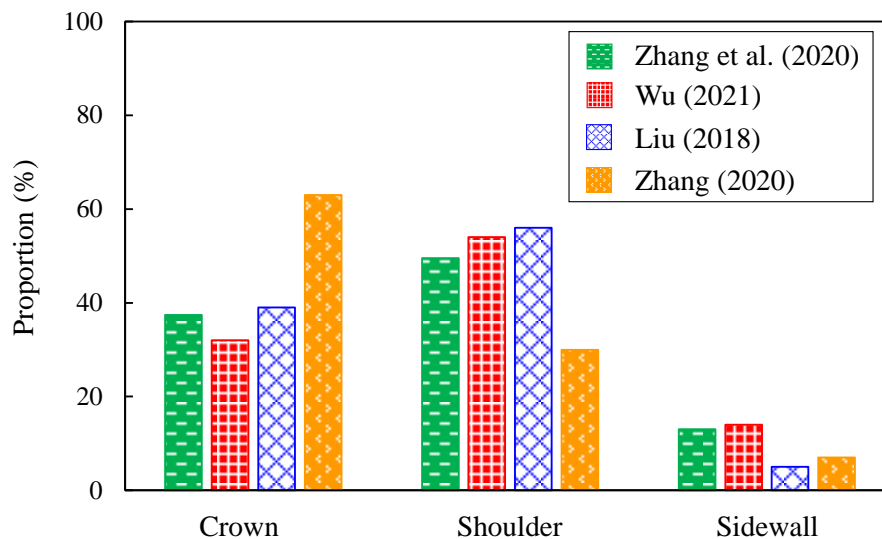


Fig. 2.2 Statistics of void location: data sources are from Zhang et al. (2020), Wu (2021), Liu (2018), and Zhang (2020).

Regarding the distribution of insufficient lining thickness, Zhang (2012) conducted a statistical analysis and found that more than 85% of the linings satisfy the thickness requirements, while among the linings that do not meet the thickness requirements, the degree of insufficient thickness is concentrated in the interval of 0.75-1. Liu et al. (2019) summarized the distribution of tunnel defects in the Liaoning province and indicated that

the effective thickness is 10% smaller than the minimum design thickness. Lu et al. (2022) detected three insufficient thickness defects along the lining section, which are 20cm for the shoulder, 10cm for the crown, and 7cm for the right sidewall. Xiang et al. (2013) applied the GPR technique to conduct a health diagnosis of tunnel structure and found that the average qualified rate of lining thickness is 79.87%. Liu et al. (2020) applied the geological radar to detect the lining thickness and found that the areas with insufficient thickness are mainly distributed near the vault, which is also the area where the damage is located, further indicating that the tunnel quality defect is the incentive of the damage.

2.3 Formation causes of typical tunnel quality defects

2.3.1 *Void quality defects*

To better prevent and repair tunnel quality defects, it is crucial to systematically reveal the causes of defects. Wang et al. (2014) indicated that insufficient backfilling and poor work technique would lead to voids. Voznesenskii and Nabatov (2017) pointed out that voids can be caused by construction work near tunnels and natural or manufactured objects. Yasuda et al. (2017) indicated that the main causes of voids are the method of tunnel support and the gravity effect. Ye et al. (2021) divided the causes of tunnel defects into two categories, including human factors and non-human factors. Note that void formation can be affected by various factors. To explore the reasons for the formation of voids, the causes were summarized from different aspects with a hierarchical structure model, as shown in Fig. 2.3. The first-level control layer can be divided into three aspects, construction stage, geological conditions, and tunnel support structure, respectively. Further, the corresponding first-level control layer is divided into several second-level control layers based on affiliation. For example, the construction stage of the first-level control layer can be divided into three second-level control layers, before construction, under construction, and after construction, respectively. Then, according to the established hierarchical structure model, the specific formation causes corresponding to the second-level control layer can be summarized in Table 2.3.

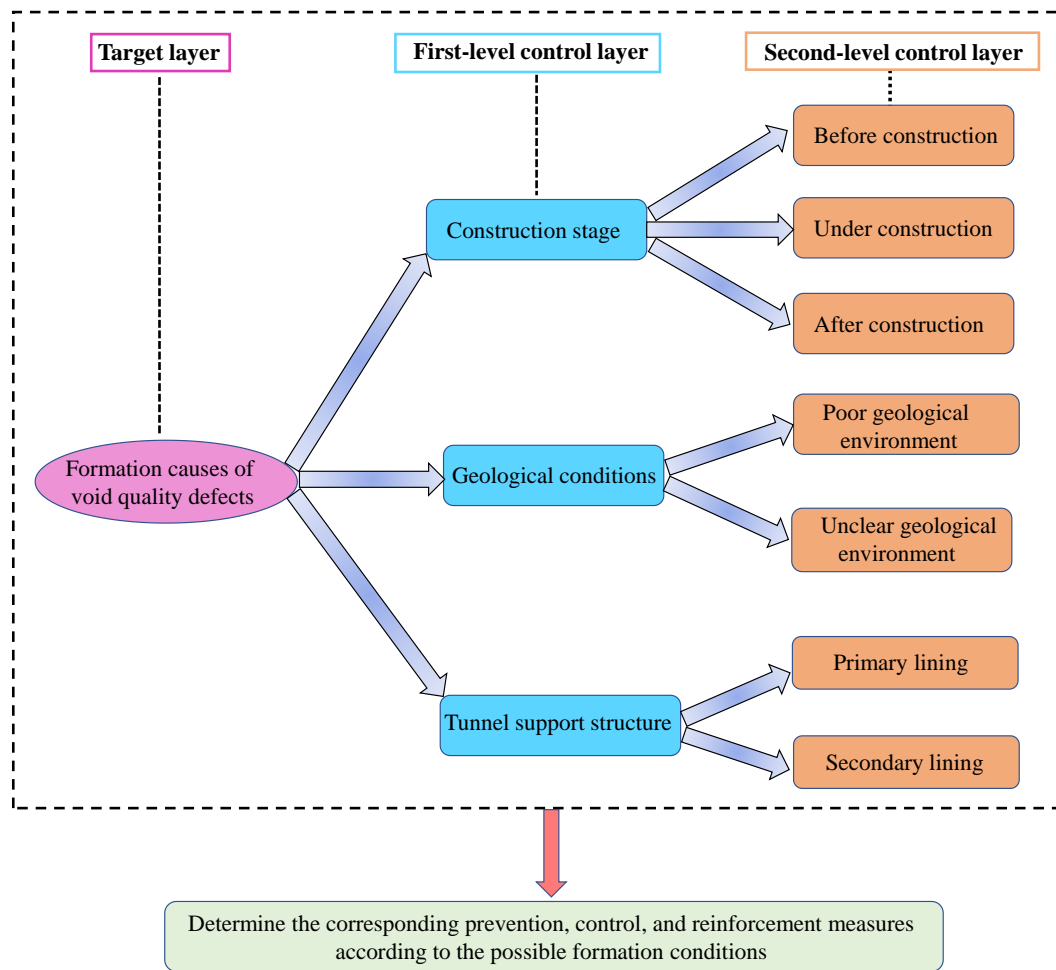


Fig. 2.3 Analysis model for the formation of void quality defects.

Taking the construction stage as an example, the reason for the formation of void defects in the stage before construction is mainly caused by design problems (Ma et al. 2019). For the stage under construction, the void defects are primarily caused by over-excavation (He et al. 2021), improper backfilling (Wang et al. 2014), improper construction of the waterproof board and formwork installation (Zhao et al. 2019), and poor construction (Wang et al. 2014). Concerning the stage after construction, the void defects are mainly caused by concrete gravity (Yasuda et al. 2017), a load of train cyclic (Wan et al. 2021), insufficient operation management concrete (Zhang et al. 2020), degradation of lining and rock mass (Gao et al. 2014), shrinkage of concrete (Yuan et al. 2010), construction work close to the tunnel (Voznesenskii and Nabatov 2017), and environmental meteorology (Wan et al. 2021). In addition, the reasons for the formation of voids were also summarized in Table 2.3, and the void formation causes that can be

effectively avoided were summarized. Special attention should be paid to the formation of void defects that are difficult to avoid effectively. According to the possible formation conditions of void defects, corresponding prevention, control, and repair schemes can be formulated. Overall, the established model can deepen the emergence of voids at different stages and further provide a basis for determining corresponding maintenance and protection measures.

Table 2.3 Main formation causes of void quality defects under different perspectives.

First-level control layer	Second-level control layer	Formation causes	References
Construction stage	Before construction	✓ Designed problems	Ma et al. (2019)
	Under construction	✓ Over-excavation ✓ Improper backfilling ✓ Improper construction of waterproof board and formwork installation ✓ Poor construction	He et al. (2021) Wang et al. (2014) Zhao et al. (2019) Wang et al. (2014)
	After construction	✧ Concrete gravity ✧ Load of train cyclic ✓ Insufficient operation management ✧ Degradation of lining and rock mass ✧ Shrinkage of concrete ✧ Construction work close to tunnels ✧ Environmental meteorology	Yasuda et al. (2017) Wan et al. (2021) Zhang et al. (2020) Gao et al. (2014) Yuan et al. (2010) Voznesenskii and Nabatov (2017) Wan et al. (2021)
Geological conditions	Poor geological environment	✧ Water infiltration into leaking joints ✧ Karstification, running soil, and waste landfills ✧ Clastic loss caused by water seepage ✧ Reinforcement corrosion ✧ Geological corrosion ✧ Faults and other unfavorable geological bodies	Meguid and Dang (2009) Voznesenskii and Nabatov (2017) He et al. (2021) Gao et al. (2014) Feng et al. (2018) Xu et al. (2021)
	Unclear geological environment	✓ Human factors ✓ Construction technology	Ye et al. (2021) Hu et al. (2019)
Tunnel support structure	Primary lining	✓ Overbreak and lack of backfilling ✧ Method of tunnel support: sheet pile ✓ Waterproof board hangs loosely ✓ Insufficient pressure of shotcrete	Xue and Yang (2017) Yasuda et al. (2017) Yuan et al. (2010) Yuan et al. (2010)
	Secondary lining	✧ Effect of dynamic loading ✓ Concrete pouring quality ✓ Construction technique and quality ✧ Settlement of formwork ✓ Technical factors	Meguid and Dang (2009) Yuan et al. (2010) Zhao et al. (2019) Zhang et al. (2013) Xu et al. (2021)

Note: the symbol ✓ indicates that voids could be effectively avoided, while ✧ should be paid special concern.

2.3.2 Insufficient lining thickness

Lining with insufficient thickness is prone to cracks and other diseases, which seriously affects the serviceability and durability of the tunnel structure (Liu et al. 2020; Yu et al. 2017). Therefore, it is meaningful to systematically summarize the causes of insufficient thickness. To explore the reasons for the formation of lining insufficient thickness, the causes were summarized from different perspectives with a hierarchical structure model, as presented in Fig. 2.4. It is noted that the first-level control layer can be divided into three aspects, construction stage, geological conditions, and tunnel support structure, respectively. Subsequently, the corresponding first-level control layer is divided into several second-level control layers according to affiliation. Then, according to the established hierarchical analysis structure model, the specific formation causes corresponding to the second-level control layer can be summarized in Table 2.4.

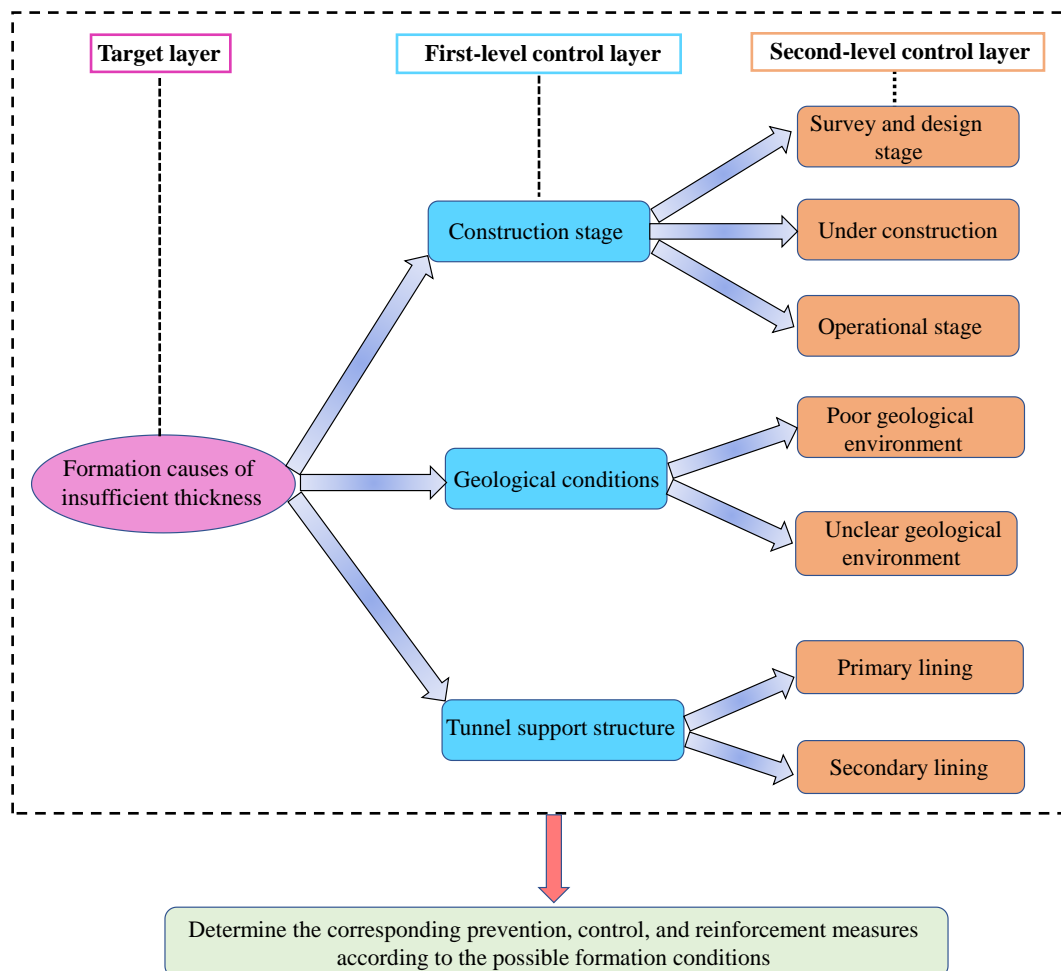


Fig. 2.4 Analysis model for the formation of lining insufficient thickness.

Table 2.4 Main causes of insufficient lining thickness under different perspectives.

First-level control layer	Second-level control layer	Formation causes	References
Construction stage	Survey and design stage	<ul style="list-style-type: none"> ✓ Incorrect design ✓ Inaccurate classification of rock mass grade ✓ Low requirements for waterproofing 	<ul style="list-style-type: none"> Ye et al. (2021) Yu et al. (2017) Jiang and Fan (2016)
	Under construction	<ul style="list-style-type: none"> ✓ Underbreak of rock mass ✓ Imperfect construction ✓ Inadequate pouring of concrete ✓ Human factors 	<ul style="list-style-type: none"> Zhang et al. (2021) Fu et al. (2019) Zhang et al. (2021) Zhao et al. (2019)
	Operational stage	<ul style="list-style-type: none"> ✧ Shrinkage of concrete ✓ Insufficient curing of lining concrete ✧ Concrete damage and carbonization ✧ Degradation of the lining 	<ul style="list-style-type: none"> Ye and Zhang (2020) Zhao et al. (2019) Li and Chen (2011) Gao et al. (2014)
Geological conditions	Poor geological environment	<ul style="list-style-type: none"> ✧ The action of saline soil ✧ Complex geological conditions 	<ul style="list-style-type: none"> Wang and Ji (2017) Ding et al. (2020)
	Unclear geological environment	<ul style="list-style-type: none"> ✓ Construction procedure ✓ Human factors 	<ul style="list-style-type: none"> Yu et al. (2017) Zhao et al. (2019)
Tunnel support structure	Primary lining	<ul style="list-style-type: none"> ✓ Poorly construction ✓ Rock mass lack-excavation ✧ Chemical reactions ✓ Poorly formed and uneven tunnels ✧ Deformation of rock mass ✓ Technique factors ✓ Inaccurate laying of concrete 	<ul style="list-style-type: none"> Ye et al. (2020) Yu et al. (2017) Niu et al. (2015) Yu et al. (2017) Jiang and Li (2020) Yu et al. (2017) Yu et al. (2017)
	Secondary lining	<ul style="list-style-type: none"> ✓ Construction quality of waterproof board, template installation, and Concrete pouring and curing ✓ Inadequate construction management 	<ul style="list-style-type: none"> Zhao et al. (2019) Jiang and Fan (2016)

Note: the symbol ✓ indicates that the insufficient lining thickness could be effectively avoided, while ✧ should be paid special concern.

Taking the construction stage as an example, the formation of lining defects for the survey and design stage is mainly caused by incorrect design (Ye et al. 2021), inaccurate classification of rock mass grade (Yu et al. 2017), and low requirements for waterproofing (Jiang and Fan 2016). For the stage under construction, the main causes can be divided as underbreak of rock mass (Zhang et al. 2021), imperfect construction (Fu et al. 2019), inadequate pouring of concrete (Zhang et al. 2021), and human factors (Zhao et al. 2019). Concerning the operational stage, the main causes include the shrinkage of concrete (Ye and Zhang 2020), insufficient curing of lining concrete (Zhao et al. 2019), concrete damage and carbonization (Li and Chen 2011), and degradation of the lining (Gao et al. 2014). Furthermore, the reasons for the formation of insufficient thickness were also

summarized in Table 2.4, and the formation causes that can be effectively prevented were summarized and marked. Concerning reasons that can be effectively avoided, efforts should be made to eliminate the effect in practice. According to the possible formation conditions of insufficient thickness, corresponding control schemes should be formulated. The established hierarchical structure model can provide a basis for the prevention of lining insufficient thickness.

2.4 Conclusions

In this chapter, the tunnel health inspection and formation causes of typical quality defects were systematically reviewed. The common nondestructive testing techniques for tunnel quality defects were summarized. On this basis, the main causes of void defects and insufficient thickness were analyzed from different perspectives by constructing a hierarchical structure model. The main conclusions of this chapter are as follows:

- (1) Different inspection techniques have different application areas and different inspection efficiencies. In addition, the engineering background should be considered to determine the appropriate inspection technique.
- (2) The distribution characteristics of tunnel quality defects were discussed, which can guide health inspection and design basis for model test and numerical model construction.
- (3) Concerning the formation causes of tunnel quality defects, two levels of control layers were determined. The first-level control layer can be divided into three aspects, construction stage, geological conditions, and tunnel support structure, respectively. According to the affiliation, seven secondary control layers were identified. Further, the formation causes of defects corresponding to the secondary control layers were reviewed. Subsequently, the formation causes that can be effectively avoided were marked, which provides the basis for defect prevention.

References

- Asakura T, Kojima Y. Tunnel maintenance in Japan. *Tunnelling and Underground Space Technology*, 2003, 18(2-3), 161-169.
[https://doi.org/10.1016/S0886-7798\(03\)00024-5](https://doi.org/10.1016/S0886-7798(03)00024-5)

- Bian K, Liu J, Xiao M, Liu ZP. Cause investigation and verification of lining cracking of bifurcation tunnel at Huizhou Pumped Storage Power Station. *Tunnelling and Underground Space Technology*, 2016, 54, 123-134.
<https://doi.org/10.1016/j.tust.2015.10.030>
- Cao R, Ma M, Liang R, Niu C. Detecting the Void behind the Tunnel Lining by Impact-Echo Methods with Different Signal Analysis Approaches. *Applied Sciences*, 2019, 9(16), 3280. <https://doi.org/10.3390/app9163280>
- Chatelain JL, Gueguen P, Guilier B, Frechet J, Bondoux F, Sarrault J, Sulpice P, Neuville JM. A User-friendly Instrument Dedicated to Ambient Noise (Microtremor) Recording for Site and Building Response Studies. *Seismological Research Letters*, 2000, 71(6), 698-703. <https://doi.org/10.1785/gssrl.71.6.698>
- Deng XS, Du T, Yuan Q, Zhong X. Tunnel lining thickness and voids detection by GPR. *Electronic Journal of Geotechnical Engineering*, 2015, 20(7), 2019-2030.
- Ding Z, Ji X, Li X, Ren Z, Zhang S. Influence of Symmetric and Asymmetric Voids on Mechanical Behaviors of Tunnel Linings: Model Tests and Numerical Simulations. *Symmetry*, 2019, 11(6), 802. <https://doi.org/10.3390/sym11060802>
- Ding Z, Wen J, Ji X, Zhang S. Experimental Investigation of the Mechanical Behavior of NC Linings in consideration of Voids and Lining Thinning. *Advances in Civil Engineering*, 2020, 2020, 8876785. <https://doi.org/10.1155/2020/8876785>
- Fan YJ, Gong L, Wang LC, Zhang ZX, Lu F, Liu SQ, Qiu WG. Remediation Technology for the Long Segment and Large-scale Cavity behind Vault Linings of an Operating Railway Tunnel. *Railway Standard Design*, 2020, 64(11), 116-121, 135.
- Feng D, Wang X, Zhang B. Specific evaluation of tunnel lining multi-defects by all-refined GPR simulation method using hybrid algorithm of FETD and FDTD. *Construction and Building Materials*, 2018, 185, 220-229.
<https://doi.org/10.1016/j.conbuildmat.2018.07.039>
- Fu J, Xie J, Wang S, Yang J, Yang F, Pu H. Cracking performance of an operational tunnel lining due to local construction defects. *International Journal of Geomechanics*, 2019, 19(4), 04019019. [https://doi.org/10.1061/\(ASCE\)GM.1943-5622.0001371](https://doi.org/10.1061/(ASCE)GM.1943-5622.0001371)
- Gao Y, Jiang YJ, Li B. Estimation of effect of voids on frequency response of mountain tunnel lining based on microtremor method. *Tunnelling and Underground Space Technology*, 2014, 42, 184-194. <https://doi.org/10.1016/j.tust.2014.03.004>

- Gao Y, Jiang YJ, Li B. Voids delineation behind tunnel lining based on the vibration intensity of microtremors. *Tunnelling and Underground Space Technology*, 2016, 51, 338-345. <https://doi.org/10.1016/j.tust.2015.10.032>
- Geng Q, Ye Y, Wang X. Identifying void defects behind Tunnel composite lining based on transient electromagnetic radar method. *NDT & E International*, 2022, 125, 102562. <https://doi.org/10.1016/j.ndteint.2021.102562>
- Gong L, Qiu WG, Wang LC, Wang XY. Accurate Detection Technologies for Larger Hollows Behind Linings of Operating Railway Tunnel. *Tunnel Construction*, 2016, 36 (12), 1507-1511.
- Han W, Jiang YJ, Li NB, Koga D, Sakaguchi O, Chen, HB. Safety evaluation and failure behavior of degraded tunnel structure with compound diseases of voids and lining defects. *Arabian Journal of Geosciences*, 2021a, 14, 1531.
- Han W, Jiang YJ, Li NB, Luan HJ, Wu XL. Study on cracking behavior of tunnel linings with the diseases of void and lining insufficient thickness. *IOP Conference Series: Earth and Environmental Science*, 2021b, 861, 042113
- He BG, Liu ER, Zhang ZQ, Zhang Y. Failure modes of highway tunnel with voids behind the lining roof. *Tunnelling and Underground Space Technology*, 2021, 117, 104147. <https://doi.org/10.1016/j.tust.2021.104147>
- Hu X, Jiang X, Li K, Cui X. Research on Tunnel Lining Cavity Treatment Technology of a Metro Tunnel in Chongqing. *IOP Conference Series: Earth and Environmental Science*, 2019, 304, 032031. <https://doi.org/10.1088/1755-1315/304/3/032031>
- Ikeda Y, Suzuki Y, Suzuki Y, Adachi N, Nozawa T. Damage detection of actual building structures through singular value decomposition of power spectrum density matrices of microtremor response. *Aij Journal Technology Design*, 2010, 16(32), 69-74. <https://doi.org/10.3130/aijt.16.69>
- Jiang HL, Fan HB. Cause Analysis and Treatment Study of Insufficient Secondary Lining Thickness of Highway Tunnel. *Urban Roads Bridges & Flood Control*, 2016, (4), 113-116. <https://doi.org/10.16799/j.cnki.csdqyfh.2016.04.035>
- Jiang XH, Li K. Analysis and Safety Assessment of Lining Thickness Defects in Highway Tunnels. *IOP Conference Series: Materials Science and Engineering*, 2020, 741, 012079. <https://doi.org/10.1088/1757-899X/741/1/012079>

- Konishi S, Kawakami K, Taguchi M. Inspection Method with Infrared Thermometry for Detect Void in Subway Tunnel Lining. *Procedia Engineering*, 2016, 165, 474-483.
<https://doi.org/10.1016/j.proeng.2016.11.723>
- Lalagüe A, Lebens MA, Hoff I, Grøv E. Detection of Rockfall on a Tunnel Concrete Lining with Ground-Penetrating Radar (GPR). *Rock Mechanics and Rock Engineering*, 2016, 49, 2811-2823. <https://doi.org/10.1007/s00603-016-0943-y>
- Li C, Li MJ, Zhao YG, Liu H, Wan Z, Xu JC, Xu XP, Chen Y, Wang B. Layer recognition and thickness evaluation of tunnel lining based on ground penetrating radar measurements. *Journal of Applied Geophysics*, 2011, 73(1), 45-48.
- Li G, Xie JS, Huo QL, Feng L. Measuring Principle and Development Prospect of 3D Laser Scanner. *Mechanical Engineer*, 2015, (9), 135-137.
- Li M, Chen HK. Experimental research on tunnel health criterion of deficiency in lining thickness. *Rock and Soil Mechanics*, 2011, 32, 570-577.
<https://doi.org/10.16285/J.RSM.2011.S1.092>
- Liu C. Study on mechanical characteristics of tunnel structure under the condition of void behind arch lining. Master's Thesis, Qingdao University of Technology, Qingdao, 2018.
- Liu C, Zhang DL, Zhang SL. Characteristics and treatment measures of lining damage: A case study on a mountain tunnel. *Engineering Failure Analysis*, 2021a, 128, 105595.
<https://doi.org/10.1016/j.engfailanal.2021.105595>
- Liu DW, Deng Y, Yang F, Xu GY. Nondestructive testing for crack of tunnel lining using GPR. *Journal of Central South University of Technology*, 2005, 12, 120-124.
<https://doi.org/10.1007/s11771-005-0384-3>
- Liu R, Li S, Zhang G, Jin W. Depth detection of void defect in sandwich-structured immersed tunnel using elastic wave and decision tree. *Construction and Building Materials*, 2021b, 305, 124756. <https://doi.org/10.1016/j.conbuildmat.2021.124756>
- Liu SH, Shi Y, Sun R, Yang JS. Damage behavior and maintenance design of tunnel lining based on numerical evaluation. *Engineering Failure Analysis*, 2020, 109, 104209.
<https://doi.org/10.1016/j.engfailanal.2019.104209>
- Liu Y, Tang CA, Wang PY, Guan YP, Wang SH. Study on Disease Mechanism and Theoretical Quantification Method of Tunnel Structure. *Advances in Civil Engineering*, 2019, 2019, 4398524.

- Lu P, Qiao D, Wu C, Wang S, He X, Zhang W, Zhou H. Effect of defects and remediation measures on the internal forces caused by a local thickness reduction in the tunnel lining. *Underground Space*, 2022, 7(1), 94-105.
<https://doi.org/10.1016/j.undsp.2021.06.001>
- Ma M, Cao R, Niu C, Zhang H, Liu W. Influence of Soil Parameters on Detecting Voids behind a Tunnel Lining Using an Impact Echo Method. *Applied Sciences*, 2019, 9(24), 5403. <https://doi.org/10.3390/app9245403>
- Meguid MA, Dang HK. The effect of erosion voids on existing tunnel linings. *Tunnelling and Underground Space Technology*, 2009, 24(3), 278-286.
<https://doi.org/10.1016/j.tust.2008.09.002>
- Nakamura Y. A method for dynamic characteristics estimation of subsurface using microtremor on the ground surface. *Railway Technical Research Institute, Quarterly Reports*, 1989, 30 (1), 25-33.
- Niu DT, Wang YD, Ma R, Wang JB, Xu SH. Experiment study on the failure mechanism of dry-mix shotcrete under the combined actions of sulfate attack and drying-wetting cycles. *Construction and Building Materials*, 2015, 81, 74-80.
<https://doi.org/10.1016/j.conbuildmat.2015.02.007>
- Peng M, Wang D, Liu L, Shi Z, Shen J, Ma F. Recent Advances in the GPR Detection of Grouting Defects behind Shield Tunnel Segments. *Remote Sensing*, 2021, 13(22), 4596. <https://doi.org/10.3390/rs13224596>
- Prego FJ, Solla M, Nieto XN, Arias P. Assessing the applicability of ground-penetrating radar to quality control in tunneling construction. *Journal of Construction Engineering and Management*, 2016, 142(5), 06015006.
[https://doi.org/10.1061/\(ASCE\)CO.1943-7862.0001095](https://doi.org/10.1061/(ASCE)CO.1943-7862.0001095)
- Qin L, Xie XY, Tang Y, Wang ZZ. Experimental Study on GPR Detection of Voids inside and behind Tunnel Linings. *Journal of Environmental and Engineering Geophysics*, 2020, 25 (1), 65-74. <https://doi.org/10.2113/JEEG18-085>
- Tang HX, Long SG, Li T. Quantitative evaluation of tunnel lining voids by acoustic spectrum analysis. *Construction and Building Materials*, 2019, 228, 116762.
- Tuladhar R, Yamazaki F, Warnitchai P, Saita J. Seismic microzonation of the greater Bangkok area using microtremor observations. *Earthquake Engineering and Structural Dynamics*, 2004, 33(2), 211-225. <https://doi.org/10.1002/eqe.345>

- Voznesenskii AS, Nabatov VV. Identification of filler type in cavities behind tunnel linings during a subway tunnel surveys using the impulse-response method. *Tunnelling and Underground Space Technology*, 2017, 70, 254-261.
<https://doi.org/10.1016/j.tust.2017.07.010>
- Wan L, Xie X, Wang L, Li P, Yin H. Cavity Location Method for Operational Metro Tunnels Based on Perturbation Theory. *KSCE Journal of Civil Engineering*, 2021, 25, 2300-2313. <https://doi.org/10.1007/s12205-021-1691-4>
- Wang J, Huang H, Xie X, Bobet A. Void-induced liner deformation and stress redistribution. *Tunnelling and Underground Space Technology*, 2014, 40, 263-276.
<https://doi.org/10.1016/j.tust.2013.10.008>
- Wang ZJ, Ji XF. Influence of Thickness Inadequacy of Invert Lining on Tunnel Structural Safety Performance. *Railway Engineering*, 2017, 57(8), 61-64.
- Wu XL. Study on the Influence of Voids behind Early Support of Highway Tunnel on Structure Safety and Crack Evolution. Master's Thesis, Shandong University of Science and Technology, Qingdao, 2021.
- Xiang L, Zhou HL, Shu Z, Tan SH, Liang GQ, Zhu J. GPR evaluation of the Damaoshan highway tunnel: A case study. *NDT & E International*, 2013, 59, 68-76.
<https://doi.org/10.1016/j.ndteint.2013.05.004>
- Xie X, Zeng C, Wang Z. GPR signal enhancement using band-pass and K–L filtering: a case study for the evaluation of grout in a shielded tunnel. *Journal of Geophysics and Engineering*, 2013, 10(3), 034003.
<https://doi.org/10.1088/1742-2132/10/3/034003>
- Xu F, Li H, Yao H, An MS. Detection method of tunnel lining voids based on guided anchoring mechanism. *Computers and Electrical Engineering*, 2021, 95, 107462.
<https://doi.org/10.1016/j.compeleceng.2021.107462>
- Xue YD, Yang R. Effect of Void behind Mountain Tunnel Lining in Blasting Condition, 4th ISRM Young Scholars Symposium on Rock Mechanics. OnePetro, 2017.
- Yashiro K, Kojima Y, Shimizu M. Historical Earthquake Damage to Tunnels in Japan and Case Studies of Railway Tunnels in the 2004 Niigataken-Chuetsu Earthquake. *QR of RTRI*, 2007, 48(3), 136-141. <https://doi.org/10.2219/rtriqr.48.136>
- Yasuda N, Tsukada K, Asakura T. Elastic solutions for circular tunnel with void behind lining. *Tunnelling and Underground Space Technology*, 2017, 70, 274-285.

- <https://doi.org/10.1016/j.tust.2017.08.032>
- Ye F, Qin N, Liang X, Ouyang A, Qin Z, Su E. Analyses of the defects in highway tunnels in China. *Tunnelling and Underground Space Technology*, 2021, 107, 103658.
<https://doi.org/10.1016/j.tust.2020.103658>
- Ye ZJ, Zhang CP. Influence of Loose Contact between Tunnel Lining and Surrounding Rock on the Safety of the Tunnel Structure. *Symmetry*, 2020, 12(10), 1733.
- Ye ZJ, Zhang CP, Ye Y, Zhu WJ. Application of transient electromagnetic radar in quality evaluation of tunnel composite lining. *Construction and Building Materials*, 2020, 240, 117958. <https://doi.org/10.1016/j.conbuildmat.2019.117958>
- Yu L, Bai SJ, Liu XX, Chen L, Bao LS. Study on the Influence of Tunnel Lining Thickness on Bearing Capacity of Lining. *Journal of Shenyang Jianzhu University (Natural Science)*, 2017, 33(6), 1039-1047.
- Yuan CH, Tang XH, Wu YM. Reasons and Solutions for Cavity in Secondary Lining of Tunnel. *Transport Standardization*, 2010, (10), 109-112.
- Zhang S. Study on Influence Mechanism of Lining Defects and Bearing Capacity of Highway Tunnel Lining. Ph.D. Thesis, Lanzhou University, Lanzhou, 2020.
- Zhang S, He W, Li Y, Zou Y. Thickness Identification of Tunnel Lining Structure by Tim-Energy Density Analysis Based on Wavelet Transform. *Journal of Engineering Science and Technology Review*, 2019, 12(4), 28-37.
<https://doi.org/10.25103/jestr.124.04>
- Zhang SL. Study on Health Diagnosis and Technical Condition Assessment for Tunnel Lining Structure. Ph.D. Thesis, Beijing Jiaotong University, Beijing, 2012.
- Zhang SL, Qi XQ, Liu C, Chen DG. Distribution Characteristics of Voids Behind Lining of Highway Tunnel and Its Influence on Lining Structure. *Journal of Architecture and Civil Engineering*, 2020, 37(2), 62-70.
<https://doi.org/10.19815/j.jace.2020.02007>
- Zhang X, Su J, Xu YJ, Min B. Experimental and numerical investigation the effects of insufficient concrete thickness on the damage behaviour of multi-arch tunnels. *Structures*, 2021, 33, 2628-2638. <https://doi.org/10.1016/j.istruc.2021.06.020>
- Zhang YL, Nie ZY, Li FX. Three-dimensional Numerical Analysis of the Effect of Voids on Existing Road Tunnel Linings. *Journal of Zhengzhou University (Engineering Science)*, 2013, 34(2), 94-98.

Zhao YC, Li YL, Wei M, Duan JC. Discussion on Causes of and Preventive Measures against Tunnel Lining Voids and Inadequate Thickness. *Modern Tunnelling Technology*, 2019, 56(2), 40-43. <https://doi.org/10.13807/j.cnki.mtt.2019.02.006>

3 Fracture characteristics and cracking mechanism of linings containing typical quality defects with the FEM-CZM method

3.1 Introduction

Cracking of lining support structure is common in tunnels, which seriously threatens the safe operation of tunnel structures (Wu et al. 2017a; Malmgren et al. 2005; Xu et al. 2020; Wu et al. 2017b; Zhang et al. 2014; Zhang et al. 2018; Huang et al. 2017). In addition, tunnel quality defects such as void behind the lining and insufficient lining thickness often appear in tunnel structures (Xue and Yang 2017; Yu et al. 2017). However, quality defects can be regarded as weak positions of tunnel structures (Yu et al. 2017; Liu et al. 2020). Therefore, it is significant to clarify the cracking characteristics of linings with typical quality defects.

The main causes for the formation of void quality defects are insufficient backfilling and poor work technique (Wang et al. 2014). Regarding the formation of insufficient lining thickness, inappropriate design and construction may become the inducement factors (Yu et al. 2017). Concerning the impact of these typical tunnel quality defects, Zhang (2018) investigated the effect of the void behind the lining and insufficient lining thickness on the safety state of a double-arch tunnel structure, and the cracking characteristics were explored with the extended finite element method (XFEM). Ding et al. (2019) carried out model tests to explore the mechanical and fracture properties of reinforced concrete lining considering the symmetric and asymmetric voids, and the numerical simulation was subsequently conducted to study the damage behavior. Min et al. (2018) paid attention to the mechanical properties and failure patterns of double-arch tunnels containing void defects. Che (2020) studied the lining cracking characteristics based on the XFEM, and the characteristic of crack propagation was explored. Zhang (2020) studied the effect of lining defects on the highway tunnel lining, and the concrete

damage plasticity (CDP) model was applied to explore the cracking characteristics of linings. Gong (2019) evaluated the safety state of tunnel structure under the impact of insufficient lining thickness, and the XFEM was then applied to simulate the cracking characteristic of linings. Feng (2013) conducted a laboratory test to explore the fracture characteristics of tunnel structures with void defects, and the distribution of inner force was investigated. Zhang et al. (2017) investigated the cracking behaviors of tunnel lining with void defects, and the distribution of stress and the inner force were further studied. He et al. (2021) conducted the model test to investigate the failure modes of highway tunnels with voids behind the lining, and the crack characteristics were discussed. Fang et al. (2016) investigated the fracture characteristics and inner force of tunnel linings with void defects under external water pressure, and the influence of external water pressure was revealed. Lei et al. (2015) numerically explored the cracking behaviors of tunnel lining with void defects, and the cracking pattern was focused on. Liu et al. (2020) investigated the cracking behaviors of lining structures with insufficient thickness and the maintenance effect of the inner lining was concerned. Regarding the impact of cracks on tunnel structure, Xu et al. (2020) explored the cracking situations based on the field investigation, and the mechanical behaviors of tunnel linings with cracks were subsequently studied with the laboratory model test and numerical model. Su et al. (2020) conducted the three-dimensional model experiment to investigate the mechanical behaviors of tunnel linings with cracks, and the deformation, inner force, and fracture behaviors were concentrated. Yan et al. (2018) studied the cracking and failure characteristics of segmental linings under a derailed high-speed train impact. In addition, Wang (2010) focused on the crack patterns of linings caused by neighboring slope movement, and safety inspection techniques were provided.

Generally, the numerical techniques, such as the CDP model (Zhang 2020; Ding et al. 2019; Hafezolghorani et al. 2017; Labibzadeh and Namjoo 2020), XFEM (Zhang 2018; Che 2020; Gong 2019; Roth et al. 2015; Ru et al. 2011; Chen et al. 2020; Faron and Rombach 2020) have been extensively applied to explore the damage and cracking behaviors of the concrete structure. The cohesive zone model (CZM), proposed by Dugdale (1960) and Barenblatt (1962), recently has been widely applied to explore the

damage behavior of concrete structures (Song et al. 2006; Zhang et al. 2015; Wu et al. 2018; Liu et al. 2021). The determination of potential crack distribution can be achieved by embedding zero-thickness cohesive elements into solid elements globally (Wu et al. 2018; Jiang and Meng 2018; Wu et al. 2020; Zhang et al. 2020). Concerning the method of CZM, Jiang and Meng (2018) investigated the 3D rock fracture under the Brazilian and Uniaxial compression tests. Additionally, Chang et al. (2020) numerically studied the cracking behaviors of layered discs containing a preexisting interface crack based on the CZM method, which was further validated by Brazilian tests. Besides, Huang et al. (2020) studied the fracture behavior of sandstone under the semicircular bending test with the method of CZM, and the effects of bedding planes were considered. Zhang et al. (2020) investigated the shear behavior of jointed rocks by inserting cohesive elements into solid elements, and crack evolution was concerned in their research. Wang et al. (2019) explored the shearing process and failure types of jointed rock masses using the CZM method, and the crack evolution process was further examined.

Overall, it can be observed that the mechanical and damage characteristics of linings have been widely investigated. Previous studies on cracking performance are mostly based on a single defect type, such as voids or insufficient lining thickness. However, information on cracking characteristics of linings with multiple defect types is rather limited. The dominant quality defects affecting the lining structure also need to be further clarified. In addition, the CZM method could well describe the cracking characteristics of the concrete structure. Unfortunately, fewer appeared in arched lining structures with multiple defect types, and its application should be further discussed. Therefore, the focus of this chapter is to explore the fracture characteristics and cracking mechanism of lining structures with multiple defect types of void and insufficient lining thickness based on the FEM-CZM method. Overall, this chapter is expected to reveal the dominant defect type affecting the lining structure, further reveal the fracture characteristics and cracking mechanism of the defective lining structure, and finally determine effective crack suppression techniques.

3.2 FEM-CZM method

3.2.1 Constitutive model

3.2.1.1 Linear elastic behavior

The traction-separation model is available in ABAQUS (ABAQUS User's Manual; Jiang and Meng 2018; Wu et al. 2020; Zhang et al. 2020). Jiang and Meng (2018) utilized the traction-separation model to explore the fracture characteristics of rocks under the Brazilian disc tests and uniaxial compression tests. Wu et al. (2020) and Zhang et al. (2020) applied the model to investigate the shear failure behaviors of rock-like materials. The traction-separation model includes the linear elastic stage and the damage evolution stage (ABAQUS User's Manual; Wu et al. 2020). The elastic behavior is represented by an elastic constitutive matrix, which can be written as follows (ABAQUS User's Manual):

$$t = \begin{Bmatrix} t_n \\ t_s \\ t_t \end{Bmatrix} = \begin{bmatrix} E_{nn} & E_{ns} & E_{nt} \\ E_{ns} & E_{ss} & E_{st} \\ E_{nt} & E_{st} & E_{tt} \end{bmatrix} \begin{Bmatrix} \varepsilon_n \\ \varepsilon_s \\ \varepsilon_t \end{Bmatrix} = E\varepsilon \quad (3-1)$$

where t is the nominal traction stress vector and consists of three components t_n , t_s , and t_t ; ε is the nominal strain vector and consists of three components ε_n , ε_s , and ε_t .

3.2.1.2 Damage evolution stage

Regarding the damage evolution stage, the quadratic nominal stress criterion can be utilized for the damage initiation (ABAQUS User's Manual). The nominal stress ratios are included in a function of the quadratic nominal stress criterion, which can be expressed as follows (ABAQUS User's Manual):

$$\left\{ \frac{\langle t_n \rangle}{t_n^o} \right\}^2 + \left\{ \frac{t_s}{t_s^o} \right\}^2 + \left\{ \frac{t_t}{t_t^o} \right\}^2 = 1 \quad (3-2)$$

where the $\langle \rangle$ is the Macaulay bracket.

To characterize the damage degree, the damage variable D for linear softening can be expressed as follows (ABAQUS User's Manual; Camanho and Dávila 2002):

$$D = \frac{\delta_m^f (\delta_{em}^{\max} - \delta_m^o)}{\delta_{em}^{\max} (\delta_m^f - \delta_m^o)} \quad (3-3)$$

where δ_m^o , δ_m^f , and δ_{em}^{\max} represent the effective displacement at the initiation of damage, the effective displacement at the complete failure, and the maximum value of the effective displacement attained during the loading history, respectively.

3.2.2 Embedding process of cohesive elements

To realize the randomness and accuracy of cracking, the zero-thickness cohesive elements should be globally embedded between the solid elements (Jiang and Meng 2018; Wu et al. 2020; Wu et al. 2018; Huang et al. 2020). Therefore, the zero-thickness cohesive elements were globally inserted between every two solid elements to form a potential crack surface, the model mesh was divided dense enough to ensure the complexity and randomness of the cracking behavior. Based on this (Jiang and Meng 2018; Wu et al. 2020; Wu et al. 2018; Huang et al. 2020), the embedding process of cohesive elements can be shown in Fig. 3.1, and it is noted that the typical process consists mainly of discretizing solid elements, renumbering, and insertion of a zero-thickness cohesive element. Since in the application of the actual model, the number of solid elements may be very large, it would be very time-consuming and inefficient to manually embed zero-thickness cohesive elements globally. Therefore, an automatic embedding program was developed, which can greatly improve efficiency.

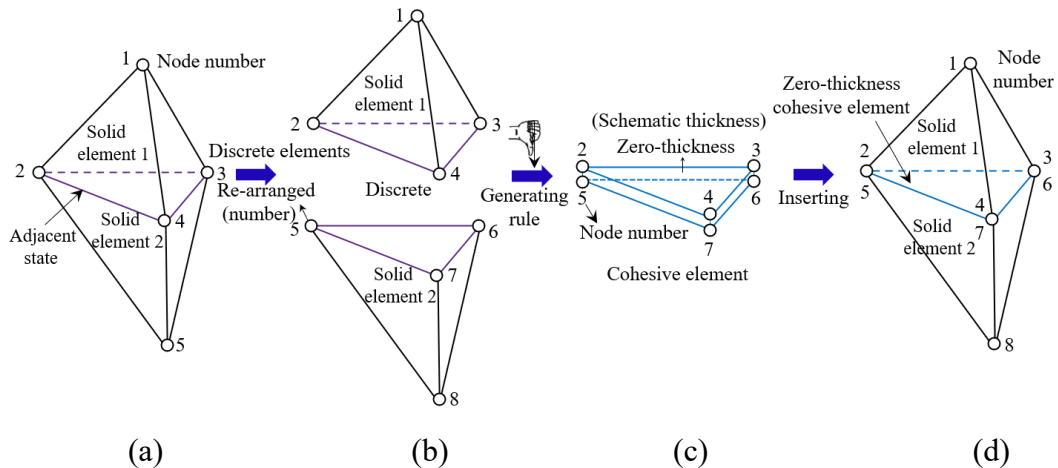


Fig. 3.1 Inserting a zero-thickness cohesive element between solid elements: (a) solid elements; (b) re-arrange nodes of solid elements; (c) zero-thickness cohesive element; (d) insertion of a zero-thickness cohesive element.

3.3 Model establishment

The numerical model established in this research can be demonstrated in Fig. 3.2. The model dimension of the tunnel structure was arranged as a 3D model with a longitudinal tunnel depth of 20m, in which multiple defect types were considered. The considered multiple defect types in this chapter are the combination of void and insufficient lining thickness, which can be referred to as combined defects. Concerning the void size, the tangential range was set as 30°, 45°, 60°, and 90°, and the length in the longitudinal direction was set as 5m. Regarding the size of the insufficient lining thickness, the range was fixed at 45°. In addition, the distance between the void and the insufficient thickness was fixed at 1m. It should be indicated that since the void shape has little effect on the tunnel structure (Liu 2007), the void thus can be set as a rectangular shape. Furthermore, it should be noted that the area with insufficient lining thickness is in contact with the rock mass. If the rock mass is not in contact with the lining in the local thickness insufficient zone, a local compound defect would be formed. To study the influence of insufficient lining thickness separately, the rock mass and lining in the model are in contact. Regarding the establishment of the numerical tunnel model, the cross-section of tunnel structure in this research was applied from the standard section of the highway tunnel (Ministry of Transport of the PRC 2004). Concerning the boundary conditions, the displacement of the rock mass on the left and right sides as well as the front and back directions were limited, and the vertical displacement at the bottom of the model was fixed. To be able to observe the cracking characteristics of the lining, a gradual vertical loading was applied to the top sides of the model, the boundary condition was also applied by Wu (2021) and Gong (2019). According to the design of tunnels and Wu (2021), the parameters of the applied materials, including tunnel rock mass and solid elements of lining structure can be displayed in Table 3.1, and parameters of cohesive elements can also be obtained by Wu (2021) as follows: initial tensile stiffness 17GPa/m, initial shear stiffness 7.35GPa/m, normal traction 6.5MPa, tangential traction 22MPa, I fracture energy 0.08N/mm, II fracture energy 0.185N/mm. The solid elements and the inserted zero-thickness cohesive elements can be presented in Fig. 3.3.

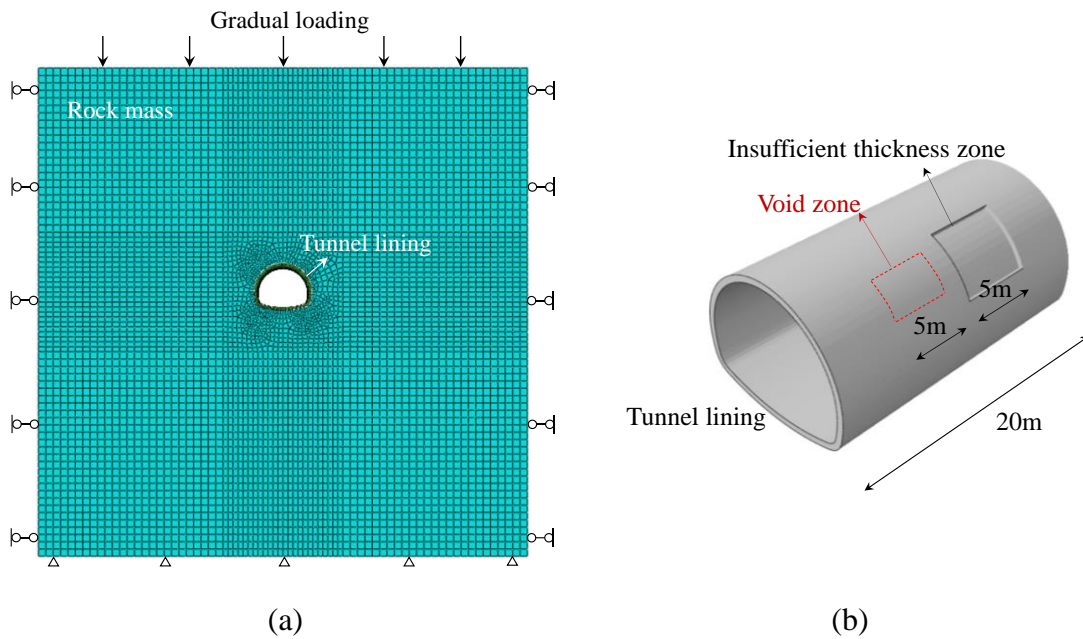


Fig. 3.2 Established numerical model: (a) grid and boundary conditions; (b) distribution of combined defects of void and insufficient thickness zone.

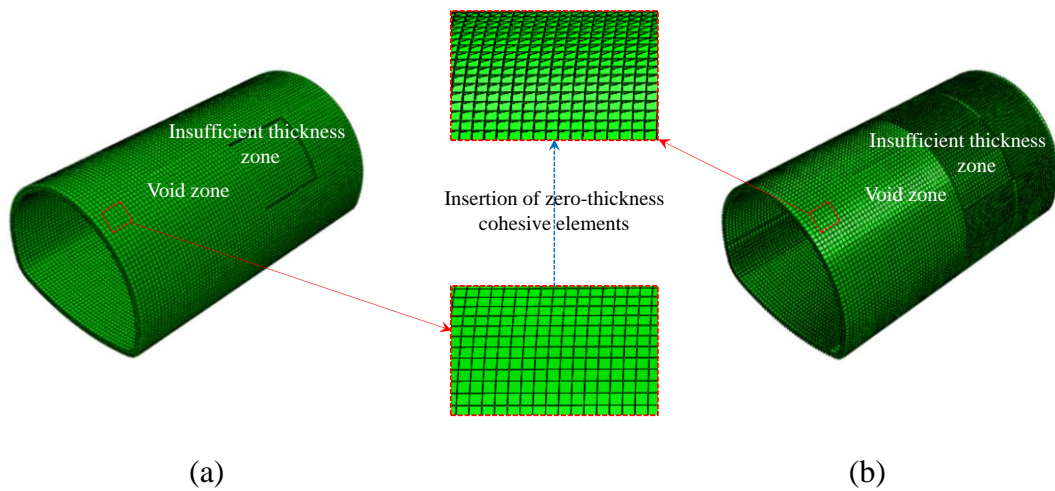


Fig. 3.3 Numerical elements: (a) solid elements; (b) inserted zero-thickness cohesive elements.

Table 3.1 Properties of tunnel rock mass and solid elements.

Parameters	Tunnel rock mass	Solid elements (Wu 2021)
ρ (kg/m ³)	1800	2200
E (GPa)	1.5	21
ν	0.35	0.2
c (Pa)	1.5×10^5	/
φ (°)	20	/

3.4 Numerical results

3.4.1 Mechanical properties

The mechanical properties of the lining with combined defects of void range of 60° were presented in Fig. 3.4. The stress properties are closely related to the defect type. Specifically, the lining is mainly subjected to an obvious tensile stress concentration on the outer surface corresponding to the void. In contrast, a significant compressive stress zone appears in the area with insufficient lining thickness. The main reason for this phenomenon is that the existence of voids eliminates the contact between the lining and the rock mass. Meanwhile, this phenomenon can be reflected in the deformation distribution, as shown in Fig. 3.5. It is observed that deform outwards phenomenon occurs at the void zone. However, regarding the lining area with insufficient thickness, the inward deformation occurs due to the effective contact between the rock mass and the lining, forming a compression zone on the outer surface.

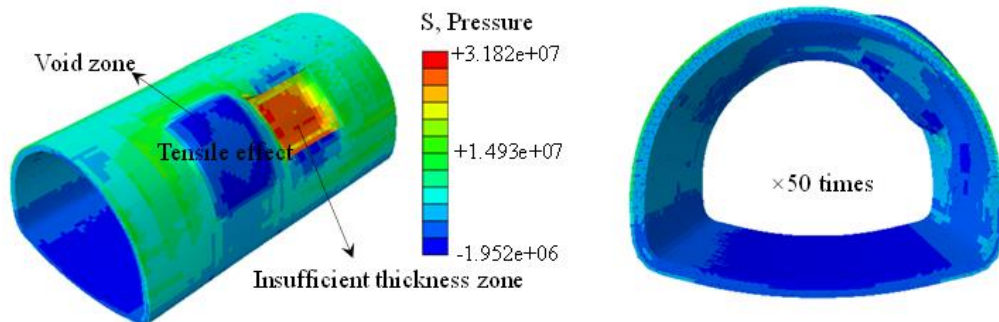


Fig. 3.4 Mechanical properties of the lining structure with combined defects.

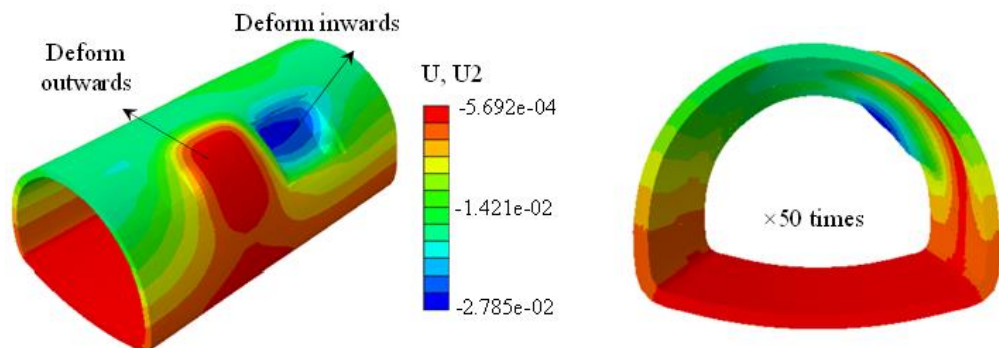


Fig. 3.5 Deformation characteristics of the lining structure with combined defects.

3.4.2 Characteristics of cracking distribution

In this section, the cracking characteristics of defective lining structures were investigated. Taking the void range of 90° as an example, the schematic of crack generation in defective linings can be exhibited in Fig. 3.6. It is observed that with the increase of the gradual load, longitudinal cohesive elements are first deleted on the lining outer surface corresponding to the void zone, resulting in longitudinal cracks. As the gradual load further increases, the cracks will further propagate and induce another cracking zone.

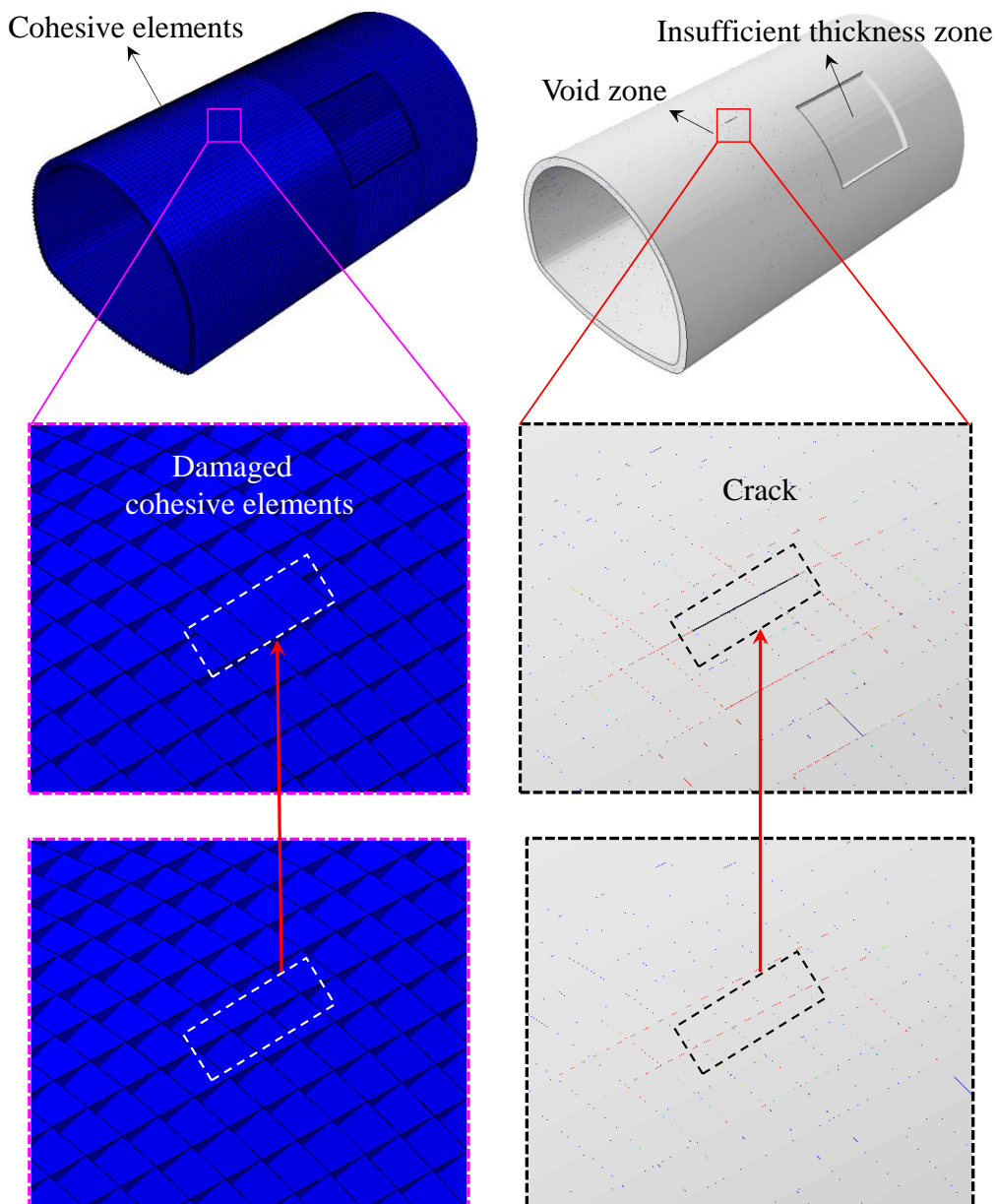


Fig. 3.6 Principle of crack generation of defective lining structures.

The cracking characteristics of linings with combined defects were explored and presented in Figs. 3.7-3.10. Taking the void range of 45° as an example, the characteristics of crack propagation were concerned, as shown in Fig. 3.8. In this chapter, three typical perspectives were selected to observe the phenomenon of lining cracking. As can be observed from perspective I in Fig. 3.8, it can be found that on the outer surface of the lining, cracks mainly appear within the void zone. The main reason for this phenomenon is that the surrounding rock and the lining are not in contact within the void zone, resulting in a sharp reduction of the safety factors (Liu 2018). This can easily lead to local failure of the lining. As the gradual loading increases, some cracks gradually appear at the area and edge of the insufficient thickness zone. The main reason for this phenomenon is the stress concentration caused by the thickness change at the edge of the defect zone. This cracking phenomenon can also be reflected by the test of Gong (2019), which can further prove the rationality of the cracking results. It is worth noting that the cracking degree of the void zone is larger than that of the area within the insufficient thickness zone. This is because the surrounding rock is in contact with the lining in the insufficient thickness zone in this research, forming a relatively well-contact state. In addition, the cracks are mainly distributed within the defect zone on the outer surface of the lining, while the other parts are not obvious in this propagation stage. Regarding the morphology of generated cracks in this research, ring cracks are prone to occur on the outer surface of the void zone, and the range gradually increases with the increment of the gradual load level. However, concerning the crack morphology within the outer surface of the lining defect zone, longitudinal cracks are mainly observed. With the increment of the applied vertical loading, the number of longitudinal cracks further increases. In addition, it is observed that significant longitudinal cracks mainly occur in the arch springing. The main reason for this phenomenon is that lower safety factors would happen at the arch springing (Liu 2018), which will be prone to cause local damage. In addition, the arch springing is also a place with a large curvature, which is prone to stress concentration. Perspective II was also presented in Fig. 3.8 to explore the fracture characteristics in the inner surface. Significant ring cracks occur at the edge of the void zone, and there are both longitudinal cracks and ring cracks generated at the void zone and the edge of the insufficient thickness zone. In addition, cross patterns of ring cracks and longitudinal cracks are prone to occur

on the inner surface of the area between the insufficient thickness zone and the void zone. As a comparison, the characteristics of crack propagation of the lining structures with the void range of 30°, 60°, and 90° were also presented in Fig. 3.7, Fig. 3.9, and Fig. 3.10. The void range can significantly affect the crack distribution. Specifically, the cracking degree of the lining outer surface corresponding to the void zone presents a positive relationship with the void range. However, the cracking degree at the outer surface of the insufficient thickness zone is not significantly affected by the variation of the void range. In addition, with the increase of the void range, the cracking of the lining outer surface is still concentrated at the defect zone, and the cracking degree in other places is not significantly affected. Regarding the fracture characteristic on the inner surface, the cracking degree exhibits a positive relationship with the void range. In addition, the range of ring cracks on the inside surface corresponding to the void edge shows a positive relationship with the void range. Overall, the cracking characteristics are significantly affected by the defect distribution.

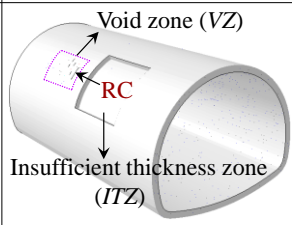
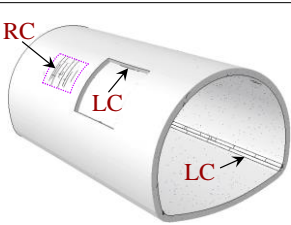
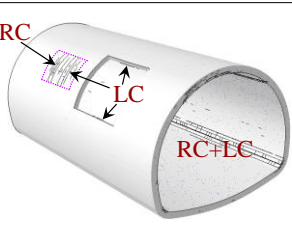
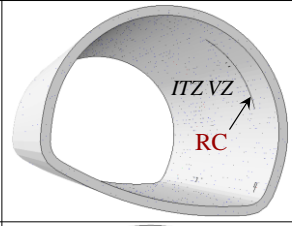
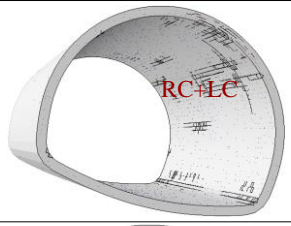
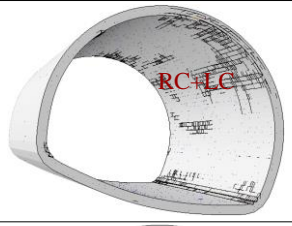
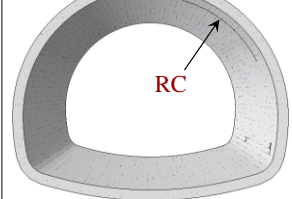
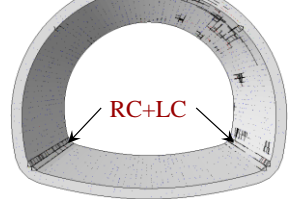
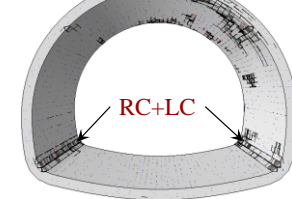
Fracture behavior	Crack propagation	Crack further propagation	Crack further propagation
Perspective I			
Perspective II			
Perspective III			

Fig. 3.7 Cracking distribution of linings with combined defects of void range of 30°.

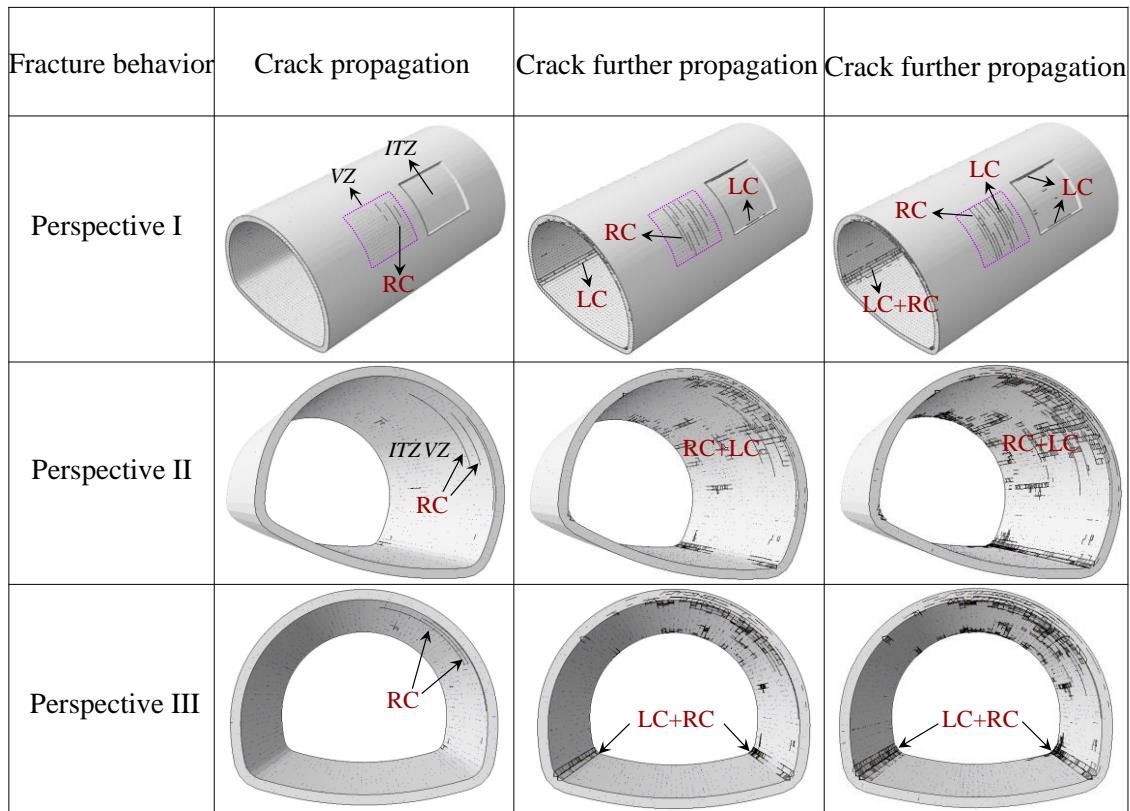


Fig. 3.8 Cracking distribution of linings with combined defects of void range of 45°.

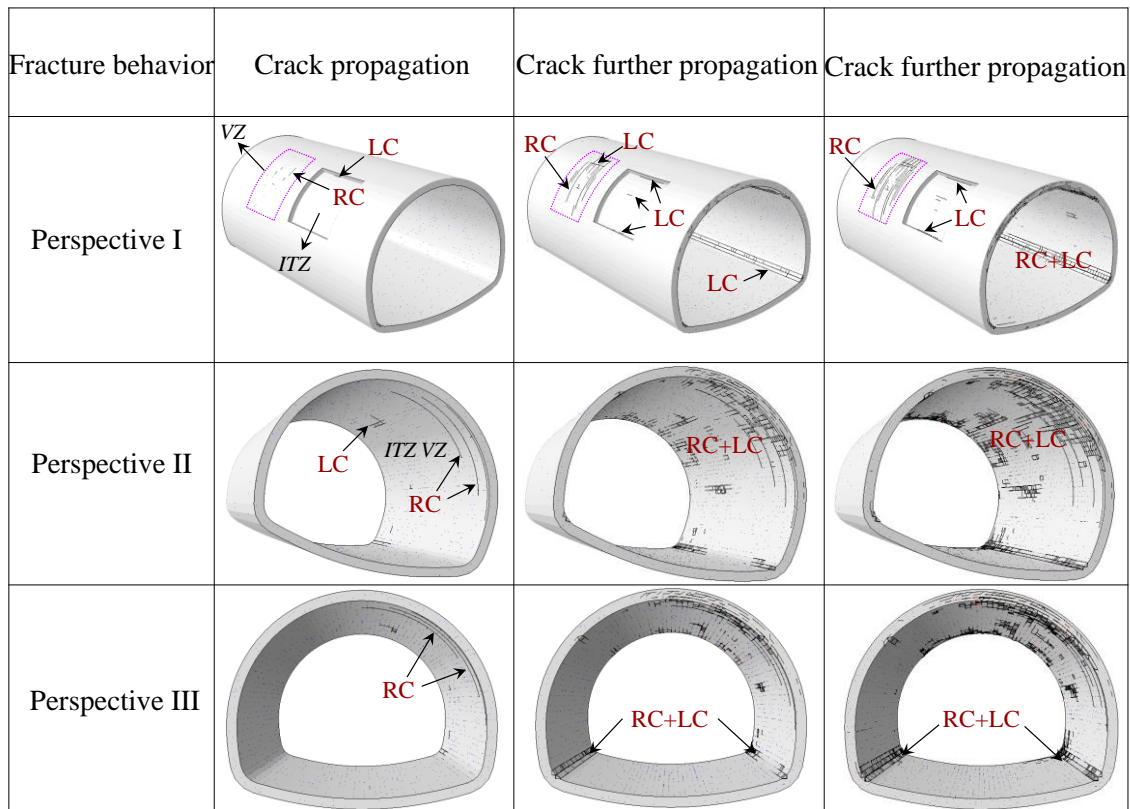


Fig. 3.9 Cracking distribution of linings with combined defects of void range of 60°.

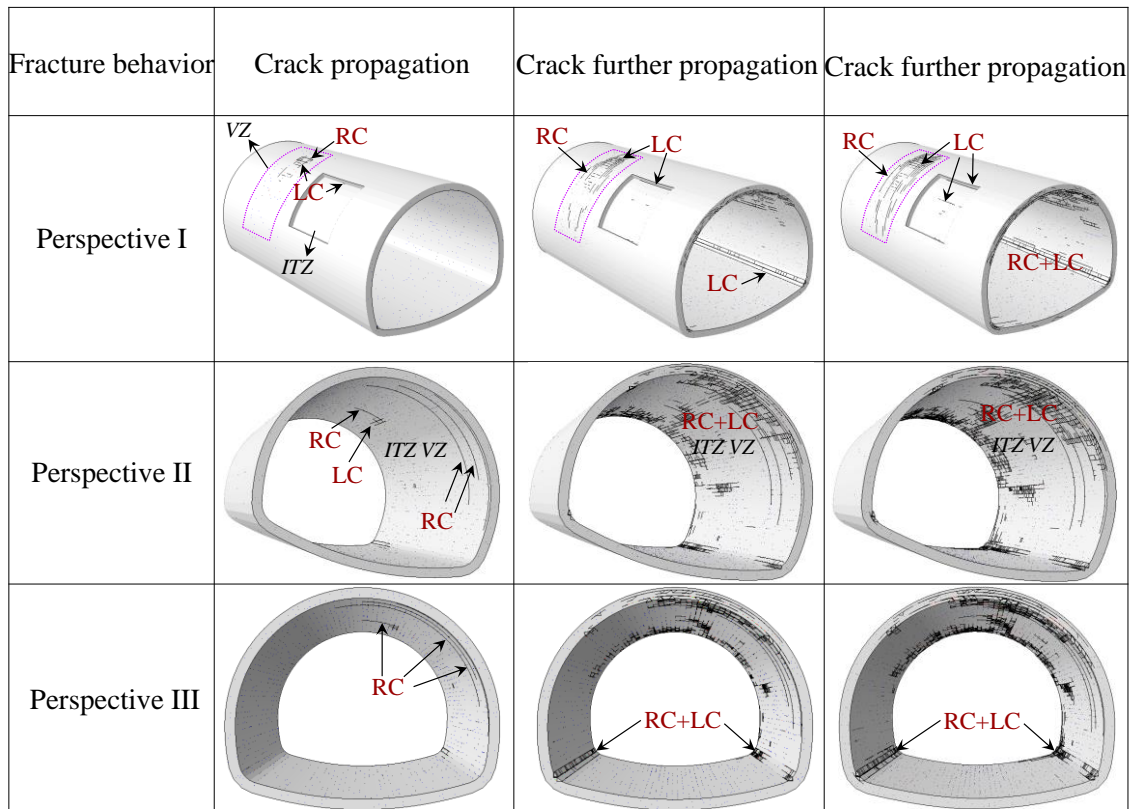
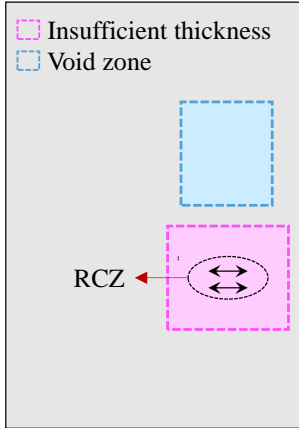
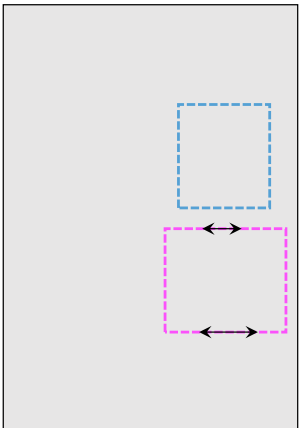
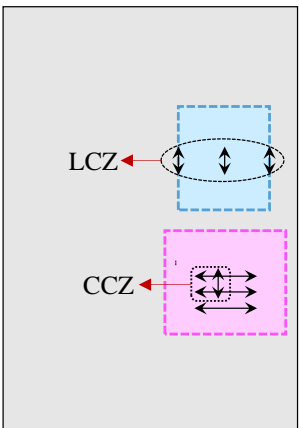
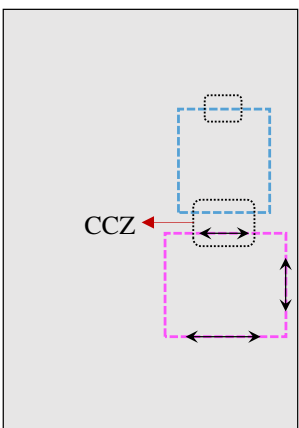


Fig. 3.10 Cracking distribution of linings with combined defects of void range of 90° .

The influence of cracks on the lining structure is closely related to morphological characteristics (He et al. 2019). Therefore, it is significant to explore the relationship between tunnel quality defects and crack morphological characteristics. In this section, the morphological characteristics of cracks of lining structures with combined defects were discussed and presented in Fig. 3.11 (compared with the research of Min et al. 2020). It is observed that the ring cracks zone (RCZ), longitudinal cracks zone (LCZ), and cross cracks zone (CCZ) is determined during crack propagation. Specifically, the RCZ is mainly distributed on the outer surface corresponding to the void zone. The LCZ primarily appears on the outer surface of the insufficient thickness zone. As the crack further propagated, CCZ appears on the outer surface of the void zone and the inner surface between the void and insufficient thickness zone. Subsequently, the comparison in fracture patterns between the lining with two typical quality defects and a single void defect was discussed. The cracking patterns of lining structures with a single void defect can be obtained from Min et al. (2020). As a comparison, RCZ both appear on the outer surface of linings corresponding to the void defect. Regarding the specific crack patterns,

the propagation paths of partial cracks at the void zone are offset along the longitudinal direction in the study of Min et al. (2020). In this study, the longitudinal cracks in the void zone were mainly caused by the failure of the longitudinal cohesive elements, forming CCZ together with the ring cracks. The main reason for this difference may be the effect of an adjacent defect of insufficient thickness. As for cracking patterns on the inner surface, ring or longitudinal cracks are prone to occur at the edge of void defects. In contrast, the inner surface of the lining corresponding to the void zone is not easy to crack, which further verifies the rationality of the results in this paper.

Cracking behavior	Outer surface	Inner surface
Crack propagation	 <p data-bbox="491 1290 616 1317">Sidewall(L)</p> <p data-bbox="770 1290 895 1317">Sidewall(R)</p>	 <p data-bbox="1289 1061 1334 1088">20m</p> <p data-bbox="911 1290 1035 1317">Sidewall(L)</p> <p data-bbox="1193 1290 1318 1317">Sidewall(R)</p>
Crack further propagation	 <p data-bbox="603 1503 727 1529">LCZ</p> <p data-bbox="619 1626 743 1653">CCZ</p>	 <p data-bbox="1046 1570 1107 1597">CCZ</p>

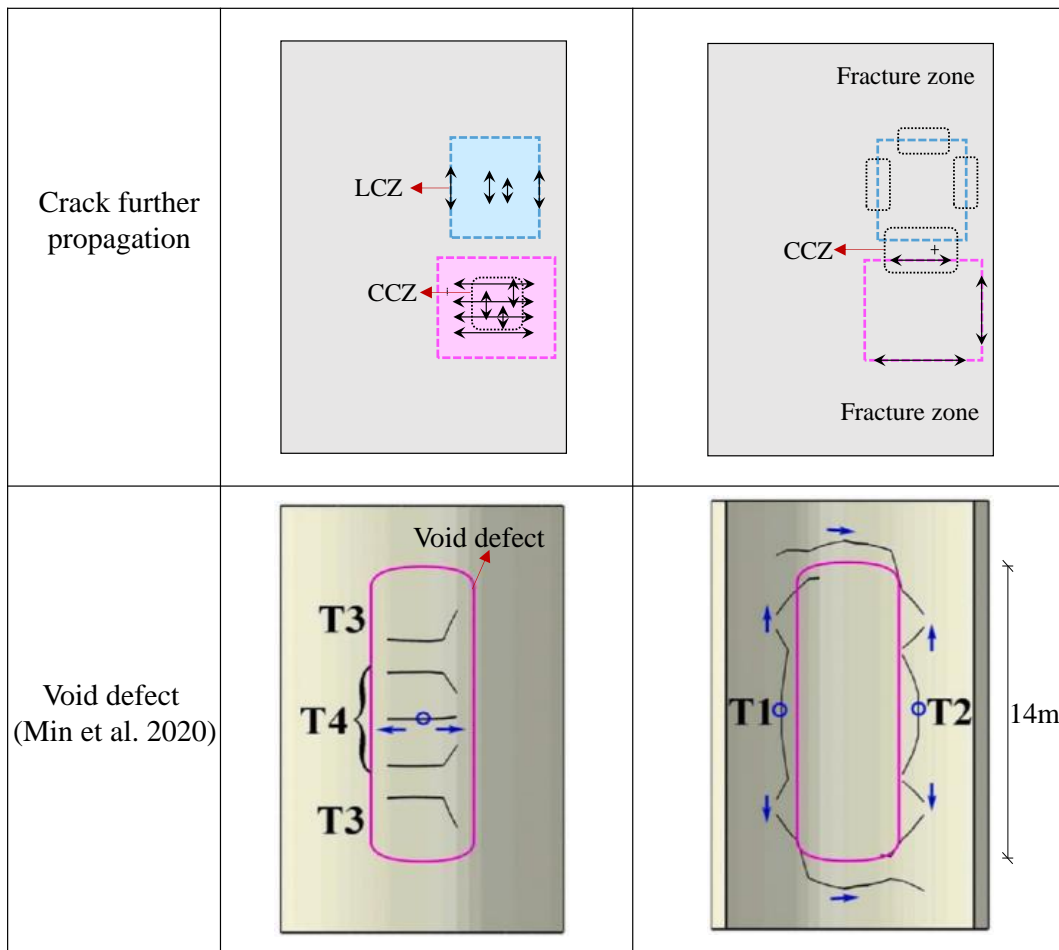


Fig. 3.11 Cracking morphological characteristics of linings with combined defects (compared with the research of Min et al. 2020).

3.4.3 Statistics of cracks

To make clear the evolution characteristics of cracks during the fracture process, the statistics of cracks were explored, including the number of damaged cohesive elements, crack area, crack volume, maximum crack width, and the proportion of tensile failure. It should be indicated that this section also focuses on exploring the effect of void range on the crack statistics of linings with combined quality defects, and the void range was set as 30° , 45° , 60° , and 90° , respectively. The statistic of the number of damaged cohesive elements can be presented in Fig. 3.12. It can be observed that with the increment of the gradual loading, the number of damaged cohesive elements tends to increase. When the applied load is in the interval of 5MPa-7MPa, the number of damaged cohesive elements

increases approximately linearly with the increase of applied gradual load. It should be indicated that 1MPa, 2MPa, 3MPa, 4MPa, 5MPa, 6MPa, and 7MPa during the gradual vertical loading process were selected as typical examples to explore the characteristics of crack statistics, as shown in the histogram of Fig. 3.12. It is noted that the number of damaged cohesive elements is relatively small when the applied gradual load does not exceed 3MPa. As the applied gradual load level further increases, the number of damaged cohesive elements changes significantly. Specifically, when the applied gradual load reaches to 5MPa-7MPa, the number of damaged cohesive elements is equal to 682, 4567, and 8614 for the void range of 45°, while for the void range of 60°, the numbers are 850, 5201, 9948, respectively. It can be observed that the number of damaged cohesive elements presents a positive relationship with the level of gradual load in the model. The number of damaged cohesive elements is significantly affected by the void range. Specifically, when the applied gradual load level is reached to 5MPa, the number of damaged cohesive elements is 523, 682, 850, and 1382 for the void range of 30°, 45°, 60°, and 90°, while the number is equal to 3802, 4567, 5201, and 7148 when the applied load level is reached to 6MPa. The main reason for the significant increase in the number of damaged cohesive elements above 5MPa is the instability of the model. Overall, the number of damaged cohesive elements exhibits a positive relationship with the increment of the void range in the model.

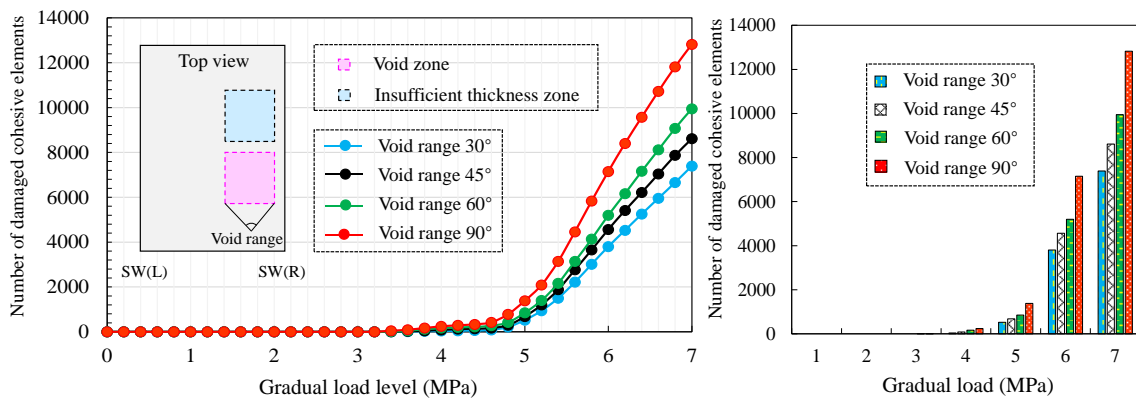


Fig. 3.12 Evolution of the number of damaged cohesive elements with the applied gradual load.

The evolution of the crack area with the applied gradual loading can be presented in Fig. 3.13. With the increase of the gradual loading, the crack area tends to increase. When the applied load is in the interval of 4MPa-5MPa, the growth rate of the crack area

gradually increases, while the crack area increases approximately linearly with the increase of applied gradual load for the loading between the 5MPa and 7MPa. Similarly, the typical loading levels of 1MPa, 2MPa, 3MPa, 4MPa, 5MPa, 6MPa, and 7MPa were also selected, as presented in the histogram of Fig. 3.13. Note that the crack area is significantly affected by the loading level. It is observed that the crack area can further increase with the increment of the applied loading. When the applied loading is larger than 5MPa, the crack area is increased sharply. The effect of the void range on the crack area can also be shown in Fig. 3.13. Taking the loading level of 6MPa as an example, the crack area is equal to 150.87cm^2 , 179.47cm^2 , 205.78cm^2 , and 282.21cm^2 , respectively. It is also observed that the crack area shows a positive relationship with the void range.

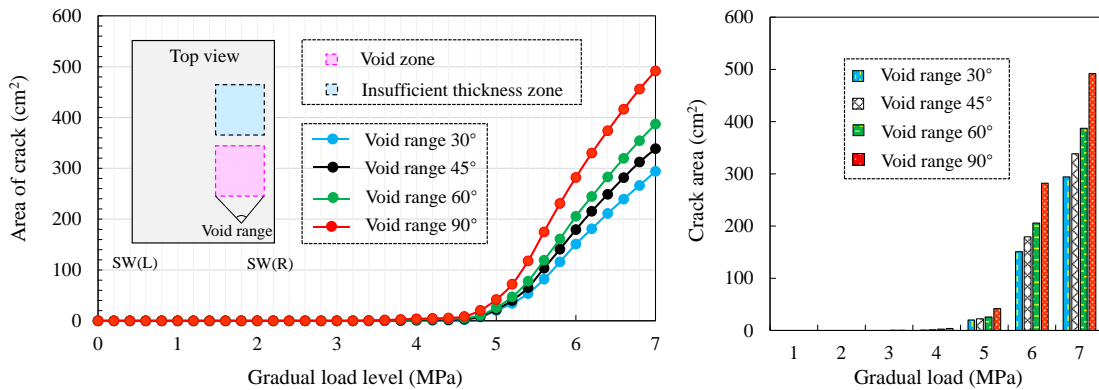


Fig. 3.13 Evolution of the crack area with the applied gradual load.

The evolution of the crack volume with the applied gradual loading can be presented in Fig. 3.14. With the increment of the loading, the crack volume increases significantly. In particular, the crack volume increases approximately linearly in the range of 6MPa to 7MPa. Analogously, typical loading levels were also selected to investigate the characteristic of crack volume. Taking the void range of 90° as an example, when the applied loading is increased from 4MPa to 7MPa, the crack volume is 0.005m^3 , 0.065m^3 , 1.01m^3 , and 2.84m^3 , respectively. In addition, the effect of the void range on the crack volume can also be shown in Fig. 3.14. Taking the applied vertical loading level of 6MPa as an example, the crack volume is 0.0609m^3 , 0.693m^3 , 0.756m^3 , and 1.01m^3 , respectively. Thus, it can be observed that the crack volume also presents a positive relationship with the void range in the established model.

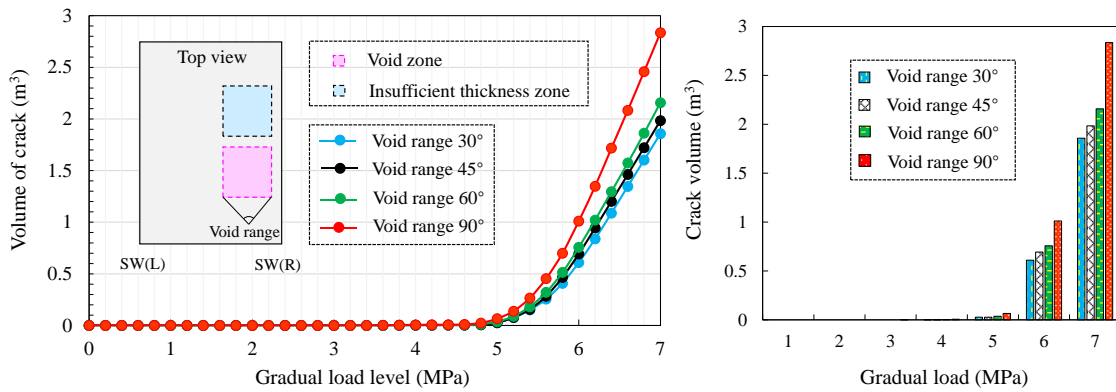


Fig. 3.14 Evolution of the volume of crack with the applied gradual load.

The evolution of the maximum crack width with the applied gradual load can be presented in Fig. 3.15. The maximum crack width varies significantly with the increasing load. Specifically, when the loading level is less than 3MPa, the maximum crack width is small. When the loading level is in the range of 4.6MPa-7.0MPa, the maximum crack width exhibits a large growth rate. Taking the void range of 60° as an example, the maximum crack width is equal to 0.00207m, 0.00991m, 0.03871m, and 0.06822m for the typical loading levels of 4MPa, 5MPa, 6MPa, and 7MPa. The effect of void range on the maximum crack width can also be presented in Fig. 3.15. Taking the loading level of 6MPa as an example, the maximum crack width is equal to 0.003794m, 0.03507m, 0.03871m, and 0.04474m for the void range of 30°, 45°, 60°, and 90°, respectively. The maximum crack width presents a non-strict positive relationship with the void range. The main reason for this phenomenon is that the maximum crack width is also affected by the spatial distribution of tunnel quality defects.

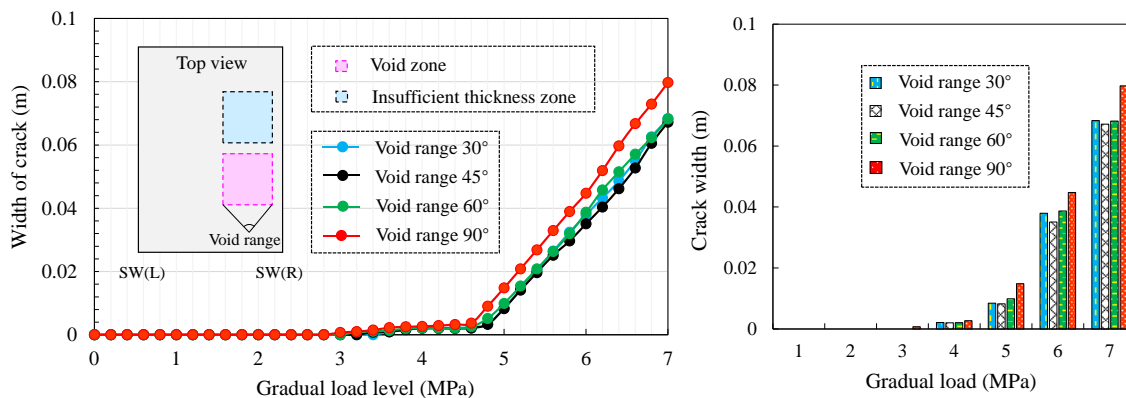


Fig. 3.15 Evolution of the maximum crack width with the applied gradual load.

In this section, the evolution of the proportion of tensile failure of the cohesive elements can be presented in Fig. 3.16. Note that the proportion of tensile failure is significantly affected by the loading level and the void range. Specifically, when the loading level is less than 3.6MPa, the cracks are roughly caused by tensile failure. With the increase in load level, the proportion of tensile failure first decreased and then increased. Taking the void range of 90° as an example, the reduction rate of tensile failure gradually increases in the range of 3.8MPa-4.8MPa but decreases in the range of 4.8MPa-5.2MPa. When the applied load level is in the range of 5.2MPa-7.0MPa, the proportion of tensile failure increases slightly. However, when the applied load level is in the range of 6.2MPa-7.0MPa, the proportion of tensile failure remains roughly unchanged. In addition, when the loading level is between 3.8MPa and 5.0MPa, the correlation between the void range and the proportion of tensile failure is not significant. In contrast, when the load level is in the range of 5.0MPa-7.0MPa, the proportion of tensile failure is basically positively correlated with the void range.

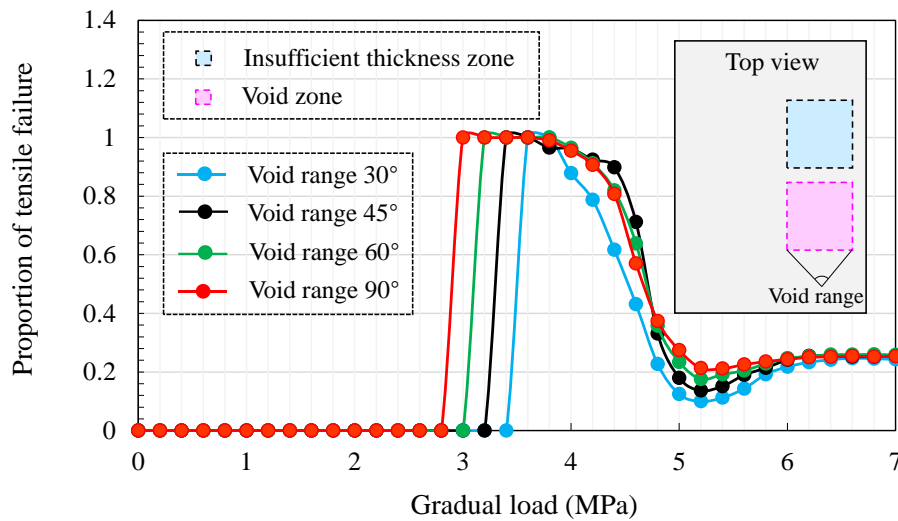


Fig. 3.16 Evolution of the proportion of tensile failure with the applied gradual load.

3.4.4 Cracking mechanism

The cracking mechanism can be identified by the damaged types of cohesive elements (ABAQUS User's Manual; Wu et al. 2020; Liu et al. 2021). It should be indicated that when the value of MMIXDMI is in the range of 0 to 0.5, the cohesive elements are dominated by tensile damage, while controlled by shear damage in the range of 0.5 to 1, when the value is equal to -1 , the cohesive elements are not damaged (ABAQUS User's

Manual; Wu et al. 2020; Liu et al. 2021). In this section, the MMIXDMI was applied to determine the cracking mechanism of the lining structure with combined quality defects of voids and insufficient thickness. The damage types of zero-thickness cohesive elements of different void ranges can be presented in Figs. 3.17-3.20. Taking the void range of 30° as an example, as shown in Fig. 3.17, the distribution of damage types of cohesive elements is significantly affected by the distribution of the void zone and the insufficient thickness zone. Regarding the lining outer surface corresponding to the void zone, the types of damaged cohesive elements are dominated by tensile damage, resulting in tensile cracks. However, concerning the outer surface of the insufficient thickness zone, the cracks are mainly caused by shear damage. The reason for different types of cracks on the outer surface of the defects is mainly due to the different mechanical properties. Specifically, as the lining structure in the void zone is not in contact with the rock mass, the outer surface of the lining exhibits a significant tensile concentration, which can easily induce tensile cracks. While for the outer surface of the insufficient thickness zone, there is no significant tensile stress concentration due to the good contact between the lining and the rock mass. In addition, it is observed that the cracks at the edge of the insufficient thickness zone are mainly caused by mixed shear and tensile damage. Concerning the damage at the arch springing, the cracks are caused by a mixed failure mode. For the damage characteristic of the inner surface, it is noted that the generated network cracks are mainly caused by the mixed failure model of shear damage and tensile damage. The comparison of the damage characteristics of tunnel linings under different void ranges can be presented in Figs. 3.17-3.20, with the increase of the void range, the degree of tensile damage on the outer surface of the void zone increases gradually. Meanwhile, the range of shear damage at the outer surface of the insufficient thickness zone is also affected. Therefore, it can be observed that the cracking mechanism of the lining structure is significantly affected by the defect type and defect distribution. The main reason for this phenomenon is that the presence of defects can change the mechanical properties of the lining structure.

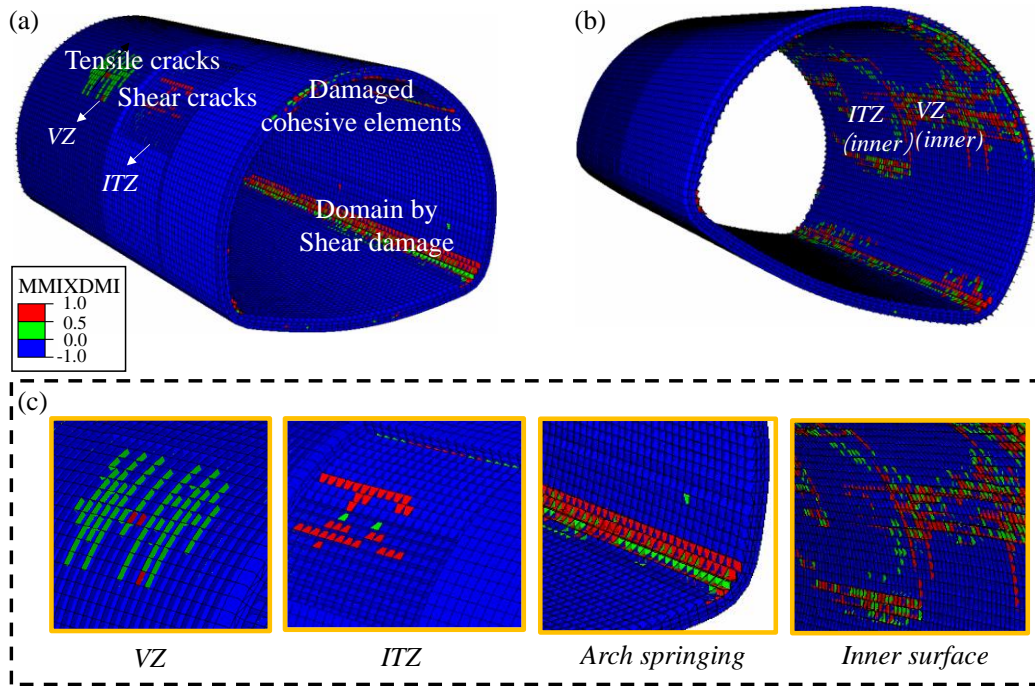


Fig. 3.17 Damage characteristics of lining structures with combined defects of void range of 30°: (a) perspective I; (b) perspective II; (c) detail cracking diagram.

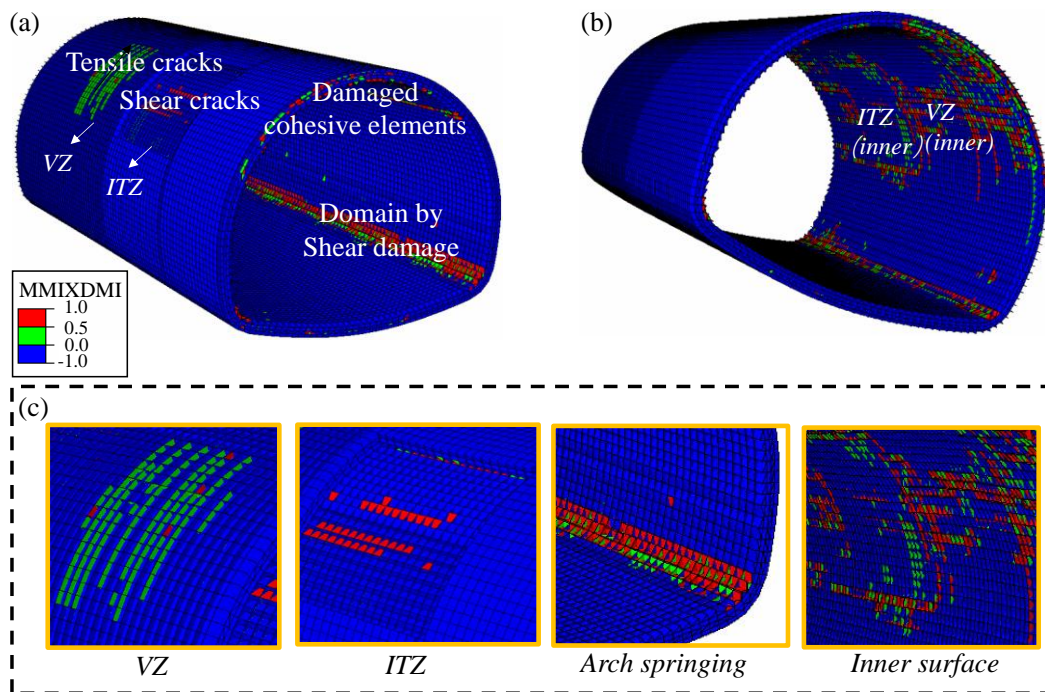


Fig. 3.18 Damage characteristics of lining structures with combined defects of void range of 45°: (a) perspective I; (b) perspective II; (c) detail cracking diagram.

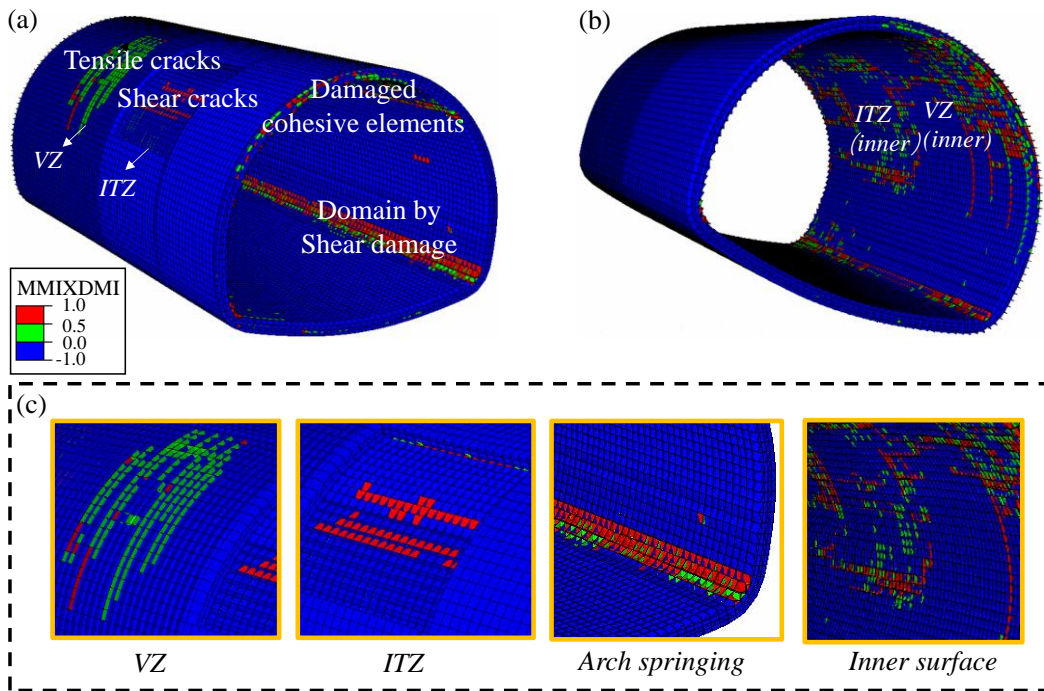


Fig. 3.19 Damage characteristics of lining structures with combined defects of void range of 60°: (a) perspective I; (b) perspective II; (c) detail cracking diagram.

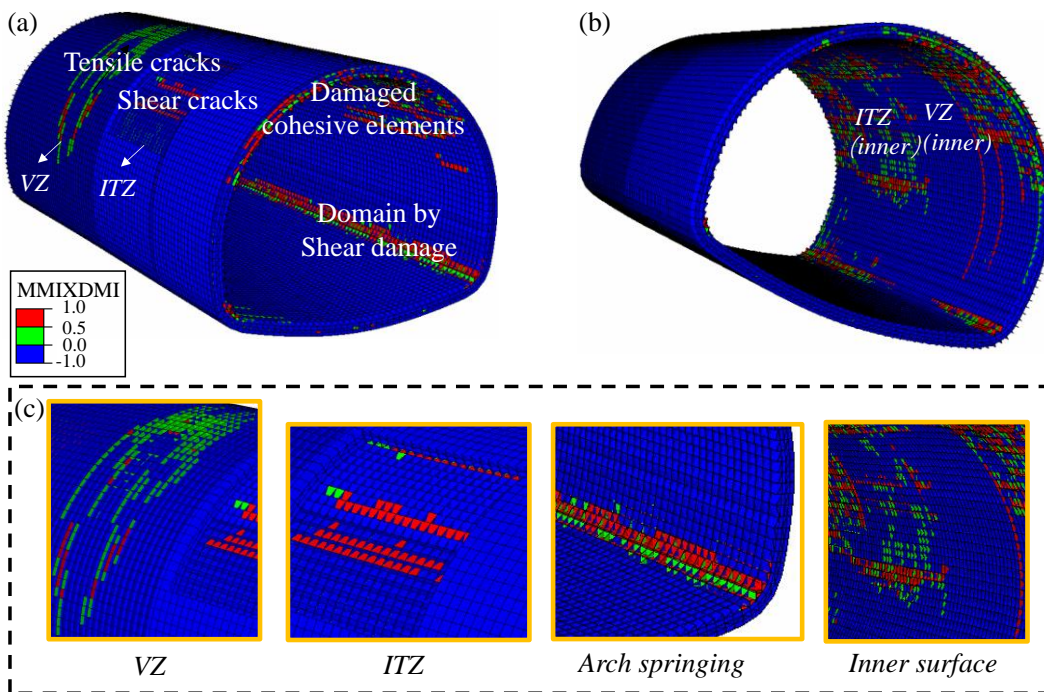


Fig. 3.20 Damage characteristics of lining structures with combined defects of void range of 90°: (a) perspective I; (b) perspective II; (c) detail cracking diagram.

3.4.5 Discussion of fracture characteristics

In this section, the fracture characteristics including the cracking mechanism and patterns of tunnel linings with combined defects were discussed in Fig. 3.21. In summary, the tensile ring cracks zone (TRCZ) is prone to occur on the outer surface of the lining corresponding to the void zone; the shear ring cracks zone (SRCZ) is prone to occur at the edge of the inner surface of the void zone; the shear longitudinal cracks zone (SLCZ) is likely to occur on the outer surface of the lining corresponding to the insufficient thickness zone. In addition, the mixed failure of cohesive elements is prone to generate at the edge of the lining sufficient thickness zone, resulting in the mixed-failure longitudinal cracks zone (MLCZ). Furthermore, the mixed-failure cross cracks zone (MCCZ) is likely to occur on the inner surface between the void and the insufficient thickness zone. Overall, the fracture characteristics are significantly affected by the distribution of the defect zone. In addition, it should be indicated that the cracking mechanism and fracture mode of the lining with combined defects were explored by the numerical model. It is meaningful to conduct a three-dimensional tunnel model test in a future study to make clear the fracture characteristics of linings deeply.

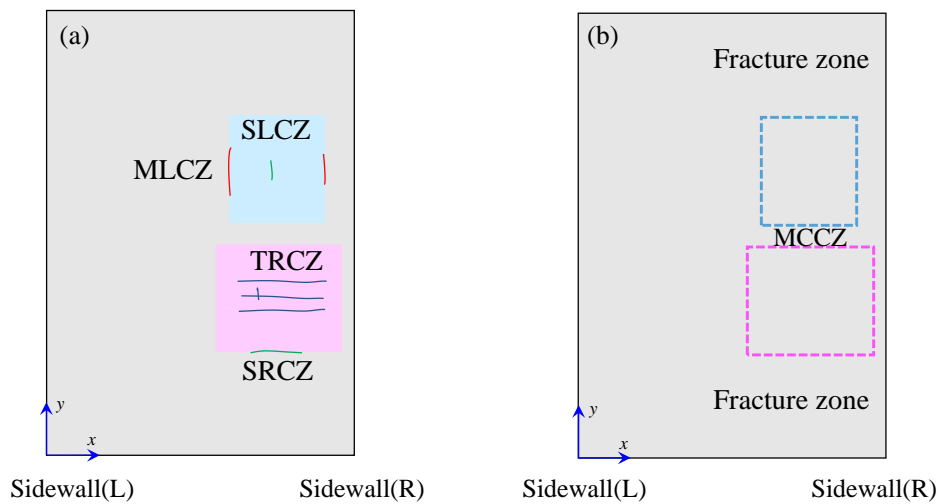


Fig. 3.21 Fracture characteristics of lining structures with combined defects: (a) outer surface; (b) inner surface.

3.5 Cracking characteristics of the reinforced lining structure

The FRP-PCM method has been widely utilized in the reinforcement of degraded lining structures due to its superior performance (FRP Grid Method Association of Japan; Jiang

et al. 2017). Liu et al. (2022) conducted a laboratory test to investigate the cracking characteristics of tunnel linings reinforced with the FRP-PCM method under bias pressure, showing that the FRP grid layer can effectively inhibit the propagation of tensile cracks. To clarify the reinforcement effect of the FRP-PCM method, the cracking characteristics were further investigated with the FEM-CZM method. The mechanical parameters of rock mass and tunnel lining were obtained by Wu (2021) from Guiling tunnel. Similarly, the distribution of tunnel defects, loading conditions, and boundary conditions can also be presented in section 3.3. As an illustration, two reinforcement techniques were identified, one is the FRP-PCM method, and the other is the combined technique of FRP-PCM and backfill method. The range of the FRP-PCM method is 180° in the tangential direction and 20m in the longitudinal direction. The performance of reinforcement parameters can be listed in Table 3.2 (Jiang et al. 2017). When the gradual load reaches to 6.4MPa, the fracture characteristics of the lining under different reinforcement schemes can be presented in Fig. 3.22. It is noted that the lining cracking characteristics changed significantly after reinforcement. If only the FRP-PCM method was applied, the cracking degree of the lining can be effectively suppressed, especially on the inner surface of the lining. On the outer surface with the insufficient thickness zone, the longitudinal cracks can be significantly optimized. However, regarding the cracking characteristics at the outer surface of the void zone, although the crack degree can be reduced to a certain extent, the reduction rate is not significant. This is mainly because the void zone is not backfilled, resulting in a significant tensile effect on the outer surface of the lining. When the combined technique of FRP-PCM and backfill was applied, the cracks on the outer surface of the void and insufficient thickness zone can be effectively suppressed. Concerning the cracking pattern, when the void zone is not backfilled, the inner surface of the lining is still prone to occur ring cracks, but longitudinal cracks are dominated after backfilling. Since the arch springing is not reinforced, cracks are also prone to occur. Overall, the repair techniques adopted in this chapter can effectively suppress the cracking.

Table 3.2 Performance of FRP grid and PCM material (Jiang et al. 2017).

Reinforcement parameters	E (MPa)	σ_t (MPa)	σ_c (MPa)	Cross-sectional area of mesh (mm ²)
FRP grid	100000	1400	—	26.4
PCM	26000	4.60	59.3	—

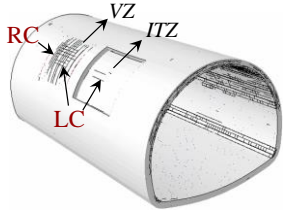
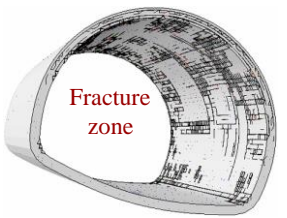
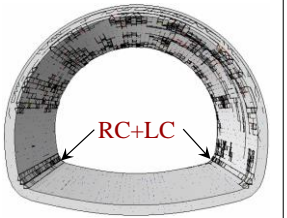
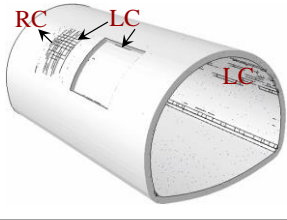
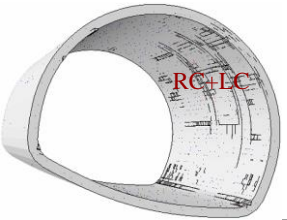
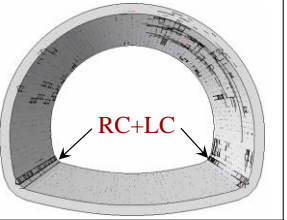
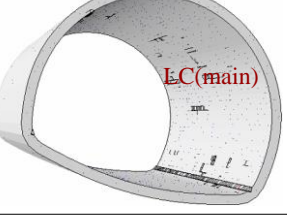
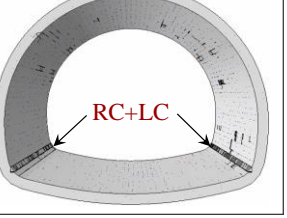
Fracture behavior	Perspective I	Perspective II	Perspective III
Without Reinforcement			
FRP-PCM method			
FRP-PCM +backfill method			

Fig. 3.22 Cracking characteristics of the defective lining structure with reinforcement.

3.6 Conclusions

In this chapter, the cracking characteristics of the lining structure containing typical quality defects of voids and insufficient thickness were investigated with the FEM-CZM method. At first, the characteristics of stress, deformation, and crack propagation were explored. Then, statistics including the number of damaged cohesive elements, crack area, crack volume, etc. were performed. Subsequently, the cracking mechanism was revealed based on the damaged cohesive elements. Finally, the cracking performance of the lining structure under different reinforcement methods was investigated. The main conclusions of this chapter can be drawn as follows:

- (1) Obvious tensile stress concentration occurs on the outer surface of the lining structure corresponding to the void zone, while the area with insufficient thickness has obvious compressive stress. In addition, the deformation characteristics at the defect are also

significantly correlated with the defect type, and the phenomenon of deformation outwards is observed in the void zone.

- (2) Cracking characteristics are significantly affected by defect distribution. The cracking degree within the void zone is larger than that of the insufficient thickness zone. As the gradual load increases, the cracking degree will further increase. The cracking patterns are significantly influenced by the defect distribution. Ring cracks are mainly prone to occur at the lining outer surface corresponding to the void zone, while longitudinal cracks are mainly likely to generate at the outer surface of the insufficient thickness zone. Cross cracks are prone to occur at the outer surface of the void zone and the inner surface between the void and the insufficient thickness zone. Combined with the characteristics of cracking degree and the cracking pattern in this model, the void quality defect can be identified as the dominant defect type affecting the lining structure.
- (3) The void range and gradual load level significantly affect the cracking characteristics. In this research, the number of damaged cohesive elements, crack area, and crack volume present a positive relationship with the void range and the applied gradual load. With the increase of load level, the proportion of tensile failure of linings with combined quality defects first decreases and then increases. When the gradual load level is large, the changes in the void range do not significantly affect the proportion of tensile failure.
- (4) The cracking mechanism is significantly affected by the defect distribution. Tensile damage is prone to occur at the lining outer surface corresponding to the void zone, while dominated by shear damage at the outer surface of the insufficient thickness zone. In addition, the distribution of cracking zones of TRCZ, SRCZ, SLCZ, MLCZ, and MCCZ is determined.
- (5) The FRP-PCM method can effectively inhibit the cracking degree of the inner surface and the outer surface corresponding to the insufficient lining thickness zone. In addition, the cracking degree on the lining outer surface corresponding to the void zone can be significantly reduced after backfilling. Overall, the cracking degree of the defective lining structure can be significantly inhibited with the combined reinforcement method of FRP-PCM and backfill.

- (6) In future work, it is meaningful to conduct three-dimensional laboratory tunnel model tests to further make clear the cracking characteristics of linings with combined defects. The inhibition of the FRP-PCM method on the cracking of defective linings can be further deepened by laboratory tunnel model tests.

References

- ABAQUS User's Manual, Abaqus Analysis User's Guide (6.14), SIMULIA.
- Barenblatt GI. The Mathematical Theory of Equilibrium Cracks in Brittle Fracture. *Advances in Applied Mechanics*, 1962, 7, 55-129.
[https://doi.org/10.1016/S0065-2156\(08\)70121-2](https://doi.org/10.1016/S0065-2156(08)70121-2)
- Camanho PP, Dávila CG. Mixed-Mode Decohesion Finite Elements for the Simulation of Delamination in Composite Materials, NASA/TM-2002-211737, 2002, 1-37.
- Chang X, Guo TF, Zhang S. Cracking behaviours of layered specimen with an interface crack in Brazilian tests. *Engineering Fracture Mechanics*, 2020, 228, 106904.
<https://doi.org/10.1016/j.engfracmech.2020.106904>
- Che ZJ. Study on the safety of the straight wall tunnel under the condition of void behind the lining. Master's Thesis, Qingdao University of Technology, Qingdao, 2020.
- Chen HB, Xu B, Wang J, Nie X, Mo YL. XFEM-Based Multiscale Simulation on Monotonic and Hysteretic Behavior of Reinforced-Concrete Columns. *Applied Sciences*, 2020, 10(21), 7899. <https://doi.org/10.3390/app10217899>
- Ding ZD, Ji XF, Li XQ, Ren ZH, Zhang S. Influence of Symmetric and Asymmetric Voids on Mechanical Behaviors of Tunnel Linings: Model Tests and Numerical Simulations. *Symmetry*, 2019, 11(6), 802.
<https://doi.org/10.3390/sym11060802>
- Dugdale DS. Yielding of steel sheets containing slits. *Journal of the Mechanics and Physics of Solids*, 1960, 8(2), 100-104.
[https://doi.org/10.1016/0022-5096\(60\)90013-2](https://doi.org/10.1016/0022-5096(60)90013-2)
- Fang Y, Guo JN, Grasmick J, Mooney M. The effect of external water pressure on the liner behavior of large cross-section tunnels. *Tunnelling and Underground Space Technology*, 2016, 60, 80-95. <https://doi.org/10.1016/j.tust.2016.07.009>
- Faron A, Rombach GA. Simulation of crack growth in reinforced concrete beams using

- extended finite element method. *Engineering Failure Analysis*, 2020, 116, 104698.
<https://doi.org/10.1016/j.engfailanal.2020.104698>
- Feng G. A Study on the Structure Security of Lining-Based on the influences of insufficient lining thickness and the voids existing at the back of lining. Master's Thesis, Beijing Jiaotong University, Beijing, 2013.
- FRP Grid Method Association of Japan. Design and construction manual of the Repair & reinforcement method for RC structures by FRP grid [O/L].
<http://www.frp-grid.com>
- Gong YP. Study on the tunnel structure safety under the impact of the lining thickness deficiency. Master's Thesis, Beijing Jiaotong University, Beijing, 2019.
- Hafezolghorani M, Hejazi F, Vaghei R, Jaafar MSB, Karimzade K. Simplified Damage Plasticity Model for Concrete. *Structural Engineering International*, 2017, 27(1), 68-78. <https://doi.org/10.2749/101686616X1081>
- He BG, Liu ER, Zhang ZQ, Zhang Y. Failure modes of highway tunnel with voids behind the lining roof. *Tunnelling and Underground Space Technology*, 2021, 117, 104147. <https://doi.org/10.1016/j.tust.2021.104147>
- He ZY, Zhong HW, Chen ZH. Safety Evaluation and Finite Element Analysis of Tunnel Lining with Cracks. *Tunnel Construction*, 2019, 39(S2), 69-77.
- Huang D, Li B, Ma WZ, Cen DF, Song YX. Effects of bedding planes on fracture behavior of sandstone under semicircular bending test. *Theoretical and Applied Fracture Mechanics*, 2020, 108, 102625. <https://doi.org/10.1016/j.tafmec.2020.102625>
- Huang H, Sun Y, Xue Y, Wang F. Inspection equipment study for subway tunnel defects by grey-scale image processing. *Advanced Engineering Informatics*, 2017, 32, 188-201. <https://doi.org/10.1016/j.aei.2017.03.003>
- Jiang HX, Meng DG. 3D numerical modelling of rock fracture with a hybrid finite and cohesive element method. *Engineering Fracture Mechanics*, 2018, 199, 280-293. <https://doi.org/10.1016/j.engfracmech.2018.05.037>
- Jiang YJ, Wang XS, Li B, Higashi Y, Taniguchi K, Ishida K. Estimation of reinforcing effects of FRP-PCM method on degraded tunnel linings. *Soils and Foundations*, 2017, 57(3), 327-340.
- Labibzadeh M, Namjoo H. Size Effects on Concrete Damaged Plasticity Model. *Current*

- Trends in Civil & Structural Engineering, 2020, 6(3), 1-5.
<https://doi.org/10.33552/CTCSE.2020.06.000637>
- Lei B, Qi TY, Chen XY, Li Y. FEM-based Contrastive Analysis of Lining Cracks Caused by Cavity behind Arch Shoulder in High-speed Railway Tunnels. *Railway Standard Design*, 2015, 59(9), 104-108.
- Liu C. Study on mechanical characteristics of tunnel structure under the condition of void behind arch lining. Master's Thesis, Qingdao University of Technology, Qingdao, 2018.
- Liu DJ, Shang Q, Li M, Zuo JP, Gao Y, Xu F. Cracking behaviour of tunnel lining under bias pressure strengthened using FRP Grid-PCM method. *Tunnelling and Underground Space Technology*, 2022, 123, 104436.
<https://doi.org/10.1016/j.tust.2022.104436>
- Liu J, Zhang XS, Lv GH, Wang K, Han B, Xie QY. Study on Crack Development of Concrete Lining with Insufficient Lining Thickness Based on CZM Method. *Materials*, 2021, 14(24), 7862. <https://doi.org/10.3390/ma14247862>
- Liu HJ. Study on Mechanical and Numerical Model for Road Tunnel Defects Diagnosis. Ph.D. Thesis, Tongji University, Shanghai, 2007.
- Liu SH, Shi Y, Sun R, Yang JS. Damage behavior and maintenance design of tunnel lining based on numerical evaluation. *Engineering Failure Analysis*, 2020, 109, 104209.
<https://doi.org/10.1016/j.engfailanal.2019.104209>
- Malmgren L, Nordlund E, Rolund S. Adhesion strength and shrinkage of shotcrete. *Tunnelling and Underground Space Technology*, 2005, 20(1), 33-48.
<https://doi.org/10.1016/j.tust.2004.05.002>
- Min B, Zhang CP, Zhang X, Wang HL, Li PF, Zhang DL. Cracking performance of asymmetric double-arch tunnels due to the voids behind linings. *Thin-Walled Structures*, 2020, 154, 106856. <https://doi.org/10.1016/j.tws.2020.106856>
- Min B, Zhang X, Zhang CP, Gong YP, Yuan TF. Mechanical Behavior of Double-Arch Tunnels under the Effect of Voids on the Top of the Middle Wall. *Symmetry*, 2018, 10(2), 703. <https://doi.org/10.3390/sym10120703>
- Ministry of Transport of the PRC. Code for Design of Road Tunnel, JTG D70-2004, 2004.
- Roth SN, Léger P, Soulaïmani A. A combined XFEM–damage mechanics approach for

- concrete crack propagation. *Computer Methods in Applied Mechanics and Engineering*, 2015, 283, 923-955. <https://doi.org/10.1016/j.cma.2014.10.043>
- Ru ZL, Zhao HB, Zhu CR. Crack propagation analysis of concrete beam subjected to three-point bending using XFEM. *Applied Mechanics and Materials*, 2011, 94-96, 1655-1658. <https://doi.org/10.4028/www.scientific.net/AMM.94-96.1655>
- Song SH, Paulino GH, Buttlar WG. Simulation of Crack Propagation in Asphalt Concrete Using an Intrinsic Cohesive Zone Model. *Journal of Engineering Mechanics*, 2006, 132 (11), 1215-1223. [https://doi.org/10.1061/\(ASCE\)0733-9399\(2006\)132:11\(1215\)](https://doi.org/10.1061/(ASCE)0733-9399(2006)132:11(1215))
- Su J, Jie YM, Niu XK, Liu C, Liu X. Mechanical Behavior of Tunnel Lining with Cracks at Different Positions. *Symmetry*, 2020, 12(2), 194. <https://doi.org/10.3390/sym12020194>
- Wang G, Zhang SB, Lian L, Zhao C, Wang K, Zhang XD. Macro-micro study on shear failure mechanism of rock joint based on zero-thickness cohesive element. *Chinese Society of Civil Engineering*. 2019, 41(12), 2224-2232
- Wang JF, Huang HW, Xie XY, Bobet A. Void-induced liner deformation and stress redistribution. *Tunnelling and Underground Space Technology*, 2014, 40, 263-276. <https://doi.org/10.1016/j.tust.2013.10.008>
- Wang TT. Characterizing crack patterns on tunnel linings associated with shear deformation induced by instability of neighboring slopes. *Engineering Geology*, 2010, 115(1-2), 80-95. <https://doi.org/10.1016/j.enggeo.2010.06.010>
- Wu XL. Study on the Influence of Voids behind Early Support of Highway Tunnel on Structure Safety and Crack Evolution. Master's Thesis, Shandong University of Science and Technology, Qingdao, 2021.
- Wu XL, Wang G, Li GX, Han W, Sun SQ, Zhang SB, Bi WL. Research on Shear Behavior and Crack Evolution of Symmetrical Discontinuous Rock Joints Based on FEM-CZM. *Symmetry*, 2020, 12(8), 1314. <https://doi.org/10.3390/sym12081314>
- Wu XZ, Jiang YJ, Masaya K, Taniguchi T, Yamato T. Study on the Correlation of Vibration Properties and Crack Index in the Health Assessment of Tunnel Lining. *Shock and Vibration*, 2017a, 2017, 5497457.
- Wu XZ, Jiang YJ, Wang JH, Masaya K, Taniguchi T, Yamato T. A New Health Assessment

- Index of Tunnel Lining Based on the Digital Inspection of Surface Cracks. *Applied Sciences*, 2017b, 7(5), 507. <https://doi.org/10.3390/app7050507>
- Wu ZJ, Zhang PL, Liu QS, Li WF, Jiang WZ. Dynamic Failure Analysis of Reinforced Concrete Slab Based on Cohesive Element Under Explosive Load. *Engineering Mechanics*, 2018, 35(8), 79-90.
- Xu GW, He C, Chen ZQ, Liu CK, Wang B, Zou YL. Mechanical behavior of secondary tunnel lining with longitudinal crack. *Engineering Failure Analysis*, 2020, 113, 104543. <https://doi.org/10.1016/j.engfailanal.2020.104543>
- Xue YD, Yang R. Effect of Void behind Mountain Tunnel Lining in Blasting Condition. 4th ISRM Young Scholars Symposium on Rock Mechanics, 2017.
- Yan QX, Xu YJ, Zhang WL, Geng P, Yang WB. Numerical analysis of the cracking and failure behaviors of segmental lining structure of an underwater shield tunnel subjected to a derailed high-speed train impact. *Tunnelling and Underground Space Technology*, 2018, 72, 41-54. <https://doi.org/10.1016/j.tust.2017.11.002>
- Yu L, Bai SJ, Liu XX, Chen L, Bao LS. Study on the influence of tunnel lining thickness on bearing capacity of lining. *Journal of Shenyang Jianzhu University (Natural Science)*, 2017, 33(6), 1039-1047.
- Zhang H, Zhang HW, Su F. The Introduction and Application of Cohesive Zone Model on Asphalt Concrete Fracture Behavior. *Applied Mechanics and Materials*, 2015, 744-746, 1320-1323.
- Zhang S. Study on Influence Mechanism of Lining Defects and Bearing Capacity of Highway Tunnel Lining. Ph.D. Thesis, Lanzhou University, Lanzhou, 2020.
- Zhang S, Wang G, Jiang Y, Wu X, Li G, He P, Yu J, Sun L. Study on Shear Mechanism of Bolted Jointed Rocks: Experiments and CZM-Based FEM Simulations. *Applied Sciences*, 2020, 10(1), 62. <https://doi.org/10.3390/app10010062>
- Zhang W, Zhang Z, Qi D, Liu Y. Automatic Crack Detection and Classification Method for Subway Tunnel Safety Monitoring. *Sensors*, 2014, 14(10), 19307-19328. <https://doi.org/10.3390/s141019307>
- Zhang X. A research on the impact of the voids behind lining and lining thickness deficiencies on the safety of a double-arch tunnel structure. Ph.D. Thesis, Beijing Jiaotong University, Beijing, 2018.

Zhang X, Zhang CP, Feng G, Han KH. Experimental studies on effect of voids behind tunnel linings on progressive failure process of tunnel structures. *Chinese Journal of Geotechnical Engineering*, 2017, 39(6), 1137-1144.

Zhang XP, Jiang YJ, Sugimoto S. Seismic damage assessment of mountain tunnel: A case study on the Tawarayama tunnel due to the 2016 Kumamoto Earthquake. *Tunnelling and Underground Space Technology*, 2018, 71, 138-148.

4 Mechanical properties and failure mechanism of degraded linings with void quality defects

4.1 Introduction

The lining can be regarded as the main guarantee for the long-term safe operation of tunnel structure (Tonon 2010). However, as time passes, the lining structure will inevitably be degraded, seriously affecting the durability of linings (Jiang et al. 2017; Higashi et al. 2014). Furthermore, as obtained in the previous chapter, the void quality defect is identified as the dominant defect type affecting the lining structure. This can be considered the typical incentive for many other tunnel lining diseases (Nie et al. 2015; Gao et al. 2016; Wang et al. 2014). Therefore, it is significant to investigate the influence of the void quality defect on the degraded lining structure and to determine effective techniques that can effectively eliminate the adverse effects of void defects.

Regarding the theoretical analysis of the effect of voids on the tunnel structure, the elastic solutions for the two-dimensional circular tunnel with the void defect behind the lining were presented by Yasuda et al. (2017). Subsequently, Yasuda et al. (2019) proposed the three-dimensional seismic response of a cylindrical tunnel with voids behind the lining. Concerning the numerical investigation of the void effect, Zhang et al. (2015) performed a two-dimensional finite element method (FEM) to evaluate the effect of double voids behind the lining on the tunnel structure, and the distribution of inner lining force, as well as the safety factors, was explored. Li et al. (2020) carried out a two-dimensional numerical model to investigate the distribution of inner force with voids behind the lining, and the effect of void location and void size was discussed. Zhang et al. (2020) established a two-dimensional FEM model to explore the effect of void size on the lining structure, and a three-dimensional model with a single void behind the lining was further established to make clear the effect of the longitudinal length of the void on the tunnel structure. In addition, Jiang et al. (2017) and Jiang and Zhang (2020) explored the effect of void defects on the degraded lining structure under the loosening pressure based on a two-dimensional finite difference method (FDM). Xu et al. (2020) investigated the damage patterns of tunnel linings with void defects based on the FDM model. Concerning the laboratory tests, Zhang et al. (2017) concentrated on the effect of voids

behind the lining on the progressive failure of tunnel structure, and the inner force of the lining was also investigated. Furthermore, Ding et al. (2019) studied the influence of symmetric and asymmetric voids on the mechanical and cracking behaviors of tunnel lining.

Typical reinforcement designs, such as the backfill grouting method (Shah et al. 2018; Ye et al. 2022; Mao et al. 2020), fiber-reinforced shotcrete method (Jeon et al. 2016; Jeng et al. 2002), and the carbon fiber sheet method (Lee and Lee 2002), have been widely applied. Recently, the FRP material has become one of the most meaningful reinforcement methods for concrete structures because of its favorable properties (Ceroni 2010; Bournas et al. 2015; Rajak et al. 2019). The representative is the FRP-PCM method (Jiang et al. 2017; Yamaguchi et al. 2014; Han et al. 2021a). Concerning the application of the FRP-PCM method on degraded tunnel linings, the typical construction process can be presented in Fig. 4.1 (FPR Grid Method Association of Japan). According to the FRP Grid Method Association of Japan and Han et al. (2021b), the typical construction process of the FRP-PCM method can mainly be divided into the following: repairing the surface of degraded linings, fixing the FRP grids with rivets, and spraying the PCM to FRP grids to form a complete reinforcement system. Regarding the reinforcement behavior of the FRP-PCM method, Guo et al. (2018) investigated the bonding behavior and stress transfer mechanism of FRP grid and concrete with PCM material, and the damaged condition of the test specimens was concerned. Guo et al. (2019) explored the shear behavior of the reinforced concrete (RC) beams strengthened by the FRP-PCM method, and the reinforcing behavior of the shear capacity of RC beams was evaluated based on the effective strain of the FRP grids. Wang et al. (2020) conducted the four-point bending tests to make clear the shear behavior of reinforced concrete strengthened by the FRP-PCM method, and the effect of the arrangement of the FRP grids was also concerned. In addition, Jiang et al. (2017) established a two-dimensional numerical model to investigate the reinforcement effect of the FRP-PCM method on the degraded tunnel structure with void defects. Further, the concept of section repair rate was proposed to explore the reinforcing behavior of the FRP-PCM method on degraded tunnel linings (Jiang et al. 2020). In addition, in the previous chapter, it is noted that the cracking in the lining inner surface can be significantly inhibited with the FRP-PCM method.

The influence of the void quality defect on tunnel structures, such as inner force distribution and failure characteristics, has been extensively investigated based on two-dimensional modeling, while information regarding the three-dimensional effect of voids

is rather limited. However, the distribution of multiple voids in the longitudinal direction can also commonly occur. Furthermore, the FRP-PCM method has been applied to reinforce the degraded tunnel linings. Unfortunately, fewer studies focused on its three-dimensional longitudinal reinforcement effect. Therefore, the focus of this chapter is to study the three-dimensional effects of voids on the mechanical properties and failure mechanism of degraded lining structures, and the reinforcement effect of the FRP-PCM method on the degraded linings with void defects was subsequently analyzed. Overall, this chapter is expected to improve the understanding of the failure and reinforcement of degraded lining structures with void defects.



Fig. 4.1 Application of the FRP-PCM method on degraded tunnel linings (FPR Grid Method Association of Japan): (a) surface treatment; (b) fix the FRP grids; (c) spray the PCM; (d) after the construction.

4.2 Model establishment

The distribution of multiple voids in the longitudinal direction can be divided into two categories, continuous form and discontinuous void form, as shown in Fig. 4.2 (Wu 2021). To illustrate the characteristics of influence between voids, the discontinuous void distribution form was applied. The numerical model established in this chapter can be demonstrated in Fig. 4.3. The model dimension was arranged as a three-dimensional model with a longitudinal size of 20 m, in which double void defects behind the lining

were considered. In this chapter, the cross-section of the tunnel structure was obtained from the standard section of the highway tunnel (Ministry of Transport of the PRC 2004). Regarding the constitutive model, the Mohr-Coulomb failure criterion was applied to describe the mechanical properties of the ground, tunnel linings, and back-filling materials. It should be noted that the urethane materials were applied as the back-filling materials due to the characteristics of high strength and quick hardening (Jiang et al. 2017). In this research, the defect of double voids behind the lining was considered, the distribution of double void defects can also be presented in Fig. 4.3. Specifically, the distribution of the double voids was divided into two types respectively symmetrical and asymmetrical distribution. Concerning the void size, the range was all fixed as 60° , the length in the longitudinal direction was set as 5 m and 3 m, respectively, and the distance between the two voids was set as 1 m. Since the void shape has little effect on the tunnel structure (Liu 2007), the void in the cut surface can be thus set as a rectangular shape. In addition, the far-field stress state (Yasuda et al. 2017) was applied to the three-dimensional deep tunnel model. Furthermore, the effect of the ground class on the reinforcement effect of the FRP-PCM method was investigated, and the common ground class CII and DI in Japan were applied (Jiang et al. 2017). Concerning the degraded behavior of tunnel linings, the deterioration degree of the lining was assumed as 20% and 40%, and the related parameters were acquired by the reduction factor. In this research, the FRP-PCM method was applied to reinforce the degraded tunnel linings, and the parameters of the corresponding materials in this research can be displayed in Table 4.1 (Jiang et al. 2017) and Table 4.2 (Jiang et al. 2017).

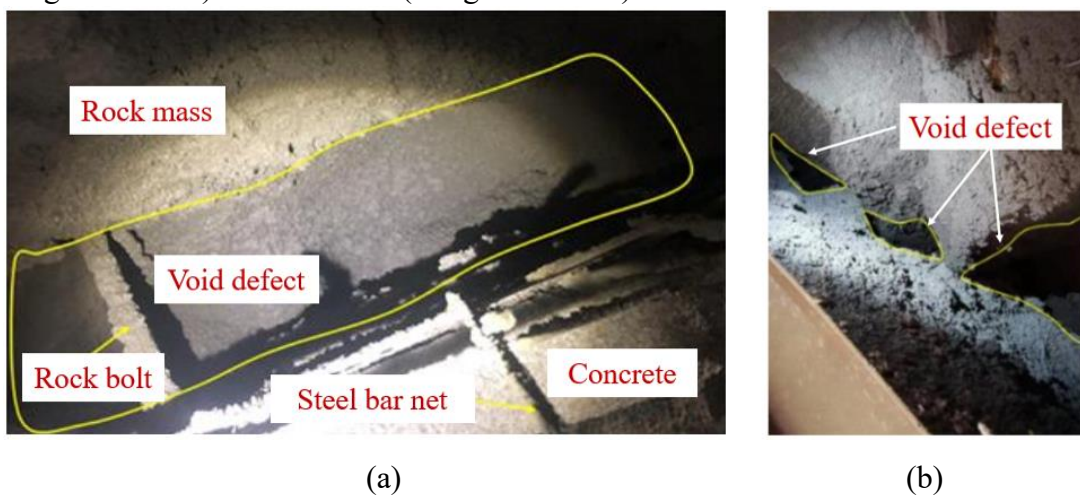


Fig. 4.2 Distribution forms of void quality defects (Wu 2021): (a) continuous void form(Wu 2021); (b) discontinuous void form (Wu 2021).

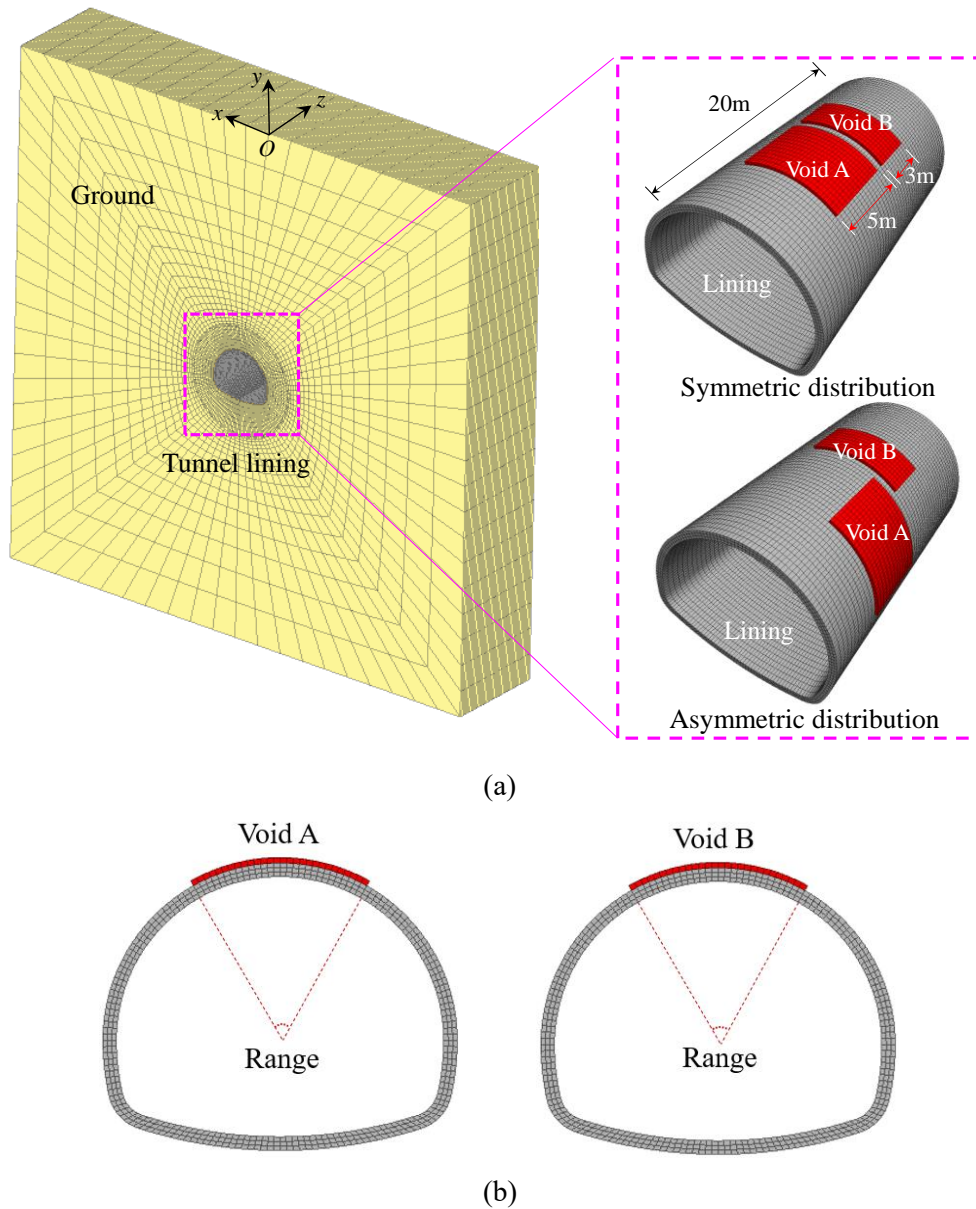


Fig. 4.3 Numerical model of tunnel structure with double voids behind the lining: (a) model overview; (b) symmetric distribution of void defects.

Table 4.1 Parameters of ground, lining, and backfill materials (Jiang et al. 2017).

Properties	Ground class		Lining	Backfill material
	CII	DI		
γ (kN/m ³)	22.6	21.6	24	9.8
E (MPa)	980	490	24500	12.0
ν	0.3	0.35	0.20	0.13
c (MPa)	0.98	0.49	6.99	0.50
φ (deg)	40.0	35.0	40.0	10.0

Table 4.2 Parameters of FRP grid and PCM material (Jiang et al. 2017).

Reinforcement materials	E (MPa)	σ_t (MPa)	c_s (MPa)	φ_s (deg)	k_s (MPa/mm)
FRP grid	100000	1400	2.217	17.7	5.298
PCM	26000	4.60			—

4.3 Mechanical properties and failure characteristics

To better present the interaction between the tunnel lining and the rock mass, the solid elements can be applied to describe tunnel linings in FLAC3D (Itasca Consulting Group 2002; Yao et al. 2007). While the inner force such as bending moment and axial force cannot be reflected evidently, it is further difficult to provide reinforcing guidance for the tunnel structure, for example, the safety factor method (Ministry of Transport of the PRC 2004). The normal stress on the section corresponding to the center of mass of the two elements can be determined (Pan 1995). The outermost and innermost solid elements were applied to identify the stress and the center of mass to further calculate the inner force of the tunnel lining in the FLAC3D platform (Yao et al. 2007). The normal stress on the surface of the solid element can be written as follows (Yao et al. 2007):

$$\begin{cases} \sigma_{n1} = 0.5(\sigma_{\theta1} + \sigma_{\theta2}) + 0.5(\sigma_{\theta1} - \sigma_{\theta2}) / i \\ \sigma_{n2} = 0.5(\sigma_{\theta1} + \sigma_{\theta2}) - 0.5(\sigma_{\theta1} - \sigma_{\theta2}) / i \end{cases} \quad (4-1)$$

where $\sigma_{\theta1}$, $\sigma_{\theta2}$ are the normal stresses of the innermost and outermost solid elements; σ_{n1} , σ_{n2} are the normal stresses of the outer edges of the innermost and outermost solid elements; i is the number of element layers inversely.

Subsequently, the bending moment M and axial force N can be written as follows (Yao et al. 2007):

$$\begin{cases} M = bh^2 (\sigma_{n1} - \sigma_{n2}) / 12 \\ N = bh (\sigma_{n1} + \sigma_{n2}) / 2 \end{cases} \quad (4-2)$$

where b and h represent the width and thickness of the section, respectively.

4.3.1 Distribution of inner force

4.3.1.1 Distribution of bending moment

4.3.1.1.1 Effect of void layout

In this section, taking the distribution of the bending moment as an example, as shown in Fig. 4.4. To determine the effect of voids on the inner force, it is necessary to explore the distribution of the bending moment when there is no defect (Han et al. 2021a). Hence, the three-dimensional view and the tangential view of bending moment for the lining without void defects can be presented in Fig. 4.4. The three-dimensional view can be obtained by unfolding the lining along the inverted arch. It should be indicated that in this research the bending moment with the positive value represents bending outwards, which means that the external face is under tension. As can be observed from Fig. 4.4, there are significant differences in the distribution of bending moments at different positions of the lining. Specifically, the maximum bending moment is located at the arch springing, indicating that the lining is significantly bending outwards. The bending moment shows an overall decreasing trend from the arch springing to the crown, and the location such as the shoulder and crown have a smaller bending moment. In addition, it is observed that the sign of the value of the bending moment would have a significant change from the arch springing to the inverted arch, indicating that the lining changes from bending outwards to bending inwards.

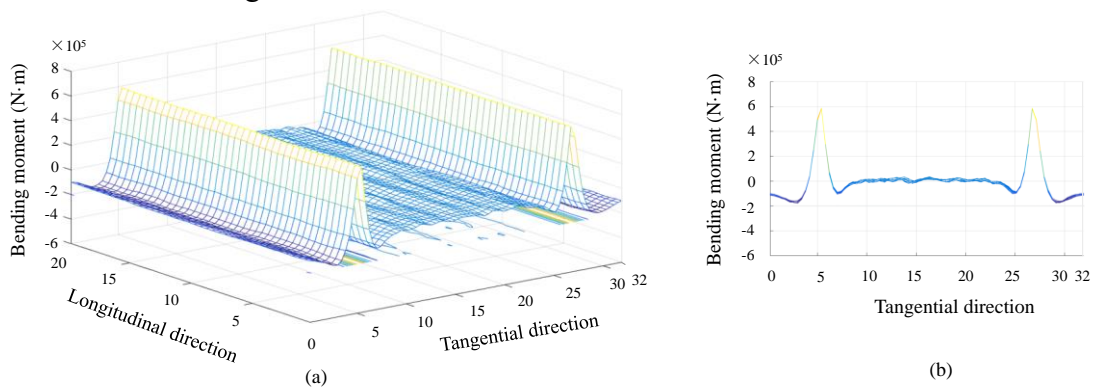


Fig. 4.4 Distribution of bending moment of tunnel lining without void defects: (a) three-dimensional view; (b) tangential view.

When there are double symmetrical voids behind the lining, the distribution of lining bending moment can be presented in Fig. 4.5. Compared with the bending moment of the tunnel lining without void defects in Fig. 4.4, the bending moment in the void-affected zone changes more evidently than in other parts of the lining. Specifically, the bending

moment changes significantly within the area of the void zone, indicating that the lining changes to bending outwards in this case. In addition, obvious bending inwards phenomenon is observed at the lining adjacent to the void-affected zone. Furthermore, it is observed that the void mainly affects the distribution of bending moment around it, while the effect is not significant when the position is far away from the void. Similarly, when void A is located at the right shoulder, and void B is located at the crown, the three-dimensional distribution and the tangential view of the bending moment can be presented in Fig. 4.6(a) and Fig. 4.6(b). Analogously, it is noted that the bending moment varies significantly within the area of the void-affected zone. In addition, when the void is distributed on the shoulder, the bending outwards effect is more pronounced than that of the crown. Furthermore, Liu (2018) established the two-dimensional defective tunnel model with ABAQUS. The distribution of bending moment of the lining structure can be shown in Fig. 4.6(c) (Liu 2018) and Fig. 4.6(d) (Liu 2018), and the bending outwards phenomenon is also observed. Furthermore, previous investigations revealed the two-dimensional bending outwards effect of the lining within the void zone (Zhang et al. 2015; Zhang et al. 2020; Liu 2018), which could further illustrate the reliability of the three-dimensional distribution of bending moment in this research.

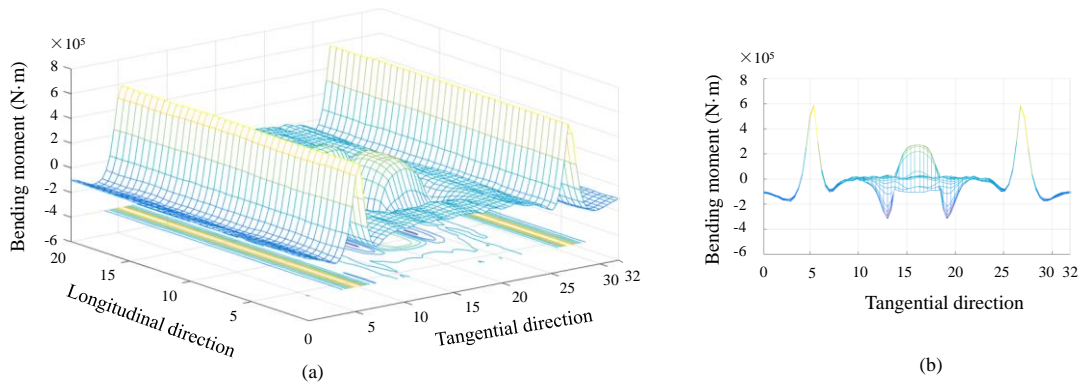
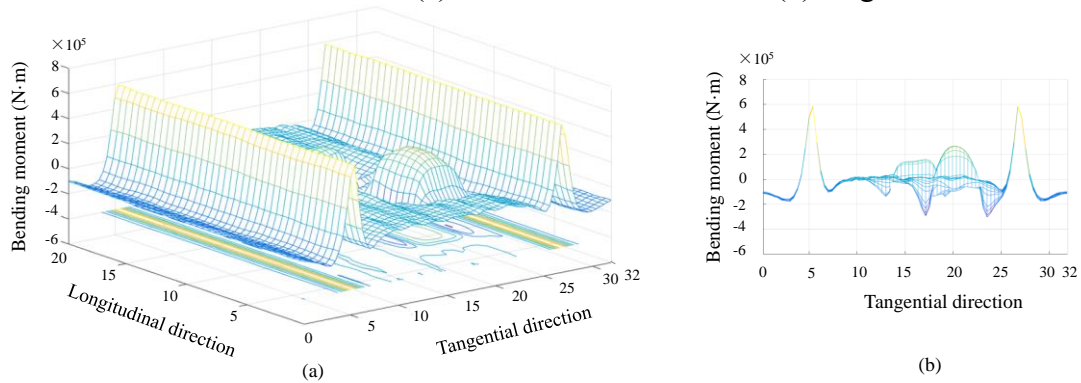


Fig. 4.5 Distribution of bending moment of tunnel linings with symmetrically distributed void defects: (a) three-dimensional view; (b) tangential view.



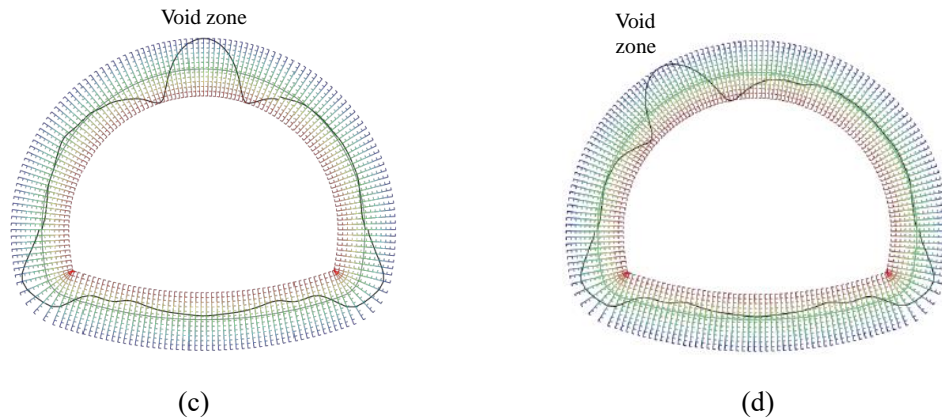


Fig. 4.6 Bending moment of linings with void defects: (a) three-dimensional view; (b) tangential view; (c) Results of bending moment of the two-dimensional model with a void at the crown (Liu 2018); (d) Results of bending moment of the two-dimensional model with a void at the shoulder (Liu 2018).

4.3.1.1.2 Effect of distance between double voids

In this section, the effect of the longitudinal distance between the double voids on the inner force was investigated. Taking the symmetrically distributed voids as an example, the longitudinal distance between double voids was set as 0.5m and 2.0m. The influence of the longitudinal distance between double voids on the bending moment can be presented in Fig. 4.7 and Fig. 4.8. The longitudinal distance does not affect the overall change trend along the tangential direction. The bending outwards phenomenon of the lining corresponding to the void-affected zone is also observed. When the longitudinal distance between the voids changes, the three-dimensional distribution characteristics of the bending moment are affected near the voids, and the effect on the bending moment is not obvious far away from the void zone.

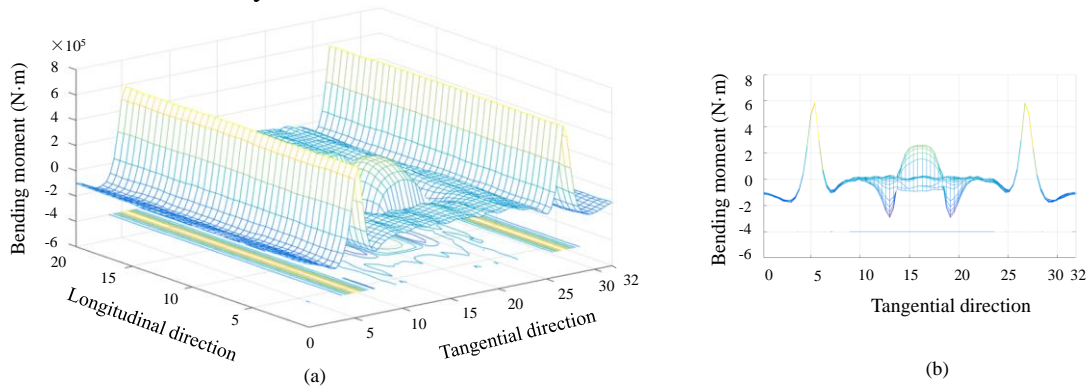


Fig. 4.7 Distribution of bending moment of tunnel linings with symmetrically distributed voids (0.5m): (a) three-dimensional view; (b) tangential view.

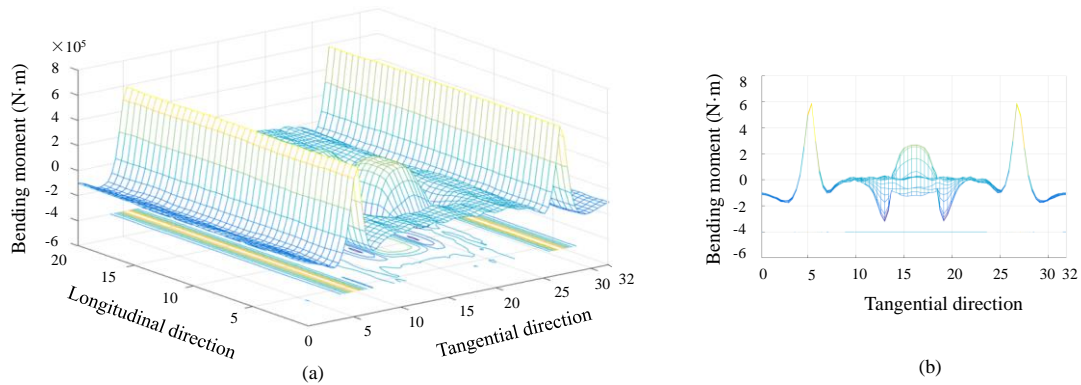


Fig. 4.8 Distribution of bending moment of tunnel linings with symmetrically distributed void defects (2m): (a) three-dimensional view; (b) tangential view.

4.3.1.2 Distribution of axial force

4.3.1.2.1 Effect of void layout

In this section, the three-dimensional distribution and tangential view of the axial force of the deep-buried tunnel lining without void defects were presented in Fig. 4.9. In this research, the axial force with the negative value represents the compression. As can be seen from Fig. 4.9, there are significant differences in the distribution of axial force at different locations of the lining. The axial force decreases from the arch springing to the inverted arch.

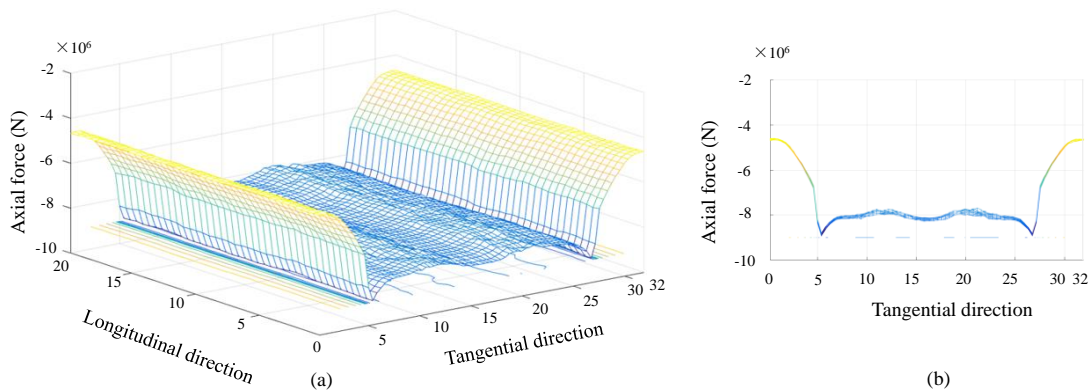


Fig. 4.9 Distribution of axial force of tunnel lining without void defects: (a) three-dimensional view; (b) tangential view.

In this section, the effect of void distribution on the axial force was investigated and presented in Fig. 4.10 and Fig. 4.11. As shown in Fig. 4.10, the axial force within the void-affected zone changes more evidently than other parts of the lining compared with the axial force of the tunnel lining without void defects. Specifically, the axial force within

the void zone and the area adjacent to the void zone along the tangential direction shows a significant decreasing trend, and the decrease in void A is greater than that of void B. Furthermore, in this research, it is observed that the void mainly affects the distribution of axial force around it. Similarly, when void A is located at the right shoulder, and void B is located at the crown, the three-dimensional distribution and the tangential view of the axial force can be presented in Fig. 4.11. Analogously, the axial force shows a significantly decreasing trend within the void zone and the area adjacent to the void zone along the tangential direction. In addition, the decrease in void A is greater than that of void B. Furthermore, with the comparison between Fig. 4.10 and Fig. 4.11, it is noted that the distribution characteristics of axial force are significantly affected by the distribution of the void zone. When the void is on the shoulder, the degree of reduction of axial force is more pronounced than that of the crown.

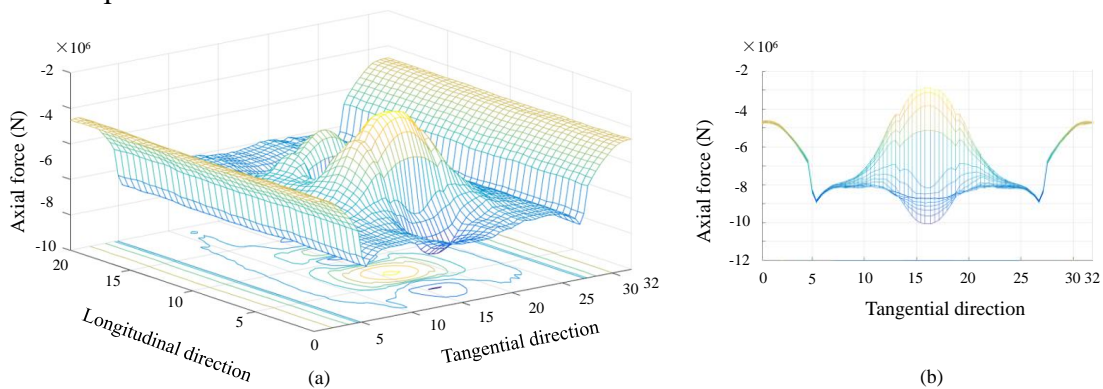


Fig. 4.10 Distribution of axial force of tunnel lining with the symmetrically distributed voids: (a) three-dimensional view; (b) tangential view.

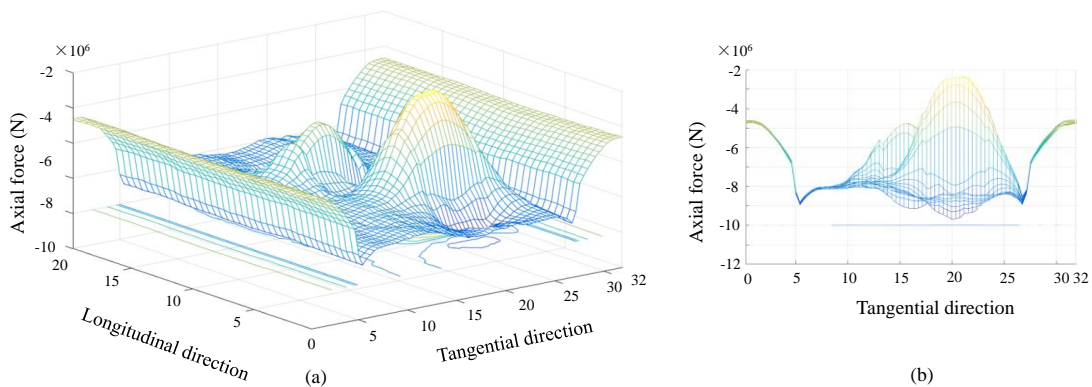


Fig. 4.11 Distribution of axial force of tunnel lining with asymmetrically distributed voids: (a) three-dimensional view; (b) tangential view.

4.3.1.2.2 Effect of distance between double voids

In this section, the effect of the longitudinal distance between the double voids on the axial force was investigated. Taking the symmetrically distributed voids as an example, the longitudinal distance between the double voids was set as 0.5m and 2.0m. The influence of the longitudinal distance between the double voids on the axial force can be presented in Fig. 4.12 and Fig. 4.13. It is noted that the longitudinal distance does not affect the overall change trend along the tunnel tangential direction. When the longitudinal distance between the voids changes, the characteristics of the three-dimensional distribution of the axial force are mainly influenced near the voids. It is noted that the range of reduction of the axial force at void A is affected by the distance between the double voids. In addition, the effect of distance on the change of axial force is not obvious far away from the void zone.

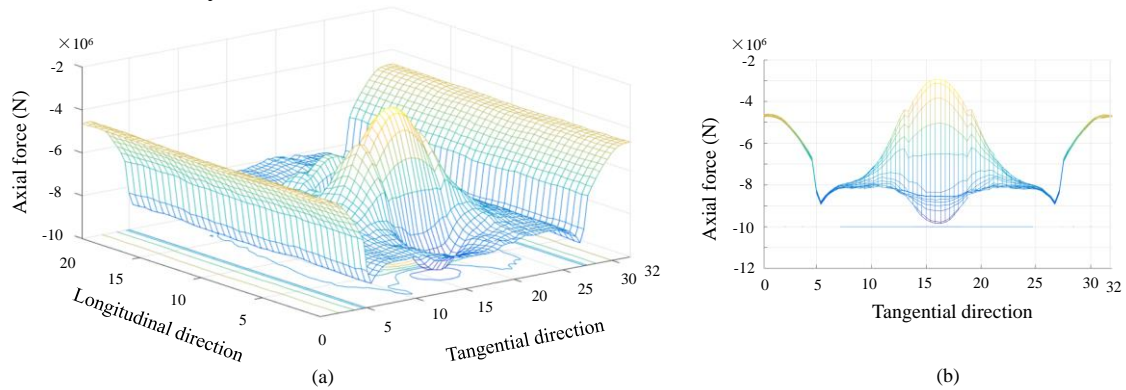


Fig. 4.12 Distribution of axial force of tunnel lining with symmetrically distributed voids (0.5m): (a) three-dimensional view; (b) tangential view.

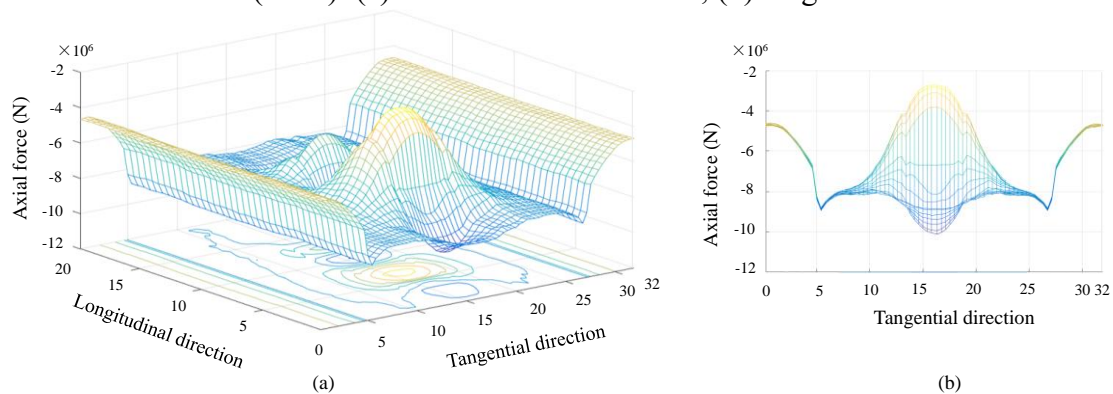
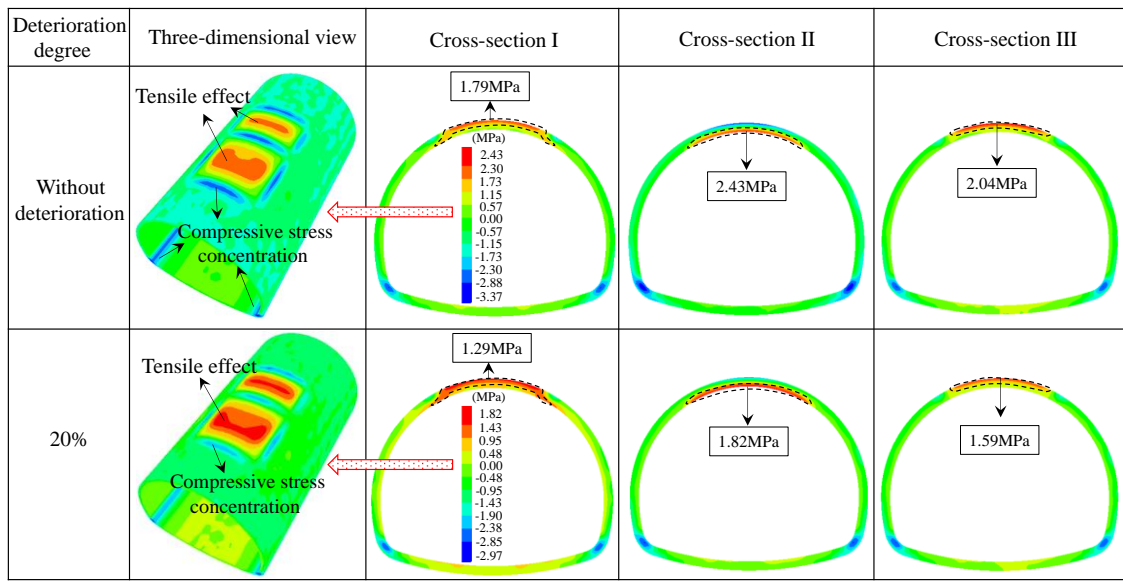


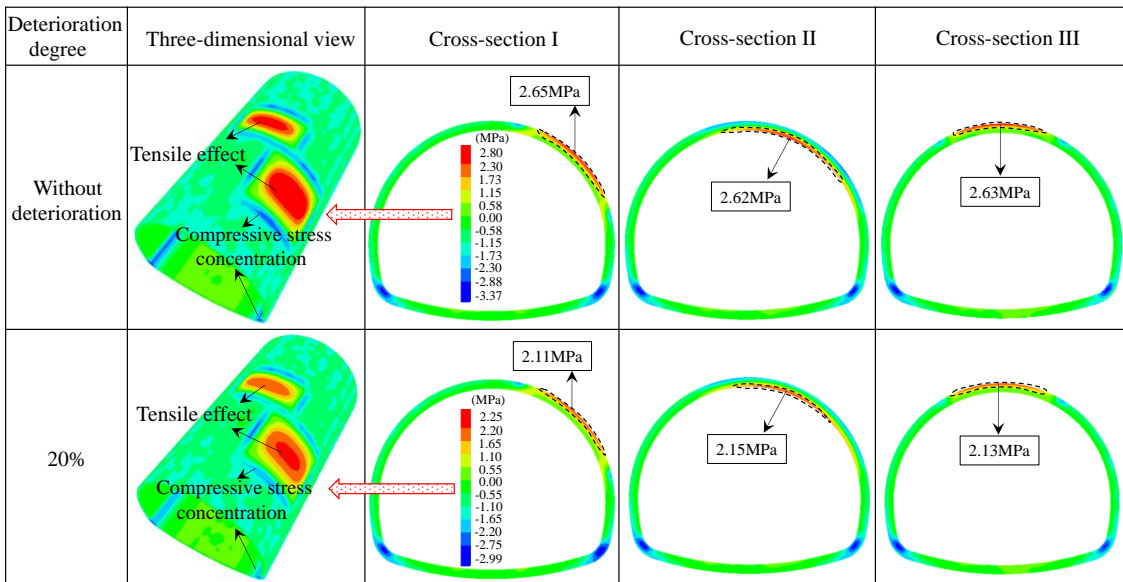
Fig. 4.13 Distribution of axial force of tunnel lining with asymmetrically distributed voids (2m): (a) three-dimensional view; (b) tangential view.

4.3.2 *Distribution of principal stress*

When double void defects are both distributed on the crown, the distribution of principal stress can be presented in Fig. 4.14(a). When the lining is not degraded, it can be observed from the three-dimensional (3D) view that the lining at the center of the void bears a significant tensile effect, while compressive stress concentration occurs at the edge of the void zone and the arch springing. To investigate the stress distribution of the lining intuitively, three typical cross-sections were selected, $z = 8$ m (cross-section I), 10 m (cross-section II), and 12 m (cross-section III), respectively. Note that the outer surface of the lining where cross-section I is located generates an obvious tensile effect, which decreases from the lining outside to the inside. As can be observed from cross-section II, the inner surface of the lining shows the tensile effect. Additionally, the stress distribution in cross-section III is similar to that of cross-section I. Furthermore, when the lining degradation degree is 20%, it can be observed that the stress distribution characteristics are similar to those when the lining is not degraded. Meanwhile, tensile stress concentration is prone to occur on the outer surface of the lining where the void is located and the inner surface between the double voids. Here, it should be indicated that the reason for the asymmetric distribution of stress is closely related to the distribution of grids. Analogously, when void A is at the right shoulder and void B is at the crown, the stress distribution characteristics of the lining can be presented in Fig. 4.14(b). The stress distribution characteristics are similar to the situation when both voids are located at the crown. Due to tensile cracks are prone to occur on the concrete lining, an investigation of the value of tensile stress is meaningful. When the lining is not degraded, the maximum tensile stress is 2.80 MPa for the asymmetrically distributed void, which is larger than the 2.43 MPa for the double voids at the crown. Similarly, the maximum tensile stress is 2.25 MPa for the asymmetrically distributed void with a deterioration of 20%, which is also larger than the 1.82 MPa for the double voids at the crown. Analysis of the three typical cross-sections I, II, and III for the symmetrically distributed voids reveals that the maximum tensile stress occurs at the inner surface of the lining between the double voids. However, concerning the asymmetrically distributed voids, the stress distribution is significantly affected by the lining deterioration degree. Specifically, when the lining is not degraded, the maximum tensile stress for the three typical cross-sections occurs at the outer surface of the lining where void A is located, while on the inner surface of the lining between the double voids for the lining deterioration of 20%. Consequently, the stress distribution is significantly affected by the spatial distribution of void defects.



(a)



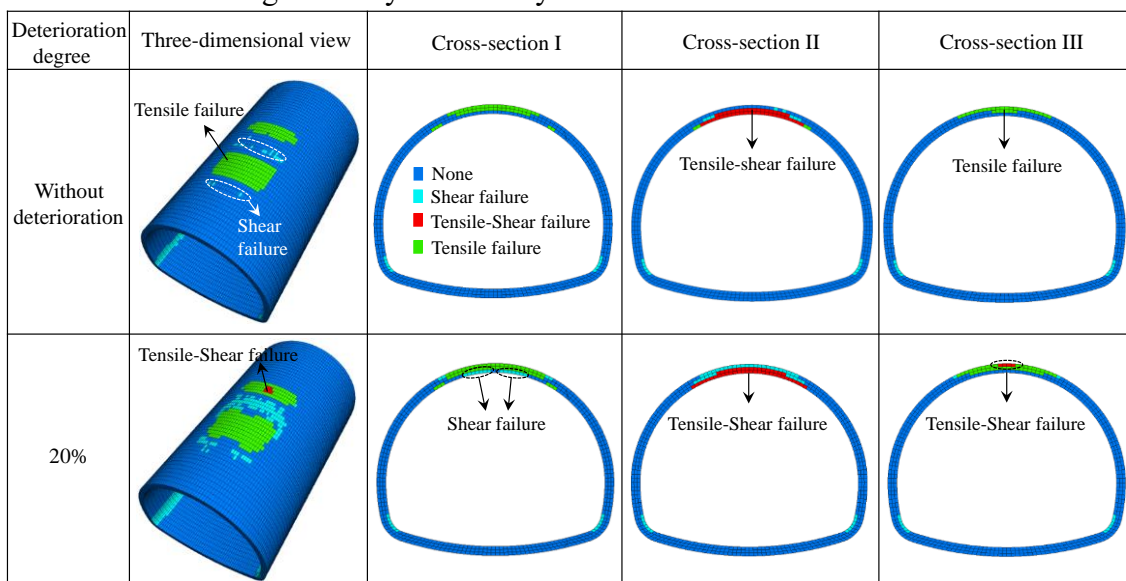
(b)

Fig. 4.14 Distribution of principal stress considering the index of deterioration degree: (a) symmetrically distributed voids; (b) asymmetrically distributed voids.

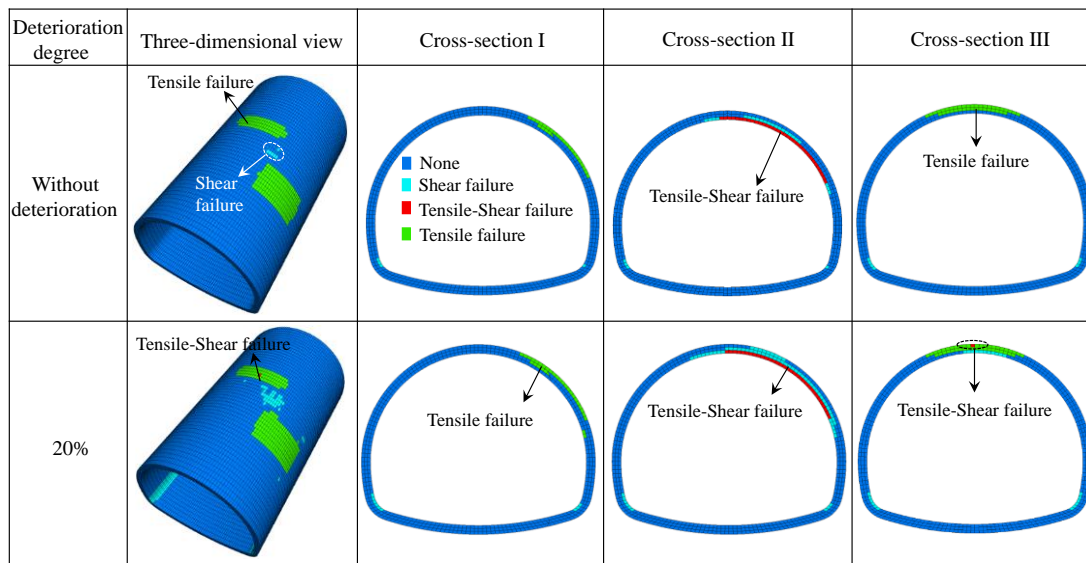
4.3.3 Distribution of failure zone

When the double voids are both distributed on the crown, the distribution of areas prone to plastic failure zone in the calculation process can be presented in Fig. 4.15(a). When the lining is not degraded, plastic tensile failure is prone to occur on the outer surface of the lining corresponding to the void zone, while significant plastic shear failure is prone to generate on the outer surface of the lining between the double voids. To present the

failure distribution of the lining intuitively, three typical cross-sections I, II, and III were also considered. Concerning the distribution of plastic failure in cross-sections I and III, it is noted that there is no plastic failure in the innermost layer of the lining corresponding to the void zone, and tensile failure also occurs in the middle layer, but the failure range is less than that of the outermost layer. Regarding the failure characteristic of cross-section II, the plastic tensile-shear failure is prone to occur in the innermost layer of the lining between the double voids. With the long operation of the tunnel, the lining will inevitably be degraded, taking the lining deterioration degree of 20% as an example, the distribution of areas prone to plastic failure zone in the calculation process can also be summarized in Fig. 4.15(a). Note that the proportion of the plastic failure zone increases compared to the lining without the deterioration, and the plastic shear failure zone also appears in the innermost layer of cross-section I, and the area of the shear failure adjacent to the void defects also increases obviously. In addition, it is observed from cross-section III that the shear-tensile failure is prone to appear on the crown at the outer surface of the lining corresponding to void B. Similarly, when void A is at the right shoulder, and void B is at the crown, the distribution of the plastic failure zone in the calculation process can be presented in Fig. 4.15(b). It should be indicated that plastic shear failure is also prone to occur at the outer surface of the lining between the double voids, while the range of the shear failure is smaller than that of the symmetrical voids. In addition, when the lining is not degraded, the plastic shear failure at the arch springing of the lining with the asymmetric voids is not obvious as that of the symmetric voids. Overall, the plastic failure characteristics are significantly affected by the void distribution.



(a)



(b)

Fig. 4.15 Distribution of plastic failure zone considering the index of lining deterioration: (a) symmetrically distributed voids; (b) asymmetrically distributed voids.

4.4 Reinforcement characteristics of the FRP-PCM method

In this section, the FRP-PCM method was applied to reinforce the degraded tunnel lining with a deterioration degree of 20%, the distribution of the failure zone in the calculation process can be presented in Fig. 4.16. It should be indicated that the region reinforced by the FRP-PCM method covered an arc length of 180° on the upper wall of the tunnel here. Concerning the failure behavior of symmetrically distributed voids, the plastic failure degree reduces significantly compared with lining without the reinforcement. Specifically, the degree of tensile plastic failure at the void zone is significantly reduced, and the plastic shear plastic zone on the outer surface of the lining between the double voids can also be significantly suppressed. In addition, the failure zone at the inner surface corresponding to void A is eliminated (cross-section I). Regarding the plastic failure of the asymmetrically distributed voids, it is noted that failure degree can also be significantly reduced. Furthermore, it is observed that the shear failure on the lining outer surface between the double voids reduces obviously.

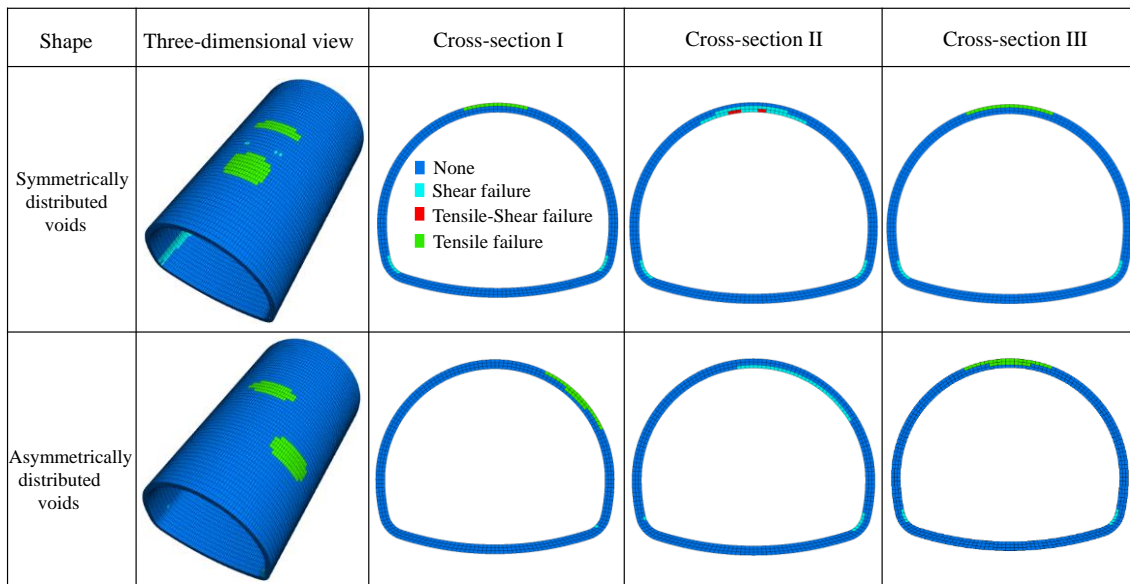
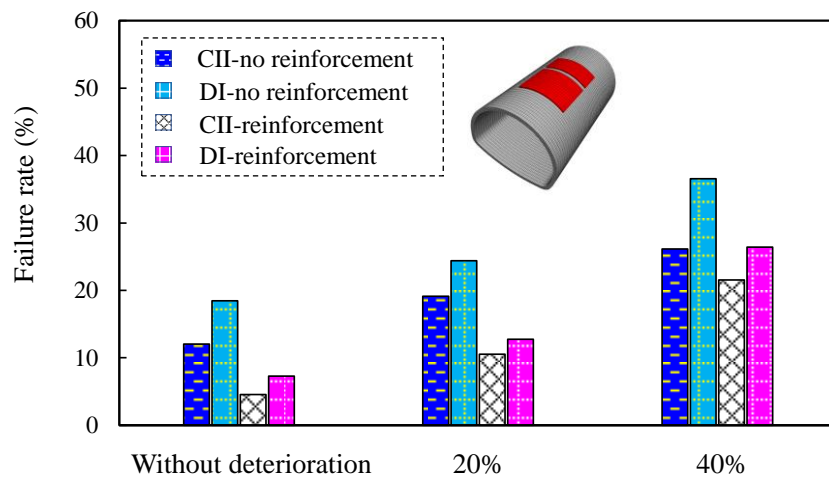


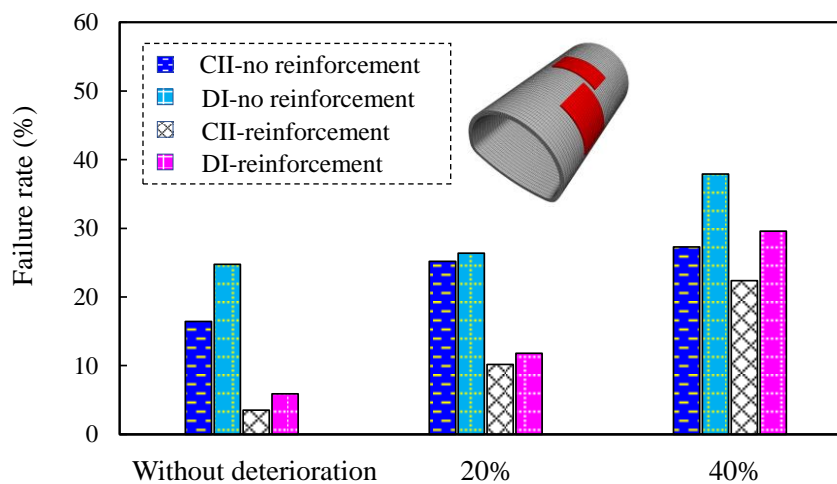
Fig. 4.16 Distribution of failure zone under the reinforcement of the FRP-PCM method.

In this section, the failure rate of tunnel lining under the reinforcement of the FRP-PCM method was evaluated and presented in Fig. 4.17. It should be indicated that the effect of the ground class and lining deterioration degree on the failure behavior was also considered in this part. Fig. 4.17(a) presents the failure rate of lining in the calculation process with the symmetrically distributed voids. It is observed that the failure rate can be significantly affected by the ground class and the lining deterioration degree. For example, when the tunnel lining is not degraded, the failure rate of the lining under the ground class of CII is 12.02%, while 18.45% for the DI. In addition, the larger the degree of lining deterioration, the greater the lining failure rate. When the FRP-PCM method was applied to reinforce the degraded tunnel lining, the failure rate can be significantly reduced. For example, when the lining is not degraded, the failure rate can be reduced to 4.54% and 7.28% for the ground class of CII and DI, respectively. When the degradation degree of the lining is 20%, the failure rate of the lining with the reinforcement is 10.54% and 12.74% for the ground class of CII and DI. Analogously, the failure rate of tunnel lining with the asymmetrically distributed voids can be presented in Fig. 4.17(b). It is observed that the degree of lining deterioration and the grade of the ground class have a similar effect on the failure rate of tunnel linings as the symmetrical voids. It is also noted that the failure rate reduces obviously with the reinforcement of the FRP-PCM method.

In addition, when the lining is not degraded, the failure rate of asymmetrically distributed voids is larger than that of symmetrically distributed voids by comparing Fig. 4.17(a) and Fig. 4.17(b). Therefore, the failure rate is affected by the spatial location of the void defects. It should be indicated that it is helpful to carry out the three-dimensional tunnel model experiments strengthened by the FRP-PCM method to further make clear the reinforcement effect in future work.



(a)



(b)

Fig. 4.17 Failure rate of the lining with different lining deterioration degrees and the ground class: (a) symmetrically distributed voids; (b) asymmetrically distributed voids.

4.5 Discussion

With the long-term operation of tunnel structure, the phenomenon of lining cracking is prone to occur due to the various environmental factors, resulting in significant negative effects (Xu et al. 2020). This section discussed the potential cracking zone based on the characteristics of the failure zone and the stress distribution, as shown in Fig. 4.18 (compared with the research of Min et al. 2020). It should be indicated that the potential cracking areas marked are the roughly distributed zone, and the distribution of the specific crack morphologies can be achieved by the XFEM (Chen et al. 2020) or the CZM method (Song et al. 2006). As shown in Fig. 4.18, three typical perspectives were selected to discuss the potential cracking zone, the outer lining surface, the inner surface, and the two-dimensional cross-section, respectively. Specifically, when the lining is not degraded, the tensile cracking zone (TCZ) is prone to occur at the outer surface of the lining within the void-affected zone, while the shear cracking zone (SCZ) is prone to generate between the double voids. Regarding the inner lining surface between the double voids, the tensile-shear cracking zone (TSCZ) is prone to occur. Concerning the cracking characteristics on the two-dimensional cross-section, an obvious compressive stress concentration zone is generated at the arch springing, resulting in a potential compressive failure. When the lining is with a deterioration degree of 20%, the TSCZ is prone to occur at the outer surface of the lining within the smaller void zone. In addition, the SCZ is prone to occur at the inner surface of the lining within the larger void zone. To verify the rationality of potential cracking distribution in this study, a rough comparison was conducted with the cracking patterns of the tunnel linings with void defects performed by Min et al. (2020). It is observed that the effect of the void defect on the damage zone of tunnel lining is similar. In addition, it should be indicated that the approximate distribution range of the potential cracking zone was discussed, and it is helpful to carry out the three-dimensional tunnel model tests to deeply determine the detailed damage characteristics.

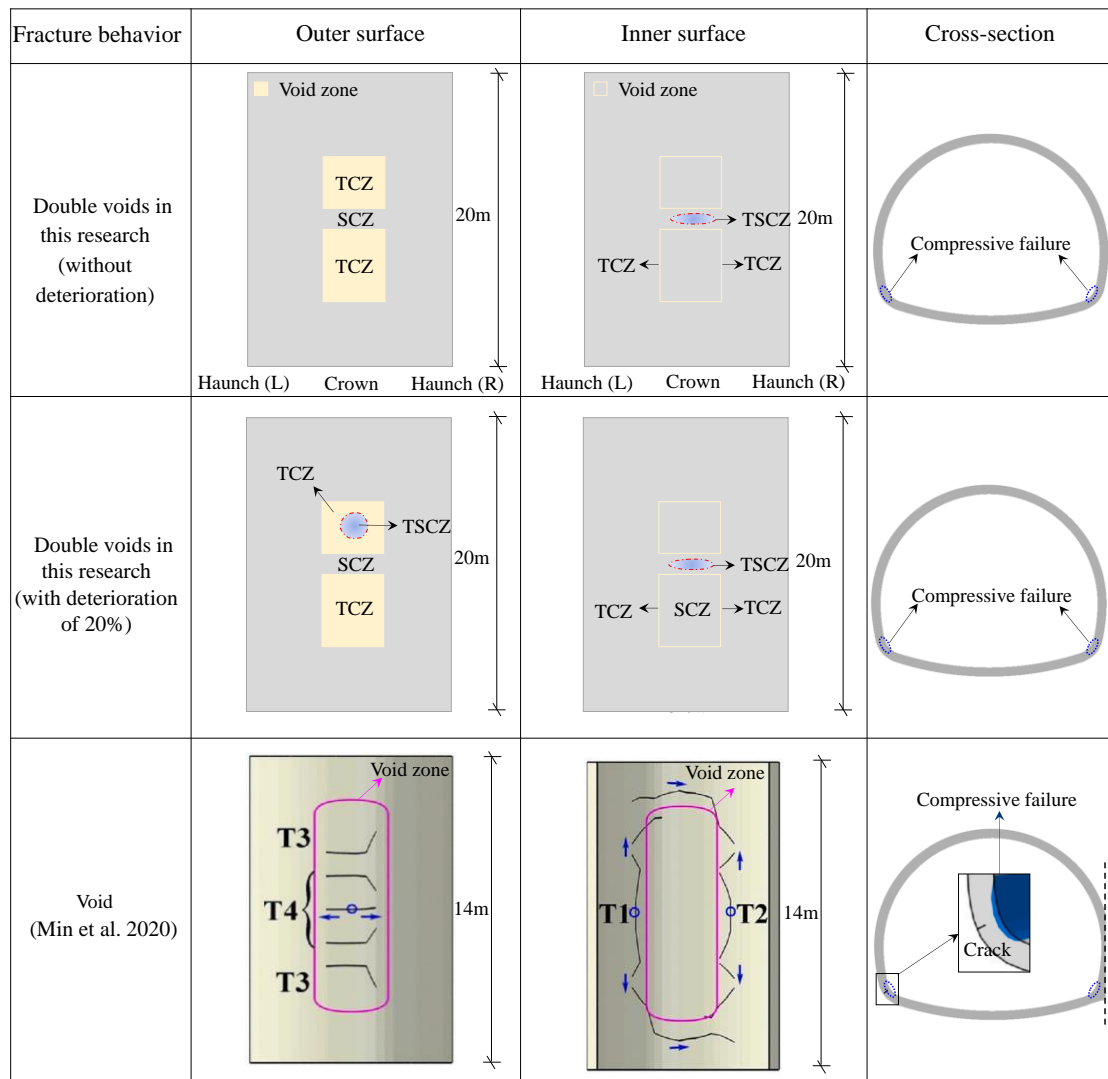


Fig. 4.18 Potential cracking distribution of tunnel linings with double void defects (compared with the research of Min et al. 2020).

4.6 Conclusions

In this chapter, the distribution characteristics of the plastic failure and inner force of the lining with the existence of three-dimensional void defects in the tunnel structure were investigated. Subsequently, the reinforcement effect of the FRP-PCM method was evaluated. Finally, the potential cracking zone was discussed. The main conclusions of this research can be drawn as follows:

- (1) Concerning the three-dimensional distribution of the bending moment of tunnel lining with double void defects, the obvious bending outwards phenomenon is observed within the void-affected zone, while significant bending inwards phenomenon occurs

at the lining adjacent to the void zone. In addition, the void defect mainly affects the distribution of bending moment near it, while not obviously far from the void. For the spatial distribution of asymmetric double voids in this research, the bending outwards phenomenon is more pronounced at the shoulder. Furthermore, the three-dimensional distribution of axial force is significantly affected by void distribution and the distance between voids.

- (2) Regarding the area between the double voids, plastic shear failure is prone to occur at the outer surface, while tensile-shear failure is likely to generate at the inner surface. However, plastic tensile failure is prone to occur within the outer surface corresponding to the void zone. The distribution characteristics of the failure zone are affected by the spatial distribution of voids. The range of shear failure at the outer surface between the double voids for the model with the asymmetrical voids is less than that of the symmetrical voids.
- (3) Concerning the reinforcement characteristics of the FRP-PCM method on tunnel linings with double void defects, it is found that the plastic shear failure on the outer surface between the double voids can be significantly suppressed, and the failure rate of tunnel lining reduces significantly.
- (4) The distribution of potential cracking zones of tensile cracking zone (TCZ), shear cracking zone (SCZ), tensile-shear cracking zone (TSCZ), and compressive failure zone was discussed based on the failure and the stress distribution. To further make clear and optimize the failure characteristics and the damage mechanism of tunnel structure with void defects, the three-dimensional tunnel model test with multiple void defects should be conducted in future work.

References

- Bournas DA, Pavese A, Tizania W. Tensile capacity of FRP anchors in connecting FRP and TRM sheets to concrete. *Engineering Structures*, 2015, 82, 72-81.
<https://doi.org/10.1016/j.engstruct.2014.10.031>
- Ceroni F. Experimental performances of RC beams strengthened with FRP materials. *Construction and Building Materials*, 2010, 24, 1547-1559.
<https://doi.org/10.1016/j.conbuildmat.2010.03.008>
- Chen HB, Xu B, Wang J, Nie X, Mo YL. XFEM-Based Multiscale Simulation on Monotonic and Hysteretic Behavior of Reinforced-Concrete Columns. *Applied Sciences*, 2020, 10(21), 7899. <https://doi.org/10.3390/app10217899>
- Ding ZD, Ji XF, Li XQ, Ren ZH, Zhang S. Influence of Symmetric and Asymmetric Voids on Mechanical Behaviors of Tunnel Linings: Model Tests and Numerical

- Simulations. *Symmetry*, 2019,11(6), 802. <https://doi.org/10.3390/sym11060802>
- FRP Grid Method Association of Japan. Design and construction manual of the Repair & reinforcement method for RC structures by FRP grid [O/L], <http://www.frp-grid.com/01.html>
- Gao Y, Jiang YJ, Li B. Voids delineation behind tunnel lining based on the vibration intensity of microtremors. *Tunnelling and Underground Space Technology*, 2016, 51, 338-345. <https://doi.org/10.1016/j.tust.2015.10.032>
- Guo R, Pan Y, Cai LH, Hino S. Bonding behavior of CFRP grid-concrete with PCM shotcrete. *Engineering Structures*, 2018, 168, 333-345. <https://doi.org/10.1016/j.engstruct.2018.04.059>
- Guo R, Cai LH, Hino S, Wang B. Experimental Study on Shear Strengthening of RC Beams with an FRP Grid-PCM Reinforcement Layer. *Applied Sciences*, 2019, 9(15), 2984. <https://doi.org/10.3390/app9152984>
- Han W, Jiang YJ, Li NB, Koga D, Sakaguchi O, Chen HB. Safety evaluation and failure behavior of degraded tunnel structure with compound diseases of voids and lining defects. *Arabian Journal of Geosciences*, 2021a, 14, 1531. <https://doi.org/10.1007/s12517-021-07489-2>
- Han W, Jiang YJ, Zhang XP, Koga D, Gao Y. Quantitative assessment on the reinforcing behavior of the CFRP-PCM method on tunnel linings. *Geomechanics and Engineering*, 2021b, 25(2), 123-134. <https://doi.org/10.12989/gae.2021.25.2.123>
- Higashi Y, Li B, Jiang YJ. Analytical Evaluation of Tunnel Reinforcement Effect by PCM Shotcrete Method Using FRP Grid. *Journal of Society of Materials Science, Japan*, 2014, 63(6), 451-458. <https://doi.org/10.2472/jsms.63.451>
- Itasca Consulting Group, Inc., *FLAC3D User's Manual*, 2002.
- Jeng F, Lin ML, Yuan SC. Performance of toughness indices for steel fiber reinforced shotcrete. *Tunnelling and Underground Space Technology*, 2002, 17(1), 69-82. [https://doi.org/10.1016/S0886-7798\(01\)00065-7](https://doi.org/10.1016/S0886-7798(01)00065-7)
- Jeon JK, Kim WS, Kim GY, Jeon CK. Polyamide Fiber Reinforced Shotcrete for Tunnel Application. *Materials*, 2016, 9(3), 163. <https://doi.org/10.3390/ma9030163>
- Jiang YJ, Wang XS, Li B, Higashi Y, Taniguchi K, Ishida K. Estimation of reinforcing effects of FRP-PCM method on degraded tunnel linings. *Soils and Foundations*, 2017, 57(3), 327-340. <https://doi.org/10.1016/j.sandf.2017.05.002>
- Jiang YJ, Zhang XP. Evaluation of reinforcement effect of FRP-PCM method in tunnel lining. *Hazard Control in Tunnelling and Underground Engineering*, 2020, 2(1), 11-19.
- Lee JK, Lee JH. Nondestructive evaluation on damage of carbon fiber sheet reinforced concrete. *Composite Structures*, 2002, 58(1), 139-147. [https://doi.org/10.1016/S0263-8223\(02\)00029-6](https://doi.org/10.1016/S0263-8223(02)00029-6)

- Li JJ, Fang Y, Liu C, Zhang YX, Lu WH. Performance investigation of tunnel lining with cavities around surrounding rocks. *Advances in Civil Engineering*, 2020, 2020, 1364984. <https://doi.org/10.1155/2020/1364984>
- Liu C. Study on mechanical characteristics of tunnel structure under the condition of void behind arch lining. Master's Thesis, Qingdao University of Technology, Qingdao, 2018.
- Liu HJ. Study on Mechanical and Numerical Model for Road Tunnel Defects Diagnosis. Ph.D. Thesis, Tongji University, Shanghai, 2007.
- Mao JH, Yuan DJ, Jin DL, Zeng JF. Optimization and application of backfill grouting material for submarine tunnel. *Construction and Building Materials*, 2020, 265, 120281. <https://doi.org/10.1016/j.conbuildmat.2020.120281>
- Min B, Zhang CP, Zhang X, Wang HL, Li PF, Zhang DL. Cracking performance of asymmetric double-arch tunnels due to the voids behind linings. *Thin-Walled Structures*, 2020, 154, 106856. <https://doi.org/10.1016/j.tws.2020.106856>
- Ministry of Transport of the PRC. Code for Design of Road Tunnel, JTG D70-2004, 2004.
- Nie ZY, Zhang CL, Li FX. Effect of void behind lining on seismic performance of tunnel. *China Earthquake Engineering Journal*, 2015, 37, 138-143.
- Pan CS. Numerical method of Tunnel Mechanics. China Railway Publishing House, Beijing, 1995. (in Chinese)
- Rajak DK, Pagar DD, Menezes PL, Linul E. Fiber-Reinforced Polymer Composites: Manufacturing, Properties, and Applications. *Polymers*, 2019, 11(10), 1667. <https://doi.org/10.3390/polym11101667>
- Shah R, Lavasan AA, Peila D, Todaro C, Luciani A, Schanz T. Numerical Study on Backfilling the Tail Void Using a Two-Component Grout. *Journal of Materials in Civil Engineering*, 2018, 30, 04018003. [https://doi.org/10.1061/\(asce\)mt.1943-5533.0002175](https://doi.org/10.1061/(asce)mt.1943-5533.0002175)
- Song SH, Paulino GH, Buttlar WG. Simulation of Crack Propagation in Asphalt Concrete Using an Intrinsic Cohesive Zone Model. *Journal of Engineering Mechanics*, 2006, 132, 1215-1223. [https://doi.org/10.1061/\(ASCE\)0733-9399\(2006\)132:11\(1215\)](https://doi.org/10.1061/(ASCE)0733-9399(2006)132:11(1215))
- Tonon F. Sequential excavation, NATM and ADECO: What they have in common and how they differ. *Tunnelling and Underground Space Technology*, 2010, 25(3), 245-265. <https://doi.org/10.1016/j.tust.2009.12.004>
- Wang B, Wang Z, Uji K, Zhang J, Guo R. Experimental investigation on shear behavior of RC beams strengthened by CFRP grids and PCM. *Structures*, 2020, 27, 1994-2010. <https://doi.org/10.1016/j.istruc.2020.07.050>
- Wang JF, Huang HW, Xie XY, Bobet A. Void-induced liner deformation and stress redistribution. *Tunnelling and Underground Space Technology*, 2014, 40, 263-276. <https://doi.org/10.1016/j.tust.2013.10.008>

- Wu XL. Study on the Influence of Voids behind Early Support of Highway Tunnel on Structure Safety and Crack Evolution. Master's Thesis, Shandong University of Science and Technology, Qingdao, 2021.
- Xu GW, He C, Wang J, Zhang JB. Study on the damage evolution of secondary tunnel lining in layered rock stratum. *Bulletin of Engineering Geology and the Environment*, 2020, 79, 3533-3557. <https://doi.org/10.1007/s10064-020-01775-1>
- Yamaguchi K, Guo R, Hino S, Miyano N. Shearing capacity and adhesive characteristic of reinforced interface for RC beam with haunch retrofitted by CFRP covering PCM shotcrete. *Proc Jpn Concr Inst*, 2014, 36(2), 1261-1266.
- Yao CC, Yu HL, Zhang Y. Method of solving the safety factor of lining strength based on FLAC3D software. *Sichuan Architecture*, 2007, 27(2), 115-116. (in Chinese)
DOI: 10.3969/j.issn.1007-8983.2007.02.050
- Yasuda N, Tsukada K, Asakura T. Elastic solutions for circular tunnel with void behind lining. *Tunnelling and Underground Space Technology*, 2017, 70, 274-285.
<https://doi.org/10.1016/j.tust.2017.08.032>
- Yasuda N, Tsukada K, Asakura T. Three-dimensional seismic response of a cylindrical tunnel with voids behind the lining. *Tunnelling and Underground Space Technology*, 2019, 84, 399-412. <https://doi.org/10.1016/j.tust.2018.11.026>
- Ye F, Qin N, Han X, Liang X, Gao X, Ying K. Displacement infiltration diffusion model of power-law grout as backfill grouting of a shield tunnel. *European Journal of Environmental and Civil Engineering*, 2022, 26(5), 1820-1833.
<https://doi.org/10.1080/19648189.2020.1735524>
- Zhang CP, Feng G, Zhang X, Han KH, Zhang DL. Effect of double voids behind the lining of safety state of tunnel structure. *Chinese Journal of Geotechnical Engineering*, 2015, 37, 487-493.
- Zhang SL, Qi XQ, Liu C, Chen DG. Distribution characteristic of voids behind the lining of highway tunnel and its influence on lining structure. *Journal of Architecture and Civil Engineering*, 2020, 37, 62-70.
- Zhang X, Zhang CP, Feng G, Han KH. Experimental studies on effect of voids behind tunnel linings on progressive failure process of tunnel structures. *Chinese Journal of Geotechnical Engineering*, 2017, 39(6), 1137-1144.
<https://doi.org/10.11779/CJGE201706021>

5 Failure and time-dependent characteristics of linings with compound quality defects

5.1 Introduction

Tunnel quality defects, such as voids and insufficient lining thickness, often occur during the stage of tunnel construction and operation (Jiang et al. 2017; Gao et al. 2016; Yu et al. 2017). However, the defects may not exist independently, which means that there is a compound or combined defect form of voids and insufficient lining thickness (Yin et al. 2020). As shown in chapters 3 and 4, the void quality defect and insufficient thickness have significant adverse effects on lining structures. For compound defect types, the interaction between the void and insufficient thickness complicates the failure mechanism and mechanical properties of the lining. Consequently, making clear the influence of compound defects on the degraded tunnel structure and searching for an effective reinforcement design are necessary.

Concerning the quality defect of voids behind the lining, Wang et al. (2014) performed a two-dimensional finite element method (FEM) analysis to explore the effect of voids on the lining deformation and stress redistribution. To investigate the safety state of lining with voids, the detailed two-dimensional distribution of inner lining force was provided (Li et al. 2020; Zhang et al. 2020; Zhang et al. 2015). Meguid and Dang (2009) conducted a two-dimensional elastoplastic analysis to explore the impact of voids on the inner force of the lining. In addition, Yasuda et al. (2017) proposed the two-dimensional elastic solutions for a deep-buried circular tunnel with a void behind the lining, and the effect of voids on the stress state of the support structure was explored. She et al. (2008) experimental investigated the deformation characteristic and bearing capacity of tunnel structures with voids behind the lining. Regarding the defect of insufficient lining thickness, Zhang et al. (2017) conducted a two-dimensional FEM analysis to explore the impact of insufficient lining thickness on tunnel structure, the distribution of inner force, including the bending moment and axial force, was detailed investigated. Yang (2011) established an evaluation system for the risk of defects behind the tunnel lining based on the risk management theory. In addition, Wang et al.'s (2013) experiment studied the

effect of insufficient lining thickness on the mechanical behavior of the tunnel structure.

Recently, the FRP-PCM method has emerged as one of the most existing and promising reinforced technologies for concrete due to its favorable properties (Guo et al. 2020; Wang et al. 2020; Zhang et al. 2021). Several investigations have indicated that beams strengthened by the FRP were able to avoid debonding failure, resulting in a good flexural performance in terms of strength and ductility (Ceroni 2010; Esfahani et al. 2007; Chajes et al. 1994; Guo et al. 2018a; Wang and Li 2006; Guo et al. 2018b). In addition, Jiang et al. (2017) performed laboratory direct shear tests and bending tests to investigate the bonding behavior between the FRP grids and the concrete. The schematic of compound quality defects and the reinforcement can be shown in Fig. 5.1(a). Due to the existence of rock mass fissures and the void, it is easy to induce shear failure (Han et al. 2020), and the void should be backfilled. Meanwhile, since the degree of insufficient thickness is serious, the FRP-PCM method can be applied to reinforce the lining. The schematic diagram of the detailed application of the FRP-PCM method can be shown in Fig. 5.1(b) (Jiang and Zhang 2020; Higashi et al. 2014; Technical Committee on FRP grid method 2007; FRP Grid Method Association of Japan). Further, Jiang and Zhang (2020) performed a two-dimensional numerical model to investigate the reinforcement behavior of the FRP-PCM method on degraded tunnel structures with a single void defect.

It is evident that most of the previous studies focused mainly on the effect of tunnel quality defects on the inner force distribution and failure characteristics of tunnel structure based on a two-dimensional numerical model, while information on the three-dimensional modeling is rather limited. In addition, most previous studies focus mainly on the impact of a single defect type, such as voids or insufficient lining thickness, whereas information on compound defects is much rare. Furthermore, the FRP-PCM method could be better to reinforce the degraded concrete structure. Unfortunately, few revealed the reinforcement effect for degraded tunnel lining with compound defects, and its reinforcing effect should be further discussed and evaluated. Moreover, with the long operation of the tunnel structure, the time-dependent characteristics of the influence of the compound defect on the lining structure and the reinforcement effect should also be clarified. Therefore, in this chapter, the influence of compound quality defects on the mechanical properties, safety state, failure mechanism, and time-dependent characteristics of degraded lining structures was explored. Meanwhile, the reinforcement effect of the FRP-PCM method was also evaluated.

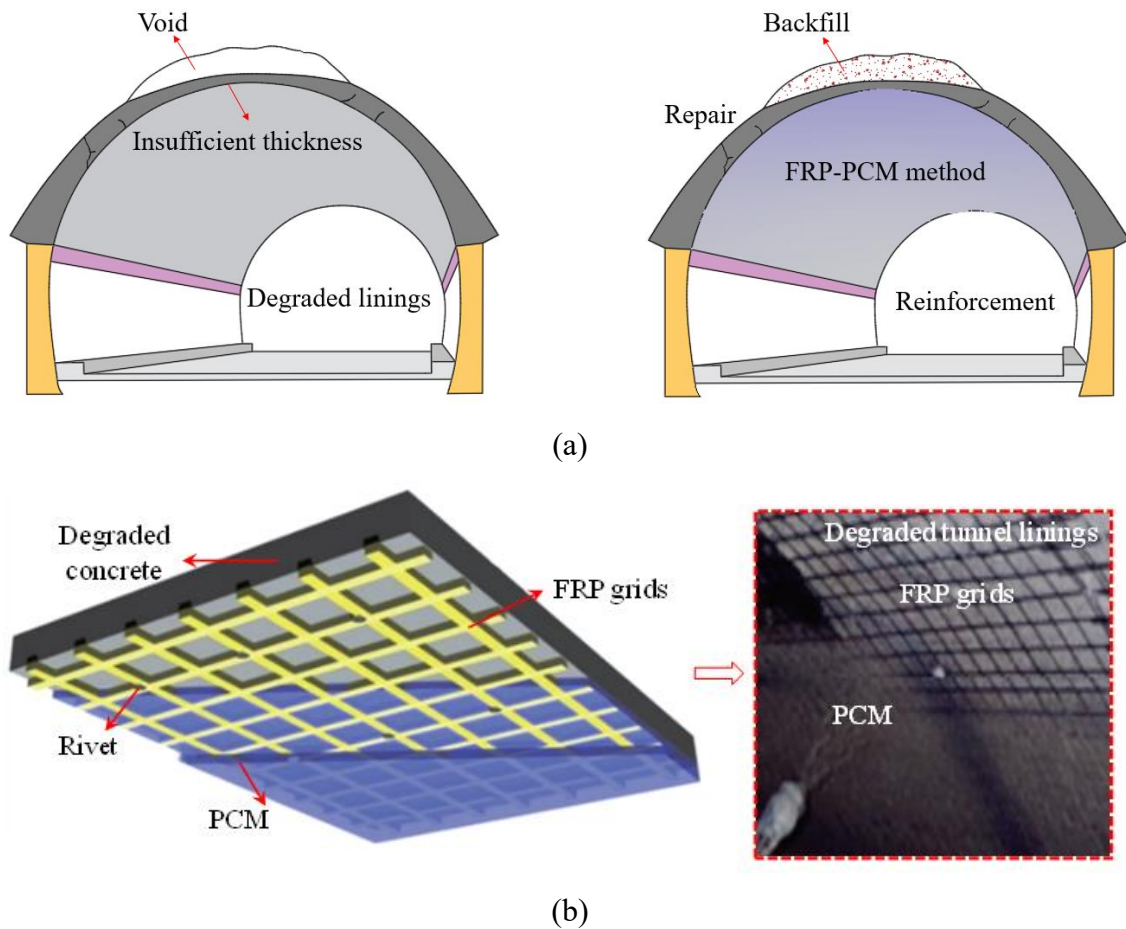


Fig. 5.1 Reinforcement of degraded linings: (a) schematic of compound quality defects and the reinforcement; (b) detailed application of the FRP-PCM method (Jiang and Zhang 2020; Higashi et al. 2014; Technical Committee on FRP grid method 2007; FRP Grid Method Association of Japan).

5.2 Model establishment

In this paper, the three-dimensional numerical model can be presented in Fig. 5.2(a). Regarding the boundary conditions, the entire numerical modeling was subjected to three-dimensional ground stresses of 0.8MPa. Concerning the tunnel cross-section in the numerical model, the standard section of the highway tunnel was adopted (Ministry of Transport of the PRC 2004). With respect to the constitutive model, the Mohr-Coulomb criterion was adopted to describe the mechanical properties of rock mass, linings, and FRP-PCM materials, respectively. In this research, the effect of the multiple tunnel compound defects was mainly focused on, and the distribution of compound defects can be presented in Fig. 5.2(b). It should be indicated that the void in this research is caused

by insufficient lining thickness, that is, the lining defects, inducing no contact between the rock mass and lining. With respect to the lining thickness, the normal lining thickness is 0.45m, and the area within insufficient lining thickness is 0.3m. Concerning the size of the compound defects, the range is all fixed as 50° , and the longitudinal length is all set as 4.5m. The cross-section I is $z=7.25\text{m}$, and cross-section II is $z=12.25\text{m}$. In addition, the ground class of CII, DI, and DII were considered. Furthermore, deterioration degrees of 10%, 30%, and 50% were mainly considered, and the corresponding parameters for lining deterioration can be obtained through the corresponding reduction rate. Subsequently, the types of FRP grids, CR4, CR6, and CR8, were selected to reinforce the degraded tunnel linings with compound quality defects. The parameters of the corresponding materials can be displayed in Table 5.1 (Jiang et al. 2017) and Table 5.2 (Jiang et al. 2017).

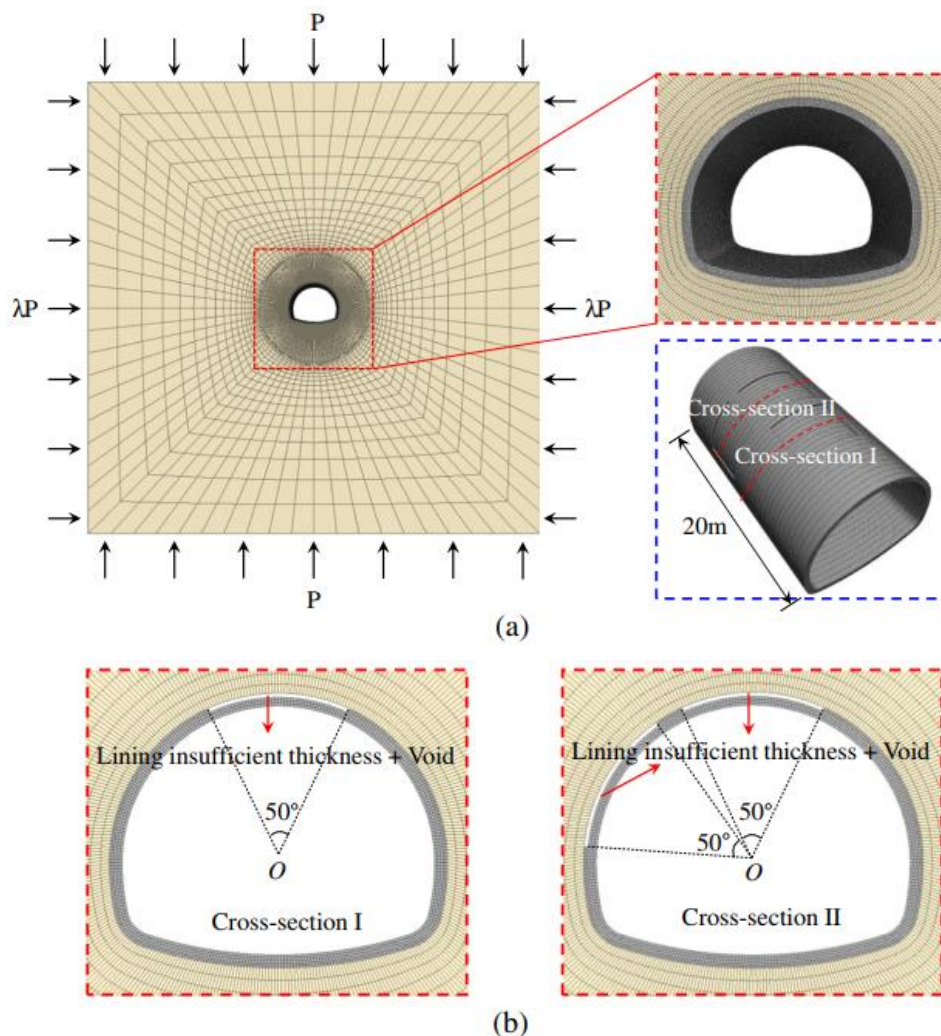


Fig. 5.2 Model establishment: (a) boundary conditions; (b) lining compound defects.

Table 5.1 Parameters of ground, lining, and backfill materials (Jiang et al. 2017).

Properties	Ground class			Tunnel lining	Backfill
	CII	DI	DII		
γ (kN/m ³)	22.6	21.6	20.6	24	9.8
E (MPa)	980	490	147	24500	12.0
ν	0.3	0.35	0.35	0.20	0.13
c (MPa)	0.98	0.49	0.196	6.99	0.50
φ (deg)	40.0	35.0	30.0	40.0	10.0

Table 5.2 Parameters of FRP grids and PCM material (Jiang et al. 2017).

Reinforcement materials		E	σ_t	φ_s	Cross-sectional area (mm ²)
		(MPa)	(MPa)	(deg)	
FRP grid	CR4				6.6
	CR6	100000	1400		17.5
	CR8			17.7	26.4
PCM		26000	4.60		—

5.3 Numerical results

5.3.1 Mechanical characteristics

5.3.1.1 Distribution of principal stress

The stress distribution of tunnel linings can be presented in Fig. 5.3. As observed in the 3D view, a significant tensile stress concentration occurs on the outer surface of the lining corresponding to the compound quality defects. While at the edge of the insufficient lining thickness, a compressive stress concentration phenomenon generates. By comparing different cross-sections, it can be observed that the stress distribution is significantly affected by the defect distribution. As presented in cross-section I, the outer surface of the area with the insufficient thickness of the lining bears a significant tensile effect and shows a gradual decrease from the outside to the inside. Concerning cross-section III, a compressive effect generates at the crown outside, but a significant tensile stress concentration phenomenon occurs at the lining inside the surface. Analogously, this phenomenon is also found in the shoulder. Regarding cross-section II, the outer surface

of these two areas with the insufficient thickness of the lining bears a significant tensile effect. However, significant compressive stress concentrations at the edges where the lining thickness is insufficient. In the area between double compound defects, the stress distribution characteristics are just the opposite, that is, the compressive effect on the outer surface of the lining gradually transforms into the tensile effect on the inner surface. In addition, it can be observed that the arch springing is identified as an area of significant compressive stress concentration.

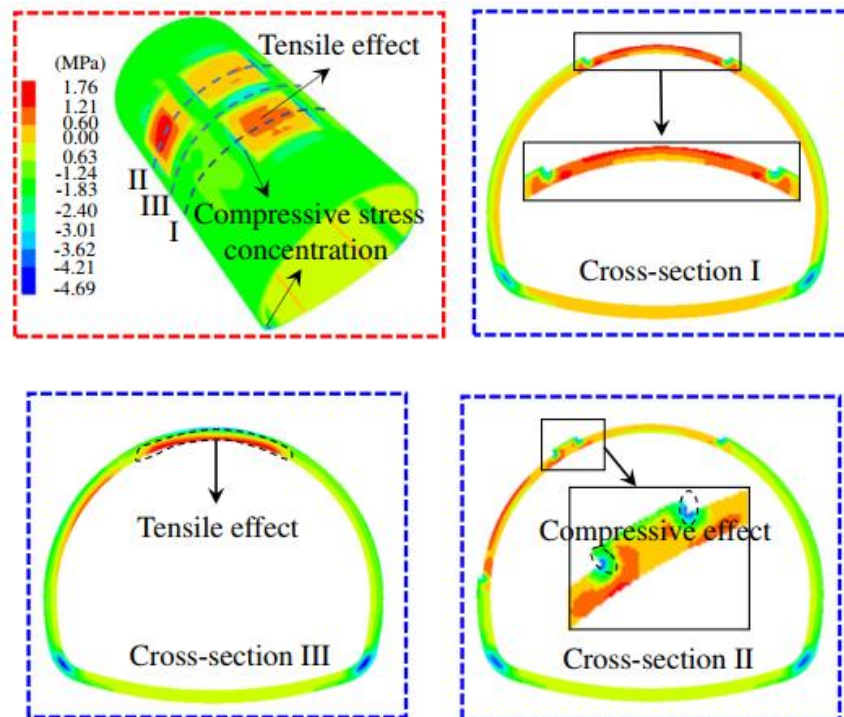


Fig. 5.3 Distribution of principal stress of degraded tunnel linings.

5.3.1.2 Distribution of inner force

To determine the effect of tunnel compound defects on the safety state of the lining, it is necessary to explore the distribution of inner force (Ministry of Transport of the PRC 2004). The distribution of lining inner force (taking the bending moment as an example) can be displayed in Fig. 5.4. As shown in Fig. 5.4, it reveals that the bending moment along the tunnel tangential direction within the defect-affected area changes evidently compared to that of other parts in the lining. Within the range of the void defects, the sign of the bending moment is significantly changed, and a significant bending outward phenomenon occurs. This finding can be attributed to the reason that the existence of the void eliminates the contact effect between the rock mass and the lining. Furthermore, the

two-dimensional distribution of the inner force of tunnel linings with the quality defect was investigated, and the phenomenon of bending outwards was also observed within the defect zone (Zhang et al. 2015; Zhang et al. 2020; Liu 2018), which can verify the reliability of the model in this research. Similarly, it should be indicated that the axial force can also be obtained with the method (Yao et al. 2007).

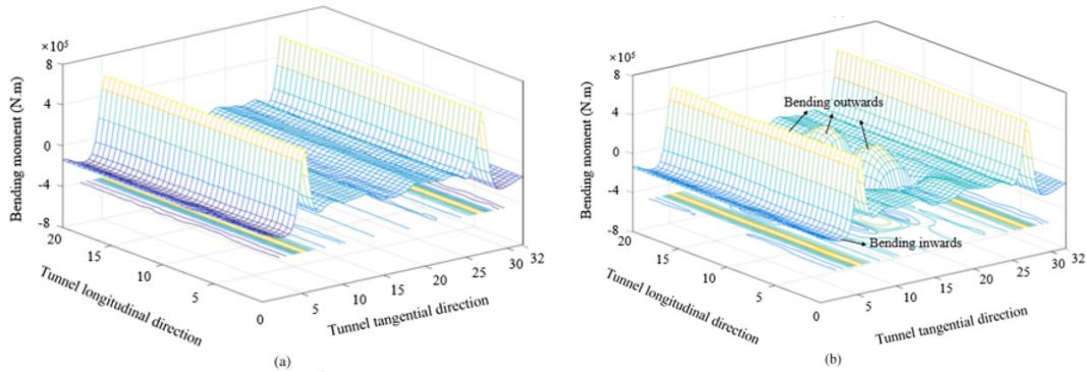


Fig. 5.4 Distribution of bending moment: (a) without compound defects; (a) with compound quality defects.

5.3.2 Distribution of failure zone

5.3.2.1 Effect of degradation degree

In this section, the effect of lining deterioration degree on the areas prone to plastic failure in the calculation process of tunnel lining was explored and presented in Fig. 5.5. When the lining deterioration degree is 0.1, the plastic failure zone on the outer surface of the lining corresponding to the compound defects can be roughly divided into two layers from the inside to the outside, namely the tensile failure zone and the shear failure zone. To investigate the damage distribution on the inner side of the lining conveniently, three typical cross-sections (I~III) were also selected in this study. As shown in cross-section I, tensile plastic failure occurs on the outwards surface of the lining with insufficient thickness, while tensile-shear failure is dominant on the inner surface. Regarding cross-section III, it can be observed that no failure zone occurs in the outermost layer of the lining, there is a significant shear failure zone in the middle area of the lining, and there is a tensile-shear failure zone on the inner surface of the lining. In addition, with respect to cross-section II, tensile failure is dominant in the area with insufficient lining thickness, and only a small part of the tensile-shear failure zone occurs on the inner surface of insufficient lining thickness. When the lining deterioration degree is 0.3, the

types of failure zone on the outer surface of the lining corresponding to the compound defects can be roughly divided into three layers from the inside to the outside, tensile-shear failure, tensile failure, and shear failure, respectively. However, when the lining deterioration degree is 0.5, there is basically no tensile failure on the outside of the crown, and it can be roughly divided into two layers, namely the tension-shear failure zone and the shear failure zone. In addition, it should be indicated that when the lining deterioration degree is 0.3 and 0.5, it can be observed that the outer surface of the lining in contact with the surrounding rock also has a shear failure zone, but when the lining deterioration degree is 0.1, no failure zone occurs. As can be observed from cross-section I, when the lining deterioration degree is changed from 0.1 to 0.5, the failure type within the range of the compound defect zone is changed from the main tensile plastic failure to the main tensile-shear failure. In addition, the failure rate presents a positive relationship with the lining deterioration degree.

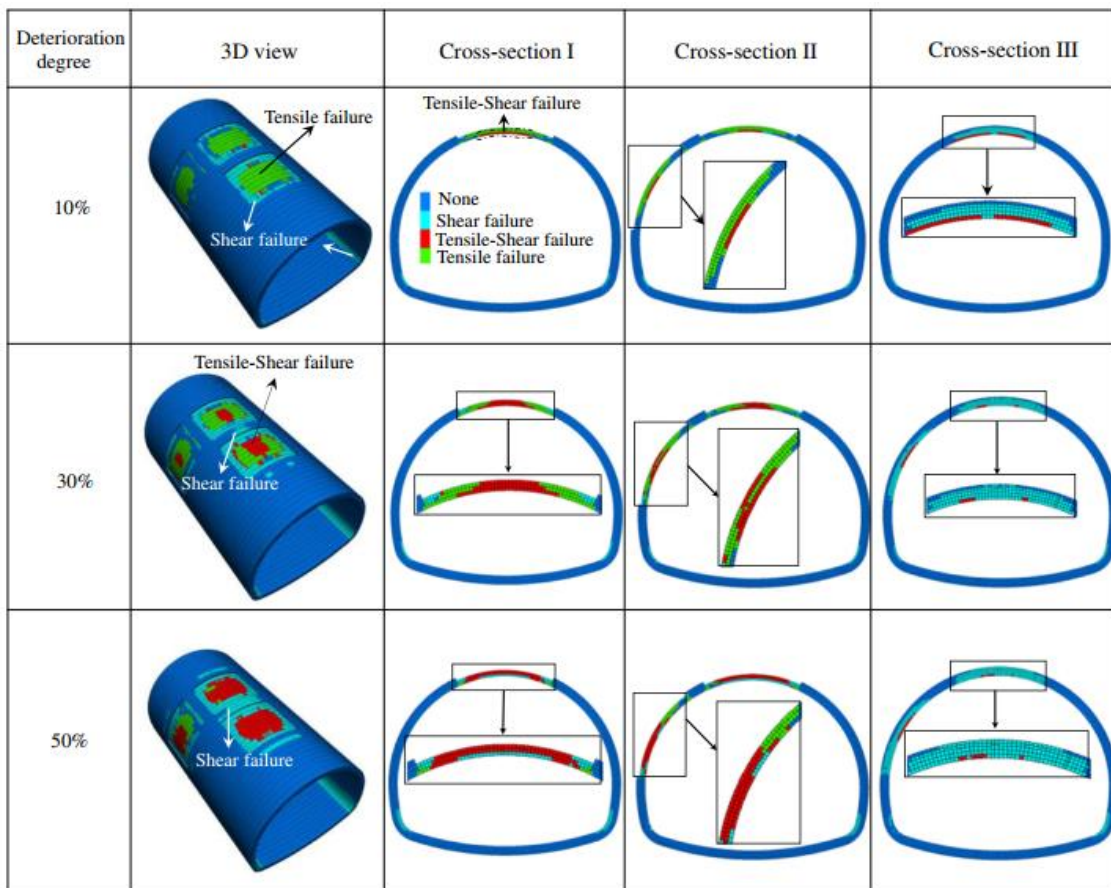


Fig. 5.5 Effect of lining degradation degree on the distribution of lining failure zone.

5.3.2.2 Effect of ground class

In this section, the effect of ground class on the areas prone to lining failure in the calculation process was investigated and shown in Fig. 5.6. Obviously, the grade of ground class significantly affects the distribution of the lining plastic failure zone. Specifically, when the ground class is DI, the lining suffers a large range of tensile-shear failure zone at the crown, while the central position of the shoulder compound defect is subjected to tensile-based failure. Shear failure occurs on edges where the lining thickness is insufficient. However, when the ground class is DII, the types of failure zone on the outer surface of the lining corresponding to compound defects can be roughly divided into two layers from the inside to the outside, the tensile-shear failure zone, and the shear failure zone, respectively. It should be indicated that the outer surface of the lining in contact with the rock mass occurs shear failure zone, but when the ground class is CII, no failure zone occurs. In addition, as observed from the cross-section I~III, the failure rate increases significantly as the degree of the ground class changes from CII to DII. It is noted that when the ground class is DII, it is easier to induce tensile-shear failure on the inner side of the lining. Furthermore, when the ground class is DII, a large-scale shear failure occurs at the shoulder of cross-section III.

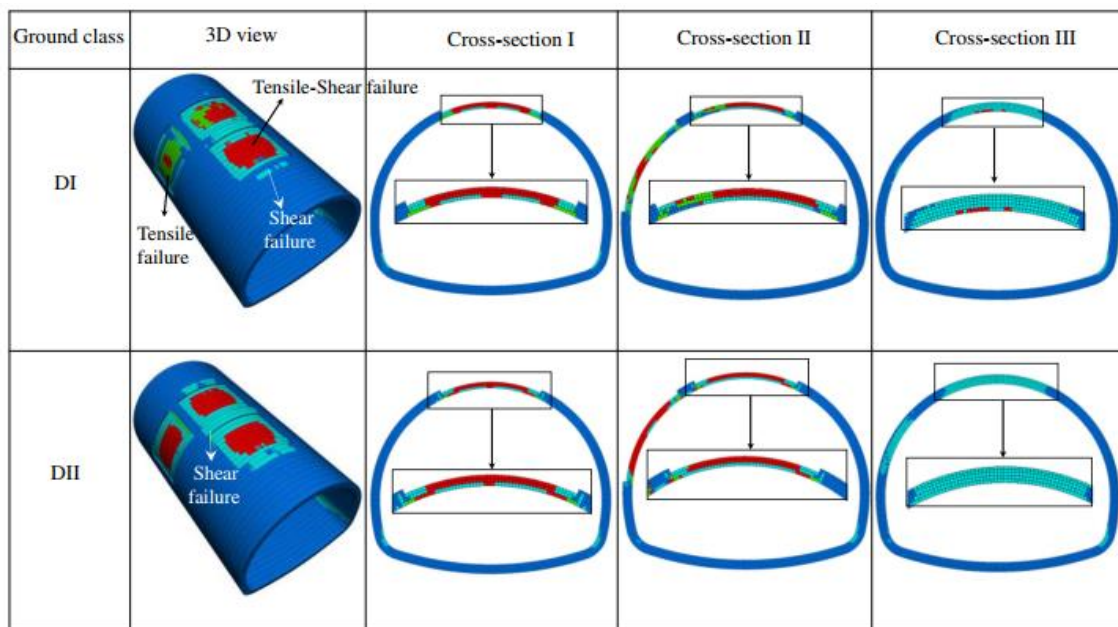


Fig. 5.6 Effect of ground class on the distribution of lining failure zone.

Analogously, the potential cracking zone of linings with compound defects was discussed according to the characteristics of the failure zone and the stress distribution

(Fig. 5.7). It should be indicated that the cracking areas marked are the roughly distributed zone, and the distribution of specific crack morphologies can be achieved by the XFEM (Chen et al. 2020) or the CZM method (Jiang and Meng 2018). Regarding the lining with a low degradation rate, as shown in Fig. 5.7(a), the potential cracking zone in the lining defect zone exhibits two layers from the inside to the outside, namely the tensile cracking zone (TCZ) and the shear cracking zone (SCZ). Concerning the lining with a low degradation rate, as shown in Fig. 5.7(b), the potential cracking zone in the lining defect zone exhibits three layers from the inside to the outside, tensile-shear cracking zone (TSCZ), TCZ, and SCZ, respectively. As shown in Fig. 5.7(c), concerning the low-grade rock mass (DII in this research), the potential cracking zone in the lining defect zone exhibits two layers from the inside to the outside, TSCZ, and SCZ, respectively. In addition, the SCZ is prone to occur between the lining defect zone. In addition, it should be indicated that the approximate distribution range of the damage zone was discussed, and it is helpful to carry out the tunnel model tests to determine the detailed failure characteristics under the three-dimensional ground stress in future work.

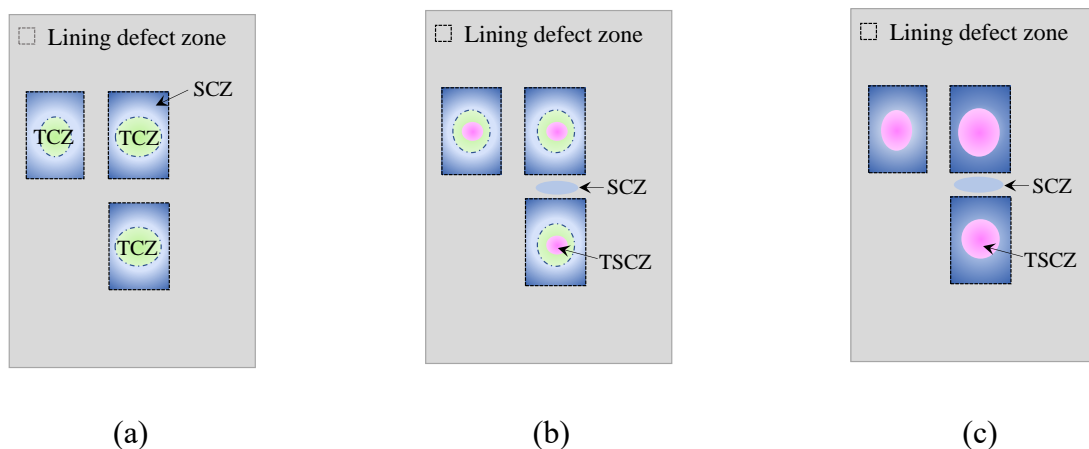


Fig. 5.7 Potential cracking zone on the outer surface of linings with compound defects: (a) low degradation rate; (b) large degradation rate; (c) low grade of the rock mass.

5.3.3 Reinforcement effect of the FRP-PCM method

5.3.3.1 Evaluation of safety state

To make clear the safety state under the reinforcement, three typical cross-sections were selected, $z=7.25\text{m}$ (cross-section I), 9.75m (cross-section III), and 12.25m (cross-section II), respectively. The arch range of the reinforcement is 240° in this section. As

shown in Fig. 5.8(a), it is observed that the type of FRP grids can affect the safety state of the tunnel lining. When the CR4, CR6, and CR8 grids were applied, the safety factors at the crown are 2.14, 3.18, and 3.46, respectively. As observed from cross-section II, when the FRP-PCM method was utilized for the reinforcement, the safety factors increase significantly with the larger grade of FRP grids. However, for the grade of CR4, the safety factors of the crown and the left shoulder are 2.16 and 1.41, respectively, and for CR6 and CR8, the safety factors of the lining can satisfy the safety state. As presented in cross-section III, as the grade of the FRP grids increases, the safety factor shows a non-linear increasing trend.

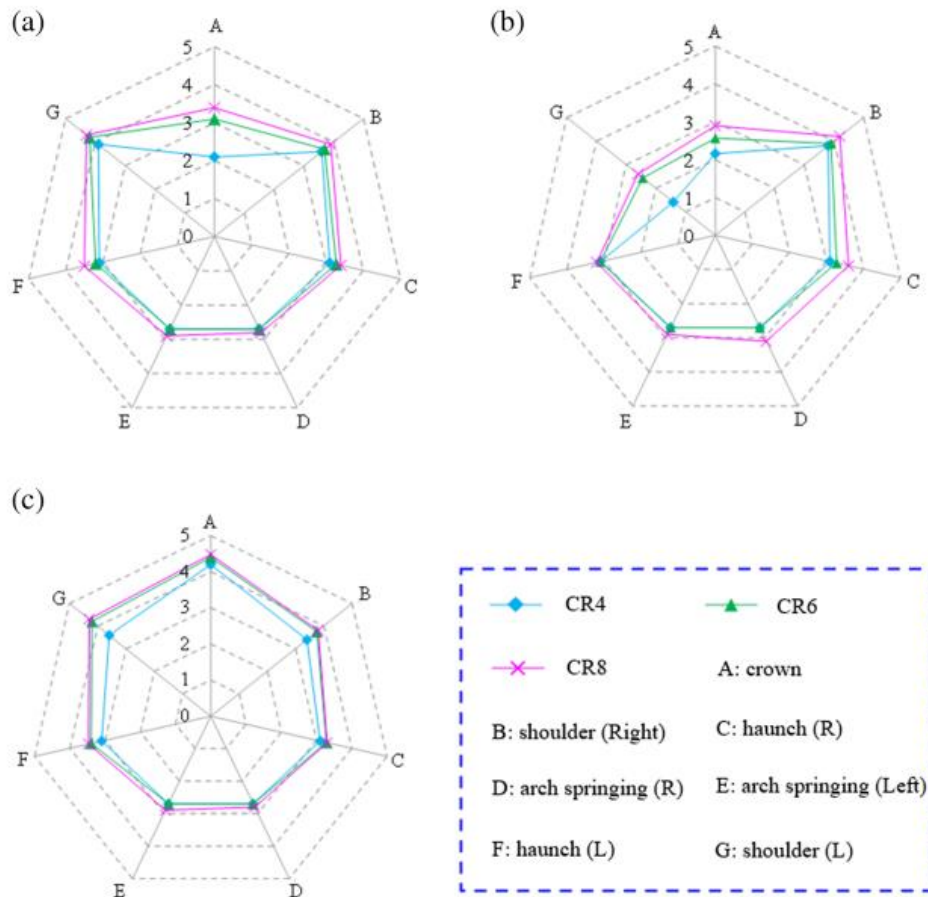


Fig. 5.8 Distribution of safety factors of linings under the reinforcement: (a) cross-section I; (b) cross-section II; (c) cross-section III.

5.3.3.2 Failure rate

To evaluate the reinforcement effect of the FRP-PCM method on degraded tunnel lining with compound defects, three grades of FRP grids (CR4, CR6, and CR8) were

adopted, and the region of the reinforcement covered an arc length of 180° . The distribution of the failure rate can be presented in Fig. 5.9. It is observed that when the lining is not reinforced, the failure rate of the lining is 13.38%, 14.85%, 19.37%, and 21.73% for the lining deterioration degree of 0, 0.1, 0.3, and 0.5, respectively. When the FRP-PCM method was applied, the damage rate of the lining displays a decreasing trend, and the degree of reduction is different for different deterioration degrees. Specifically, when the lining is without degradation, the failure rates are 7.71%, 5.23%, and 3.82% for the FRP grades CR4, CR6, and CR8, respectively. When the deterioration degree of the lining is 0.1, the failure rate is 8.93%, 7.24%, and 6.18%, respectively. When the lining is with a degradation degree of 0.3, the failure rate of the lining is 13.53%, 10.22%, and 8.53%, respectively. Similarly, when the lining is with a deterioration degree of 0.5, the damage rate is 15.91%, 12.23%, and 9.92%, respectively. Therefore, it can be found that as the grade of the FRP grids increases, the failure rate shows a non-linear decrease trend. To clarify the reinforcement effect of the FRP-PCM method on tunnel linings more deeply, it is necessary to conduct the model test in future work.

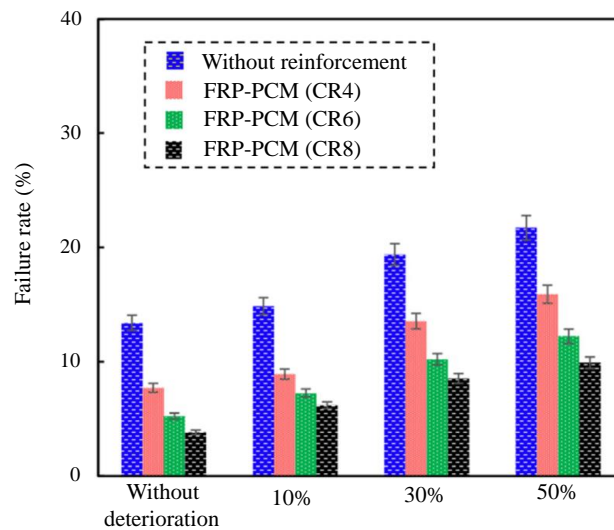


Fig. 5.9 Failure rate of the degraded lining under the reinforcement of the FRP-PCM method.

5.4 Time-dependent characteristics

5.4.1 Model overview

The above-established three-dimensional model mainly investigated the failure characteristics and reinforcement performance of linings with compound defects, while

the corresponding time-dependent characteristics were not considered. Therefore, the time-dependent properties of the effect of compound defects on linings were explored in this section. To improve computational efficiency, the two-dimensional model was established. The boundary conditions and the defect description can be obtained in section 5.2. The model arrangement can be exhibited in Fig. 5.10. The effect of defect location and defect range was mainly explored in this section. Concerning the rheological model, the Burgers model can be depicted as a combination of Maxwell and Kelvin elements (Kargar et al. 2020), which has been widely and effectively applied in the time-dependent analysis of rock mass (Higashi 2014; Hu et al. 2018). Therefore, in this section, the Burgers model was applied to the ground. Concerning the reinforcement arrangement, the range of the FRP-PCM method is 180° . The corresponding applied parameters can be listed in Table 5.2 (Jiang et al. 2017) and Table 5.3 (Higashi 2014; Jiang et al. 2017).

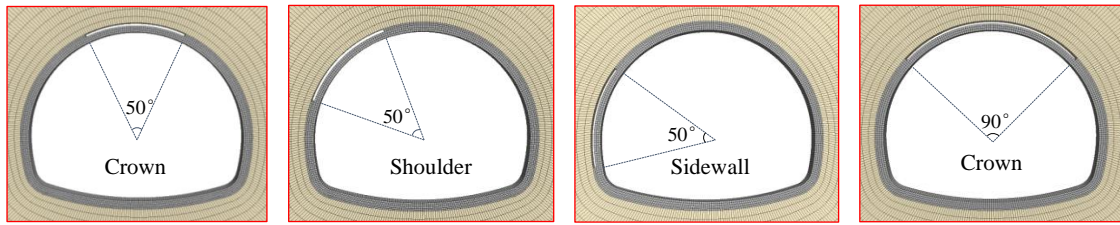


Fig. 5.10 Model arrangement.

Table 5.3 Parameters of the established model (Higashi 2014; Jiang et al. 2017).

Properties	Ground	Tunnel lining	Backfill
E (MPa)	1000	24500	12.0
ν	0.3	0.20	0.13
c (MPa)	0.8	6.99	0.50
φ (deg)	30	40.0	10.0
G^K (MPa)	604		
$\mu^K(10^{10} \text{ Pa}\cdot\text{s})$	4.04		
G^M (MPa)	385		
$\mu^M(10^{10} \text{ Pa}\cdot\text{s})$	3.83		

5.4.2 Numerical results

5.4.2.1 Mechanical properties

In this section, the characteristics of mechanical properties over time were explored. The evolution of the principal stress was presented in Fig. 5.11. When the defective lining

is unreinforced (UR), as shown in Fig. 5.11(a), the tensile stress concentration phenomenon occurs on the outer surface of the defect zone and the inner side of the defect edge. As time increases, the range and degree of the tensile stress concentration become further significant. In addition, the principal stress evolution characteristics at the arch foot also change significantly with time. When the time reaches 5 years and 10 years, the outer edge of the arch foot exhibits a significant tensile effect while compressive stress concentration for the inner side. Therefore, it can be observed that the stress distribution at the defect area deteriorates significantly over time. Correspondingly, the principal stress distribution of the defective lining reinforced by the FRP-PCM method and the backfill method can be presented in Fig. 5.11(b). The corresponding values of defective lining structure reduce obviously with reinforcement. Specifically, the tensile stress concentration phenomenon on the outer surface of the defect zone and inside the defect edge is significantly suppressed. With the increase of time, there is no tensile stress concentration phenomenon in the defect area. As for the stress distribution of the defective lining structure at the arch springing, the tensile stress concentration and compressive stress concentration are not improved significantly. The main factor for the phenomenon is the reinforcement range. Overall, the FRP-PCM method and the backfill method can reduce the stress concentration of the defective lining and optimize the mechanical distribution.

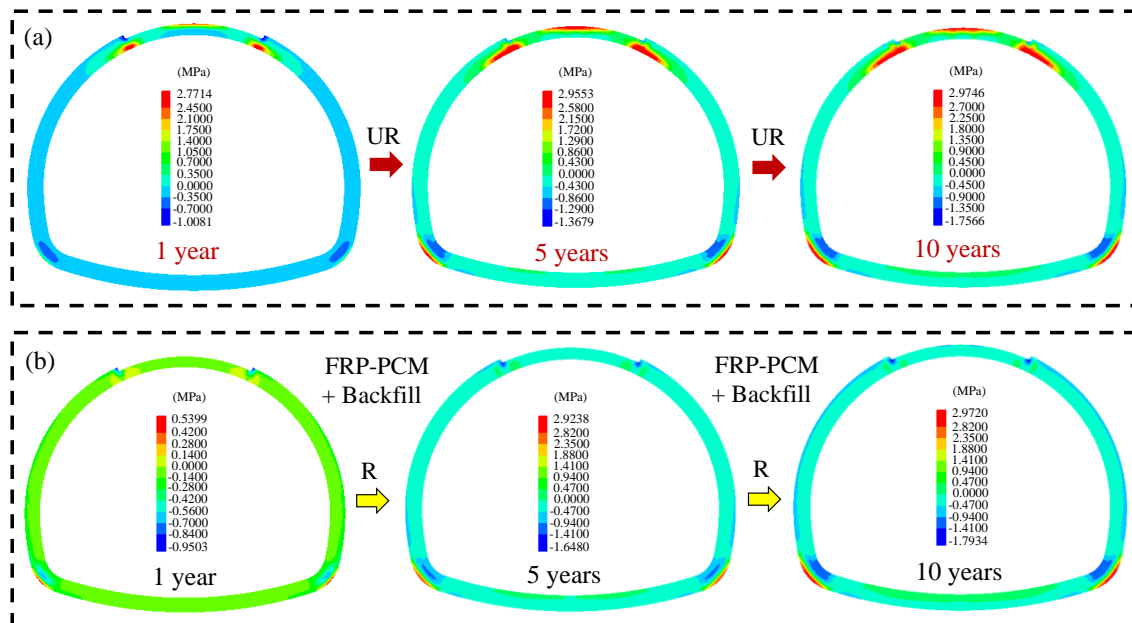


Fig. 5.11 Evolution of the distribution of principal stress of defective linings over time: (a) without reinforcement; (b) with reinforcement.

Similarly, the time-dependent characteristic of maximum shear stress can be presented in Fig. 5.12. If no countermeasures were applied to the defective linings, as exhibited in Fig. 5.12(a), the maximum shear stress increases significantly with time. It is noted that the increase in shear stress at the arch springing is greater than that at the defect area. In addition, concerning the rheological time of 1 year, large shear stress occurs at the inner side of the crown and the arch springing, resulting in local stress concentration. The time-dependent characteristics of maximum shear stress with reinforcement can be presented in Fig. 5.12(b). As time increases, the maximum shear stress increases obviously. In addition, the maximum shear stress at the inner side of the defect zone is significantly reduced compared with the unreinforced defective linings. Furthermore, the maximum shear stress of the defective linings at the arch springing is not significantly reduced. Overall, it is noted that the FRP-PCM method and the backfill method can significantly reduce the shear stress of the compound defective lining within the reinforcement zone, optimizing the mechanical performance.

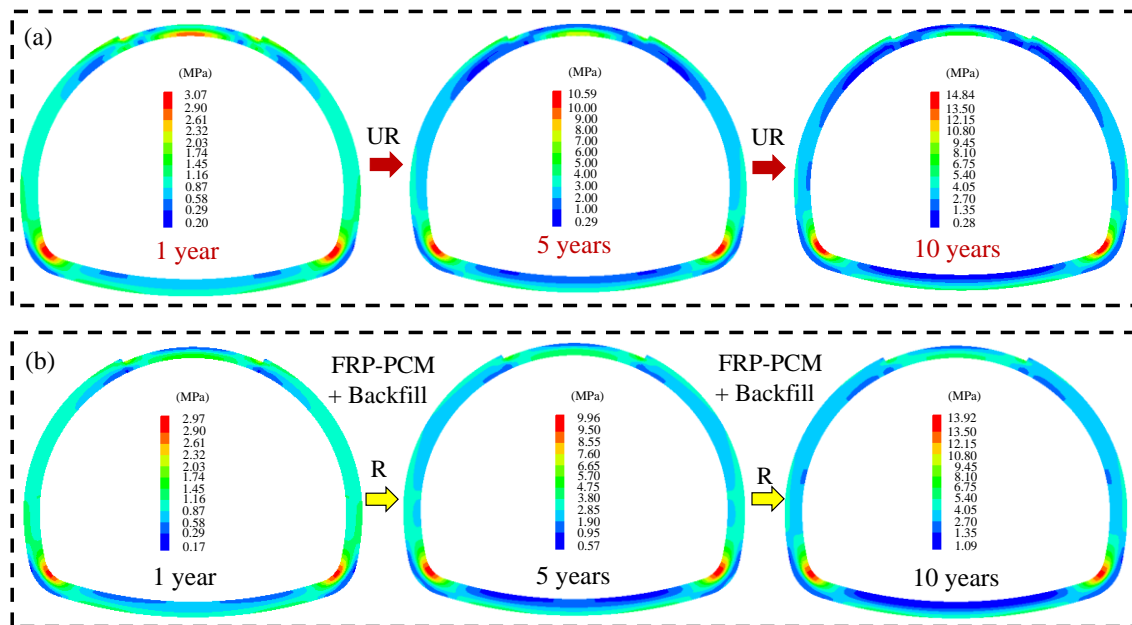
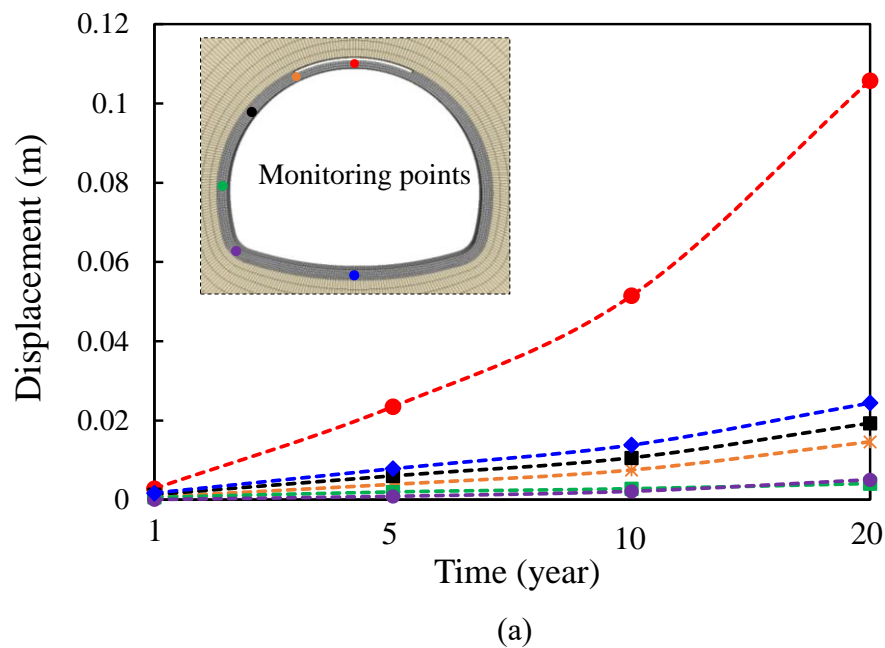


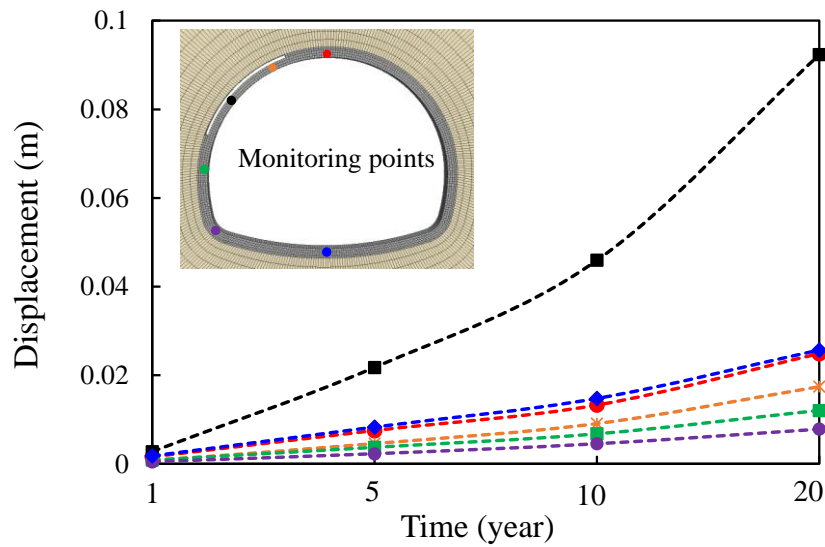
Fig. 5.12 Evolution of the distribution of maximum shear stress of lining structure over time (a) without reinforcement; (b) with reinforcement.

5.4.2.2 Displacement evolution characteristics

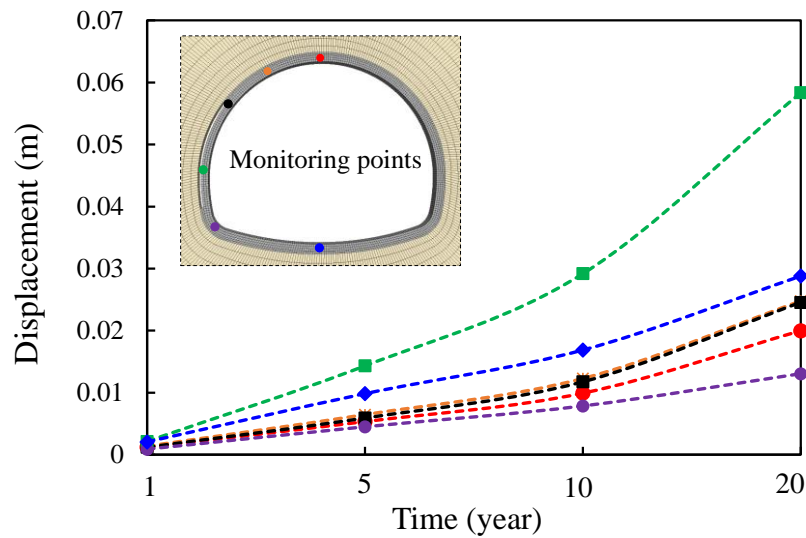
5.4.2.2.1 Effect of defect location

In this section, the effect of defect location on the displacement evolution characteristics at typical measuring points was investigated, as presented in Fig. 5.13. Defect locations were set at the crown, shoulder, and sidewall, respectively. As shown in Fig. 5.13, the displacement at typical measuring points presents a significant positive correlation with time. However, the displacement of each measuring point is significantly affected by the defect location. Specifically, when the location of the lining defect is at the crown, as shown in Fig. 5.13(a), the maximum displacement is near the defect center zone, while a minor displacement is at the arch springing. In addition, the growth rate of the displacement in the defect center area with time is larger than that in the non-defect area or outside the defect zone. Similar characteristics are observed for the defect location of the shoulder and sidewall. Furthermore, by comparing the displacement of different defect locations in the time of 20 years, it can be observed that the displacements at the center of the defect area are 0.105m, 0.092m, and 0.058m, respectively. When the defect is at the crown, the displacement at the defect center changes significantly with time. In addition, when the compound quality defect is located at the sidewall, the dispersion between the defect center and other typical measuring points is smaller than in other locations.





(b)



(c)

Fig. 5.13 Evolution of displacement over time: (a) crown; (b) shoulder; (c) sidewall.

5.4.2.2.2 Effect of reinforcement

As presented in the last section, the displacement increases significantly with time. Therefore, it is crucial to take corresponding countermeasures to suppress the rapid development of deformation. When the defective lining structure was reinforced with the FRP-PCM method and backfill method, the distribution of lining displacement at 10 years can be exhibited in Fig. 5.14. With the comparison between Fig. 5.14(a) and Fig. 5.14(b), the distribution of lining displacement can be significantly influenced by the reinforcement. In particular, the displacement at the defect area can reduce significantly. Specifically, the displacement at the compound defect zone is 0.0515m, but 0.0007m for

the defective lining with the reinforcement. In addition, the deformation direction at the crown is easy to be upward when there is no reinforcement but downward after reinforcement. The main reason for this phenomenon is that when the defect is not repaired, the lining structure and the rock mass are not in contact. After the reinforcement, the poor contact between the lining and the rock mass is eliminated. The displacement of defective lining structures can be significantly reduced by the FRP-PCM and the backfill method.

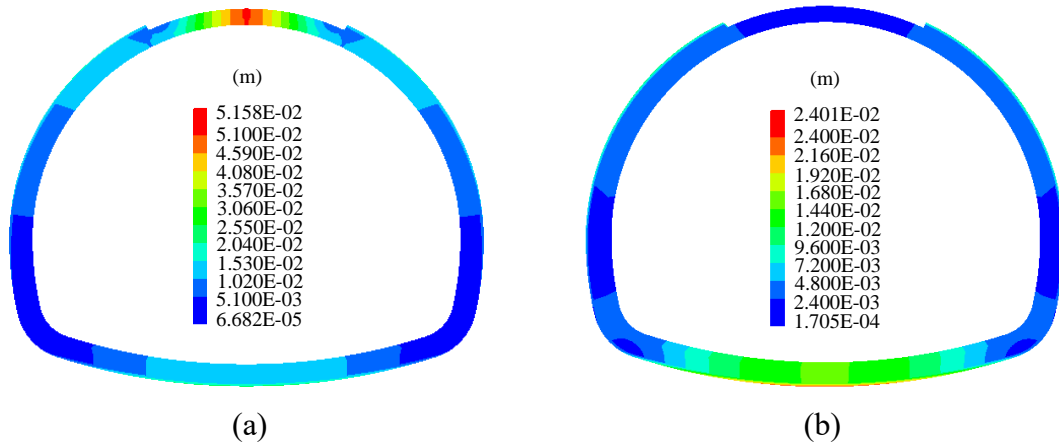


Fig. 5.14 Distribution of displacement at 10 years: (a) without reinforcement; (b) with reinforcement.

5.4.2.3 Plastic failure distribution

5.4.2.3.1 Effect of defect location

When the lining structure is unreinforced, the effect of defect location on the time-dependent characteristic of plastic failure in the calculation process can be presented in Fig. 5.15. It should be indicated that the defect locations were set at the shoulder and sidewall in this section as a comparison. Regardless of whether the defect is located at the shoulder or sidewall, significant plastic tensile failure and shear failure zones are observed at 5 years. When the defect is at the shoulder, as shown in Fig. 5.15(a), plastic tensile failure is observed on the inner surface of the defect edge and the outer surface of the arch springing, while shear failure occurs on the outer surface of the defect edge. However, for the defect location of the sidewall, as shown in Fig. 5.15(b), plastic failure is not observed at the arch springing close to the defect, while the plastic failure of the arch springing away from the defect is similar to that of the shoulder. As shown in Fig. 5.15, the range of plastic failure increases with time. In particular, the tensile failure zone occurs at the inverted arch when the time is 20 years. The plastic failure proportion at the inverted arch

for the defect located at the sidewall is larger than that of the shoulder. Therefore, it can be concluded that the plastic failure characteristics of lining structures with compound defects are significantly affected by the defect location. Meanwhile, the failure characteristic of linings presents a significant time dependence.

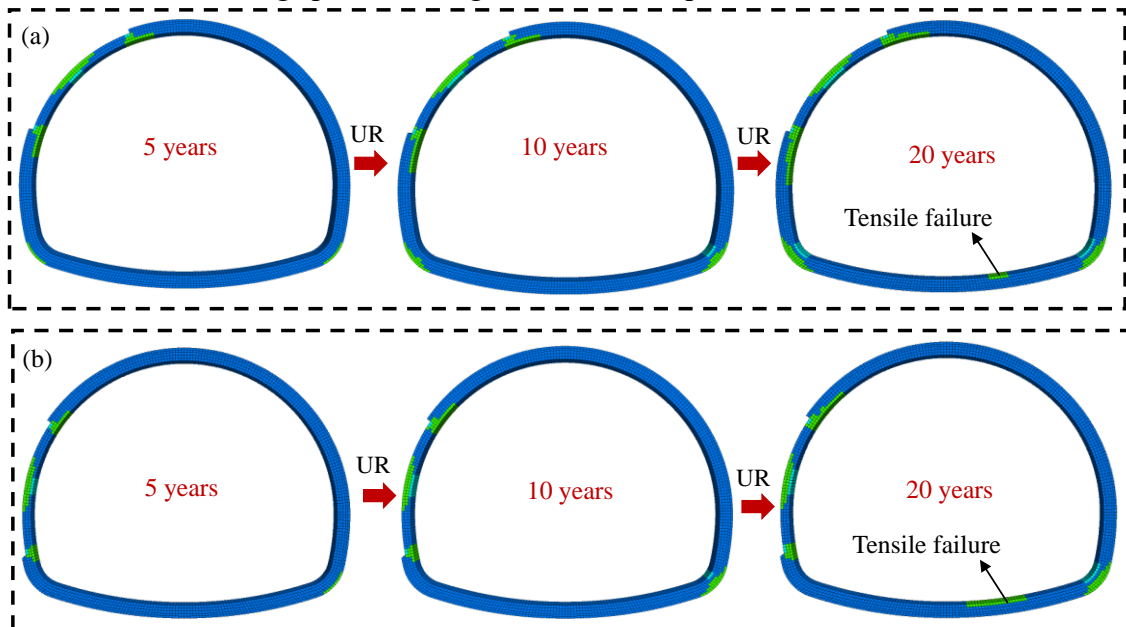


Fig. 5.15 Effect of defect location on the time-dependent characteristic of plastic failure:
(a) shoulder; (b) sidewall.

5.4.2.3.2 Effect of defect range

The effect of defect range on the time-dependent characteristic of plastic failure in the calculation was investigated, as presented in Fig. 5.16. As for the defect range of 50° , the plastic tensile failure occurs on the outer surface of the defect zone, but plastic shear failure generates on the inner surface when the time is 5 years. In addition, tensile failure appears at the inner surface of the defect edge and the outer surface of the arch springing, while shear failure occurs on the outer surface of the defect edge. When the lining structure is unreinforced, the range of the plastic failure zone gradually increases with time. The plastic shear failure zone appears on the inner side of the arch springing at 10 years, and a large-scale tensile failure zone occurs on the inverted arch at 30 years. In the comparison between Fig. 5.16(a) and Fig. 5.16(b), the plastic failure range on the inner surface of the defect zone of the defect range of 90° is smaller than that of the 50° . Concerning the plastic failure of defective linings with the reinforcement, the proportion reduces significantly compared to without reinforcement. Specifically, the plastic failure zone at the crown reduces significantly, and the plastic failure zone at the arch springing

reduces to a small range. Therefore, the FRP-PCM method and the backfill method can effectively inhibit the plastic failure zone of the deep-burned tunnel structure with compound quality defects. However, the optimization effect is limited for the area outside the reinforcement range. In addition, to more realistically reflect the properties of defect linings, it may also be an effort to consider temperature effects in future work.

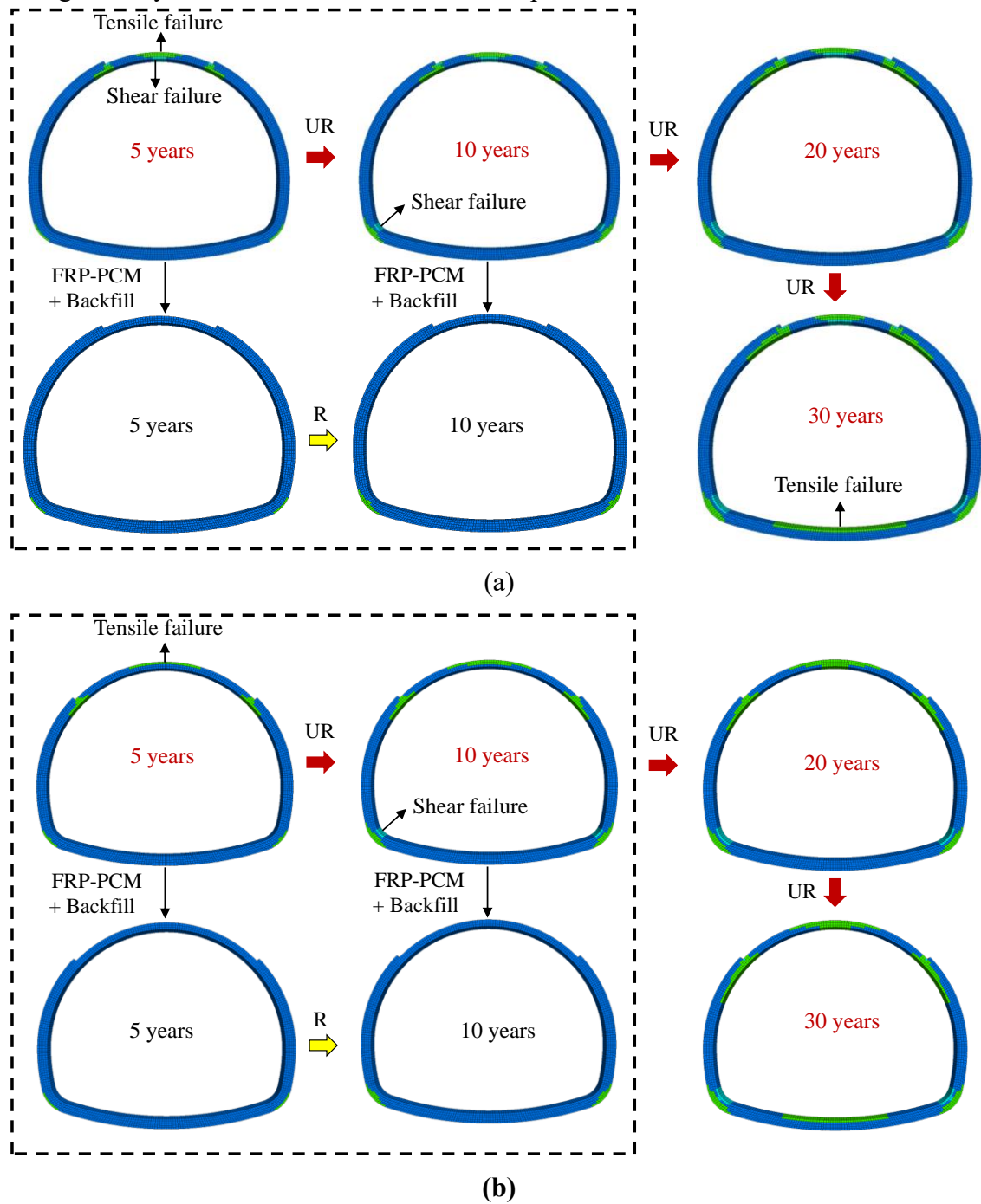


Fig. 5.16 Effect of defect range on the time-dependent characteristic of plastic failure: (a) defect range of 50°; (b) defect range of 90°.

5.5 Conclusions

In this chapter, the failure and time-dependent characteristics of linings with compound quality defects were investigated. Meanwhile, the reinforcement effect of the FRP-PCM method and the backfill method was evaluated. The main conclusions can be drawn as follows:

- (1) Concerning the deep-buried tunnel with compound quality defects, tensile stress concentration is prone to occur on the outside surface of the lining within the defect zone, while on the inside surface of the area between the double defect zones. In addition, a compressive stress concentration phenomenon is prone to generate at the edge of the compound defect zone. The bending outward phenomenon of the lining within the compound defect zone is observed.
- (2) Failure characteristics are significantly affected by the lining deterioration degree and the ground class. The higher the deterioration degree, the more prone to tensile-shear plastic failure in the compound defect zone. Otherwise, the more likely it is for tensile failure. Concerning the failure behavior for the ground class of DII, a significant ring layer failure phenomenon occurs, that is, the inner layer is the tensile-shear failure, and the outer layer is the plastic shear failure. In addition, the distribution of potential cracking zones of TCZ, SCZ, and TSCZ was determined.
- (3) The FRP-PCM method can effectively reduce the plastic failure zone of the tunnel lining with compound defects. As the grade of the FRP grids increases, the failure rate shows a non-linear decrease trend. The safety state of tunnel linings exhibits a positive relationship with the grade of the FRP grids.
- (4) The FRP-PCM method and backfill method can effectively optimize the time-dependent properties of mechanics and deformation of linings with compound defects. Although the proportion of plastic failure at the defect zone increases with time, effective optimization can be obtained by the FRP-PCM method and backfill method.

References

- Ceroni F. Experimental performances of RC beams strengthened with FRP materials. *Construction and Building Materials*, 2010, 24(9), 1547-1559.
- Chajes MJ, Thomson TA, Januszka TF, Finch WW. Flexural strengthening of concrete beams using externally bonded composite materials. *Construction and Building Materials*, 1994, 8(3), 191-201. [https://doi.org/10.1016/s0950-0618\(09\)90034-4](https://doi.org/10.1016/s0950-0618(09)90034-4)

- Chen HB, Xu B, Wang J, Nie X, Mo YL. XFEM-Based Multiscale Simulation on Monotonic and Hysteretic Behavior of Reinforced-Concrete Columns. *Applied Sciences*, 2020,10(21), 7899. <https://doi.org/10.3390/app10217899>
- Esfahani MR, Kianoush MR, Tajari AR. Flexural behavior of reinforced concrete beams strengthened by CFRP sheets. *Engineering Structures*, 2007, 29(10), 2428-2444 <https://doi.org/10.1016/j.engstruct.2006.12.008>
- FRP Grid Method Association of Japan. Design and construction manual of the Repair & reinforcement method for RC structures by FRP grid [O/L], <http://www.frp-grid.com/01.html>
- Gao Y, Jiang YJ, Li B. Voids delineation behind tunnel lining based on the vibration intensity of microtremors. *Tunnelling and Underground Space Technology*, 2016, 51, 338-345. <https://doi.org/10.1016/j.tust.2015.10.032>.
- Guo R, Hu WH, Li MQ, Wang B. Study on the flexural strengthening effect of RC beams reinforced by FRP grid with PCM shotcrete. *Composite Structure*, 2020, 239, 112000. <https://doi.org/10.1016/j.compstruct.2020.112000>
- Guo R, Pan Y, Cai LH, Hino S. Bonding behavior of CFRP grid-concrete with PCM shotcrete. *Engineering Structures*, 2018a, 168, 333-345.
- Guo R, Pan Y, Cai LH, Hino S. Study on design formula of shear capacity of RC beams reinforced by CFRP grid with PCM shotcrete method. *Engineering Structures*, 2018b, 166, 427-440. <https://doi.org/10.1016/j.engstruct.2018.03.095>
- Han W, Jiang YJ, Luan HJ, Du YT, Zhu YG, Liu JK. Numerical investigation on the shear behavior of rock-like materials containing fissure-holes with FEM-CZM method. *Computers and Geotechnics*, 2020, 125, 103670.
- Higashi Y. Reinforcement Effect and Design Analysis Model of FRP Grid for Deformation Tunnel. Ph.D. Thesis, Nagasaki University, Nagasaki, 2014.
- Higashi Y, Li B, Jiang YJ. Analytical Evaluation of Tunnel Reinforcement Effect by PCM shotcrete Method Using FRP Grid. *Journal of the Society of Materials Science, Japan*, 2014, 63, 451-458. <https://doi.org/10.2472/jsms.63.451>
- Hu K, Feng Q, Li H, Hu Q. Study on Creep Characteristics and Constitutive Model for Thalam Rock Mass with Fracture in Tunnel. *Geotechnical and Geological Engineering*, 2018, 36, 827-834. <https://doi.org/10.1007/s10706-017-0357-y>
- Jiang YJ, Wang XS, Li B, Higashi Y, Taniguchi K, Ishida K. Estimation of reinforcing effects of FRP-PCM method on degraded tunnel linings. *Soils and Foundations*, 2017, 57(3), 327-340. <https://doi.org/10.1016/j.sandf.2017.05.002>

- Jiang YJ, Zhang XP. Evaluation of reinforcement effect of FRP-PCM method in tunnel lining. *Hazard Control in Tunnelling and Underground Engineering*, 2020, 2(1), 11-19.
- Jiang HX, Meng DG. 3D numerical modelling of rock fracture with a hybrid finite and cohesive element method. *Engineering Fracture Mechanics*, 2018, 199, 280-293.
<https://doi.org/10.1016/j.engfracmech.2018.05.037>
- Kargar AR, Haghgouei H, Babanouri N. Time-dependent analysis of stress components around lined tunnels with circular configuration considering tunnel advancing rate effects. *International Journal of Rock Mechanics and Mining Sciences*, 2020, 133, 104422. <https://doi.org/10.1016/j.ijrmms.2020.104422>
- Li J, Fang Y, Liu C, Zhang, Y, Lu W. Performance investigation of tunnel lining with cavities around surrounding rocks. *Advances in Civil Engineering*, 2020, 2020, 1364984.
- Liu C. Study on mechanical characteristics of tunnel structure under the condition of void behind arch lining. Master's Thesis, Qingdao University of Technology, Qingdao, 2018.
- Meguid MA, Dang HK. The effect of erosion voids on existing tunnel linings. *Tunnelling and Underground Space Technology*, 2009, 24(3), 278-286.
<https://doi.org/10.1016/j.tust.2008.09.002>
- Ministry of Transport of the PRC. Code for Design of Road Tunnel, JTG D70-2004, 2004.
- She J, He C, Wang B, Wang Y. Study on Effect of Cavities behind Linings on Bearing Capacity of Tunnel Structure by Model Test. *Journal of Highway and Transportation Research and Development*, 2008, 25, 104-110.
- Technical Committee on FRP grid method. Reinforcement method by FRP grid for concrete structure; Manual of design and construction (draft) Technical Committee on FRP Grid Method, 2007.
- Wang B, Li TB, He C, She J. Model Test of Effect of Lining Thinning on Tunnel Structure Bearing Capacity. *Journal of the China Railway Science*, 2013, 35, 106-114.
- Wang B, Wang ZP, Uji K, Zhang JL, Guo R. Experimental investigation on shear behavior of RC beams strengthened by CFRP grids and PCM. *Structures*, 2020, 27, 1997-2010. <https://doi.org/10.1016/j.istruc.2020.07.050>
- Wang JF, Huang HW, Xie XY, Bobet A. Void-induced liner deformation and stress redistribution. *Tunnelling and Underground Space Technology*, 2014, 40, 263-276.
<https://doi.org/10.1016/j.tust.2013.10.008>

- Wang W, Li G. Experimental study and analysis of RC beams strengthened with CFRP laminates under sustaining load. *International Journal of Solids and Structures*, 2006, 43(6), 1372-1387. <https://doi.org/10.1016/j.ijsolstr.2005.03.076>
- Yang P. Risk Assessment on the Defects behind Lining of Road Tunnels. *China Safety Science Journal*, 2011, 21, 130-135.
- Yao CC, Yu HL, Zhang Y. Method of solving the safety factor of lining strength based on FLAC3D software. *Sichuan Architecture*, 2007, 27(2), 115-116. (in Chinese)
DOI: 10.3969/j.issn.1007-8983.2007.02.050
- Yasuda N, Tsukada K, Asakura T. Elastic solutions for circular tunnel with void behind lining. *Tunnelling and Underground Space Technology*, 2017, 70, 274-285.
<https://doi.org/10.1016/j.tust.2017.08.032>
- Yin H, Liu Z, Guo Y. Analysis of stress characteristics of lining structure under the influence of combined defects. *Journal of Railway Science and Engineering*, 2020, 17(8), 2037-2045.
- Yu L, Bai SJ, Liu XX, Chen L, Bao LS. Study on the influence of tunnel lining thickness on bearing capacity of lining. *Journal of Shenyang Jianzhu University (Natural Science)*, 2017, 33(6), 1039-1047.
- Zhang CP, Feng G, Zhang X, Han KH, Zhang DL. Effect of double voids behind the lining of safety state of tunnel structure. *Chinese Journal of Geotechnical Engineering*, 2015, 37, 487-493.
- Zhang CP, Zhang X, Feng G, Zhang DL. Influence of Insufficient Lining Thickness on the Safety of a Tunnel Structure. *Modern Tunnelling Technology*, 2017, 54, 137-143.
- Zhang FW, Dai JG, Wang ZL, Wang MQ, Leng YB, Xu QF. Bond durability of epoxy and cement- bonded CFRP reinforcement to concrete interfaces subject to water immersion. *Materials and Structures*, 2021, 54, 53.
<https://doi.org/10.1617/s11527-021-01641-w>
- Zhang SL, Qi XQ, Liu C, Chen DG. Distribution characteristic of voids behind the lining of highway tunnel and its influence on lining structure. *Journal of Architecture and Civil Engineering*, 2020, 37(2), 62-70.

6 Dynamic response of tunnel structures with quality defects of void and lining defect

6.1 Introduction

Recent earthquakes, such as the 2008 Wenchuan earthquake in China (Shen et al. 2014; Li 2012), and the 2016 Kumamoto earthquake in Japan (Zhang et al. 2018; Zhang et al. 2019), caused severe damage to tunnel structures. The dynamic effect, such as ground explosion (Yang et al. 2010), and earth motions (Kirzhner and Rosenhouse 2000), present a noticeable impact on the stability of tunnels. Unfortunately, tunnel quality defects frequently occur in tunnels, resulting in the lining being more susceptible to damage under dynamic action (Xin et al. 2018). Therefore, it is crucial to clarify the dynamic response of tunnel linings with quality defects and determine effective reinforcement methods.

Concerning the dynamic behaviors of tunnel structures, Yasuda et al. (2019) theoretically explored the three-dimensional seismic response of the tunnel structure with the void defect. Jones and Hunt (2011) developed a semi-analytical method for the coupling model of tunnel-soil considering the void defect on ground vibration. Xin et al. (2018) conducted shaking table tests of the scaled tunnel with void defects under the seismic loading, and the effect of voids on damage behaviors was focused on. Yan et al. (2019) carried out shaking table tests of tunnel structures with void defects, and the damage patterns of lining structures were investigated. Zhu et al. (2015) explored the effect of void location, void size, grade of rock mass, and tunnel depth on the seismic response of tunnel structures. In addition, Shen et al. (2014) conducted a field investigation on the damage behaviors of mountain tunnels after the Wenchuan earthquake. Jiang et al. (2014) explored the effect of tunnel depth on the seismic response of mountain tunnels, and the peak acceleration and displacement under different tunnel depths were mainly investigated. Chen et al. (2010) conducted a series of shaking table tests to explore the seismic characteristics of tunnels under non-uniform earthquake waves.

Regarding the reinforcement techniques of tunnel structure under earthquakes, Li (2014) applied rock bolts to reinforce the working faces of tunnel structure, and the

influence of distributed density of rock bolts on the reinforcement effect was investigated. Zhu et al. (2014) used various methods such as the grouting reinforcement ring method, shock absorption layer method, and ultra-excavation method to explore the reinforcement effect of tunnel structures under seismic load. Cui et al. (2014) determined the repair technologies for seismic damage of tunnel linings with three stages, and some typical reinforcement methods such as shotcrete, fiber composite material, and arch reinforcement were applied. In addition, various techniques have been applied to ensure the serviceability of the structure, such as the fiber-reinforced concrete method (Li et al. 2017; Guler et al. 2019; Jeon et al. 2016; Guler and Yavuz 2019; Jeng et al. 2002; Guler et al. 2021), the carbon fiber sheet method (Lee and Lee 2002), the steel arch method (Dong et al. 2017), spray slurry method (Jiang and Fan 2016), and the fiber-reinforced plastic (FRP) method (Gaurav and Singh 2018, Mofidi and Chaallal 2014; Jiang et al. 2017). Concerning the reinforcing effect of FRP composites on reinforced concrete (RC), Brunton et al. (2012) conducted punching shear tests to assess the shear capacity of concrete decks reinforced by FRP grids. Maalej and Leong (2005) experimental investigated the interfacial shear stress, and the failure modes of RC beams strengthened in flexural with FRP composites. Rabia et al. (2019) investigated the effect of the porosity on the shear interfacial stresses of the beam strengthened with FRP composites, and the reinforcing effect was also clarified. Fang et al. (2016) conducted a four-point bending experiment of composite concrete slabs reinforced by FRP grids, and the effects of FRP grid rib spacing, grid rib height, and sheet thickness were considered. In addition, other investigations indicated that beams reinforced by FRP can obtain good performance (Sumathi and Arun 2017, Setvati and Mustaffa 2018). Concerning the reinforcing effect of the FRP-PCM method, Jiang et al. (2017) conducted laboratory direct shear tests and bending tests to investigate the bonding behavior between the PCM and the concrete reinforced by the FRP grids, and three grades of CFRP grids (CR4, CR6, and CR8) were considered. Guo et al. (2018) proposed a new evaluation method for the shear capacity of RC beams reinforced by the FRP-PCM method, and the effect of the arrangement of the FRP grids was investigated. In addition, Wang et al. (2021) evaluated the reinforcement effect of the FRP-PCM method on tunnel linings under dynamic loading from the perspectives of plastic failure zone and axial stress distribution.

Currently, the dynamic response of tunnel structures has been widely investigated,

while information on systematically revealing the effects of quality defects is rather limited. In addition, the FRP-PCM method, as a promising strengthening technique, has been widely applied for the reinforcement of degraded tunnel structures. However, previous studies mainly focus on the reinforcement effect under static conditions, and the reinforcement effect under dynamic conditions is rare. Therefore, its application should be further discussed and evaluated. Overall, the focus of this chapter is to systematically explore the dynamic response and the reinforcement behaviors of tunnel structures with quality defects.

6.2 Numerical model

6.2.1 *Model establishment*

The numerical model established in this chapter can be shown in Fig. 6.1. Concerning the size of the numerical model, the cross-section of the tunnel structure can be obtained from the Ministry of Transport of the PRC (Ministry of Transport of the PRC 2004). The horizontal distance from the tunnel wall to the model boundary was determined as two times the excavation diameter, which was applied by Wang et al. (2021). In this chapter, the effect of tunnel quality defects on the dynamic response of tunnel structures was explored. The distribution of defects in this chapter can be presented in Fig. 6.2(a). The defect types can be divided into void defects and lining defects. It should be indicated that the void defect is caused by the rock mass defect in the established model, while the lining defect is induced by insufficient lining thickness. Due to the effect of defect shape on the dynamic response of tunnel structures is not the focus of this chapter, the defect shapes of voids and lining defects are unified. The lining structure is divided into two layers to facilitate defect modeling. Specifically, the outermost layer is the potential area where the thickness of the lining is insufficient. Similarly, the rock mass is divided into one layer of the same thickness, which is regarded as the potential area of the void defect. In addition, several measuring points were arranged to determine the dynamic response characteristics at typical locations, and the distribution can be shown in Fig. 6.2(b).

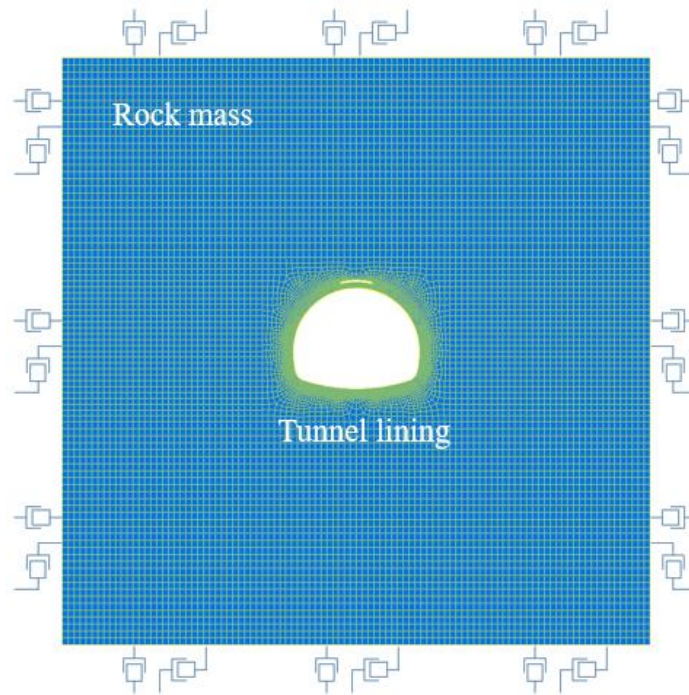


Fig. 6.1 Numerical analysis model.

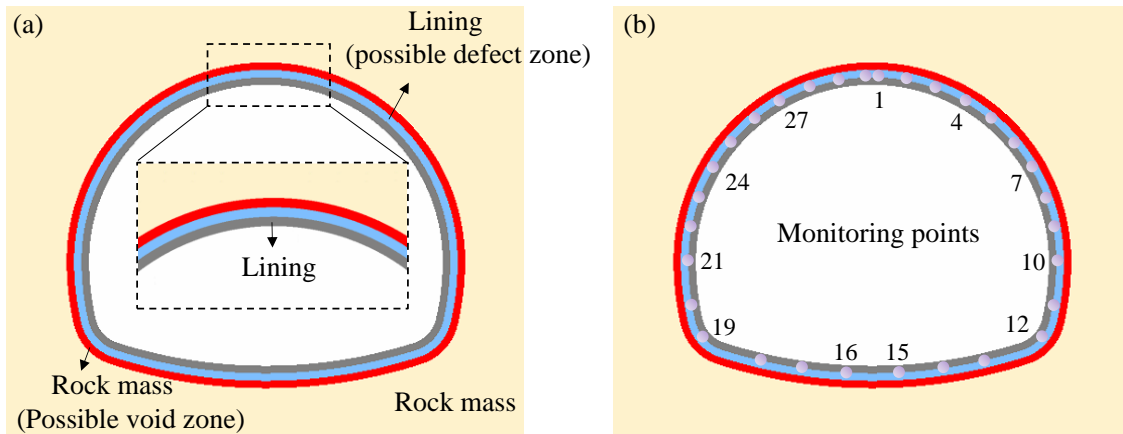


Fig. 6.2 Model arrangement: (a) distribution of tunnel quality defects; (b) monitoring points.

6.2.2 Calculation conditions

The boundary conditions in the dynamic analysis are different from the static calculation boundary. In the static calculation, the left and right boundaries of the model should be fixed horizontally, and the lower boundary should be fixed (Wang 2017). Concerning the boundary conditions for the model of seismic analysis, the free-field boundary conditions were applied in the seismic analysis and simulated by viscous dashpots (Wang 2017; Wang et al. 2021; Itasca Consulting Group 2002). Concerning the

reinforcement techniques of tunnel lining under dynamic load, three methods were mainly applied, the backfill method, FRP-PCM method, and the combined method of FRP-PCM and backfill, respectively. Specifically, the backfill material of urethane can be applied to fill the defect zone due to its favorable properties, such as quick hardening and high strength (Jiang et al. 2017). In addition, the FRP-PCM method was utilized to reinforce the upper inner wall of tunnel linings. Concerning the constitutive model, the Mohr-Coulomb failure criterion was applied to describe the mechanical property of the ground, and the elastic material was set for the lining structure. The corresponding materials of rock mass (CII), tunnel linings, the FRP-PCM, and the backfill can be obtained in Table 4.1 (Jiang et al. 2017) and Table 4.2 (Jiang et al. 2017).

6.2.3 Input motion

Since the established model is a two-dimensional plane strain problem, two vibration directions of the input wave, horizontal and vertical, should be considered. In this section, microseism and strong seismic were considered separately to clarify the dynamic response. The Gaussian white noise (Kushnir et al. 2014) was often concerned in previous research, and the applied microseism of Gaussian white noise, which can be generated from MATLAB, can be shown in Fig. 6.3. The typical El Centro seismic (United States Geological Survey, Report of CALTEC 1971; Malhotra 2001) was applied as the strong seismic as shown in Fig. 6.4 (National Strong-Motion Program, United States Geological Survey). In addition, the dynamic waves are processed with zero drift before being applied to the numerical model to improve the integral performance of wave records (Li and Yang 2010).

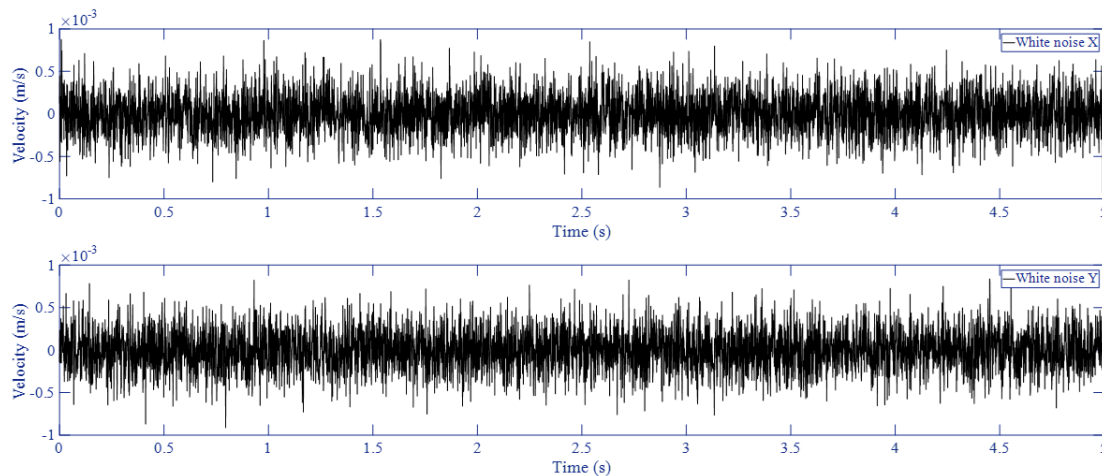


Fig. 6.3 Curve of velocity-time history of Gaussian white noise.

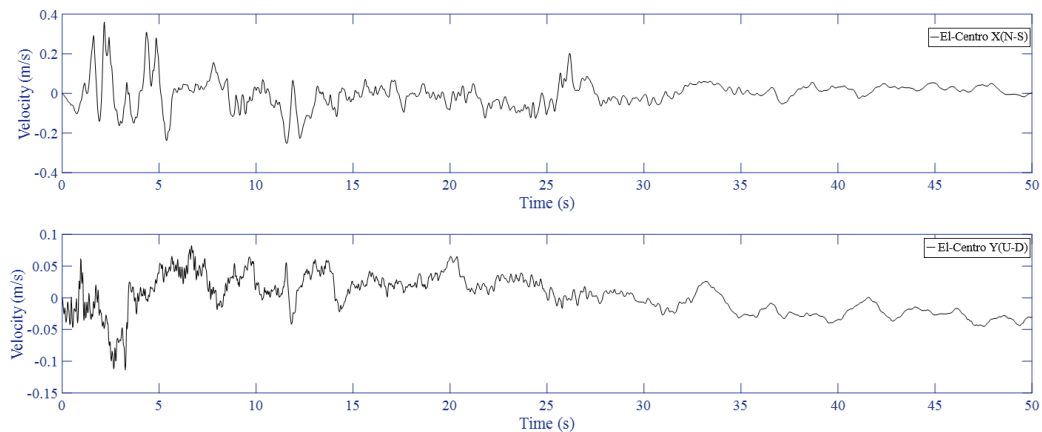


Fig. 6.4 Processed velocity history of El Centro applied to the numerical model (National Strong-Motion Program, United States Geological Survey).

6.3 Mechanical and physical properties

6.3.1 Characteristics of principal stress

In this section, the effect of void range on principal stress of defective linings under El-Centro was investigated, as presented in Fig. 6.5. When there is no void behind the lining, most of the lining is under compression, and the obvious compressive stress concentration occurs in the arch springing. When there is a void behind the lining, an obvious tensile stress concentration is observed on the outside of the lining corresponding to the void zone. In addition, as observed in the model, the degree of tensile stress concentration presents a significant positive relation with the void range. Taking the void range of 60° as an example, the edge of the inner surface of the lining corresponding to the void zone exhibits a significant tensile effect. As a result, the void range significantly affects the stress distribution. When the defective tunnel lining was reinforced with the FRP-PCM and backfill method, the principal stress distribution can also be presented in Fig. 6.5. The reinforcement measures can significantly reduce the stress concentration characteristics. To verify the correctness of the established model, it is meaningful to conduct a comparative analysis with other research results. Nie et al. (2015) explored the influence of void on the seismic performance of the tunnel structure using ABAQUS, and the distribution of stress and plastic zone was investigated. The stress distribution between Fig. 6.6(a) (this study) and Fig. 6.6(b) (Nie et al. 2015) is compared. It can be observed that the effects of voids are similar, which verifies the rationality of the numerical results in this study.

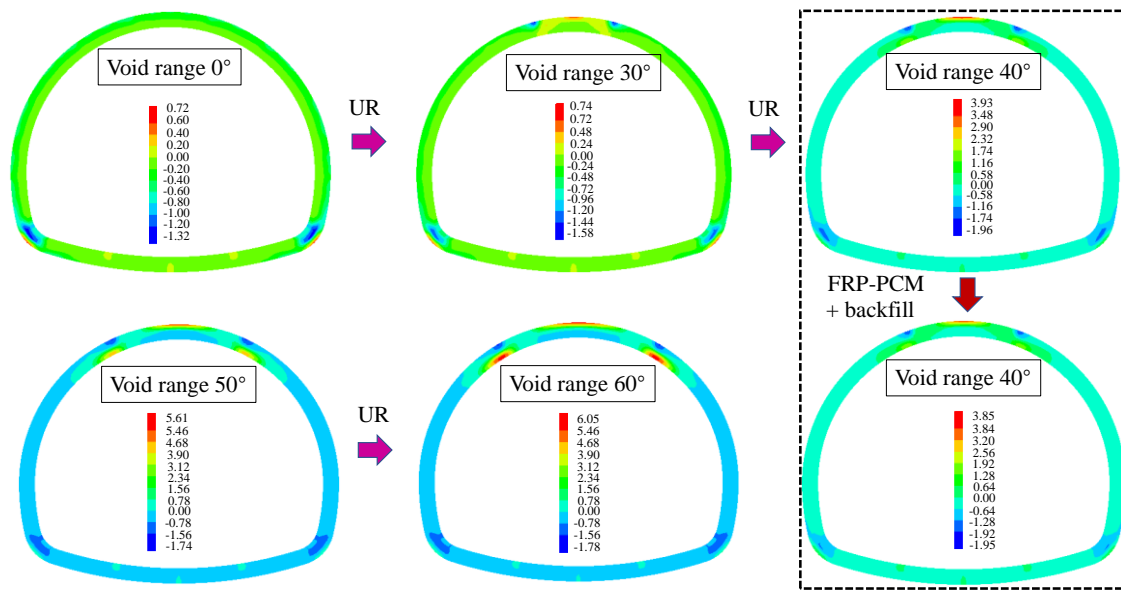


Fig. 6.5 Effect of void range on the distribution of principal stress (Unit: MPa).

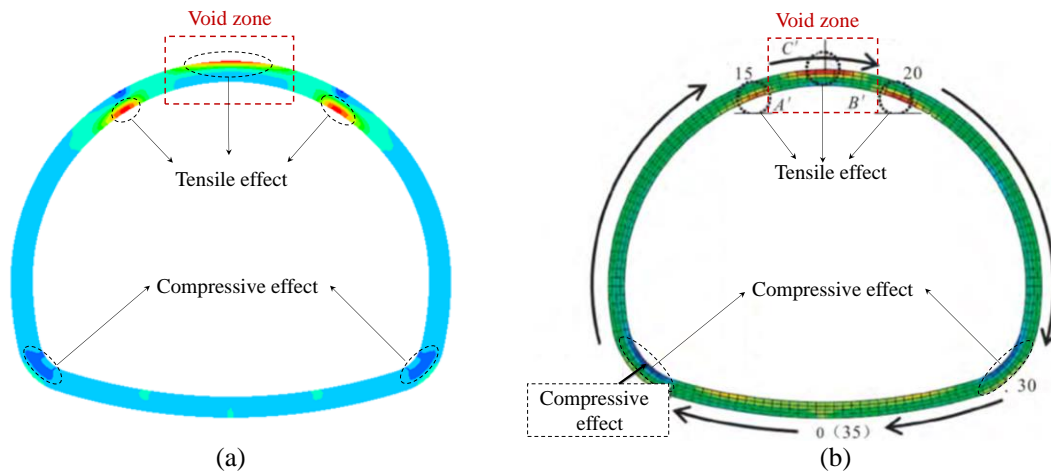


Fig. 6.6 Stress distribution of linings with void defects under earthquake: (a) results of this study; (b) results of stress distribution (Nie et al. 2015).

6.3.2 Characteristics of maximum shear stress

The effect of void range on the distribution of maximum shear stress under the El-Centro was explored, as exhibited in Fig. 6.7. When there is no void, the maximum shear stress occurs at the inner side of the arch springing. When there is a void behind the lining, a significant stress concentration phenomenon occurs at the inner side of the lining corresponding to the void zone. In addition, the maximum shear stress positively correlates with the void range. The effect of reinforcement methods of FRP-PCM and

backfill was also explored and exhibited in Fig. 6.7. Regarding the reinforcement effect of the lining structure with a void range of 40° , the maximum shear stress can be reduced.

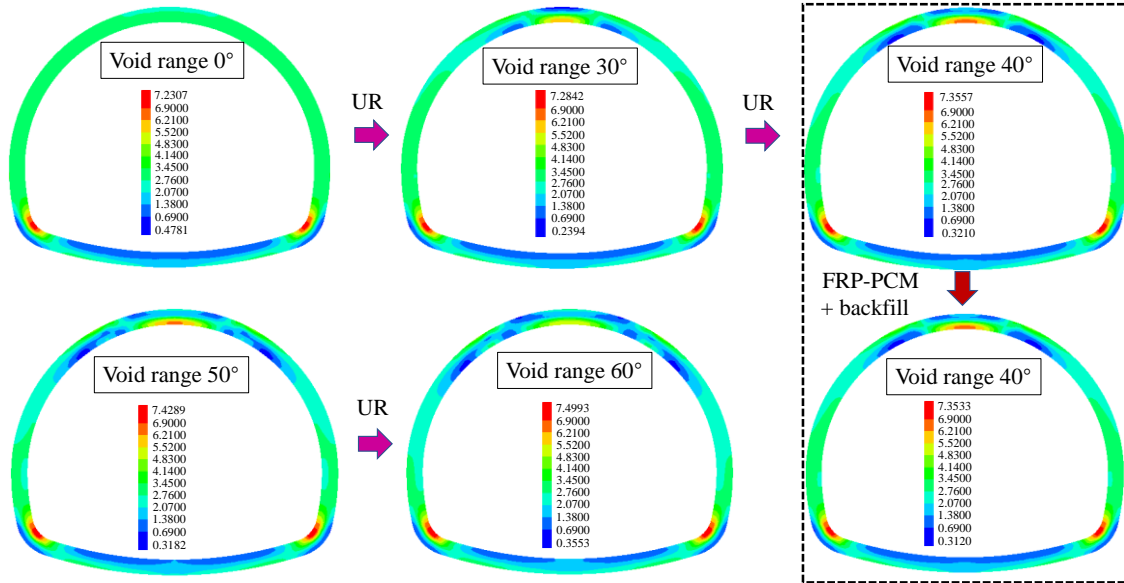


Fig. 6.7 Effect of void range on the distribution of maximum shear stress (Unit: MPa).

6.3.3 Distribution of peak acceleration

6.3.3.1 Effect of defect type

In this section, the effect of defect type on the peak acceleration under the white noise was investigated, as shown in Fig. 6.8. The location of the void defect and lining defect was set at the crown, and the defect range was 40° . As presented in Fig. 6.8, the peak acceleration exhibits significant differences at various positions of the intact lining. Specifically, in the established model, the peak acceleration is relatively small at the crown and shoulder but large at the arch springing and inverted arch. In addition, the distribution of peak acceleration is greatly affected by defects and is also closely related to the type of defects. Specifically, the peak acceleration in the void and lining defect affected zone increases significantly compared with that of the intact lining, and the increase of void defects is greater than that of the lining defect. However, for the peak acceleration in the non-defect area, the peak acceleration under the void defect is significantly larger than that of the lining defect and is basically larger than the peak acceleration of the intact lining. While for the lining defect, the peak acceleration in the non-defect zone is smaller than that of the intact lining. In addition, although the tunnel quality defects are distributed symmetrically along with the crown in the established

model, the peak acceleration is not strictly symmetrical. The main reason for this phenomenon is that the distribution of the model mesh is not entirely symmetrical.

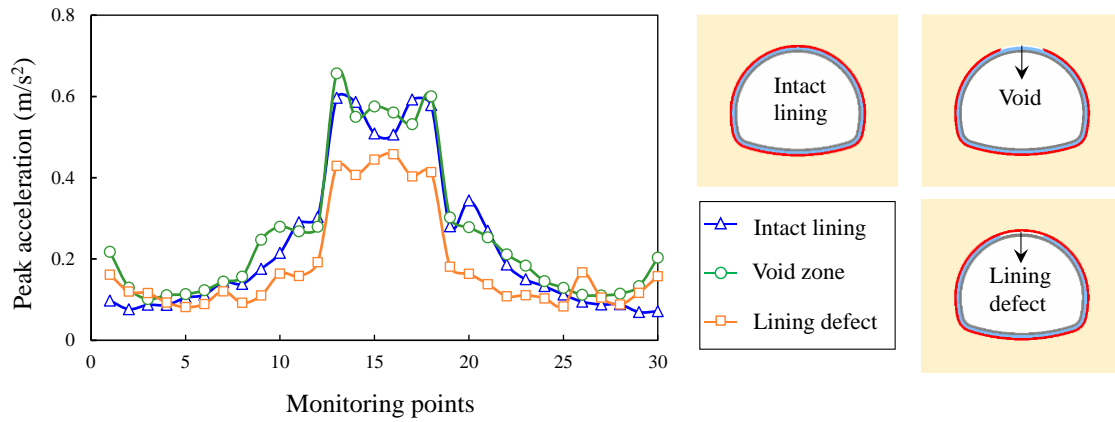


Fig. 6.8 Influence of types of tunnel quality defects on peak acceleration.

6.3.3.2 Effect of void range

In this section, the effect of void range on the distribution of peak acceleration was explored and shown in Fig. 6.9. The void location was set at the crown, and the void range was 0° , 40° , and 50° , respectively. When the tunnel structure is under the action of Gaussian white noise, as exhibited in Fig. 6.9(a), the peak acceleration roughly increases with the increase of the void range within the defect zone. For example, when the void range is 0° , the peak acceleration is 0.098m/s^2 at measure point 1, but 0.218 m/s^2 for the void range of 40° and 0.309 m/s^2 for the void range of 50° . There is no significant positive correlation between peak acceleration and void range regarding the regions outside the void zone. On the contrary, there is a downward trend in some measuring points, indicating that the impact of voids on the peak acceleration is mainly concentrated near the defect zone. The effect of the void range on the peak acceleration under El-Centro can be displayed in Fig. 6.9(b). It is observed that the impact of the void range on peak acceleration is similar to that of the white noise. The peak acceleration roughly increases with the increase of the void range within the defect zone except for a few individual monitoring points. However, as for other areas outside the void-affected zone, the void range does not significantly affect the peak acceleration. With the comparison between Fig. 6.9(a) and Fig. 6.9(b), the peak acceleration at specific measuring points exhibits a significant increasing trend under the El-Centro. In addition, taking the intact lining as an example, the peak acceleration at the inverted arch is about five times that of the crown for the white noise, while only about two times for the EI Centro. This shows that the dispersion degree of the peak acceleration along the lining structure is relatively large

under the white noise.

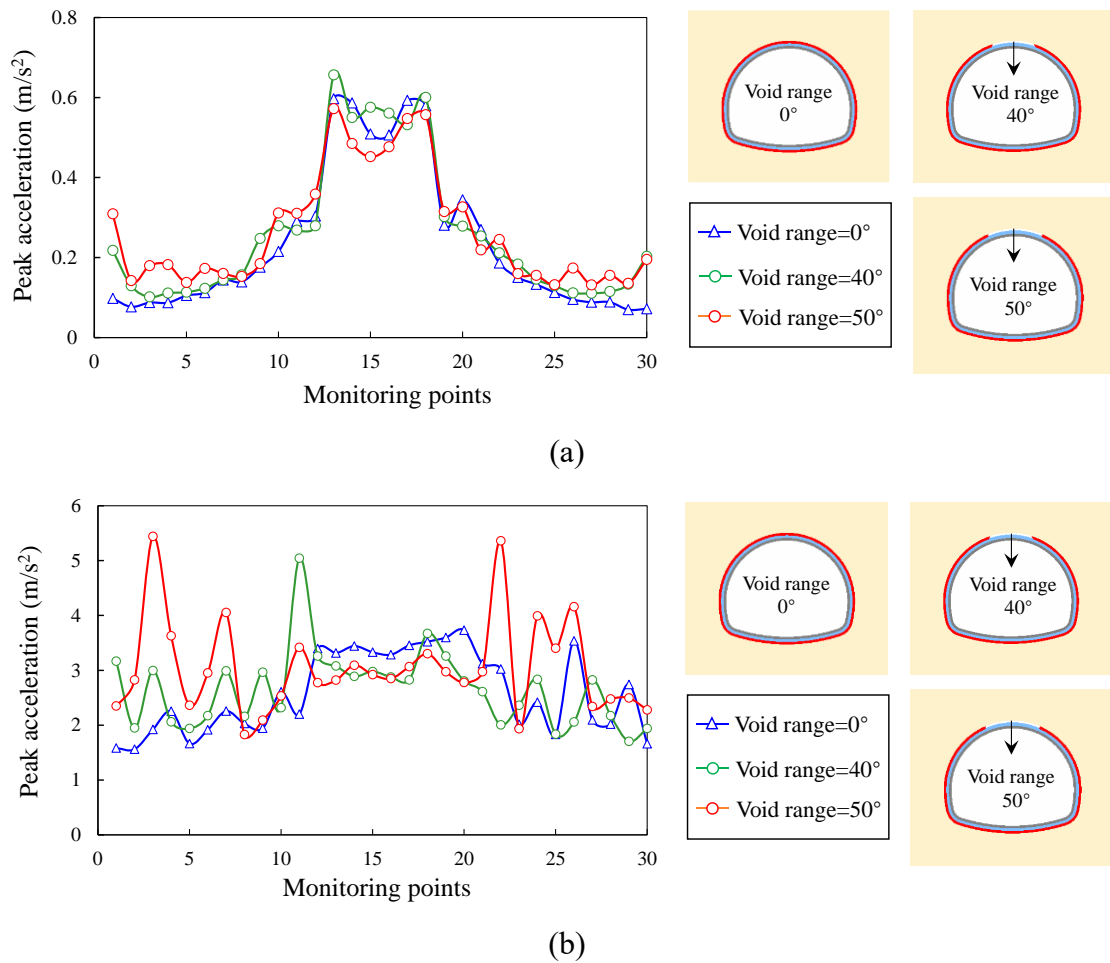


Fig. 6.9 Effect of void range on peak acceleration: (a) White noise; (b) El-Centro.

6.3.4 Distribution of peak velocity

6.3.4.1 Effect of defect type

In this section, the effect of defect type on the peak velocity along the lining structure under the white noise was explored, as shown in Fig. 6.10. The location of the tunnel defect was set at the crown, and the defect range was 40° . Concerning the intact lining, the peak velocity is relatively small at the crown and shoulder but large at the arch springing and inverted arch. When there are typical quality defects in the tunnel structure, the distribution of peak velocity can be significantly affected. Specifically, as for the measuring points 1 and 30 within the defect zone, the peak velocity of the lining in descending order is the void, lining defect, and intact lining. The main reason for this phenomenon is that the void quality defect eliminates the local elastic resistance between

the rock mass and the lining structure. However, in the non-defect area, the peak velocity of the lining structure at specific measuring points exhibits a uniform law, which are voids, intact linings, and lining defects in descending order. Overall, lining defects cause peak velocities to increase at specific measuring points in defect areas and decrease in non-defect areas. However, the main difference is that void defects lead to an increase in the peak velocity at particular measurement points. Therefore, it can be observed that the defect type significantly affects the distribution of peak velocity.

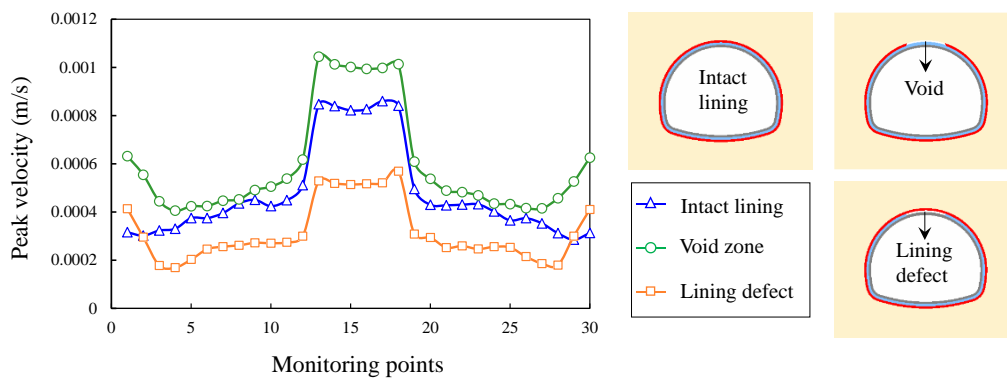


Fig. 6.10 Effect of defect type on the distribution of peak velocity.

6.3.4.2 Effect of void range

The effect of void range on the distribution of peak velocity can be shown in Fig. 6.11. When the tunnel structure is under the action of white noise, as exhibited in Fig. 6.11(a), the peak velocity within the defect zone roughly increases with the increase of the void range. For example, regarding the measuring point 1, when the void range is 0° , 30° , 40° , and 50° , the peak velocity is 0.00032m/s, 0.00039m/s and 0.00063m/s, and 0.00066m/s, respectively. Concerning the non-defect zone, the peak velocity is roughly improved but exhibits a non-strictly positive correlation with the void range. This is due to the limited effect of the void, resulting in less impact at locations farther from the void. Analogously, the distribution of peak velocity under the action of the El-Centro can be presented in Fig. 6.11(b). The effect of void range on peak velocity is similar to that of the white noise. Specifically, when void range is 0° , 30° , 40° , and 50° , the peak velocity is 0.10256 m/s, 0.10258 m/s, 0.10291m/s, and 0.10307m/s for measuring point 1, respectively. The peak velocity is 0.10120 m/s, 0.10226m/s, 0.10265m/s, and 0.1028m/s for measuring point 2, respectively. The peak velocity is 0.10199 m/s, 0.10224m/s, 0.10259m/s, and 0.10274m/s for measuring point 3. Consequently, the peak velocity in the void-affected zone positively correlates with the void range. With the comparison between Fig. 6.11(a) and

Fig. 6.11(b), the peak velocity increases significantly under the El-Centro. In addition, through the effect of void range on the dispersion degree of peak velocity, it can be seen that under the El-Centro, the void range presents less sensitivity than that of the white noise.

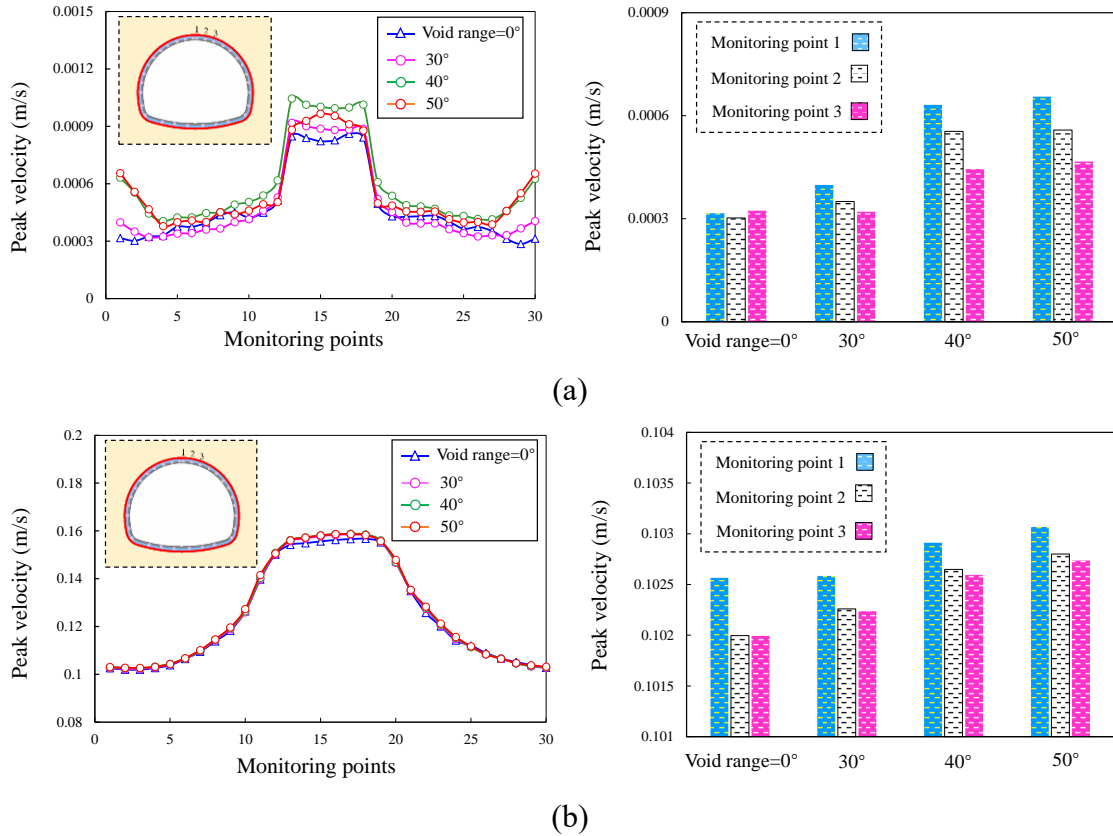


Fig. 6.11 Effect of void range on the peak velocity: (a) White noise; (b) El-Centro.

6.3.4.3 Effect of void location

In this section, the effect of void location on the distribution of peak velocity was explored. Four void locations were selected, as presented in Fig. 6.12. The distribution of peak velocity can be illustrated in Fig. 6.13. When the tunnel structure is under white noise, as exhibited in Fig. 6.13(a), the void location significantly affects the peak velocity. The maximum peak velocity of specific measuring points is consistent with the void location. Taking the measuring points 4 and 7, located in the center of the void, as examples, the peak velocity for the void location of 0° , 30° , 60° , and 90° at measuring point 4 is 0.000405m/s , 0.000502m/s , 0.000309m/s , and 0.000471m/s for the void location of 0° , 30° , 60° , and 90° . The maximum peak velocity is identified as the void location of 30° . Concerning the measuring point 7, the peak velocity is 0.000447m/s , 0.000296m/s , 0.000743m/s , and 0.000502m/s for the void location of 0° , 30° , 60° , 90° .

The maximum peak velocity is determined as the void location of 60° . Analogously, the effect of void location on the distribution of peak velocity under the El-Centro can be presented in Fig. 6.13(b). Note that the sensitivity of the void location to the peak velocity is smaller than that of the white noise. Similarly, four specific measuring points were applied to investigate the distribution of peak velocity. Except for measuring point 2, the maximum peak velocity of the specific measuring points is consistent with the void location. The main reason for this phenomenon is that under the action of strong seismic, the influence of void location on peak velocity becomes insignificant.

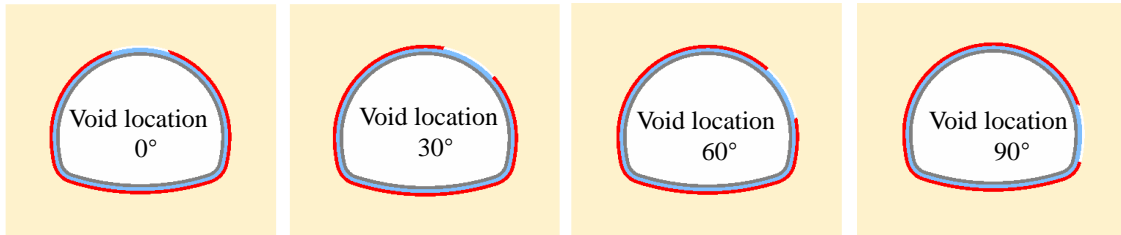


Fig. 6.12 Distribution of void location.

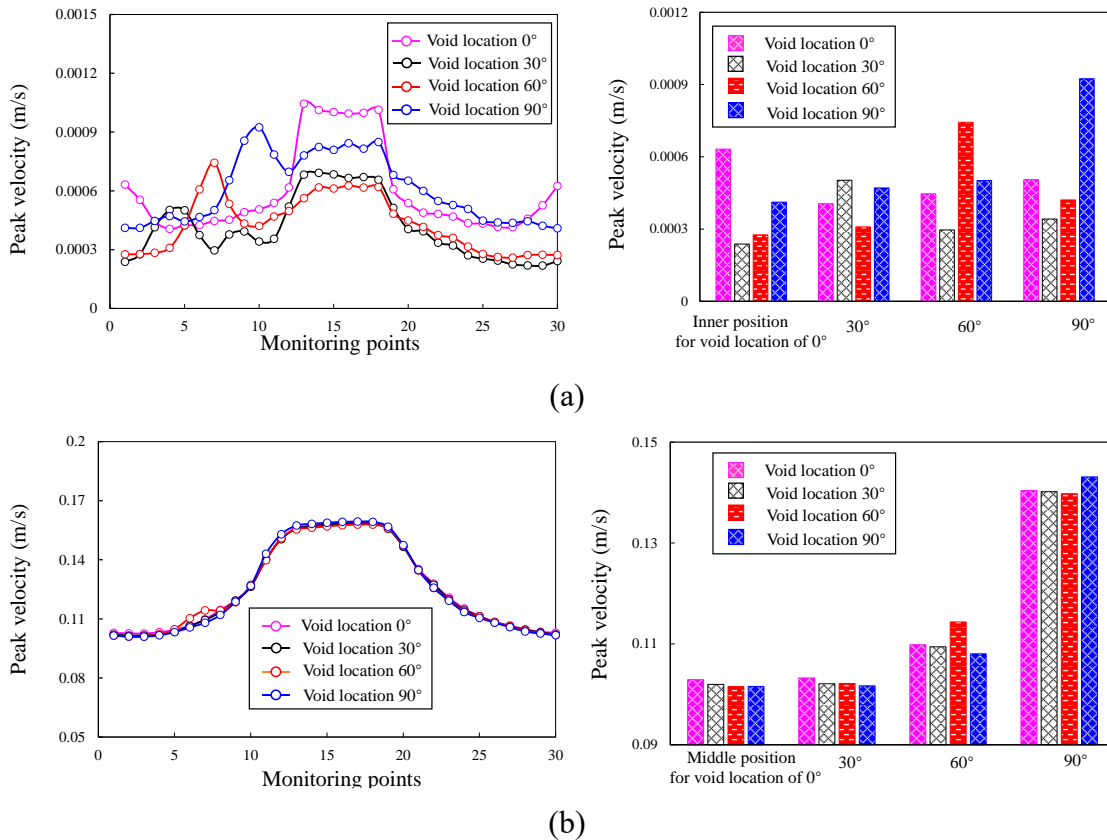


Fig. 6.13 Effect of void location on the peak velocity: (a) White noise; (b) El-Centro.

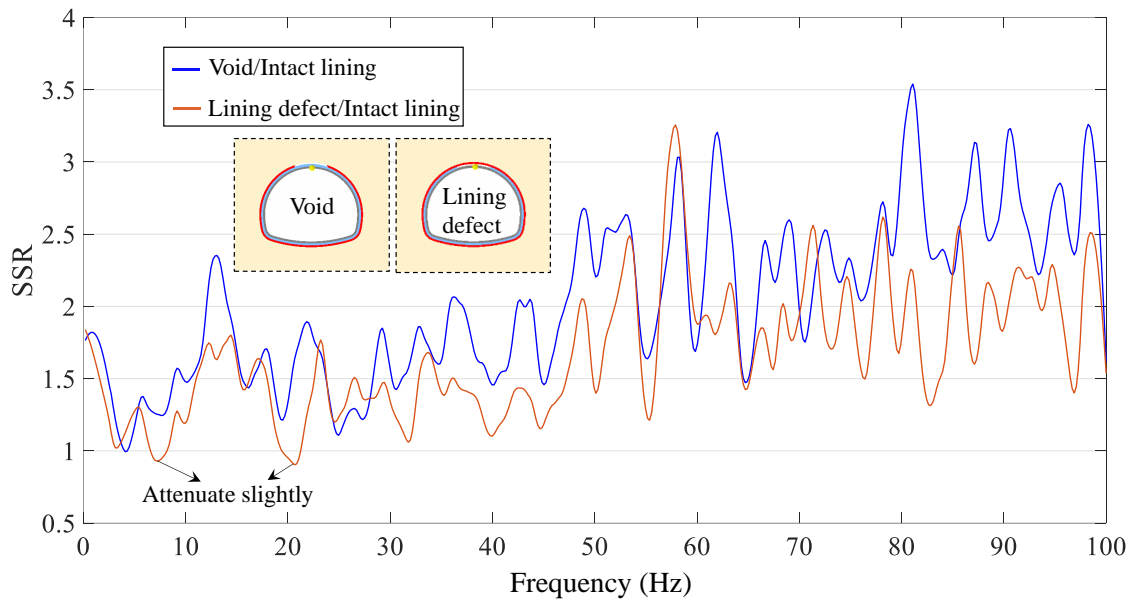
6.4 Distribution of spectrum characteristic analysis

6.4.1 Characteristics of acceleration SSR

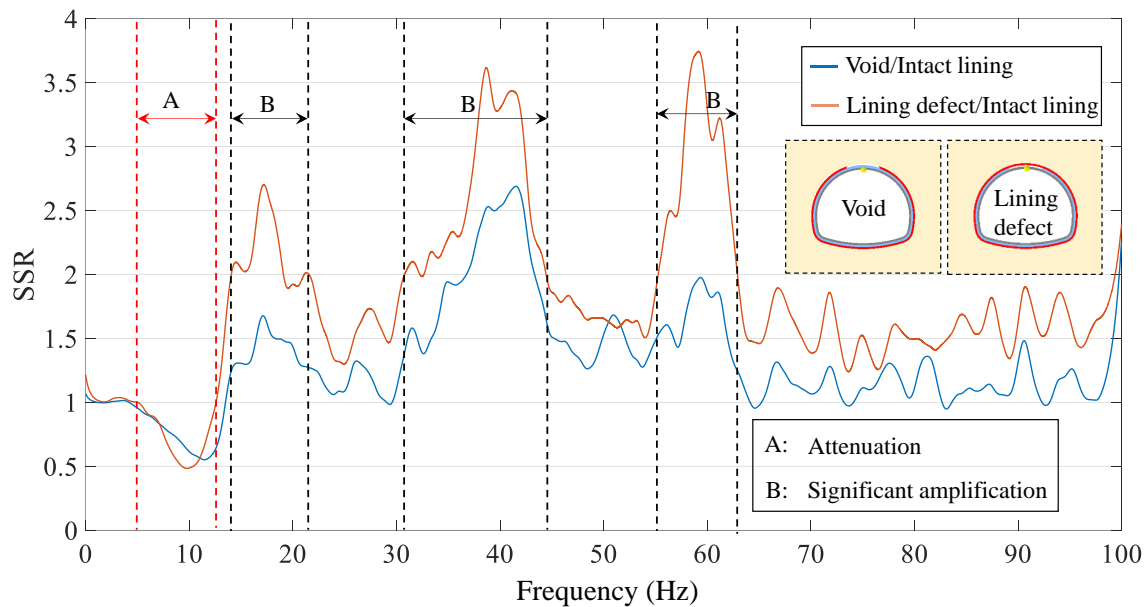
6.4.1.1 Effect of defect type

The Standard Spectral Ratio (SSR) technique, introduced by Borchardt (1970), can be regarded as the widely applied standard reference site technique (Mittal et al. 2013). The SSR represents a scaled value of amplification relative to a certain input signal (Borchardt 1970). The frequency domain was obtained from the time domain by the Fourier Transform (Bracewell 1986; Mateo and Talavera 2018). In this section, the effect of the type of tunnel quality defects on the distribution of SSR was investigated, as presented in Fig. 6.14. The acceleration SSR in this section is the ratio of the dynamic response of the defective lining structure to that of the intact lining structure. In this model, the dynamic response of the tunnel structure is amplified when $SSR > 1$ but attenuated when $SSR < 1$. The characteristics of acceleration SSR under the effect of Gaussian white noise can be presented in Fig. 6.14(a). When the frequency is around 7Hz and 21Hz, the dynamic response at the crown tends to attenuate for the defect type of lining defect. However, concerning the dynamic response at other frequencies, the dynamic response intensity tends to amplify whether it is a void defect or a lining defect. In addition, when the frequency domain is in the range of 0Hz-100Hz, the increase in the dynamic response of the void defect is roughly larger than that of the lining defect. Regarding the distribution of acceleration SSR under the El-Centro, as presented in Fig. 6.14(b), the characteristics exhibit obvious differences compared with that of the white noise. Specifically, a significant segmentation phenomenon along the frequency domain is observed. Taking the lining defect as an example, the dynamic response of acceleration at the crown shows a significant attenuation phenomenon near the frequency of 10Hz. However, a considerable intensity amplified phenomenon is observed near the frequency of 17Hz, 38Hz, and 59Hz. In this research, the degree of amplification of dynamic response intensity is further defined. Specifically, the corresponding frequency domain is defined as an amplified range when $1 < SSR < 2$; When the value of SSR is larger than 2, the corresponding frequency domain is defined as a significant amplification range. Thus, in this case, the frequency domain of 14Hz-19Hz, 32Hz-44Hz, and 55Hz-62Hz are determined as the significantly amplified range for lining defects. As for the distribution of acceleration SSR with the void defect, the significantly amplified range can be

determined as the frequency domain of 36Hz-43Hz. Concerning the frequency domain of 65Hz-100Hz, the amplified degree of the dynamic response of the lining defect is larger than that of the void defect.



(a)

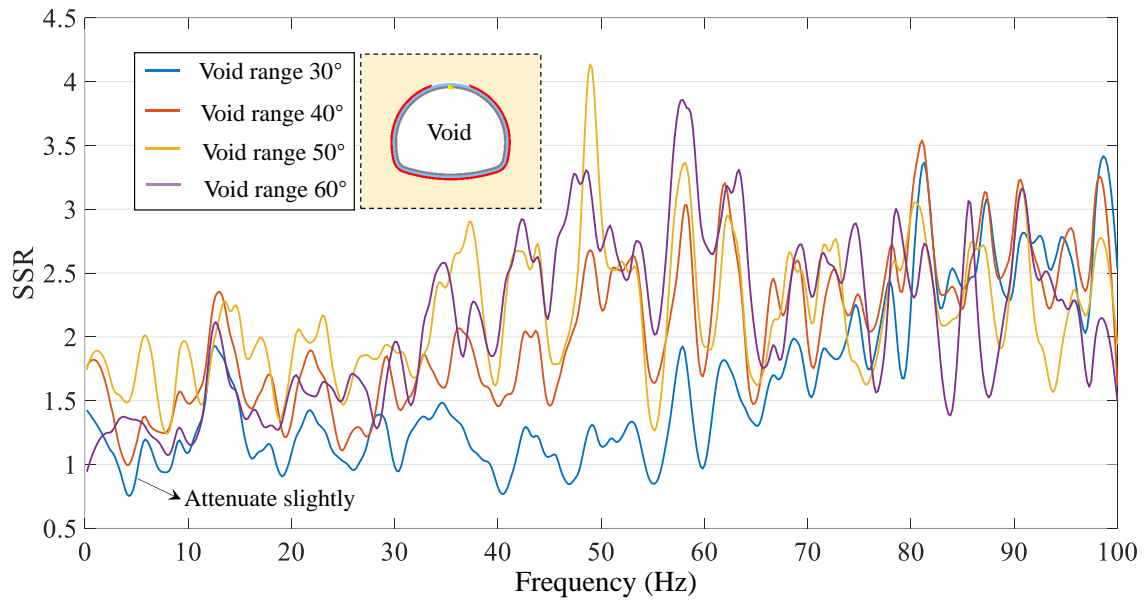


(b)

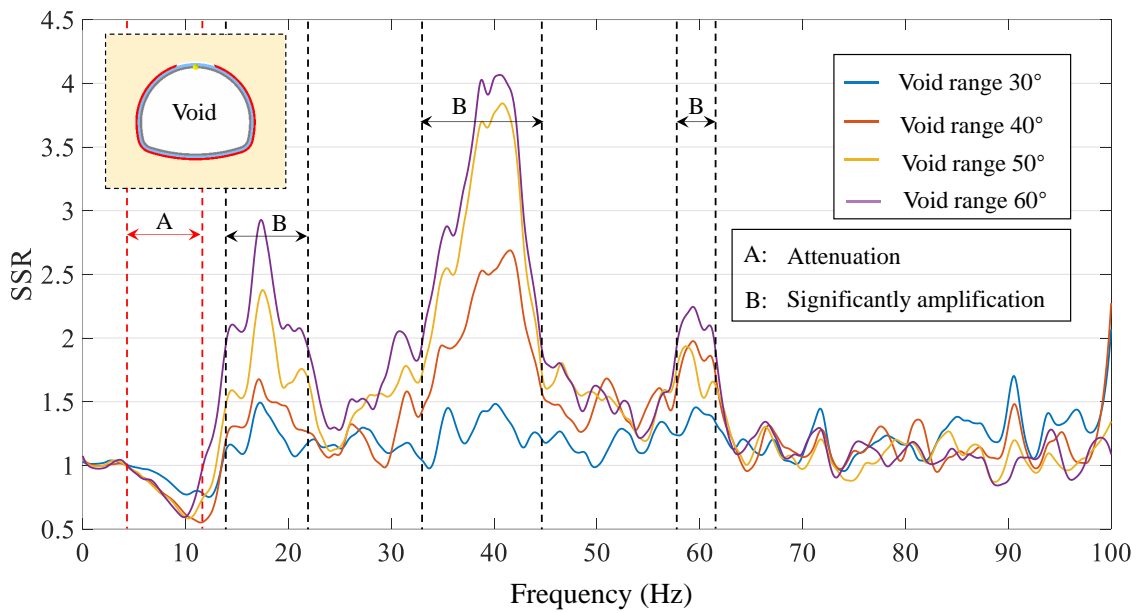
Fig. 6.14 Effect of defect type on the distribution of acceleration SSR at the crown: (a) effect of white noise; (b) effect of El-Centro.

6.4.1.2 Effect of void range

In this section, the effect of void range on the distribution of acceleration SSR was investigated and presented in Fig. 6.15. Regarding the characteristics of the acceleration SSR in the case of white noise, as shown in Fig. 6.15(a), it is observed that there is a slight attenuation phenomenon for the void range of 30° near the frequency of 4Hz, 18Hz, 30Hz, 40Hz, 47Hz, and 55Hz. While for other void ranges of 40° , 50° , and 60° , there is an amplification phenomenon within the frequency domain of 0Hz-100Hz. In addition, when the frequency domain is in the range of 0Hz-60Hz, the distribution of acceleration SSR is roughly the smallest for the void range of 30° . When the void range is 40° , 50° , and 60° , the distribution of acceleration SSR at the crown is not strictly positive with the void range. When the frequency domain is in the range of 60Hz-100Hz, the void range has no significant influence on the dynamic response intensity at the crown. Regarding the characteristics of acceleration SSR in the case of El-Centro, as presented in Fig. 6.15(b), there is an obvious partition phenomenon along with the frequency domain. Taking the void range of 60° as an example, the acceleration dynamic response intensity of the crown attenuates around 10Hz. However, the dynamic response intensity can basically be amplified within the frequency domain of 12Hz-60Hz. Especially around 18Hz, 40Hz, and 60Hz, the amplification effect is extremely significant. In addition, note that in the frequency domain of 12Hz-60Hz, the SSR exhibits a significant positive correlation with the void range. Furthermore, when the void range is relatively small, the proportion of the significant amplification range is significantly reduced. When the void range is 30° , there is no significant amplification range in the frequency domain of 0Hz-100Hz. Moreover, the change in the void range does not significantly affect the dynamic response of acceleration within the frequency domain of 0Hz-5Hz and 65Hz-100Hz. It should be indicated that the acceleration SSR is different under the effect of strong seismic and micro-seismic, which may be due to the elastic deformation of the tunnel structure under the effect of micro-seism but damage behavior under a strong seismic. Concerning the dynamic response of acceleration at other locations, as presented in Fig. 6.16, it is noted that the amplification ratio of the acceleration dynamic response intensity is roughly larger than that of the far distance to the defect zone. No matter in the sidewall or the inverted arch, there is no range of significant amplification ($SSR > 2$). In addition, it is observed that the change of the acceleration dynamic response intensity at the sidewall and the inverted arch is not significantly affected by the change of the void range at the crown.

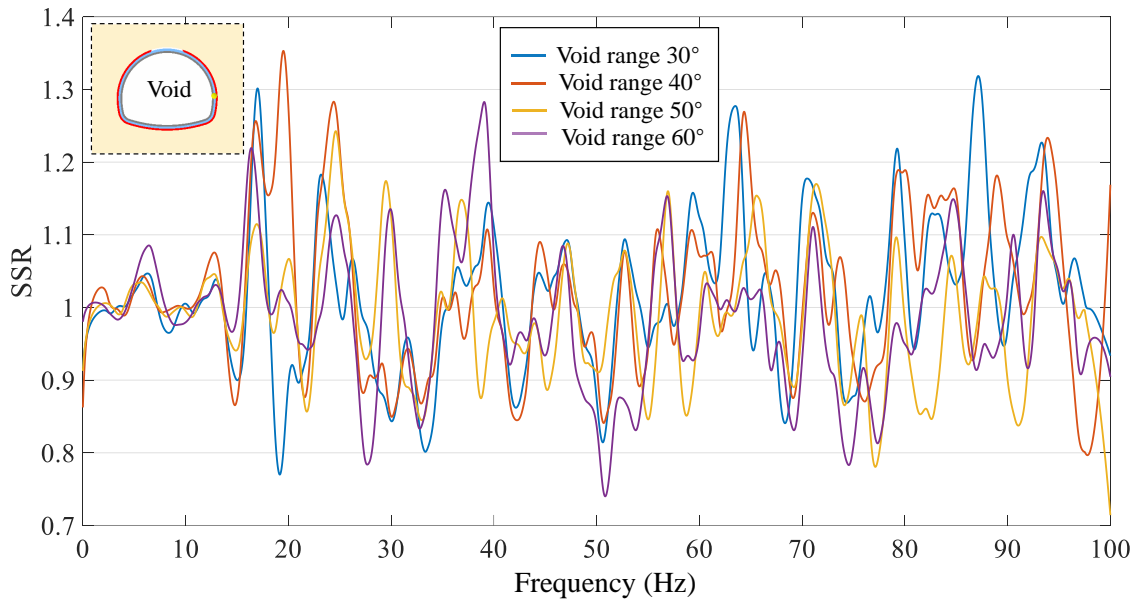


(a)

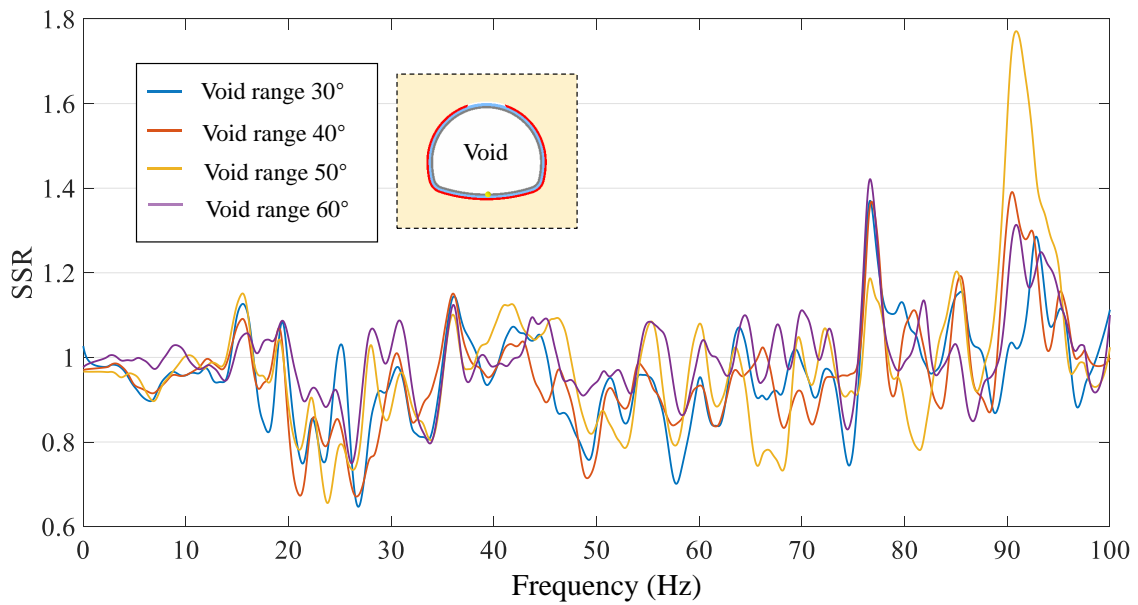


(b)

Fig. 6.15 Effect of void range on the distribution of acceleration SSR at crown: (a) effect of white noise; (b) effect of El-Centro.



(a)



(b)

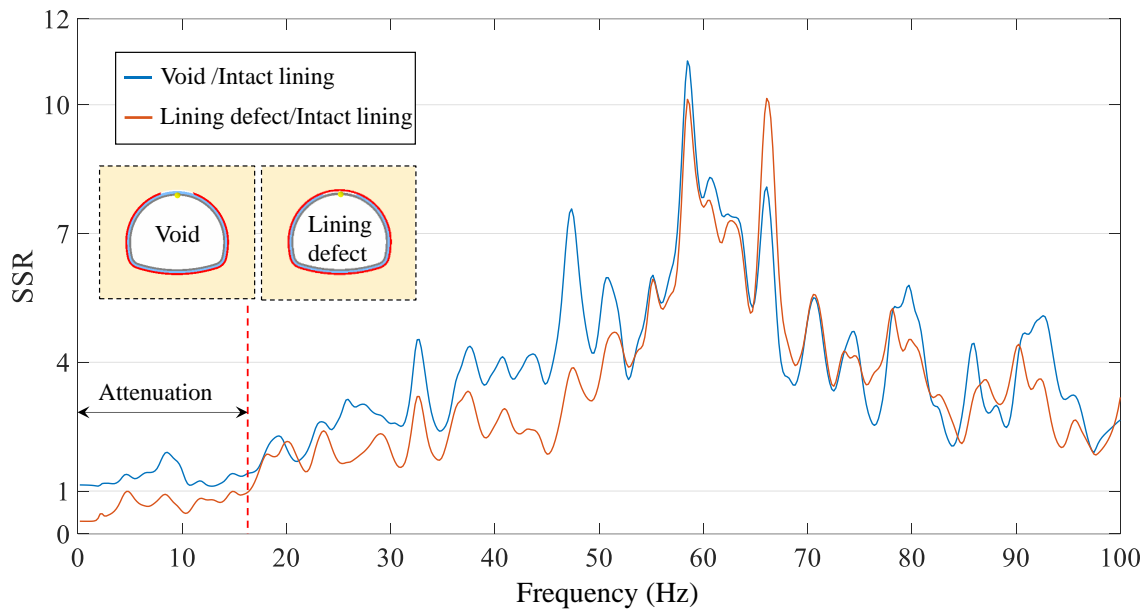
Fig. 6.16 Effect of void range on the distribution of acceleration SSR at other locations:

(a) sidewall; (b) inverted arch.

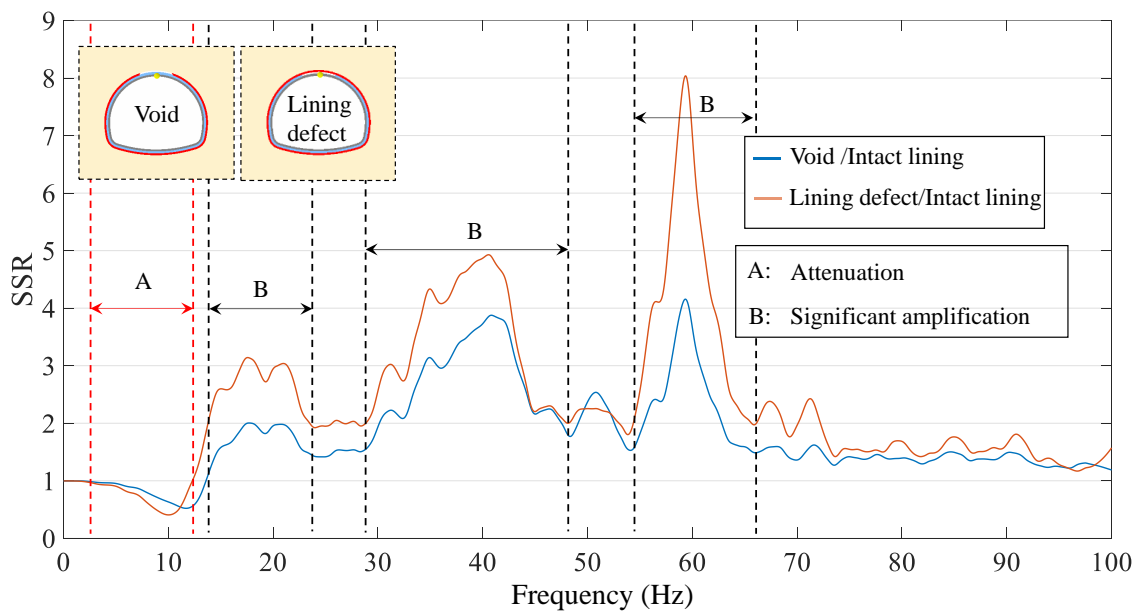
6.4.2 Characteristics of velocity SSR

6.4.2.1 Effect of defect type

In this section, the effect of defect type on the distribution of velocity SSR at the crown was explored and shown in Fig. 6.17. Concerning the characteristic of velocity SSR under the action of white noise, as exhibited in Fig. 6.17(a), the amplification of the velocity dynamic response with the void defect is roughly larger than that of the lining defect within the frequency domain of 0Hz-65Hz. It should be indicated that the effect of the lining defect on the velocity dynamic response intensity at the crown is attenuated within the frequency domain of 0Hz-17Hz, while it is amplified for the effect of the void defect. In addition, when the frequency domain is in the range of 70Hz-100Hz, the change in defect type has no significant influence on the velocity SSR at the crown, but all are in an amplified state. Regarding the characteristics of the velocity SSR in the case of El-Centro, as presented in Fig. 6.17(b), an obvious partition phenomenon occurs along with the frequency domain. Taking the lining defect as an example, when the frequency domain is 0Hz-12Hz, the dynamic response at the crown is attenuated. The maximum attenuation coefficient occurs near 10Hz. When the frequency domain is in the range of 12Hz-100Hz, the velocity dynamic response is in an amplified state. Especially around 18Hz, 40Hz, and 60Hz, the effect of amplification is extremely significant. For the type of lining defect, the frequency domain of 14Hz-23Hz, 29Hz-48Hz, and 54Hz-66Hz can be determined as the significantly amplified range. While for the defect type of void defect, the significantly amplified range is in the frequency domain of 30Hz-47Hz, 50Hz-52Hz, and 56Hz-62Hz. In addition, when the frequency is around 60Hz, the amplification coefficient of the velocity dynamic response intensity at the crown reaches the maximum within the frequency domain of 0Hz-100Hz. Specifically, the maximum amplification coefficient for the lining defect is 8.02, while 4.12 for the void defect. Furthermore, within the frequency domain of 73Hz-100Hz, the influence of change in defect type on velocity dynamic response is not significant, and the amplification coefficient is around 1.5. By comparing Fig. 6.17(a) and Fig. 6.17(b), it is noted that the effect of void on the velocity dynamic response at the crown has an amplification effect in the frequency range of 0Hz-100Hz under the microseism. In contrast, the effect of void on the velocity dynamic response is attenuated in the frequency domain of 0Hz -12Hz for the effect of strong seismic.



(a)



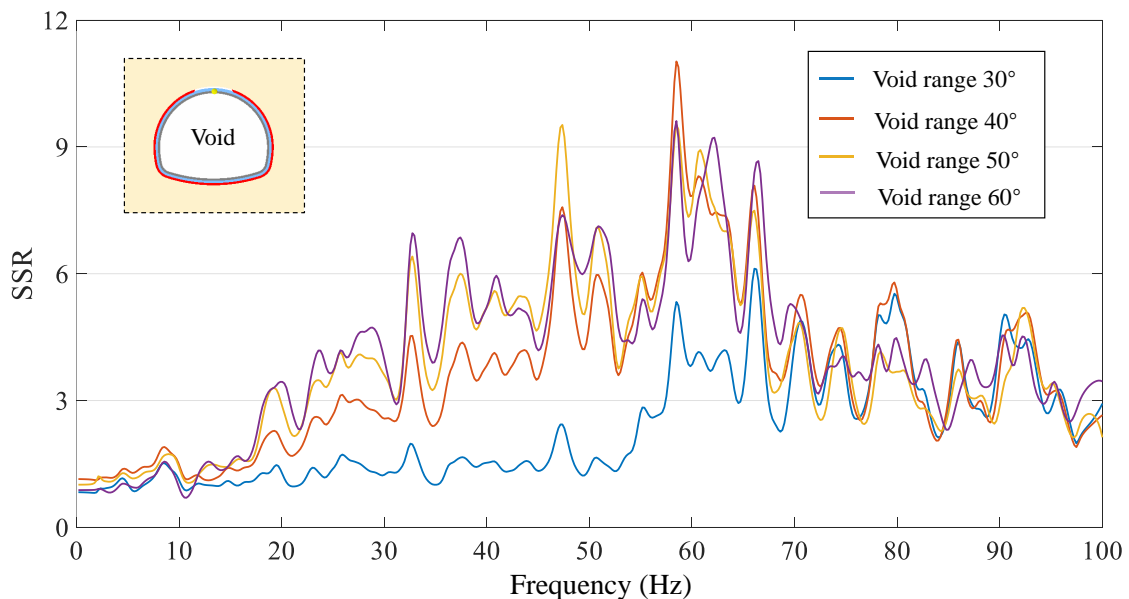
(b)

Fig. 6.17 Effect of defect type on the distribution of velocity SSR: (a) effect of white noise; (b) effect of El-Centro.

6.4.2.2 Effect of void range

In this section, the effect of void range on the distribution of velocity SSR can be

presented in Fig. 6.18. As for the impact of white noise, as shown in Fig. 6.18(a), when the frequency domain is in the range of 0Hz-65Hz, the velocity SSR at the crown is roughly the smallest for the void range of 30° . As for the void range of 40° , 50° , and 60° , the distribution of velocity SSR does not show a strictly positive correlation with the void range except for the frequency domain of 19Hz-48Hz. When the frequency domain is 70Hz-100Hz, the void range will not cause a significant change. The distribution of velocity SSR under the El-Centro can be presented in Fig. 6.18(b). The velocity dynamic response intensity is attenuated in the frequency domain of 0Hz-12Hz for a void range of 60° , and the maximum attenuated coefficient is near 10Hz. As the void range decreases, the range of frequency domain corresponding to the attenuation of the velocity dynamic response intensity at the crown gradually increases. For the frequency domain of 15Hz-100Hz, the velocity dynamic response at the crown is amplified for the void range of 30° , 40° , 50° , and 60° . Especially around 20Hz, 40Hz, and 60Hz, the amplification effect is extremely significant. In addition, an apparent positive correlation is observed between the velocity SSR and void range in the frequency domain of 15Hz-48Hz. For the void range of 60° , the frequency domain of 14Hz-48Hz, and 55Hz-62Hz can be determined as the significantly amplified range. Furthermore, within the frequency domain of 65Hz-100Hz, the amplification of the void range of 30° is the largest, while for the void range of 40° , 50° , and 60° , the influence of change in the void range on the velocity SSR at the crown is not apparent.



(a)

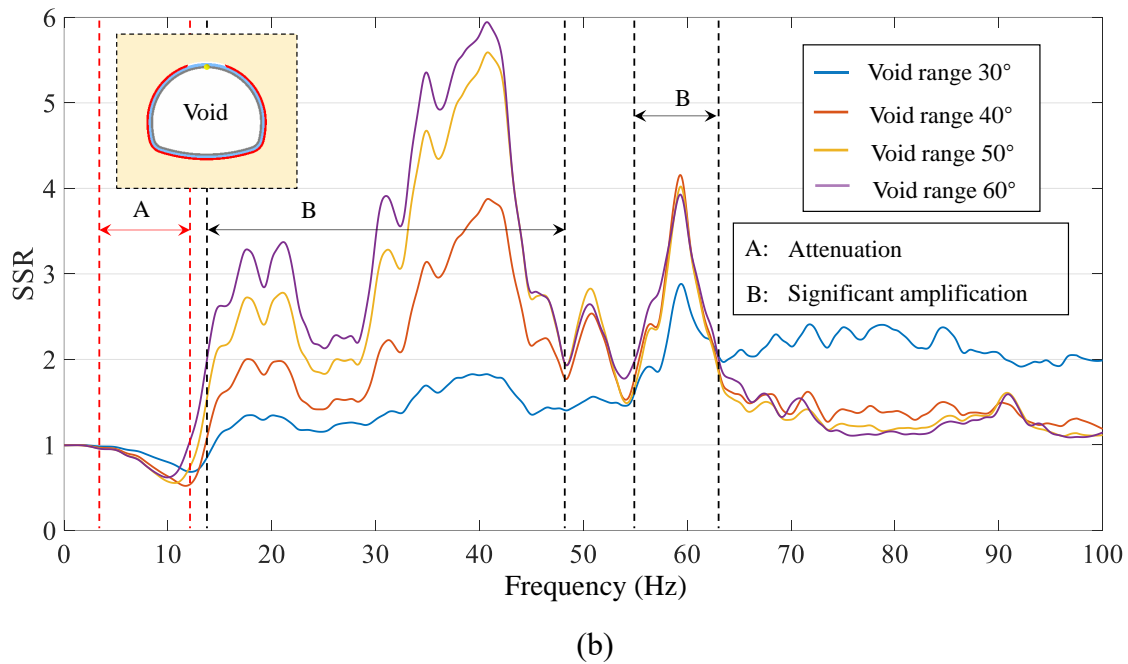
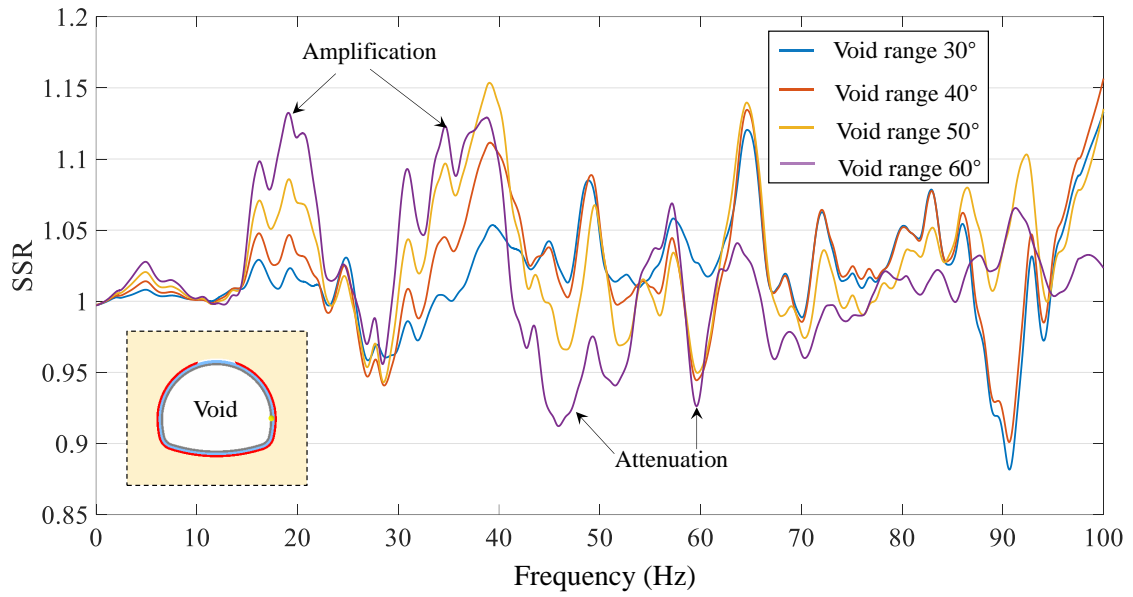
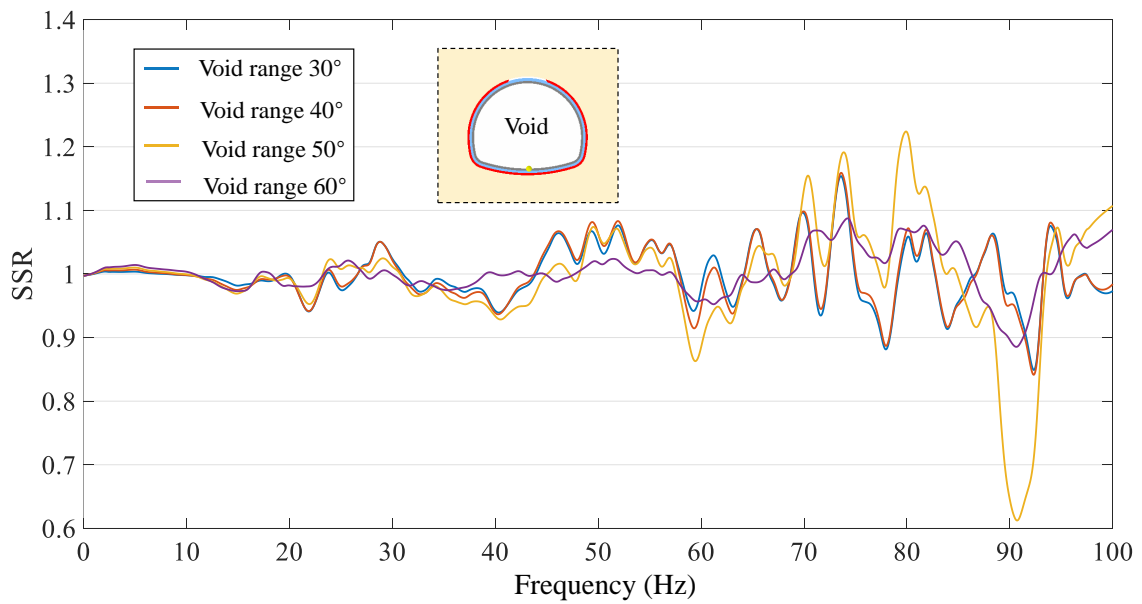


Fig. 6.18 Effect of void range on the distribution of velocity SSR at the crown: (a) effect of white noise; (b) effect of El-Centro.

In this section, the change of velocity SSR at other locations, such as the sidewall and the inverted arch, is presented in Fig. 6.19. It can be found that the effect of the void range on the velocity SSR presents significant differences at different locations. As shown in Fig. 6.19(a), taking the void range of 60° as an example, when the frequency is around 20Hz and 40Hz, the amplification coefficient of the velocity dynamic response intensity is significant, while when the frequency is around 45Hz and 60Hz, an apparent attenuation phenomenon occurs. In addition, an obvious positive correlation is observed between the velocity SSR and void range near the frequency of 5Hz, 20Hz, and 35Hz. Concerning the monitoring point at the inverted arch, as presented in Fig. 6.19(b), when the frequency domain is 0Hz-100Hz, the effect of the void range on the velocity SSR is not apparent. As for the void range of 50° , a significant attenuation phenomenon generates when the frequency is near 60Hz and 91Hz. By exploring the influence of void range on the velocity SSR at specific measuring points, it is noted that when the measuring point is within the defect range, the amplification coefficient is larger than that of a far distance to the defect zone. Overall, it can be concluded that the effect of void range on the distribution of velocity SSR is more pronounced near defects.



(a)



(b)

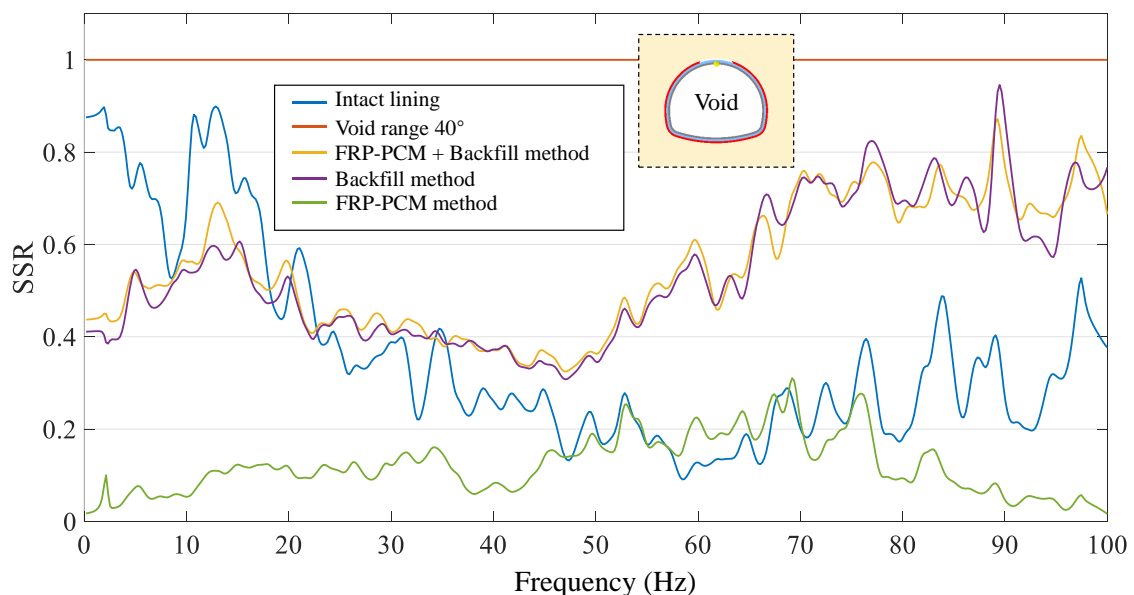
Fig. 6.19 Effect of void range on the distribution of velocity SSR at other locations: (a) sidewall; (b) inverted arch.

6.4.3 Characteristics of SSR under the reinforcement

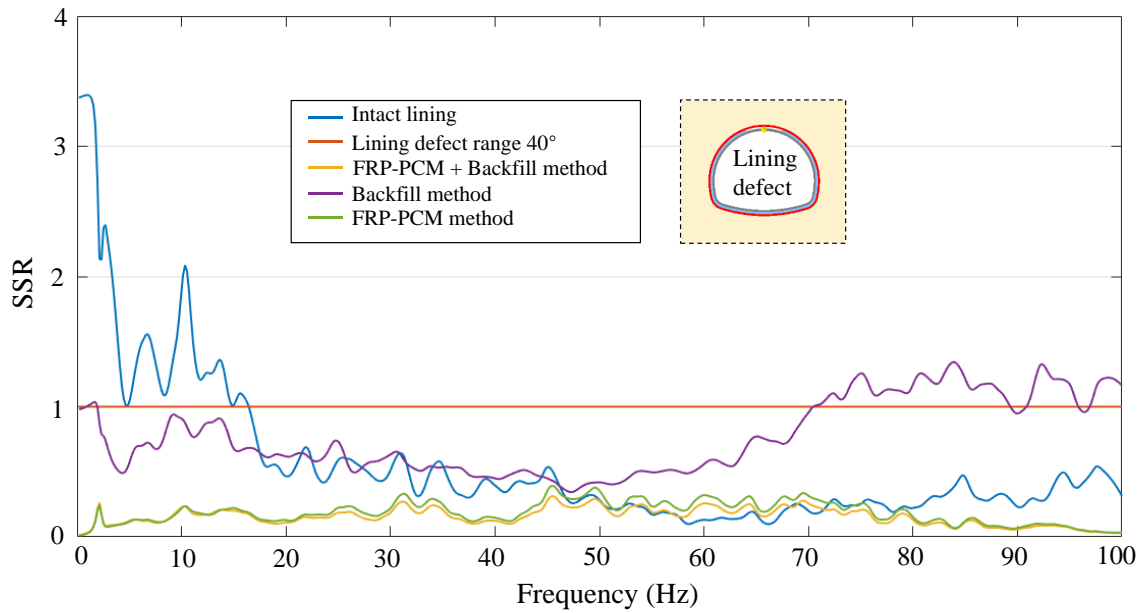
6.4.3.1 Velocity SSR

In this section, the impact of reinforcement methods on the distribution of velocity SSR was explored. When the tunnel structure is under the effect of white noise, the distribution of velocity SSR can be presented in Fig. 6.20. In this model, the velocity SSR is the ratio of the dynamic response of the defective lining structure with the reinforcement or the intact tunnel lining without reinforcement to that of the lining structure with a defect range of 40° . As for the void quality defect shown in Fig. 6.20(a), the velocity dynamic response at the crown of the repaired lining structure in the 0Hz-100Hz frequency domain is attenuated compared to that of the defective lining structure without repairment. When the defective lining structure is reinforced by the FRP-PCM method, the attenuation of velocity dynamic response intensity at the crown is the most significant compared to other reinforcement methods. In addition, when the frequency domain is 0Hz-18Hz, the attenuation of intact lining is smaller than that of the defective lining structure with the repairment, indicating that the velocity dynamic response intensity at the crown is suppressed below that of the intact lining structure. Furthermore, when the frequency domain is 57Hz-67Hz, the attenuation of the intact lining is larger than that of the repaired lining structure. This indicates that although the velocity dynamic response intensity at the crown can be attenuated, the degree of suppression is still less than that of the intact lining. The distribution of velocity SSR of tunnel structures with lining defects under different reinforcement methods can be shown in Fig. 6.20(b). When the defective lining structure is reinforced with the FRP-PCM method or the combined method of FRP-PCM and backfill, the attenuation is more significant than that of the intact lining in the frequency domain of 0Hz-45Hz and 75Hz-100Hz. This indicates that the velocity dynamic response intensity at the crown is suppressed below that of the intact lining structures. Regarding the changed behavior of velocity SSR under the backfill method, when the frequency domain is 0Hz-70Hz, the degree of attenuation is smaller than that of the other two repairment methods. However, when the frequency domain is in the range of 71Hz-100Hz, the dynamic response at the crown is roughly amplified. In addition, the dynamic response intensity at the crown is suppressed below that of the intact lining in the frequency domain of 0Hz-18Hz. By comparing Fig. 6.20(a) and Fig. 6.20(b), it is noted that the type of tunnel quality defects significantly affects the impact of repairment

schemes on the velocity SSR. An apparent difference is that the suppress performance of the combined method of FRP-PCM and backfill to the dynamic velocity response at the crown of the lining defect is more significant than the void defect. In addition, it can be observed that the combined method of FRP-PCM and backfill have similar effects on the dynamic response intensity of the crown velocity of the void defect as that of the backfill method. However, for the type of lining defect, the impact of the FRP-PCM method and the combined method of FRP-PCM and backfill on the attenuation degree of velocity dynamic response intensity at the crown is roughly similar. In addition, the dispersion degree of SSR curves between the repaired lining and the intact lining is significantly different depending on the repair method and the defect type. Theoretically, the smaller the degree of dispersion, the more ideal the repair effect may be. For example, as for the void defect, the velocity SSR under the repair of the FRP-PCM method is close to the intact lining in the frequency domain of 48Hz-80Hz, but far away in other domains. When the frequency domain is 0Hz-45Hz, the restoration effect is ideal with the combined and backfill methods. Furthermore, since the velocity SSR curve of the lining repaired by the combined method is closer to the curve repaired by the backfill method, it shows that the effect of the backfill method on the void is significant. Similarly, it can be concluded that the FRP-PCM method significantly affects the repair effect of lining defects.



(a)

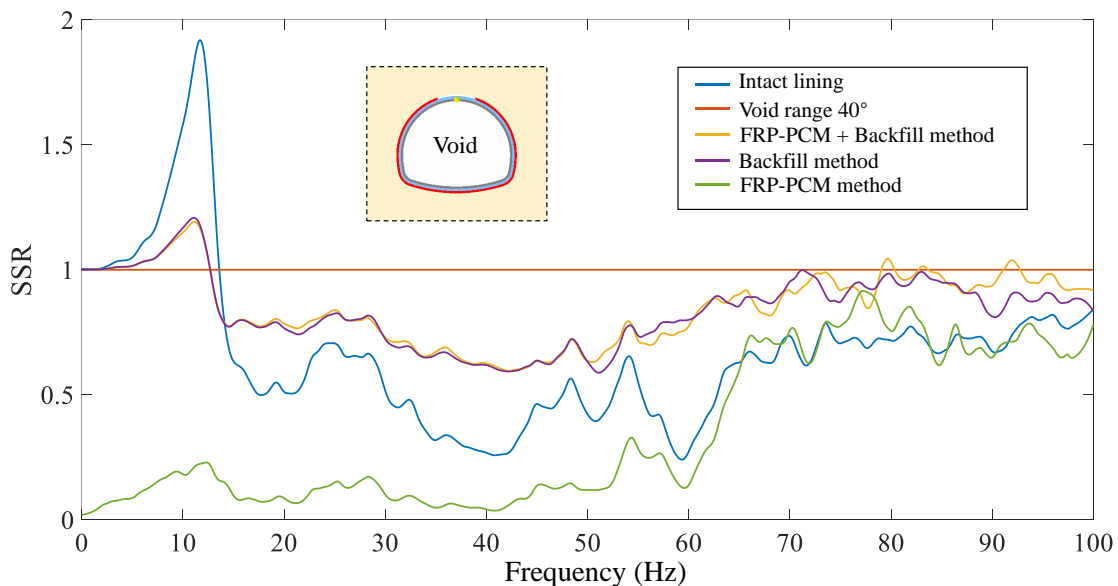


(b)

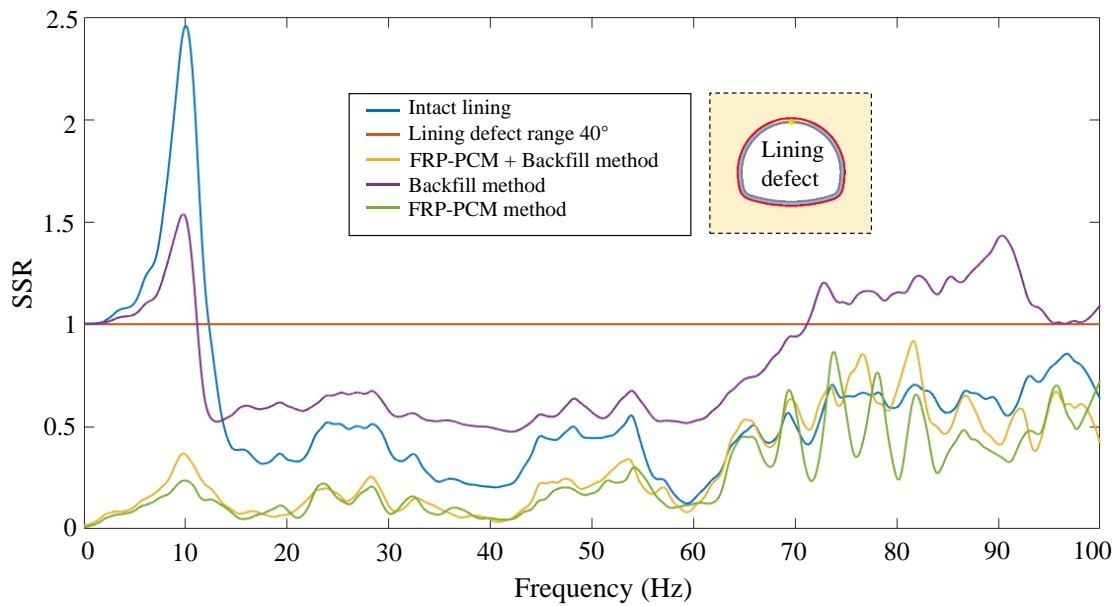
Fig. 6.20 Effect of defect type on the distribution of velocity SSR with different reinforcement methods: (a) void quality defect; (b) lining defect.

When the tunnel structure is under the effect of the El-Centro, the distribution of velocity SSR can be exhibited in Fig. 6.21. As for the void defect shown in Fig. 6.21(a), when the frequency domain is 0Hz-12Hz, the velocity dynamic response intensity at the crown amplifies under the backfill method and combined method of the FRP-PCM and backfill. When the frequency domain is 12Hz-100Hz, the velocity dynamic response intensity at the crown roughly presents a tendency of attenuation with the three repair methods, and the degree of attenuation of the FRP-PCM method is the most obvious. In addition, when the frequency domain is 0Hz-65Hz, the degree of attenuation under the FRP-PCM method is more significant than that of the intact lining, which indicates the velocity dynamic response of the repaired lining structure at the crown is suppressed below that of the intact lining. The distribution of velocity SSR of tunnel structures with lining defects under different reinforcement methods can be displayed in Fig. 6.21(b). When the frequency domain is 0Hz-11Hz and 72Hz-100Hz, the velocity dynamic response at the crown amplifies under the backfill method. However, when the frequency domain is in the range of 0Hz-100Hz, the velocity dynamic response intensity at the crown presents a tendency of attenuation under the repair of the FRP-PCM method and the combined method of FRP-PCM and backfill. In addition, when the frequency domain

is 0Hz-60Hz, the attenuation degree of the repaired lining under the FRP-PCM method and the combined method of FRP-PCM and backfill is larger than that of the intact lining. It indicates that the velocity dynamic response at the crown is suppressed below that of the intact lining. By comparing Fig. 6.21(a) and Fig. 6.21(b), it is noted that the dynamic response of velocity at the crown under the repairment is also significantly affected by the defect type. An apparent difference is that the FRP-PCM method and the combined method of FRP-PCM and backfill can dramatically suppress the dynamic response of velocity at the crown for lining defects. As for the void defect, the velocity SSR under reinforcement of the FRP-PCM method is close to the intact lining in the frequency domain of 60Hz-100Hz, but far away in other frequency domains. When the frequency domain is 57Hz-100Hz, the restoration effect of the lining defect is ideal with the combined method. Theoretically, the less dispersion from the intact lining, the more ideal the restoration effect may be. In addition, for void defects, the recovery effect of the backfill method is similar to that of the combined method, while for lining defects, the restoration effect of the FRP-PCM method is similar to that of the combined method. Overall, combined with the distribution characteristics of velocity SSR curves under each repair method, it is determined that the backfill method and the FRP-PCM method have significant effects on void quality defect and lining defect, respectively.



(a)



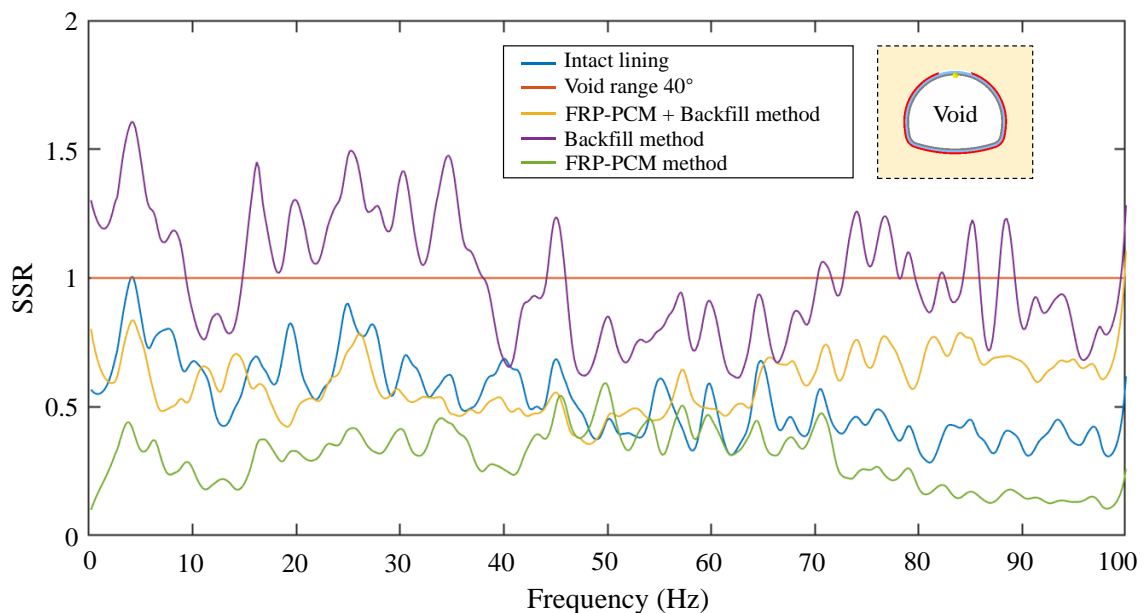
(b)

Fig. 6.21 Effect of defect type on the distribution of velocity SSR with different reinforcement methods: (a) void quality defect; (b) lining defect.

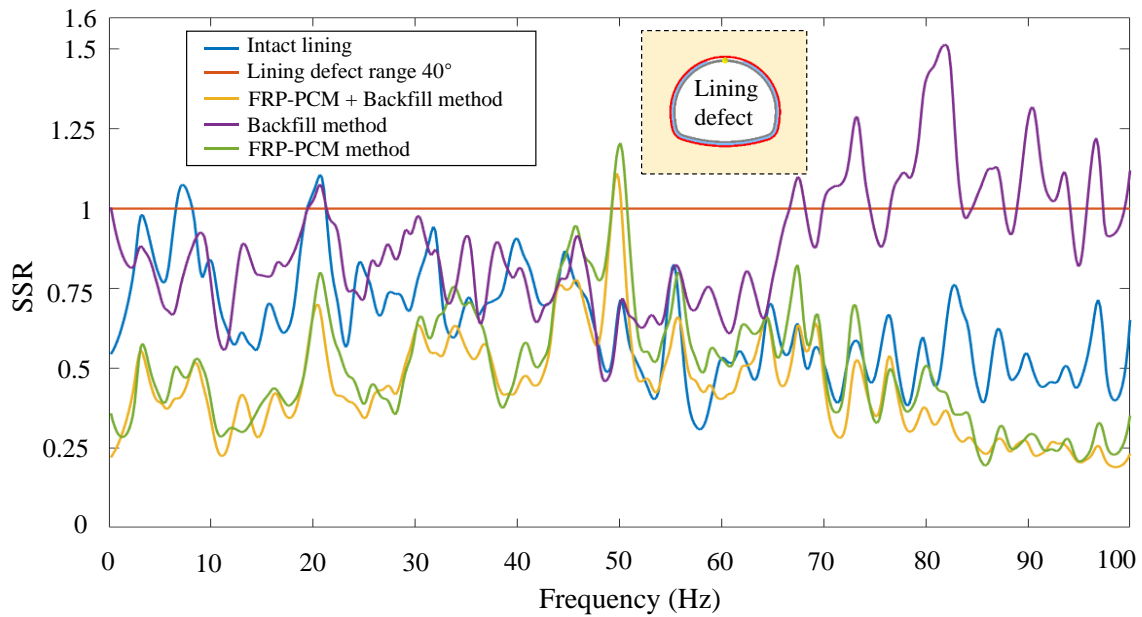
6.4.3.2 Acceleration SSR

When the tunnel structure is under the effect of the white noise, the effect of the reinforcement method on the distribution of acceleration SSR was explored and exhibited in Fig. 6.22. In this model, the acceleration SSR is the ratio of the dynamic response of acceleration of the reinforced lining structure or the intact tunnel lining without reinforcement to that of the lining structure with a defect range of 40° . As for the void quality defect shown in Fig. 6.22(a), the dynamic response of acceleration of defective lining structure under the FRP-PCM method and the combined method of FRP-PCM and backfill is significantly attenuated in the frequency domain of 0Hz-100Hz. Regarding the distribution of acceleration SSR under the repair of the backfill method, the dynamic response at the crown is attenuated around 12Hz, 50Hz, 60Hz, and 95Hz. In addition, the acceleration SSR under reinforcement of the combined method of FRP-PCM and backfill is close to the intact lining in the frequency domain of 0Hz-65Hz. However, the close degree under the combined reinforcement method is roughly similar to that under the FRP-PCM method in the frequency domain of 65Hz-100Hz. The distribution of acceleration SSR of tunnel structures with lining defects under different reinforcement methods can be displayed in Fig. 6.22(b). The dynamic response at the crown is in an attenuation state under the FRP-PCM method and combined method of FRP-PCM and

backfill except for the frequency near 50Hz. The dynamic response of acceleration is attenuated in the frequency domain of 0Hz-66Hz under the backfill repair method except near 20 Hz. When the frequency domain is 66Hz-100Hz, the dynamic response at the crown is roughly in the amplified state, and the maximum amplification coefficient is around 81Hz. In addition, as for the FRP-PCM method and the combined method of FRP-PCM and backfill, the degree of attenuation of the intact lining is smaller than that of the repaired lining structure in the frequency domain of 0Hz-31Hz and 80Hz-100Hz. It indicates that the dynamic response intensity of acceleration is suppressed below the intact lining in the specified frequency domain. In addition, the effect of the combined method of FRP-PCM and backfill on the acceleration SSR at the crown is similar to that of the FRP-PCM method. The acceleration SSR under the reinforcement of the combined method of FRP-PCM and backfill is close to the intact lining in the frequency domain of 55Hz-100Hz. However, the SSR curve of the backfill method is close to that of the intact lining in the frequency domain 10Hz-30Hz. Furthermore, the acceleration SSR at the crown is also significantly affected by the defect type. The FRP-PCM method has significant effects on the acceleration SSR of lining defects. In addition, in the frequency domain of 0Hz-100Hz, the combined method of FRP-PCM and backfill can effectively repair void defects.



(a)



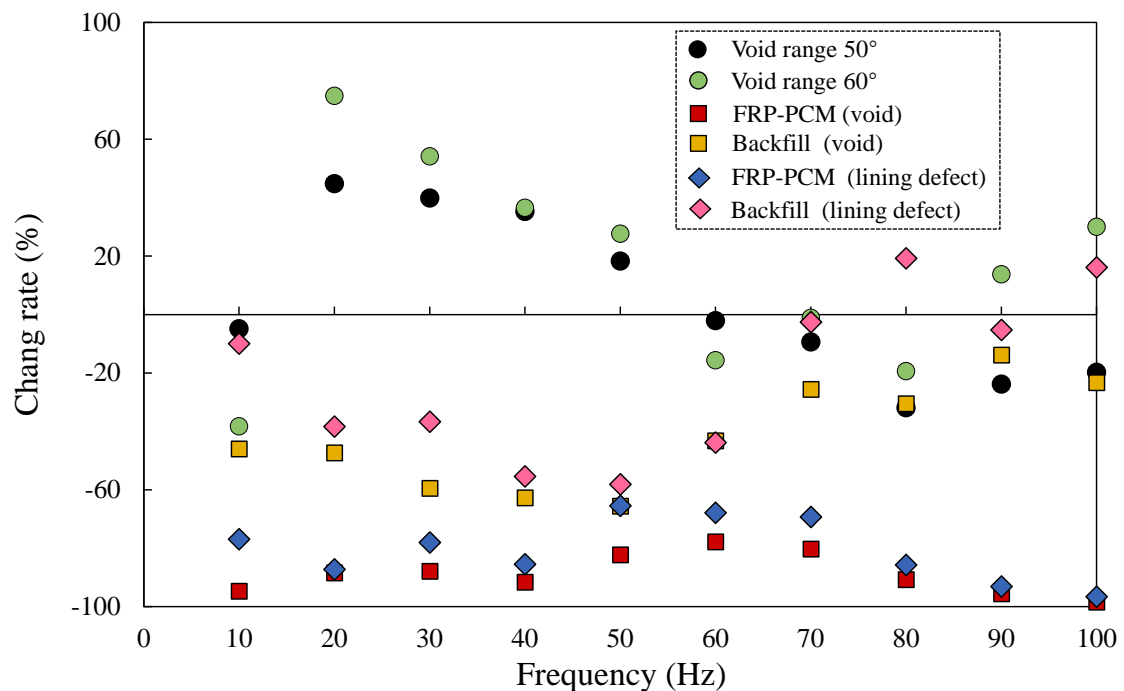
(b)

Fig. 6.22 Effect of defect type on the distribution of acceleration SSR with different reinforcement methods: (a) void quality defect; (b) lining defect.

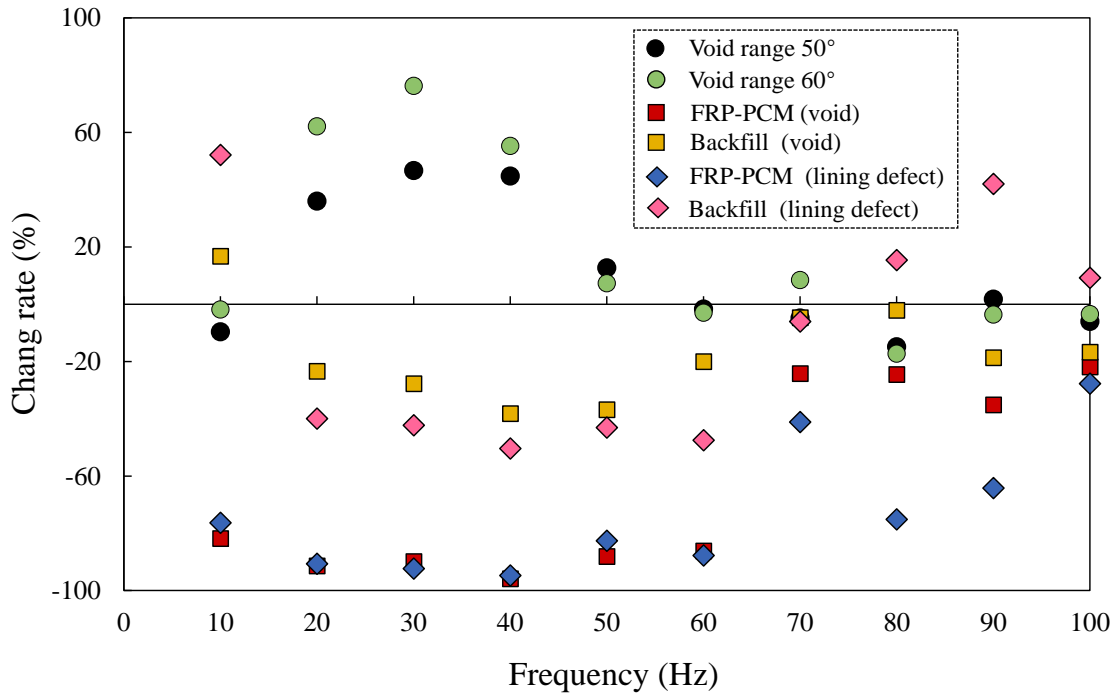
6.5 Discussion

In this section, a quantitative study was conducted to intuitively explore the influence of the defect range and reinforcement methods on the SSR at the crown near the specified frequency. The change rate of dynamic response intensity was applied to characterize and explain the influence of typical factors quantitatively. It should be indicated that the change of the dynamic response intensity in this model is compared with the case where the tunnel quality defect is 40° at crown without reinforcement. Specifically, when the change rate is less than 0%, the dynamic response intensity at the crown tends to attenuate. Otherwise, it will be amplified. The change rate of the dynamic response of velocity under the white noise can be shown in Fig. 6.23(a). When the specified frequency is around 20Hz, the increase of the void range causes a significant increase in the velocity dynamic response intensity at the crown. The change rate can reach 44.80% for the void range of 50° and 74.86% for the void range of 60° . In addition, it is observed that near the specified frequency, the reduction rate of the FRP-PCM method on the velocity dynamic response of the void defect is more significant than that of the lining defect. In particular, the

reduction rate can reach 98.37% and 96.60% near 100Hz, respectively. As for the backfill method, it is noted that the reduction rate of the void defect is more significant than that of the lining defect near the specified frequency. When the frequency is around 50Hz, the backfill method can significantly reduce the dynamic response of the crown. The reduction rate can reach 65.53% for void defects and 58.14% for lining defects. Regarding the defect type of lining defect, the backfill method amplifies the velocity dynamic response near the specific frequencies, such as 19.25% near 80Hz and 16.18% near 100Hz. The change rate of the dynamic response of velocity under the El-Centro can be presented in Fig. 6.23(b). For the effect of the FRP-PCM method, the reduction rate of lining defect is roughly more apparent than that of the void defect in specific frequencies. The reduction rate can reach 95.86% for void defects and 94.71% for lining defects near 40Hz. As for the backfill method, the reduction rate of the lining defect is more significant than that of the void defect near the specified frequency of 20Hz, 30Hz, 40Hz, 50Hz, 60Hz, and 70Hz. In addition, compared with the backfill method, the FPR-PCM method has a more obvious reduction effect on the velocity dynamic response intensity. Furthermore, the overall performance of the reinforcement effect can be determined by the degree of restoration, which was described in detail in this chapter.



(a)

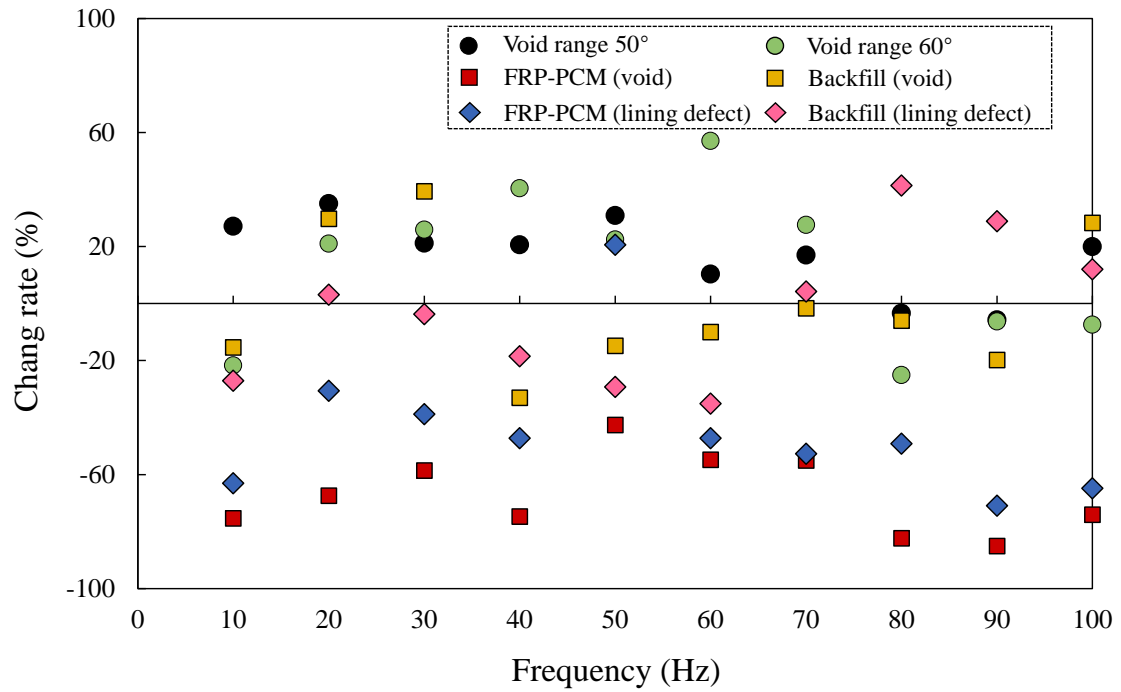


(b)

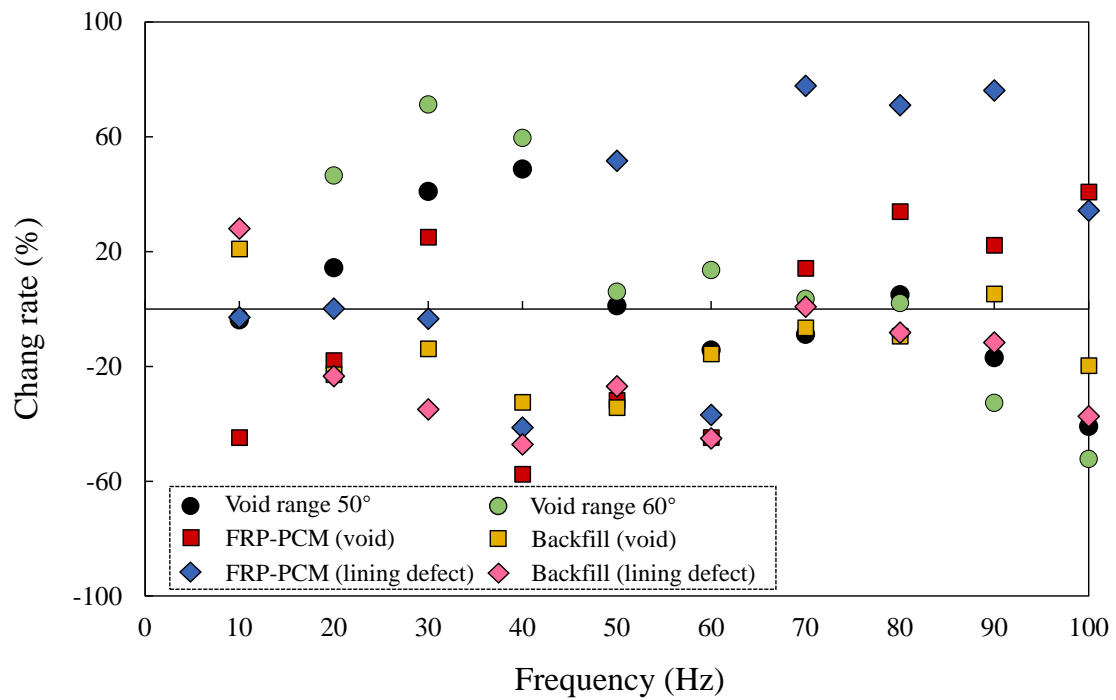
Fig. 6.23 Change rate of the dynamic response of velocity at the crown: (a) effect of white noise; (b) effect of El-Centro.

Analogously, the change rate of the dynamic response of acceleration at the crown can be exhibited in Fig. 6.24. Concerning the characteristics under the white noise shown in Fig. 6.24(a), the reduction rate of the FRP-PCM method on the void defect is more significant than that of the lining defect near specified frequencies. Notably, the reduction rate can reach 85.06% and 70.99% near 90 Hz. Regarding the change rate of the backfill method, the maximum reduction rate is 33.06% for void defects when the frequency is near 40 Hz. However, the maximum reduction rate is 35.15% for lining defects near the frequency of 60Hz. In addition, compared with the backfill method, the FRP-PCM method has a more obvious reduction effect on the acceleration dynamic response intensity. The change rate characteristics under the El-Centro can be shown in Fig. 6.24(b). For the change rate of the FRP-PCM method near specified frequencies, the maximum reduction rate is 57.5% for void defects and 41.29% for lining defects when the frequency is near 40 Hz. Regarding the reduction rate of the backfill method, the maximum reduction rate can reach 34.3% for void defects near 50Hz. The overall performance of the reinforcement can be judged by the degree of restoration, which was discussed in detail in this chapter. In future work, it is helpful to more deeply reveal the dynamic

response of defective tunnels with reinforcement by conducting model tests.



(a)



(b)

Fig. 6.24 Change rate of the dynamic response of acceleration at the crown: (a) effect of white noise; (b) effect of El-Centro.

6.6 Conclusions

In this chapter, the dynamic response of tunnel structures with quality defects of the void and lining defect was comprehensively investigated. The effect of defect parameters on the physical and mechanical properties was also investigated. The main conclusions of this chapter can be drawn as follows:

- (1) There is an apparent tensile stress concentration phenomenon on the outside of the defect, and the degree of stress concentration is roughly positively correlated with the defect range. The FRP-PCM method and the backfill method can significantly optimize the mechanical properties of the lining.
- (2) The peak acceleration and velocity of the lining are roughly relatively small at the crown and shoulder but large at the arch springing and inverted arch. The distribution of peak acceleration and velocity are significantly affected by the defect type, defect range, and defect location. The peak acceleration increases obviously within the defect range, and the increase rate under the void defect is roughly more significant than that of the lining defect. In addition, the peak acceleration and velocity of the lining approximately increase with the increase of the void range within the defect zone. Furthermore, the maximum values of peak velocity and acceleration of specific measuring points are roughly consistent with the defect location.
- (3) The distribution of acceleration SSR and velocity SSR is significantly affected by the defect type and range. Compared with the dynamic response of the lining structure without defects, the dynamic response at the crown with quality defects shows the attenuation phenomenon within the small range of frequency domain, while most other frequencies are in an amplified state. The degree of attenuation and amplification is significantly influenced by the defect type, defect range, and dynamic degree, which was discussed in detail.
- (4) The type of reinforcement method significantly affects the dynamic response. In the established model, the velocity SSR under the FRP-PCM method, backfill method, and the combined method of FRP-PCM and backfill is also significantly affected by the defect type. In general, the dynamic response can be optimized under reinforcement. Furthermore, the influence of the defect range and reinforcement methods on the dynamic response was also quantitatively discussed.

References

Borcherdt RD. Effects of local geology on ground motion near San Francisco Bay.

- Bulletin of the Seismological Society of America, 1970, 60, 29-61.
<https://doi.org/10.1785/BSSA0600010029>
- Brunton JJ, Bank LC, Oliva MG. Punching Shear Failure in Double-Layer Pultruded FRP Grid Reinforced Concrete Bridge Decks. *Advances in Structural Engineering*, 2012, 15(4), 601-613. <https://doi.org/10.1260/1369-4332.15.4.601>
- Bracewell R. *The Fourier Transform and Its Applications*, McGraw-Hill, 1986.
- Chen J, Shi X, Li J. Shaking table test of utility tunnel under non-uniform earthquake wave excitation. *Soil Dynamics and Earthquake Engineering*, 2010, 30, 1400-1416. <https://doi.org/10.1016/j.soildyn.2010.06.014>
- Cui GY, Liu WD, Zhao RH, Wang MN, Lin GJ. Research on the Evaluation Grade of Seismic Damage and Disposal Technologies of Tunnel Structure. *Journal of Railway Engineering Society*, 2014, 31(5), 74-78, 105.
- Dong ZJ, Guo SC, Xu HY, Zhou P, Zhao QC. Treatments defects of secondary lining thickness of an expressway tunnel. *Engineering Journal of Wuhan University*, 2017, 50(6), 957-962. <https://doi.org/10.14188/j.1671-8844.2017-06-024>
- Fang H, Xu X, Liu WQ, Qi YJ, Bai Y, Zhang B, Hui D. Flexural behavior of composite concrete slabs reinforced by FRP grid facesheets. *Composites Part B: Engineering*, 2016, 92, 46-62. <https://doi.org/10.1016/j.compositesb.2016.02.029>
- Gaurav A, Singh KK. Fatigue behavior of FRP composites and CNT-Embedded FRP composites: A review. *Polymer Composites*, 2018, 39(6), 1785-1808. <https://doi.org/10.1002/pc.24177>
- Guler S, Yavuz D, Korkut F, Ashour A. Strength prediction models for steel, synthetic, and hybrid fiber reinforced concretes. *Structural Concrete*, 2019, 20(1), 428-445. <https://doi.org/10.1002/suco.201800088>
- Guler S, Öker B, Akbulut ZF. Workability, strength and toughness properties of different types of fiber-reinforced wet-mix shotcrete. *Structures*, 2021, 31, 781-791. <https://doi.org/10.1016/j.istruc.2021.02.031>
- Guler S, Yavuz D. Post-cracking behavior of hybrid fiber-reinforced concrete-filled steel tube beams. *Construction and Building Materials*, 2019, 205, 285-305. <https://doi.org/10.1016/j.conbuildmat.2019.01.192>
- Guo R, Pan Y, Cai LH, Hino S. Study on design formula of shear capacity of RC beams reinforced by CFRP grid with PCM shotcrete method. *Engineering Structures*, 2018, 166, 427-440. <https://doi.org/10.1016/j.engstruct.2018.03.095>
- Itasca Consulting Group, Inc., *FLAC3D User's Manual*, 2002.
- Jeng F, Lin ML, Yuan SC. Performance of toughness indices for steel fiber reinforced shotcrete. *Tunnelling and Underground Space Technology*, 2002, 17(1), 69-82.

- [https://doi.org/10.1016/S0886-7798\(01\)00065-7](https://doi.org/10.1016/S0886-7798(01)00065-7)
- Jeon JK, Kim WS, Kim GY, Jeon CK. Polyamide Fiber Reinforced Shotcrete for Tunnel Application. *Materials*, 2016, 9(3), 163. <https://doi.org/10.3390/ma9030163>
- Jiang HL, Fan HB. Cause Analysis and Treatment Study of Insufficient Secondary Lining Thickness of Highway Tunnel. *Urban Roads Bridges & Flood Control*, 2016, (4), 113-116. <https://doi.org/10.16799/j.cnki.csdqyfh.2016.04.035>
- Jiang SP, Fang L, Lin Z. Seismic response analysis of mountain tunnels in different depths. *Rock and Soil Mechanics*, 2014, 35(1), 211-225.
- Jiang YJ, Wang XS, Li B, Higashi Y, Taniguchi K, Ishida K. Estimation of reinforcing effects of FRP-PCM method on degraded tunnel linings. *Soils and Foundations*, 2017, 57(3), 327-340. <https://doi.org/10.1016/j.sandf.2017.05.002>
- Jones S, Hunt H. Voids at the tunnel soil-interface for calculation of ground vibration from underground railways. *Journal of Sound and Vibration*, 2011, 330(2), 245-270. <https://doi.org/10.1016/j.jsv.2010.08.015>
- Lee JK, Lee JH. Nondestructive evaluation on damage of carbon fiber sheet reinforced concrete. *Composite Structures*, 2002, 58(1), 139-147. [https://doi.org/10.1016/S0263-8223\(02\)00029-6](https://doi.org/10.1016/S0263-8223(02)00029-6)
- Li B. Characteristics of the Earthquake Dynamic Response and Corresponding Reinforcement of the Tunnel Face. *Modern Tunnelling Technology*, 2014, 51(2), 56-62.
- Li T. Damage to mountain tunnels related to the Wenchuan earthquake and some suggestions for aseismic tunnel construction. *Bulletin of Engineering Geology and the Environment*, 2012, 71, 297-308. <https://doi.org/10.1007/s10064-011-0367-6>
- Li JT, Yang QS. A Correction Method for Baseline Drift of Seismic Wave. *Journal of Beijing Jiaotong University*, 2010, 34(1), 95-99.
- Li ZX, Li CH, Shi YD, Zhou XJ. Experimental investigation on mechanical properties of hybrid fibre reinforced concrete. *Construction and Building Materials*, 2017, 157, 930-942. <https://doi.org/10.1016/j.conbuildmat.2017.09.098>
- Kirzhner F, Rosenhouse G. Numerical analysis of tunnel dynamic response to earth motions. *Tunnelling and Underground Space Technology*, 2000, 15(3), 249-258. [https://doi.org/10.1016/S0886-7798\(00\)00054-7](https://doi.org/10.1016/S0886-7798(00)00054-7)
- Kushnir A, Varypaev A, Dricker Ilya, Rozhkov M, Rozhkov N. Passive surface microseismic monitoring as a statistical problem: location of weak microseismic signals in the presence of strongly correlated noise. *Geophysical Prospecting*, 2014, 62, 819-833. <https://doi.org/10.1111/1365-2478.12124>
- Maalej M, Leong KS. Effect of beam size and FRP thickness on interfacial shear stress

- concentration and failure mode of FRP-strengthened beams. *Composites Science and Technology*, 2005, 65(7-8), 1148-1158.
<https://doi.org/10.1016/j.compscitech.2004.11.010>
- Malhotra PK. Response spectrum of incompatible acceleration, velocity and displacement histories. *Earthquake Engineering and Structural Dynamics*, 2001, 30, 279-286.
- Mateo C, Talavera JA. Short-time Fourier transform with the window size fixed in the frequency domain. *Digital Signal Processing*, 2018, 77, 13-21.
<https://doi.org/10.1016/j.dsp.2017.11.003>
- Ministry of Transport of the PRC. Code for Design of Road Tunnel, JTG D70-2004, 2004.
- Mittal H, Kamal, Kumar A, Singh SK. Estimation of site effects in Delhi using standard spectral ratio. *Soil Dynamics and Earthquake Engineering*, 2013, 50, 53-61.
<https://doi.org/10.1016/j.soildyn.2013.03.004>
- Mofidi A, Chaallal O. Tests and Design Provisions for Reinforced-Concrete Beams Strengthened in Shear Using FRP Sheets and Strips. *International Journal of Concrete Structures and Materials*, 2014, 8, 117-128.
<https://doi.org/10.1007/s40069-013-0060-1>
- National Strong-Motion Program, United States Geological Survey, Menlo Park, CA. And Vibrationdata El Centro Earthquake Page.
- Nie ZY, Zhang CL, Li FX. Effect of Void behind Lining on Seismic Performance of Tunnel. *China Earthquake Engineering Journal*, 2015, 37(1), 138-143.
<http://doi.org/10.3969/j.issn.1000-0844.2015.01.0138>
- Rabia B, Daouadji TH, Abderezak R. Effect of distribution shape of the porosity on the interfacial stresses of the FGM beam strengthened with FRP plate. *Earthquakes and Structures*, 2019, 16(5), 601-609. <http://doi.org/10.12989/eas.2019.16.5.601>
- Setvati MR, Mustaffa Z. Rehabilitation of notched circular hollow sectional steel beam using CFRP patch. *Steel and Composite Structures*, 2018, 26(2), 151-161.
<https://doi.org/10.12989/scs.2018.26.2.151>
- Shen Y, Gao B, Yang X, Tao S. Seismic damage mechanism and dynamic deformation characteristic analysis of mountain tunnel after Wenchuan earthquake. *Engineering Geology*, 2014, 180, 85-98.
<https://doi.org/10.1016/j.enggeo.2014.07.017>
- Strong Motion Earthquake Accelerograms, Digitized and Plotted Data, Report of CALTEC Vol.II, Part A, EERL71-50, 1971.
- Sumathi A, Arun Vignesh S. Study on behavior of RCC beams with externally bonded FRP members in flexure. *Advances in concrete construction*, 2017, 5(6), 625-638.

- <http://doi.org/10.12989/acc.2017.5.6.625>
- Wang XS. Stability Analysis and Deformation Control Measures of Underground Structures in Complex Geological Conditions. Ph.D. Thesis, Nagasaki University, Nagasaki, 2017.
- Wang XS, Wei L, Wang ZQ, Jiang YJ, Zhang LM, Meng FZ, Cong Y. Study on the Reinforcing Effects of the FRP-PCM Method on Tunnel Linings for Dynamic Strengthening. *Geofluids*, 2021, 2021, 8926423.
<https://doi.org/10.1155/2021/8926423>
- Xin CL, Wang ZZ, Gao B. Shaking table tests on seismic response and damage mode of tunnel linings in diverse tunnel-void interaction states. *Tunnelling and Underground Space Technology*, 2018, 77, 295-304. <https://doi.org/10.1016/j.tust.2018.03.010>
- Yan GM, Shen YS, Xin CL, Gao B, Zhou PF, Zhang X, Yang JQ. Shaking table test research of the influence of voids on seismic response of tunnel structures. *Chinese Journal of Rock Mechanism and Engineering*, 2019, 38(12), 2491-2501.
- Yang Y, Xie X, Wang R. Numerical simulation of dynamic response of operating metro tunnel induced by ground explosion. *Journal of Rock Mechanics and Geotechnical Engineering*, 2010, 2(4), 373-384. <https://doi.org/10.3724/SP.J.1235.2010.00373>
- Yasuda N, Tsukada K, Asakura T. Three-dimensional seismic response of a cylindrical tunnel with voids behind the lining. *Tunnelling and Underground Space Technology*, 2019, 84, 399-412. <https://doi.org/10.1016/j.tust.2018.11.026>
- Zhang XP, Jiang YJ, Sugimoto S. Seismic damage assessment of mountain tunnel: A case study on the Tawarayama tunnel due to the 2016 Kumamoto Earthquake. *Tunnelling and Underground Space Technology*, 2018, 71, 138-148.
- Zhang XP, Jiang YJ, Hirakawa Y, Cai Y, Sugimoto S. Correlation Between Seismic Damages of Tawarayama Tunnel and Ground Deformation Under the 2016 Kumamoto Earthquake. *Rock Mechanics and Rock Engineering*, 2019, 52, 2401-2413. <https://doi.org/10.1007/s00603-018-1704-x>
- Zhu ZG, Geng YS, Wu J, Zhu YQ, Wang DY, Han XM. Research on the Effect Mechanism of Cavity behind Tunnel lining under the Earthquake Action. *Journal of Railway Engineering Society*, 2015, 9, 79-84.
- Zhu ZG, Yu JT, Sui CY, Wang DY, Zhu YQ, Sun ML. Compressive Seismic Measures for Tunnel Structure in the Area of High Intensity Active Fault. *China Railway Science*, 2014, 6, 55-62.

7 Reinforcement design of lining structure with typical quality defects and disease

7.1 Introduction

Typical quality defects and diseases, if not properly addressed, will have a non-negligible negative impact on the tunnel and seriously threaten the safety of people's lives and property. Therefore, it is crucial to determine an appropriate reinforcement design for defective and diseased linings. However, an accurate evaluation of the health state of linings is the prerequisite for a rational reinforcement design.

The health state of lining structures is generally affected by a variety of factors, such as lining defects, voids behind the lining, cracks, water leakage, etc. (Ministry of Railways of the PRC 2004). Uncertainty, ambiguity, and complexity are typical characteristics of these factors, leading to difficulties in tunnel health assessment (Yang et al. 2014). If the evaluation factors are vague, fuzzy evaluation is required (Li 2004). Concerning the fuzzy evaluation of the tunnel structure, Hong and Liu (2011) conducted a comprehensive evaluation of the health status of railway tunnels with the analytic hierarchy process (AHP), and the health assessment was conducted. Ye (2021) evaluated the influence of poor contact behind the lining on the safety state of the tunnel structure, and the influence degree was divided into four grades. Li et al. (2021) provided a five-level safety evaluation method for tunnel structures with the fuzzy mathematical theory. Yan and Zhu (2010) constructed a fire safety evaluation model of tunnel linings based on a fuzzy comprehensive evaluation (FCE) method, in which the AHP method was applied to determine the index weight. Wang et al. (2017) investigated the long-term health status of tunnel structures with the fuzzy evaluation method, and the established model was applied to the Cang Ling Tunnel. Zheng et al. (2020) conducted the risk assessment of mountain tunnels with the AHP-FCE method, and the countermeasures of risk prevention were provided. Hu et al. (2018) provided the classification standard of the evaluation index of the long highway tunnel, and the evaluation system of the safety level was established with the method of the AHP-fuzzy principle. Zhao et al. (2017) established an evaluation system of railway tunnel diseases with a fuzzy model, and the safety state of

the Yichang-Wanzhou railway tunnel was evaluated. Luo (2007) provided evaluation standards for tunnel diseases and a set of diagnostic systems for tunnel health was established. In addition, to better evaluate tunnel health, some standards have been proposed to promote the development of tunnel status assessment (Yang et al. 2014).

The health state of the tunnel lining structure is affected by multiple levels and indicators, and previous evaluation models often have shortcomings in the improper selection of evaluation indicators and unclear classification of index levels. Meanwhile, the AHP method is often applied as an important and convenient method for weight determination, and it is meaningful to further carry out combined weight analysis (Wang et al. 2019; Ye 2021). In addition, the membership degree significantly affects the evaluation results, while the determination of membership function has a subjective phenomenon in the application of the FCE model. Therefore, the purpose of this study is to reasonably reveal the degree of influence of typical quality defects and disease on the health state of lining structures, and conduct a reasonable reinforcement design. The main research contents of this chapter are as follows: at first, typical tunnel quality defects, diseases, and their main controlling factors affecting the health state of lining structures are determined by the statistical analysis method. Then, the hierarchical structure model is further constructed based on the structural relationship, and the weight is determined by the AHP-entropy weight method (EWM). Subsequently, the membership function suitable for this study is determined, and the FCE model of the degree of influence of typical quality defects and disease on the health state of the lining structure is established. To provide a suitable reinforcement design, the reinforcement techniques for lining structures are reviewed. On this basis, the reinforcement design of the defective and diseased lining is given based on the established FCE model. Finally, the process of reinforcement design for the lining structure is summarized.

7.2 Hierarchical model establishment

7.2.1 *Index analysis*

The target layer of the evaluation model in this chapter is the influence degree of typical quality defects and disease on the health state of lining structure. Concerning selecting indicators in the criterion and index layers, it is necessary to satisfy the principles of

scientific rationality, relative integrity, hierarchy et al. (He 2004). If the number of selected indicators is too few, the evaluation system may be incomplete. On the contrary, if the number or level of the index is large, the model will become complicated, which is inconvenient to be applied. Therefore, it is crucial to construct a systematic and necessary index system.

Based on the previous chapters, this chapter conducted index analysis by the method of statistical analysis of tunnel structure (Ministry of Railways of the PRC 2004; Zhang 2012; Yang et al. 2014; Hong and Liu 2011; Yi 2019; Lai et al. 2017; Luo 2007; Gong 2019). The established hierarchical structure model can be presented in Fig. 7.1. It should be pointed out that the tunnel quality defect has a significant impact on the safety state of the lining structure, such as the plastic zone distribution characteristics. In addition, the causes of lining cracks are due to the geological environment effect, a direct effect of external loading, temperature effect, drying shrinkage effect, etc. (Ye et al. 2010). In this chapter, it is assumed that the influence of each index is independent. It is observed that the hierarchical structure model includes three levels. The void behind the lining, insufficient lining thickness, and lining crack disease was identified at the criterion layer. Regarding the determination of the index layer, a total of 13 main indicators were determined. As for the void behind the lining, the index layer includes the void circumferential range, void longitudinal length, void radial height, and void spatial location. Regarding the insufficient lining thickness, the index layer includes defect circumferential range, defect longitudinal length, defect degree, and defect spatial location. It should be indicated that the definition of degree of defect C6 is the ratio of rock mass embedded into the lining structure. Concerning the lining crack disease, the index layer mainly includes crack length, crack width, crack pattern, crack depth degree and crack development state. Then, the hierarchical structure model was constructed according to the relationship between each index. Finally, a multi-index and three-level comprehensive evaluation system of the influence degree of quality defects and disease on the health status of lining structures was constructed.

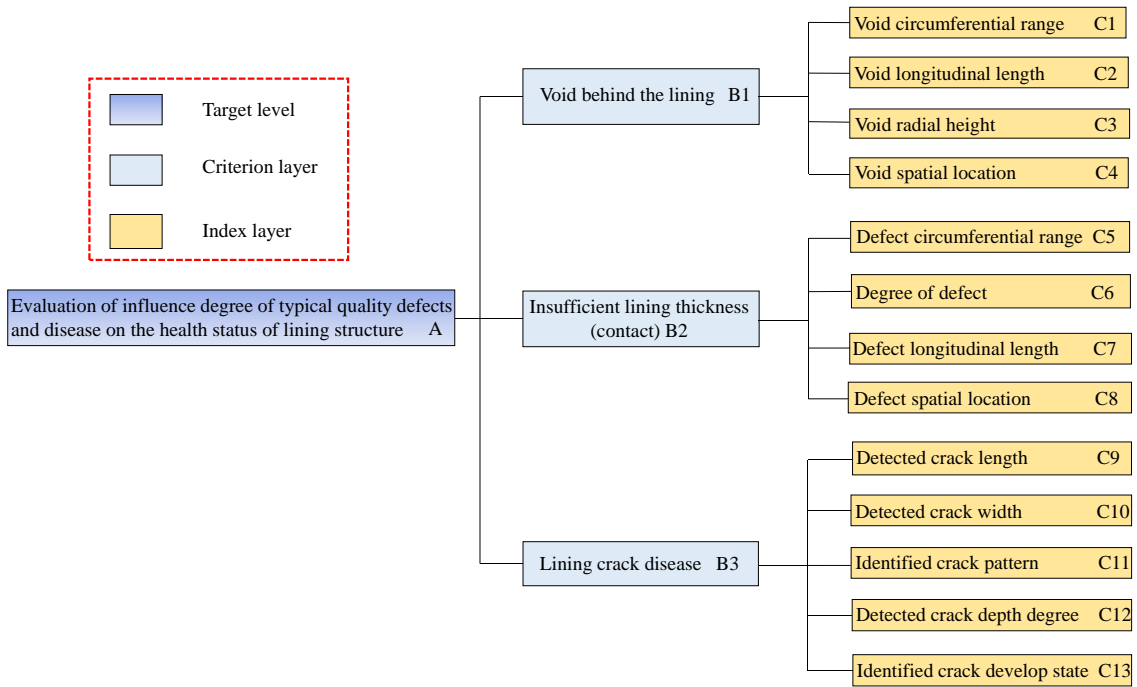


Fig. 7.1 Evaluation system.

7.2.2 Weight calculation method

The weight of each index relative to the target layer should be determined. The analytic hierarchy process (AHP) is an efficient and common method to deal with weight analysis, which was introduced by Saaty T.L.(1980). The calculation processes of the AHP introduced by Saaty T.L. can be expressed as the following formulas (Xu et al. 2011):

$$\bar{\omega}_i = \left(\prod_{j=1}^n q_{ij} \right)^{\frac{1}{n}} \quad (i = 1, 2, \dots, n) \quad (7-1)$$

$$\omega_i = \bar{\omega}_i / \sum_{j=1}^n \bar{\omega}_j \quad (i = 1, 2, \dots, n) \quad (7-2)$$

$$\lambda_{\max} = \left(\sum_{i=1}^n ((A\omega)_i / \omega_i) \right) / n \quad (7-3)$$

$$CR = \{ (\lambda_{\max} - n) / (n - 1) \} / RI \quad (7-4)$$

$$\omega_j^L = \sum_{i=1}^{n_1} \omega_i^K \psi_{ji} \quad (j = 1, 2, \dots, n_2) \quad (7-5)$$

$$CR^L = \frac{\left(\sum_{i=1}^{n_1} \omega_i^K CI_{K_i}^L \right)}{\left(\sum_{i=1}^{n_1} \omega_i^K RI_{K_i}^L \right)} \quad (7-6)$$

where q_{ij} is the element of the judgment matrix; ω_i^K is the total ranking weight vector of the factors of the upper layer (K layer); ψ_{ji} is the weight of n_2 factors of the lower layer (L layer) corresponding to K_i , and $\psi_{ji} = 0$ when the L_j and ψ_{ji} are independent; ω_j^L is the total ranking weight vector of the factors of the lower layer (L layer); $CI_{K_i}^L$ and $RI_{K_i}^L$ are the general consistency index and random consistency index of L layer corresponding to K_i ; CR^L is the total order random consistency ratio of the L layer.

Entropy is the concept of thermodynamics, which is usually applied to judge the stage of systemic disorder with information entropy (Zhang et al. 2014). The entropy weight method (EWM) can be combined to conduct the combined weight analysis (Wang et al. 2019). In this chapter, the combined weight analysis is based on the AHP-EWM. According to the subjective weight, the expert's own weight can be obtained using the EWM (Wang et al. 2019), the calculation processes can be expressed as the following formulas (Wang et al. 2019):

$$Y_{ij} = \frac{x_{ij} - \min(x_i)}{\max(x_i) - \min(x_i)} \quad (7-7)$$

$$E_j = -\ln(m)^{-1} \sum_{i=1}^n p_{ij} \ln p_{ij} \quad (7-8)$$

$$c_i = \frac{1 - E_j}{m - \sum_{i=1}^m E_j} \quad (i = 1, 2, \dots, m) \quad (7-9)$$

$$p_{ij} = y_{ij} / \sum_{i=1}^n y_{ij} \quad (7-10)$$

where $\max(x_i)$ and $\min(x_i)$ are the maximum and minimum values obtained by filtering column; Y_{ij} is the element after normalization of the positive indicator; E_j is the entropy value of expert j ; m is the number of experts; p_{ij} is the proportion of the weight of the expert j in the index i .

The combined weight can be expressed as follows (Wang et al. 2019):

$$W_i = \sum_{j=1}^m \omega_{ji} \times c_j \quad (7-11)$$

where W_i is the combined weight; ω_{ji} is the subjective weight of the expert j on the i index; c_j is the expert j 's own weight.

7.2.3 Weight analysis

In this research, the judgment matrix obtained by the experts can be presented in Tables 7.1-7.4. The weight distribution obtained by AHP can also be shown in Tables 7.1-7.4. Meanwhile, a consistency check should be conducted. When $CR < 0.1$, the judgment matrix satisfies the consistency requirements, otherwise the judgment matrix needs to be rebuilt (Wang et al. 2019; Fang et al. 2021, The SPSSAU project 2022, Ye 2021). As shown in Tables 7.1-7.4, each judgment matrix has passed the consistency check, satisfying the consistency requirement. In addition, the total ranking consistency should also be checked. The obtained overall consistency ratios CR satisfy the consistency requirement.

Table 7.1 Judgment matrix of criterion layer A.

Experts	Judgment matrix	Weight distribution	Consistency check	Preliminary judgment
1	$\begin{bmatrix} 1 & 2 & 1/3 \\ 1/2 & 1 & 1/4 \\ 3 & 4 & 1 \end{bmatrix}$	$\omega_{A-B-1} = (0.2385, 0.1365, 0.6250)$	$\lambda_{\max} = 3.018$ $CR = 0.018 < 0.1$	OK
2	$\begin{bmatrix} 1 & 1/2 & 1/4 \\ 2 & 1 & 1/2 \\ 4 & 2 & 1 \end{bmatrix}$	$\omega_{A-B-2} = (0.1429, 0.2857, 0.5714)$	$\lambda_{\max} = 3.000$ $CR = 0 < 0.1$	OK
3	$\begin{bmatrix} 1 & 2 & 1/2 \\ 1/2 & 1 & 1/3 \\ 2 & 3 & 1 \end{bmatrix}$	$\omega_{A-B-3} = (0.2970, 0.1634, 0.5396)$	$\lambda_{\max} = 3.009$ $CR = 0.009 < 0.1$	OK

Table 7.2 Judgment matrix of index layer of B1.

Experts	Judgment matrix	Weight distribution	Consistency check	Preliminary judgment
1	$\begin{bmatrix} 1 & 1/2 & 3 & 2 \\ 2 & 1 & 4 & 3 \\ 1/3 & 1/4 & 1 & 1/2 \\ 1/2 & 1/3 & 2 & 1 \end{bmatrix}$	$\omega_{B1-C-1} = (0.2776, 0.4668, 0.0953, 0.1603)$	$\lambda_{max}=4.031$ $CR=0.012<0.1$	OK
2	$\begin{bmatrix} 1 & 2 & 5 & 3 \\ 1/2 & 1 & 4 & 2 \\ 1/5 & 1/4 & 1 & 1/3 \\ 1/3 & 1/2 & 3 & 1 \end{bmatrix}$	$\omega_{B1-C-2} = (0.4724, 0.2854, 0.0725, 0.1697)$	$\lambda_{max}=4.051$ $CR=0.019<0.1$	OK
3	$\begin{bmatrix} 1 & 1/2 & 4 & 3 \\ 2 & 1 & 5 & 4 \\ 1/4 & 1/5 & 1 & 1/2 \\ 1/3 & 1/4 & 2 & 1 \end{bmatrix}$	$\omega_{B1-C-3} = (0.3059, 0.4915, 0.0777, 0.1249)$	$\lambda_{max}=4.048$ $CR=0.018<0.1$	OK

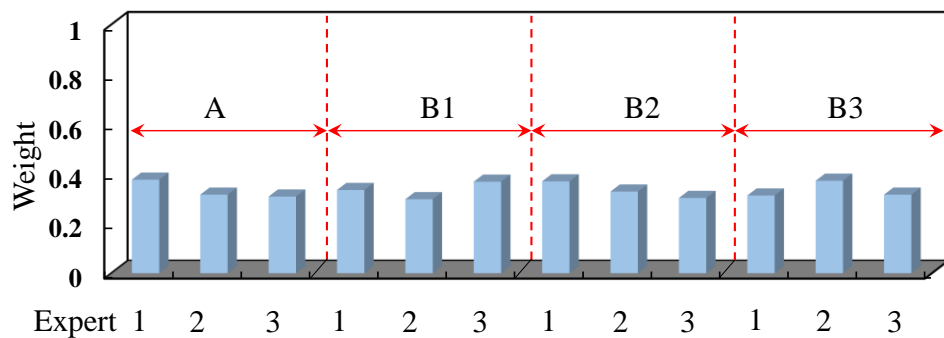
Table 7.3 Judgment matrix of index layer of B2.

Experts	Judgment matrix	Weight distribution	Consistency check	Preliminary judgment
1	$\begin{bmatrix} 1 & 1/2 & 1/4 & 2 \\ 2 & 1 & 1/3 & 3 \\ 4 & 3 & 1 & 5 \\ 1/2 & 1/3 & 1/5 & 1 \end{bmatrix}$	$\omega_{B2-C-1} = (0.1384, 0.2329, 0.5450, 0.0837)$	$\lambda_{max}=4.051$ $CR=0.019<0.1$	OK
2	$\begin{bmatrix} 1 & 1/3 & 1/2 & 2 \\ 3 & 1 & 2 & 4 \\ 2 & 1/2 & 1 & 2 \\ 1/2 & 1/4 & 1/2 & 1 \end{bmatrix}$	$\omega_{B2-C-2} = (0.1630, 0.4747, 0.2551, 0.1072)$	$\lambda_{max}=4.046$ $CR=0.017<0.1$	OK
3	$\begin{bmatrix} 1 & 1/4 & 1/3 & 1/2 \\ 4 & 1 & 2 & 3 \\ 3 & 1/2 & 1 & 2 \\ 2 & 1/3 & 1/2 & 1 \end{bmatrix}$	$\omega_{B2-C-3} = (0.0953, 0.4668, 0.2776, 0.1603)$	$\lambda_{max}=4.031$ $CR=0.012<0.1$	OK

Table 7.4 Judgment matrix of index layer of B3.

Experts	Judgment matrix	Weight distribution	Consistency check	Preliminary judgment
1	$\begin{bmatrix} 1 & 1 & 3 & 2 & 1/2 \\ 1 & 1 & 3 & 2 & 1/2 \\ 1/3 & 1/3 & 1 & 1/2 & 1/4 \\ 1/2 & 1/2 & 2 & 1 & 1/3 \\ 2 & 2 & 4 & 3 & 1 \end{bmatrix}$	$\omega_{B3-C-1} = (0.2154, 0.2154, 0.0735, 0.1208, 0.3749)$	$\lambda_{\max}=5.033$ $CR=0.007<0.1$	OK
2	$\begin{bmatrix} 1 & 1 & 4 & 2 & 1/3 \\ 1 & 1 & 4 & 2 & 1/3 \\ 1/4 & 1/4 & 1 & 1/2 & 1/5 \\ 1/2 & 1/2 & 2 & 1 & 1/4 \\ 3 & 3 & 5 & 4 & 1 \end{bmatrix}$	$\omega_{B3-C-2} = (0.1937, 0.1937, 0.0577, 0.1051, 0.4498)$	$\lambda_{\max}=5.084$ $CR=0.019<0.1$	OK
3	$\begin{bmatrix} 1 & 1 & 4 & 3 & 2 \\ 1 & 1 & 4 & 3 & 2 \\ 1/4 & 1/4 & 1 & 1/2 & 1/4 \\ 1/3 & 1/3 & 2 & 1 & 1/3 \\ 1/2 & 1/2 & 4 & 3 & 1 \end{bmatrix}$	$\omega_{B3-C-3} = (0.3150, 0.3150, 0.0632, 0.0991, 0.2077)$	$\lambda_{\max}=5.097$ $CR=0.022<0.1$	OK

Subsequently, the weight distribution obtained by EWM can be shown in Fig. 7.2. Further, the combined weights were calculated, and the obtained combined weight can be presented in Table 7.5 and Fig. 7.3.

**Fig. 7.2** Distribution of weight of experts.

As exhibited in Table 7.5, lining crack disease has the largest weight, accounting for 58.18%, followed by void behind the lining and insufficient lining thickness, accounting

for 22.63% and 19.19%, respectively. Regarding the weight of the index layer to the criterion layer, the sum weights the void longitudinal length and the void circumferential range in index layer is high at 76.79%. As for the insufficient lining thickness, the sum weight of degree of defect and defect longitudinal length is high at 75.2%. Concerning the lining crack disease, the sum weight of crack develop state, crack width, and crack length is large at 82.75%. Further, the weight order of the index layer relative to the target layer is as follows: $\omega_{C13} > \omega_{C9} = \omega_{C10} > \omega_{C2} > \omega_{C1} > \omega_{C6} > \omega_{C7} > \omega_{C12} > \omega_{C11} > \omega_{C4} > \omega_{C5} > \omega_{C8} > \omega_{C3}$. It is noted that the weight of crack develop state relative to the target layer is the largest, accounting for 20.36%. The smallest weight is determined as the void vertical height, accounting for 1.85%. The bar charts were created to visualize the weight distribution, as shown in Fig. 7.3. Fig. 7.3(a), Fig. 7.3(b), and Fig. 7.3(c) are the weight distribution of each index relative to the criterion layer, and Fig. 7.3(d) is the underlying weight of each index relative to the target layer.

Table 7.5 Weight distribution of the evaluation system.

Criterion layer	Weight	Index layer	Weight	Weight on the target layer	Ranking
Void behind the lining (B1)	0.2263	C1	0.3460	0.0783	5
		C2	0.4219	0.0955	4
		C3	0.0820	0.0185	13
		C4	0.1501	0.0340	10
Insufficient lining thickness (B2)	0.1919	C5	0.1334	0.0256	11
		C6	0.3831	0.0735	6
		C7	0.3689	0.0708	7
		C8	0.1146	0.0220	12
Lining crack disease (B3)	0.5818	C9	0.2388	0.1389	2
		C10	0.2388	0.1389	2
		C11	0.0644	0.0375	9
		C12	0.1081	0.0629	8
		C13	0.3499	0.2036	1

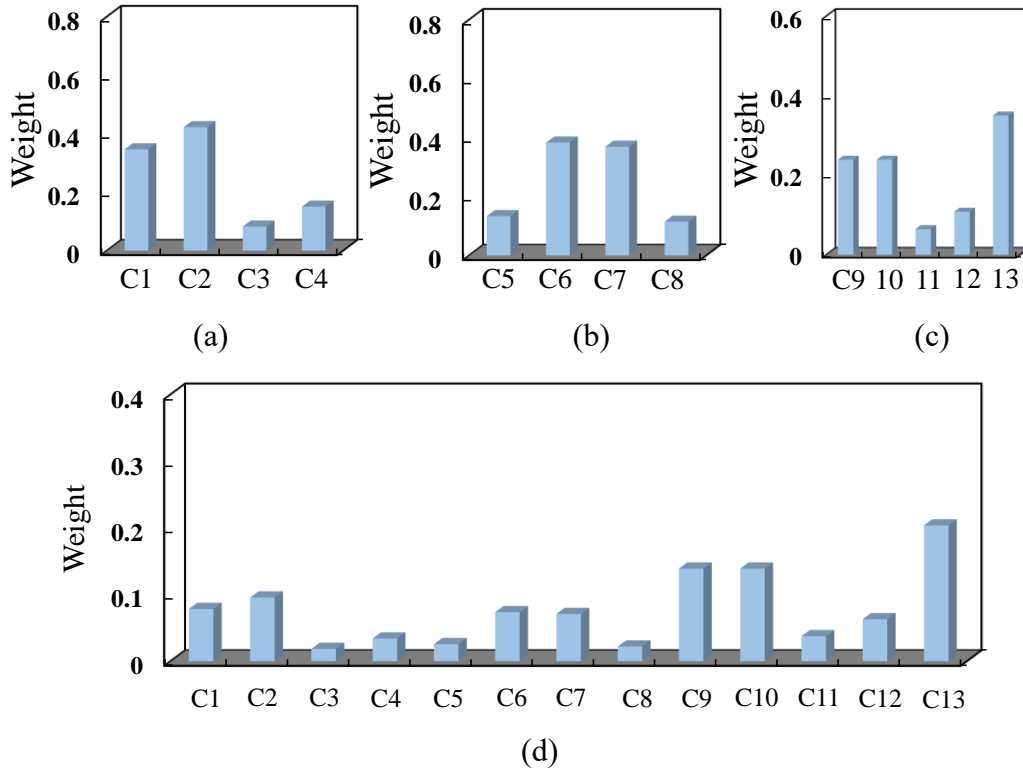


Fig. 7.3 Weight distribution: (a) index layer B1; (b) index layer B2; (c) index layer B3; (d) weight relative to the target layer.

7.3 Establishment of the FCE model

7.3.1 Principle of the FCE method

Zadeh (1965) proposed fuzzy concepts into the application category of mathematics. The principle of the FCE method is to decompose the evaluation target with indicators, describing each index and its fuzzy boundary by the membership degree (Jiang et al. 2021; Wang et al. 2019). Therefore, the primary step of the FCE method is the determination of evaluation sets and membership degree. Concerning the determination of evaluation sets, the expression can be expressed as follows (Wang et al. 2019):

$$V = \{v_1, v_2, v_3, \dots, v_n\} \quad (7-12)$$

where V is the evaluation sets; v_n is the comment; n is the number of comments.

Then, the fuzzy operation can be expressed as follows (Wang et al. 2019; Ye 2021):

$$R_i = W_i \circ S_i = (R_{i1}, R_{i2}, \dots, R_{in}) \quad (7-13)$$

where R_i is the first level fuzzy matrix; W_i is the weight vector of factor i ; S_i represents the membership degree matrix; \circ is the fuzzy compositing operator.

Correspondingly, the second fuzzy operation can be expressed as follows (Wang et al. 2019; Ye 2021):

$$Z = W \circ R \quad (7-14)$$

where W is the weight vector; R is the fuzzy matrix in the criterion layer; Z is the evaluation results.

7.3.2 Establishment of evaluation model

7.3.2.1 Evaluation set

According to the previous research (Ministry of Railways of the PRC 2004; Zhang 2012; Ye 2021; Hong and Liu 2011; Gao et al. 2018), the evaluation set of the influence degree of typical quality defects and disease on the lining structure can be divided into four levels: v_a , v_b , v_c , and v_d . Evaluation v_a indicates basically no effect, v_b means that the degree of influence is moderate, v_c denotes that the degree of influence is large, v_d demonstrates that the degree of influence is extremely significant.

7.3.2.2 Membership degree

In the established model, the discrete or qualitative evaluation index includes void spatial location, defect spatial location, crack pattern, and crack develop state. The membership degree of the discrete index can also be determined by the expert evaluation method (Liu et al. 2013). The membership degree of each qualitative index in the established model can be processed in Table 7.6.

Table 7.6 Membership degree of each qualitative evaluation index.

Membership degree	C4 (Feng 2013)	C8 (Gong 2019)	C11 (He et al.2019)	C13 (He et al. 2019)
v_a	Others	Others	Ring or others	No develop
v_b	Sidewall	Sidewall	Oblique	Develop slowly
v_c	Crown	Shoulder	Longitudinal	Develop fast
v_d	Shoulder	Crown	Mesh or cross	Develop rapidly

Regarding the continuous index, the membership function is frequently applied to determine the membership degree of each index (Liu et al. 2013). There are many membership functions, such as triangular distribution, trapezoidal distribution, Gaussian distribution, Generalized bell distribution, etc. (Ali et al. 2015). Since the degree of membership significantly affects the evaluation results, the half trapezoid model was determined to determine the degree of membership by statistical and comparative analysis methods. The membership function of the half trapezoid model can be expressed as follows (Liu et al. 2013):

$$S_{ij}(v_a) = \begin{cases} 1, & u_{ij} \leq c \\ \frac{d-u_{ij}}{d-c}, & c < u_{ij} \leq d \\ 0, & u_{ij} > d \end{cases} \quad (7-15)$$

$$S_{ij}(v_b) = \begin{cases} 0, & u_{ij} < c \text{ or } u_{ij} > e \\ \frac{u_{ij}-c}{d-c}, & c < u_{ij} \leq d \\ \frac{e-u_{ij}}{e-d}, & d < u_{ij} \leq e \end{cases} \quad (7-16)$$

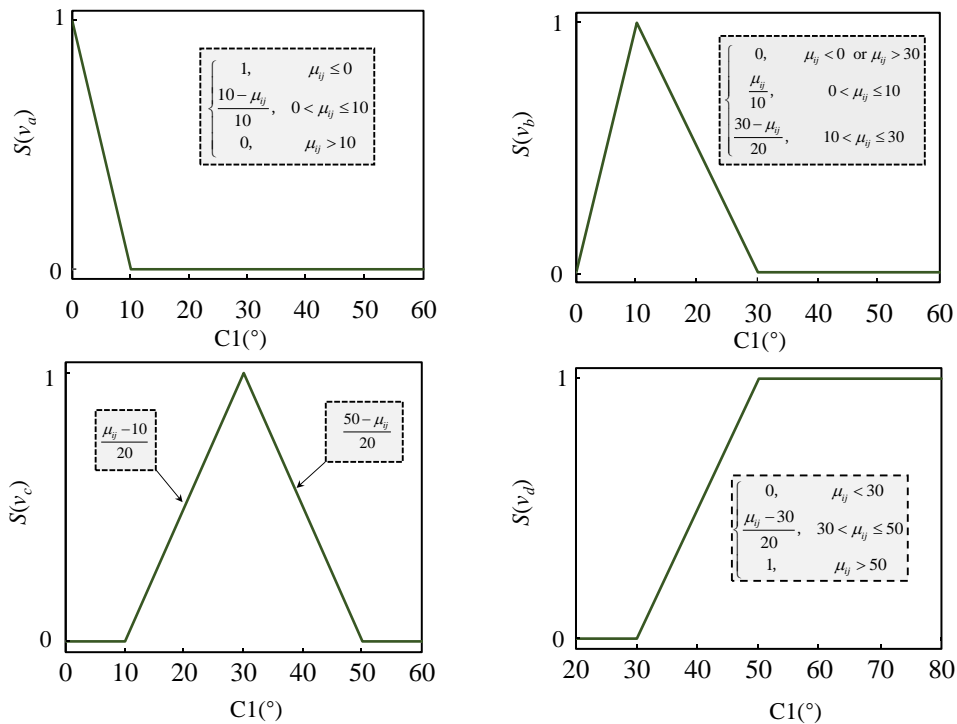
$$S_{ij}(v_c) = \begin{cases} 0, & u_{ij} < d \text{ or } u_{ij} > f \\ \frac{u_{ij}-d}{e-d}, & d < u_{ij} \leq e \\ \frac{f-u_{ij}}{f-e}, & e < u_{ij} \leq f \end{cases} \quad (7-17)$$

$$S_{ij}(v_d) = \begin{cases} 0, & u_{ij} < e \\ \frac{u_{ij}-e}{f-e}, & e < u_{ij} \leq f \\ 1, & u_{ij} > f \end{cases} \quad (7-18)$$

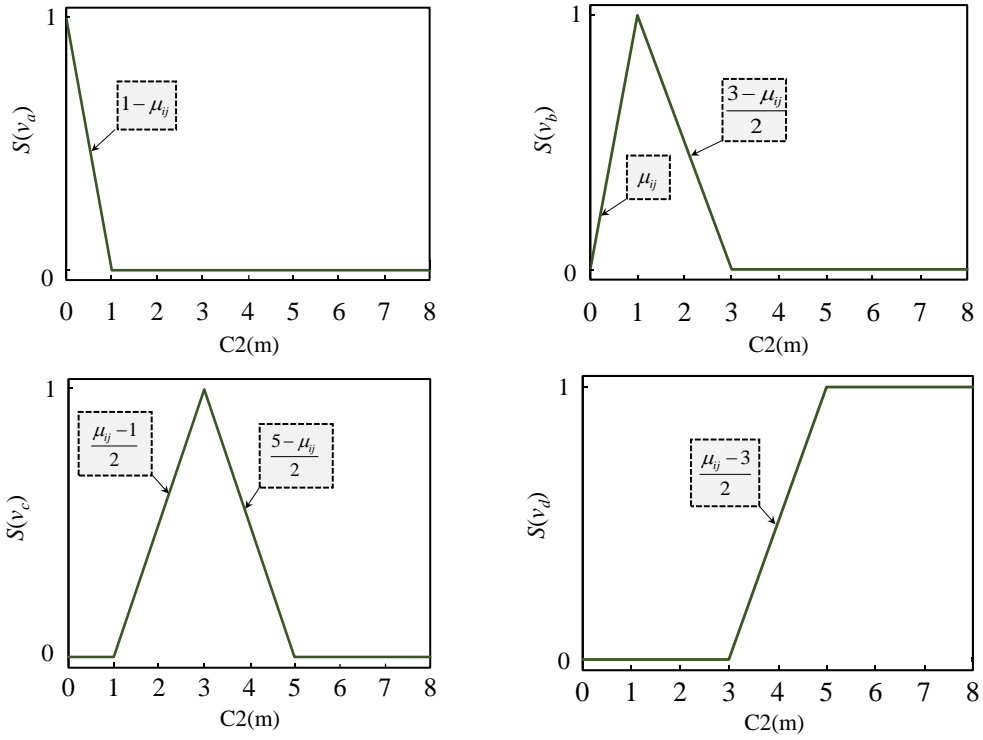
where c , d , e , and f are the extreme values and critical values in each level evaluation.

It should be indicated that the determination of the extreme values and critical values significantly affects the membership degrees. The actual characteristics of the target problem should be fully considered to determine the selection criteria of the critical value.

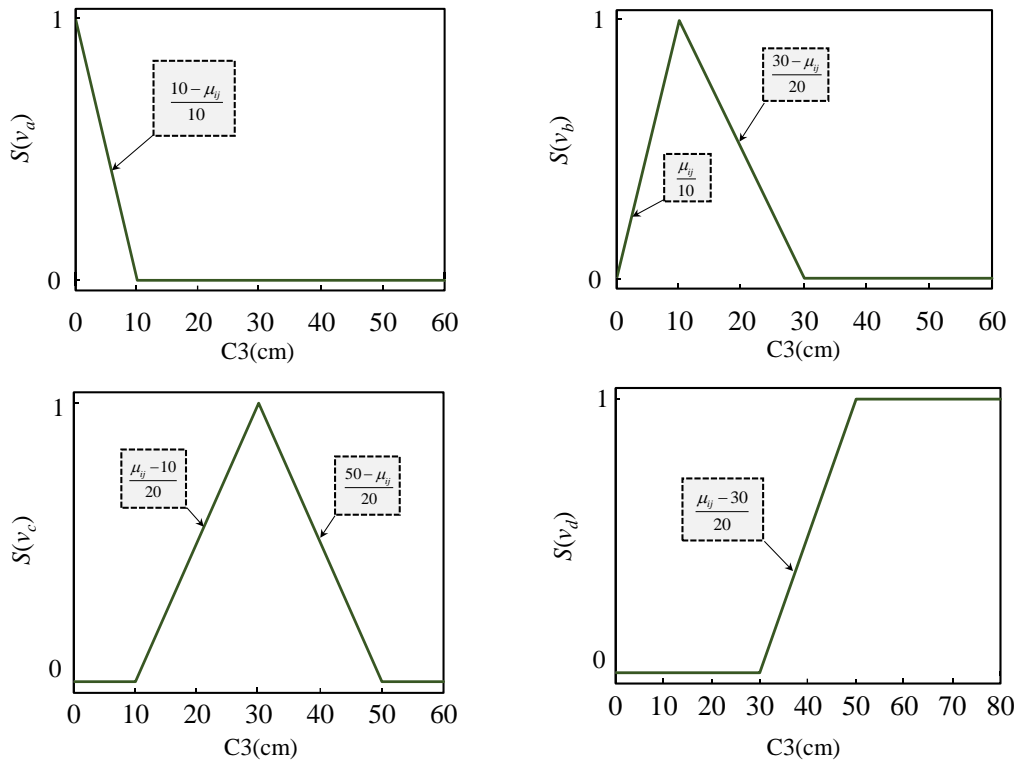
Concerning the FCE model established in this research, the target layer is to evaluate the degree of influence of quality defects and disease on the health of the lining structure. Due to the hidden characteristics and irregularity of tunnel quality defects, it is difficult to measure their distribution characteristics with a regular scale. In addition, other implicit impact factors for example adverse operating environment cannot be effectively reflected in the current model. It is meaningful to reserve a specific safety reserve space for the reinforcement design. Thus, selecting the lower limit of the corresponding level as the criterion for determining the critical value could be suitable for the evaluation model. Subsequently, the determined values, including the extreme values and critical values of each index, were substituted into the expressions (7-15)-(7-18) (Liu et al. 2013). It should be indicated that the level classification, including the extreme values and critical values of each index, could be determined according to the results in this paper and previous studies (Ren 2018; Ministry of Railways of the PRC 2004; Guan 2004; Japan Ministry of Land, Infrastructure, Transport and Tourism 2018; Zhang 2012; Gong 2019; Yang et al. 2014; Ministry of Railways of the PRC 2003; Ministry of Railways of the PRC 2001; Luo 2007), and the obtained membership function can be shown in Fig. 7.4(a)-Fig. 7.4(i).



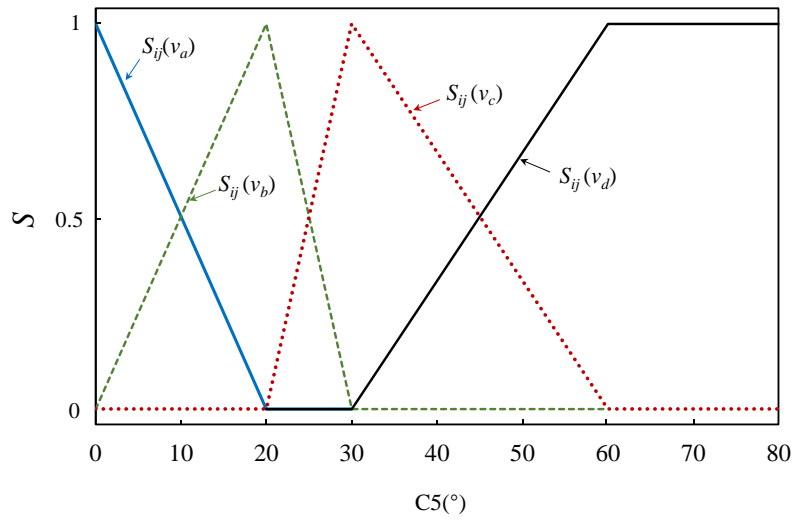
(a) Membership function of C1



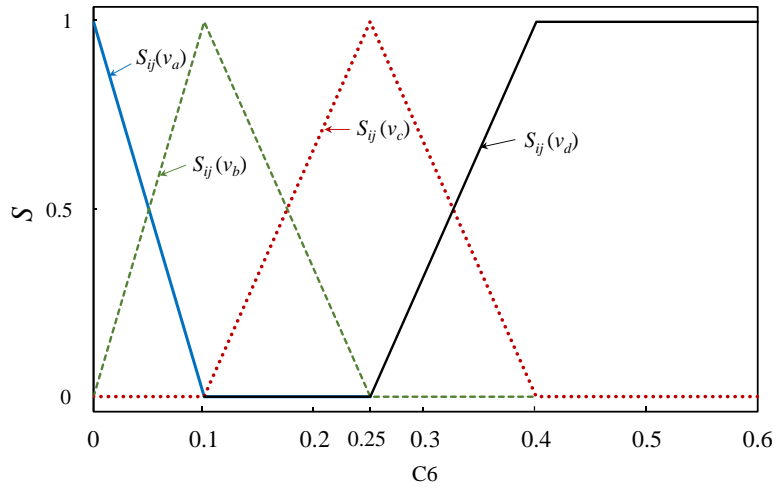
(b) Membership function of C2



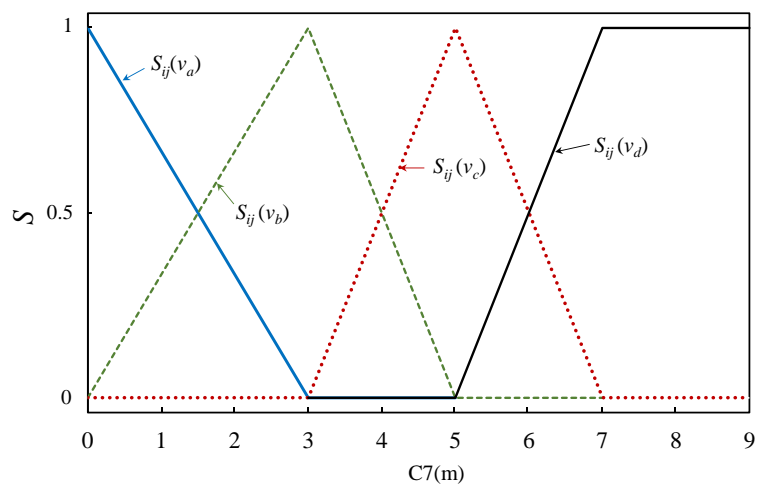
(c) Membership function of C3



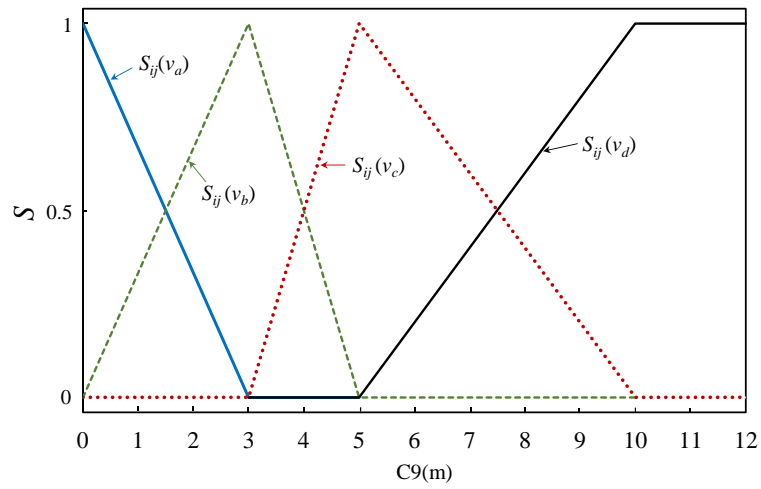
(d) Membership function of C5



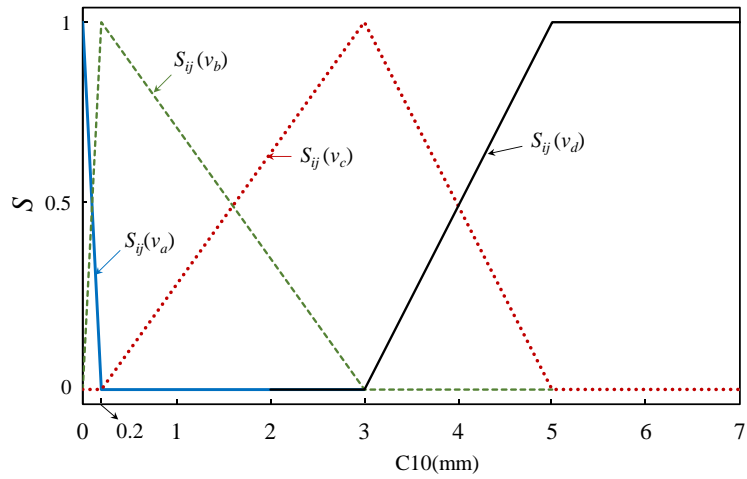
(e) Membership function of C6



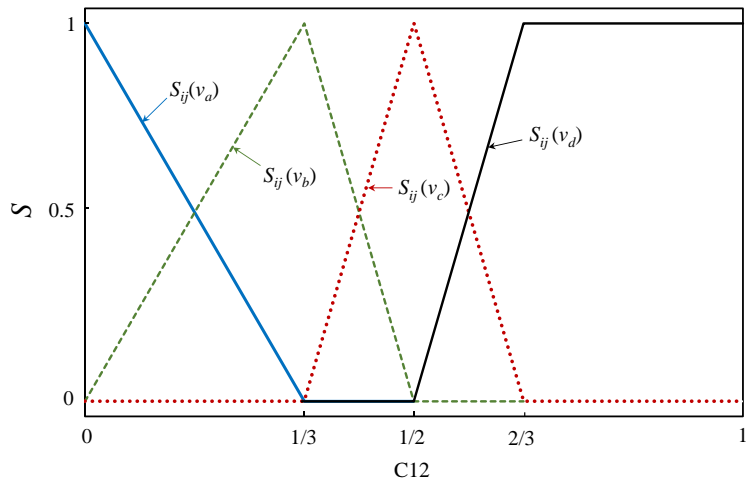
(f) Membership function of C7



(g) Membership function of C9



(h) Membership function of C10



(i) Membership function of C12

Fig. 7.4 Distribution of membership function.

7.4 Application of the established evaluation model

When a certain tunnel section has typical quality defects and diseases, the FCE model established in this chapter is applied to evaluate the degree of influence. As an example, it is assumed that the detected values of defects and diseases are shown in Table 7.7. At first, substitute the parameters of Table 7.7 into the membership function. Next, the First-level fuzzy calculation is performed in combination with the weights in Table 7.5. The calculation can be shown in Table 7.8.

Table 7.7 Specific parameter values of quality defects and diseases.

Type	Descriptions and Remarks
Void behind the lining	Void circumferential range is 40° ; Void longitudinal length is 3.5m; Void radial height is 15 cm; Void location is at the shoulder.
Insufficient lining thickness	Defect circumferential range is 25° ; Degree of defect is 0.3; Defect longitudinal length is 2 m; Defect location is at the shoulder.
Crack disease	Crack length is 4 m; width is 4.5 mm; Longitudinal crack pattern; Crack depth degree is $2/3$; Crack develops fast.

Table 7.8 First-level fuzzy evaluation.

Cases	Weight vector	Membership matrix	Fuzzy calculation
Void behind the lining	$\begin{bmatrix} 0.3460 \\ 0.4219 \\ 0.0820 \\ 0.1501 \end{bmatrix}^T$	$\begin{bmatrix} 0 & 0 & 1/2 & 1/2 \\ 0 & 0 & 3/4 & 1/4 \\ 0 & 3/4 & 1/4 & 0 \\ 0 & 0 & 0 & 1 \end{bmatrix}$	$\begin{bmatrix} 0 \\ 0.0615 \\ 0.5099 \\ 0.4286 \end{bmatrix}^T$
Insufficient lining thickness	$\begin{bmatrix} 0.1334 \\ 0.3831 \\ 0.3689 \\ 0.1146 \end{bmatrix}^T$	$\begin{bmatrix} 0 & 1/2 & 1/2 & 0 \\ 0 & 0 & 2/3 & 1/3 \\ 1/3 & 2/3 & 0 & 0 \\ 0 & 0 & 1 & 0 \end{bmatrix}$	$\begin{bmatrix} 0.1230 \\ 0.3126 \\ 0.4367 \\ 0.1277 \end{bmatrix}^T$
Crack disease	$\begin{bmatrix} 0.2388 \\ 0.2388 \\ 0.0644 \\ 0.1081 \\ 0.3499 \end{bmatrix}^T$	$\begin{bmatrix} 0 & 1/2 & 1/2 & 0 \\ 0 & 0 & 1/4 & 3/4 \\ 0 & 0 & 1 & 0 \\ 0 & 0 & 0 & 1 \\ 0 & 0 & 1 & 0 \end{bmatrix}$	$\begin{bmatrix} 0 \\ 0.1194 \\ 0.5934 \\ 0.2872 \end{bmatrix}^T$

Subsequently, the second fuzzy operation was performed in combination with the weight in Table 7.5. The process is as follows:

$$Z = [0.2263 \quad 0.1919 \quad 0.5818] \begin{bmatrix} 0 & 0.0615 & 0.5099 & 0.4286 \\ 0.1230 & 0.3126 & 0.4367 & 0.1277 \\ 0 & 0.1194 & 0.5934 & 0.2872 \end{bmatrix} \\ = [0.0236 \quad 0.1434 \quad 0.5444 \quad 0.2886]$$

Then, based on the principle of maximum membership degree (Liu et al. 2013), the level can be determined as:

$$Z = \max_{1 \leq j \leq 4} \{Z_j\} = 0.5444$$

In this case, it can be observed that the degree of influence of combined quality defects and disease on the health of lining structure is determined as v_c , which denotes that the degree of influence is large. Therefore, corresponding reinforcement should be conducted in time.

7.5 Review of reinforcement methods of tunnel linings

7.5.1 Traditional methods

7.5.1.1 Backfill method

When the degree of influence on the health state of the lining structure is large, it is necessary to carry out reinforcement designs in time. To provide a rational reinforcement design, the common repair and reinforcement methods for tunnel quality defects should be reviewed and summarized. It should be indicated that the summary was carried out from the following two aspects, namely the traditional repair techniques and the promising FRP reinforcement technique. From the research results in chapters 3 and 4 of this thesis, it can be observed that a significant tensile concentration stress zone is easily formed at the lining outer surface corresponding to the void zone. However, for the position where the rock mass and the lining are in good contact, the stress state of the lining is normal. Therefore, establishing effective contact between rock mass and the lining is the basis for repairing void defects. The backfill grouting method can fill the void, optimizing the mechanical performance between the lining and rock mass (Liu et al. 2021). This section reviewed and summarized the application of the backfill method,

including the repair subject, backfill materials, application conditions, and precautions, as shown in Table 7.9.

Table 7.9 Application of backfill method in the repair of tunnel quality defect.

References	Repair subject	Backfill materials	Application conditions	Remarks
Liu et al. (2021)	Void defect	M30 cement mortar	Small voids	Grouting pressure should be controlled in the range of 0.3MPa-0.5MPa
Lei (2020)	Void defect	Foam concrete	Void height (h) and scale are large	Grouting pressure should be controlled. Meanwhile, temporary support should be considered.
Guo et al. (2020)	Void and insufficient thickness	New type of micro-expansion grouting material	Lining thickness (L) < 20 cm. The grouting pressure may cause damage to the lining	The construction methods: Intermittent non-shrinkage backfill method ($L < 20$ cm). Opening skylight method ($L \geq 20$ cm).
Jiang et al. (2017)	Void and insufficient thickness	Urethane materials	Fast maintenance and reinforcement project	The reinforcing effect is obvious when applied with FRP materials.
Wang (2014)	Void and insufficient thickness	I: Fine stone concrete II: M35 slightly expansive cement mortar	$L < 20$ cm, material I $L \geq 20$ cm, material II	Fine stone concrete needs to add an expansion agent; Grouting pressure should be concerned.
Fan et al. (2020)	Large-scale void and insufficient thickness	I: Cement mortar. II: PE ball. III: Foam concrete. IV: PVC pipe.	$h \leq 60$ cm, I $h > 60$ cm, II $h > 130$ cm, III $h > 130$ cm, IV	The construction methods: Layered grouting method ($h \leq 60$ cm); Opening skylight method ($h > 60$ cm). When the degree of insufficient thickness is large, other additional measures should also be considered.
Zhang et al. (2021)	Void defect and damaged surface	Cement slurry	Small-size voids and local repair	Before grouting, the damaged part of the lining surfaces should be roughened. The local repair effect is confirmed.

It is noted that foam concrete (Lei 2020; Fan et al. 2020), a new type of micro-expansion grouting material (Guo et al. 2020), urethane materials (Jiang et al. 2017), cement mortar (Liu 2021; Fan et al. 2020; Zhang et al. 2021), fine stone concrete (Wang 2014), PE ball (Fan et al. 2020), and PVC pipe (Fan et al. 2020) can be utilized as backfill materials. However, the application conditions of backfill materials are closely related to

the types, distribution, and morphological characteristics of the quality defects. Particularly, Fan et al. (2020) determined the grouting materials depending on the void height. Wang (2014) identified the backfill materials with the lining thickness. In addition, the construction processes of backfill materials are also closely related to the defect size. Especially, Fan et al. (2020) identified grouting methods depending on the void height. Guo et al. (2020) identified the backfill methods with the lining thickness. Overall, the repair effect of the backfill method is significantly affected by the selection of backfill materials and the construction process. The following steps are required when the backfill method is applied to repair quality defects. At first, it is necessary to clarify the defect type and its detailed parameters, especially including the defect size and defect range. Subsequently, determine the appropriate backfill material based on the defect parameters. Finally, determine the appropriate construction technique in combination with the parameters of the defect and the backfill material. In addition, the technical details of the backfill method should be flexibly adjusted according to the specific project.

7.5.1.2 Bolt reinforcement

The rock mass above the void zone is prone to suffer large deformation, resulting in the loosening area (Jiang et al. 2017; Han et al. 2021a). When the loosening pressure is large, the plastic failure zone occurs in the lining structure (Han et al. 2021a). When there are joints, it is also likely to induce shear failure of rock mass (Han et al. 2020). Therefore, to prevent the further enlargement of the loosening area, it is crucial to reinforce the upper rock mass while repairing the void quality defect. Nie (2013) applied the bolt reinforcement method to reinforce the loosened rock mass above the void zone. Deng et al. (2013) applied the combined method of the backfill and bolt reinforcement to repair the void quality defect, and the effect of earthquake resistance was explored. Fan et al. (2020) utilized the combined technique of backfill and bolt reinforcement to repair the large-scale void quality defect behind the lining. Zhu et al. (2015) applied various repair schemes for the void quality defect and indicated that the best anti-seismic effect is the combined method of backfill, bolt, and arch surrounds scheme. He et al. (2007) conducted the laboratory model test to investigate the reinforcement effect of the combined bolt reinforcement method on tunnel defects. Overall, one of the main functions of the bolt reinforcement method is to strengthen the loosened rock mass. Therefore, when the void

has a great influence on the lining health state and there is a loosened area above the void, the bolt reinforcement method can generally obtain a significant reinforcement effect.

7.5.1.3 Reinforcement technique of inner surface

The area with insufficient lining thickness will lead to reduced stiffness and insufficient bearing capacity, which may easily induce tunnel diseases (Yu et al. 2017; Liu et al. 2020). The technology is to fix materials on the inner surface of the lining to form an integral structure, which can significantly improve the bearing capacity (Liu et al. 2020). Therefore, the inner surface reinforcement technique has been widely applied for the reinforcement of tunnel quality defects. In this section, the common reinforcement techniques of the inner surface were reviewed and exhibited in Table 7.10.

Table 7.10 Application of the reinforcement techniques of inner surface.

References	Subject	Reinforcement methods	Application conditions	Major findings or Remarks
Liu et al. (2020)	Insufficient lining thickness	Inner lining method	Damaged lining with the insufficient thickness	The method can be applied as an effective maintenance method in an operation tunnel.
Liu et al. (2021)	Insufficient lining thickness	Shotcrete support	Lining structure with cracks	The injection process can be divided into two steps to reduce the rebound of shotcrete.
Li et al. (2013)	Cracks and insufficient thickness	Carbon fiber cloth method	The local lining strength is not enough	Non-destructive testing is required to identify the disease and defect distribution.
Jiang and Fan (2016)	Insufficient lining thickness	Spray slurry method	The lining thickness is not reduced much, but there are more cracks.	Pay attention to the uniformity of shotcrete.
Sheng et al. (2020)	Insufficient lining thickness	Bonding steel plate and pouring concrete	Local range of insufficient secondary lining thickness.	It is noted that the reinforcement effect of the pouring concrete is better than that of the bonding steel plate method.
Dong et al. (2017)	Insufficient lining thickness	Steel fiber concrete and steel arch method	The lining thickness is seriously insufficient	The method can be applied to replace the reconstruction method, which is conducive to the economy.

Note that the common reinforcement technologies of inner surface mainly include the inner lining method (Liu et al. 2020), shotcrete support (Liu et al. 2021), carbon fiber

cloth method (Li et al. 2013), spray slurry method (Jiang and Fan 2016), bonding steel plate method (Sheng et al. 2020), pouring concrete method (Sheng et al. 2020), and a combined method of steel fiber concrete and steel arch (Dong et al. 2017), etc. Although the mentioned methods can effectively reinforce the quality defects, the application conditions are different. Suppose the lining structure has both insufficient thickness defects and crack diseases, the application of the carbon fiber cloth method can obtain a good reinforcement effect (Li et al. 2013). If the degree of insufficient lining thickness is serious, the combined method of steel fiber concrete and steel arch can be applied for effective reinforcement (Dong et al. 2017). In addition, the major findings and precautions of other methods were also summarized in Table 7.10. In general, when using the inner surface reinforcement method, the specific defect parameters, such as the defect degree and defect range, should be identified first. On this basis, it is also necessary to combine the specific engineering background to determine the appropriate inner surface reinforcement method.

7.5.2 FRP reinforcement method

The determination of repair materials is critical to the remediation effect of tunnel defects and diseases. The FRP materials have been widely utilized in concrete reinforcement projects, and some applications in civil structures can be summarized in Table 7.11. It is noted that FRP materials can significantly improve the mechanical properties of structures and effectively repair defective and degraded structures.

Table 7.11 Application of FRP materials in the reinforcement of civil structures.

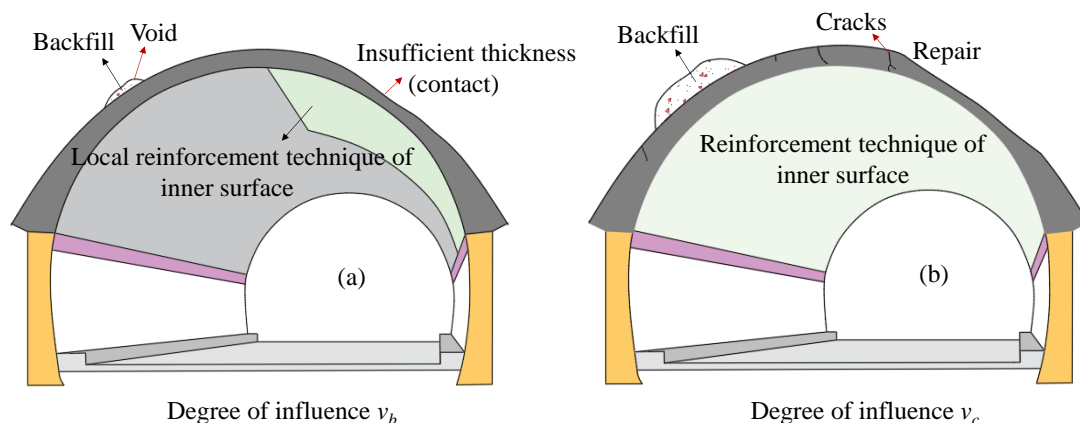
References	Building type	FRP types	Subject of strengthening	Major findings or Remarks
Liu et al. (2022)	Tunnel	FRP grids	Lining cracking	The propagation of the tensile cracks can be effectively suppressed, and the bearing capacity is improved.
Jiang et al. (2017)	Tunnel	FRP grids	Degraded linings with void defect and insufficient thickness	The reinforcement effect is influenced by the grade of FRP grids.
Wang et al. (2021)	Tunnel	FRP grids	Dynamic response under void defect and lining defect	The proportion of the plastic failure zone is reduced under reinforcement.
Higashi et al. (2014)	Tunnel	FRP grids	Degraded linings with void defect and insufficient thickness	Failure of the lining can be inhibited, and the axial stress decreases.

Hara (2015)	Tunnel	FRP corrugate sheet	Degraded lining concrete structure	The proposed corrugate sheet can make the crack visible and flow the water through the concrete.
Han et al. (2021b)	Tunnel	FRP grids	Degraded lining structure with void quality defects	The plastic failure rate of lining structures can be significantly reduced.
Yang et al. (2019)	Tunnel	FRP cloth	Resistance of the tunnel to underwater explosions	The rigidity and bear loading performance can be improved significantly.
Keller et al. (2007)	Bridge	FRP sheet	Flexural behavior of bridge deck	The feasibility of a lightweight hybrid-FRP bridge deck was verified.
Stallings et al. (2000)	Bridge	FRP plates	Repair aging and damaged concrete structures	The stress of the reinforcing bar and the vertical midspan deflections can be reduced.
Schnerch et al. (2007)	Bridge	FRP strips	Steel bridges reinforced with CFRP materials	The guidelines and installation techniques were presented, and high modulus CFRP materials can be applied to reinforce steel bridges.

7.6 Reinforcement design of lining structures

In the review of lining reinforcement, the determination of reinforcement schemes, including the reinforcement method, materials, range, etc., are closely related to the defect parameters. Although the quality defects can be effectively determined, nevertheless, it is still difficult to identify a clear boundary between a large defect and a small defect. The corresponding judgment in practice is primarily based on experience, resulting in great subjectivity and randomness. To solve this problem, boundary determination can be transformed into the degree of influence. Therefore, the reinforcement designs of defective linings can be carried out combined with the FCE model. In addition, Nie (2013) applied a hierarchical method for the reinforcement design of the defective tunnels. Based on Nie (2013), and aiming at the problem that composite defects and diseases may exist in actual tunnels, this chapter develops reinforcement schemes for linings with a variety of defects and diseases. In this section, the corresponding reinforcement design was carried out combined with the established FCE model, as shown in Fig. 7.5. It should be indicated that the lining and rock mass in the area of insufficient lining thickness is in a contact state. As presented in Fig. 7.5(a), it is assumed that the degree of influence of tunnel quality defects on the lining health is moderate, local repair and reinforcement measures need to be taken, that is, the backfill method can be applied to repair the void

defect, and the reinforcement technique of inner surface can be utilized within the lining thickness is insufficient. As shown in Fig. 7.5(b), it is assumed that the degree of influence of quality defects and disease on the health status of the lining is large, and the inner surface reinforcement technique is valuable to apply to the entire tunnel section. According to the degree of cracking, appropriate methods can be selected for crack repair. Further, as exhibited in Fig. 7.5(c), when the degree of influence on the health status of the lining structure is extremely significant, it is necessary to carry out backfill repair, cracks repair, and inner surface reinforcement. When there is a loosened rock mass area over the void, the mechanical properties of the lining will be significantly affected (Jiang et al. 2017), and bolt reinforcement is valuable applied to the void-affected zone (Nie 2013). It should be indicated that the number and range of bolts should be determined and adjusted according to the actual condition. As exhibited in Fig. 7.5(d), it is assumed that the degree of influence of quality defects and disease on the health status of the lining is extremely large, and the single index of the insufficient thickness and crack disease also present a significant influence, it is recommended to apply the FRP-PCM method to strengthen the inner lining surface. Further, as presented in Fig. 7.5(f), it is assumed that the overall thickness of the lining is insufficient, the cracking phenomenon is serious, and a large void exists behind the lining, the local reconstruction can be considered. It should be indicated that the backfill materials, construction processes, crack repair methods, the reinforcement materials on the inner surface, and the grade of FRP grids should be determined combined with the actual condition. It should also be pointed out that determining the distribution of defects and diseases is the premise for effective reinforcement design. The specific reinforcement design is closely related to the actual characteristics of the tunnel, so it should be flexibly adjusted.



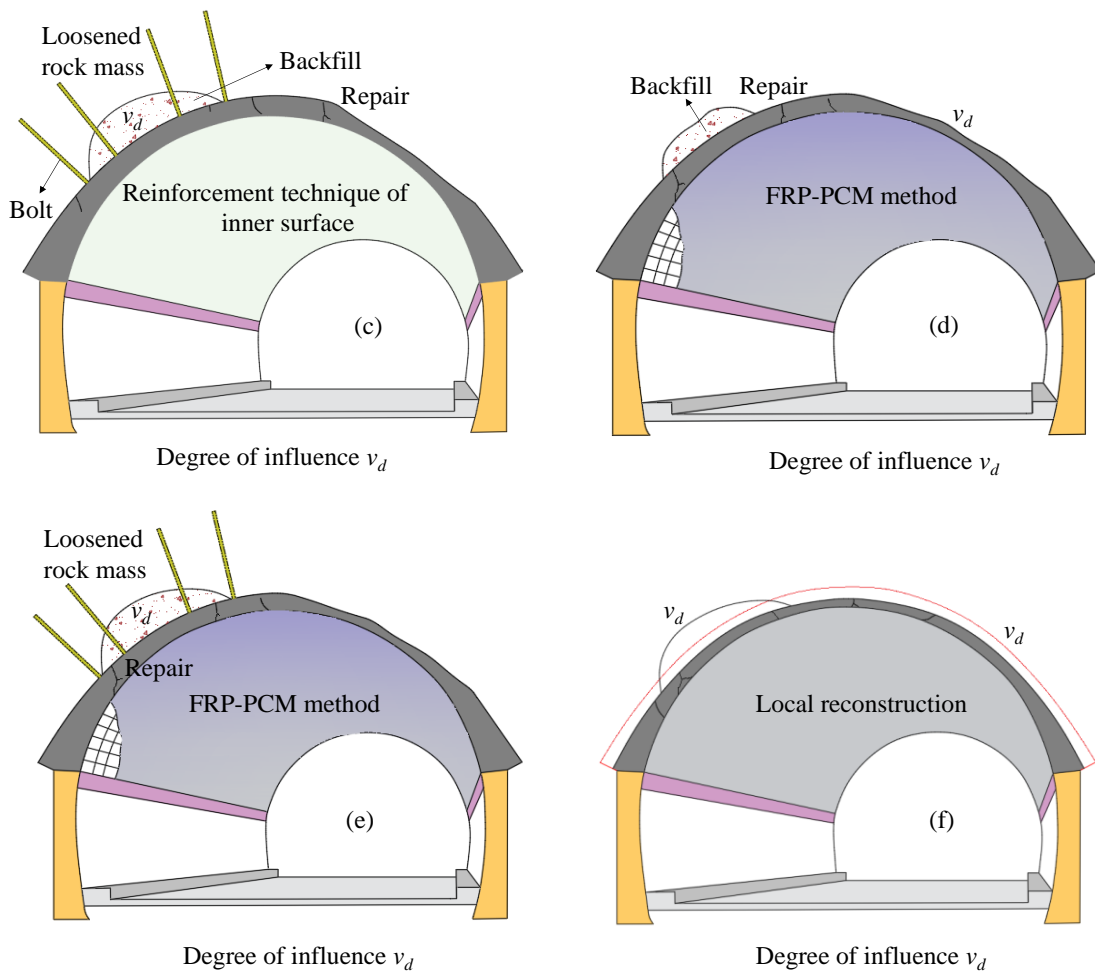


Fig. 7.5 Diagram of reinforcement schemes under the typical degree of influence: (a) T1; (b) T2; (c) T3; (d) T4; (e) T5; (f) T6.

Based on the principle of the FCE model (Hong and Liu 2011; Wang et al. 2019; Ye 2021; Jiang et al. 2021), the process of reinforcement design of linings was summarized in Fig. 7.6. It mainly includes the establishment of a hierarchical structure model, weight analysis, and the establishment of the FCE model. Subsequently, the reinforcement design of defective lining structures can be determined according to the evaluation results. As an example, this chapter presents the reinforcement design of lining structures under typical defects and diseases, as shown in Fig. 7.5. With the evaluation results of the overall influence degree and the single influence degree, the reinforcement design in Fig. 7.5 can be determined by Fig. 7.7. In addition, it is necessary to determine the reinforcement effect. If the reinforcement effect is not satisfied, the corresponding designs should be re-executed.

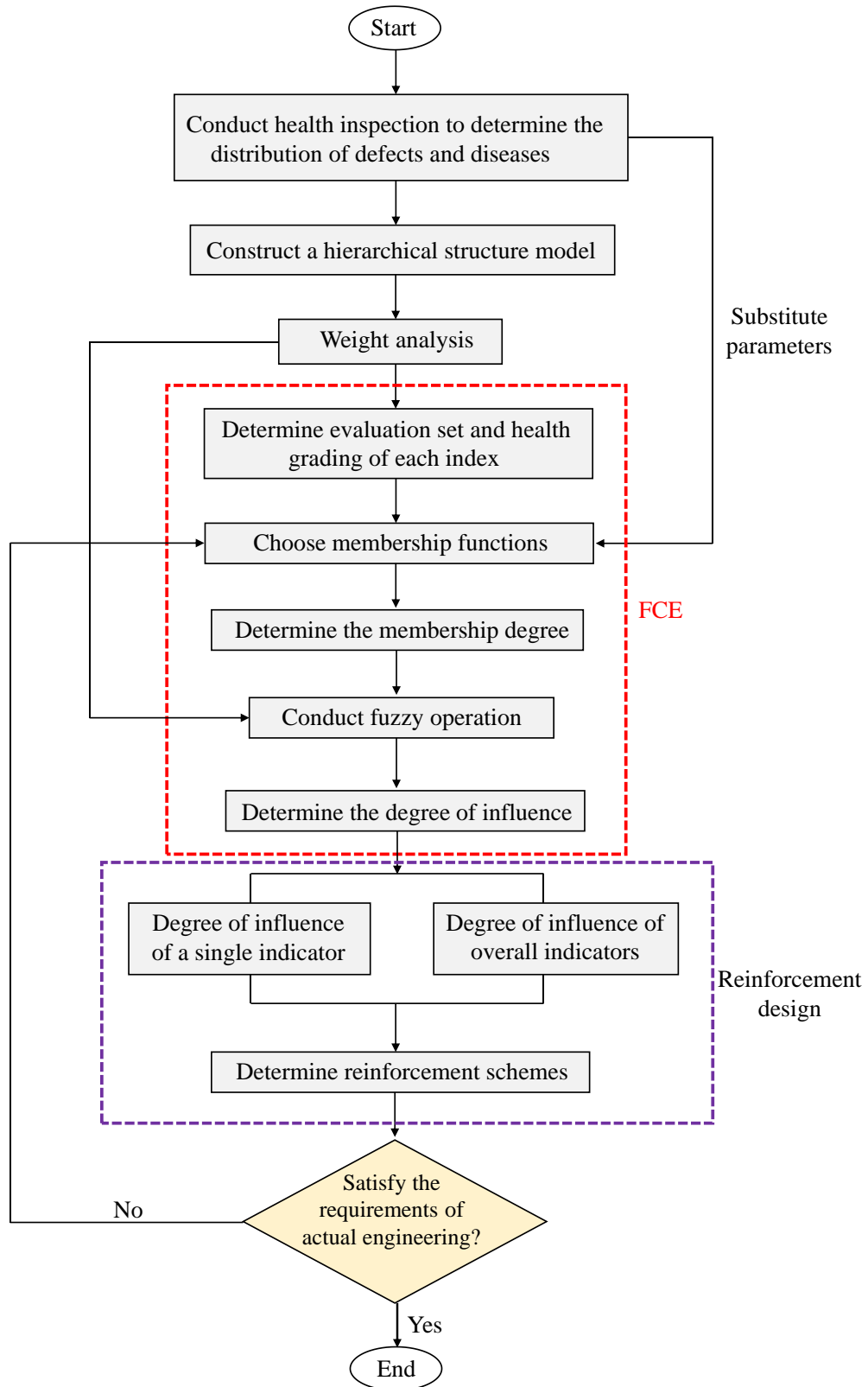


Fig. 7.6 Flowchart of reinforcement design of lining structure.

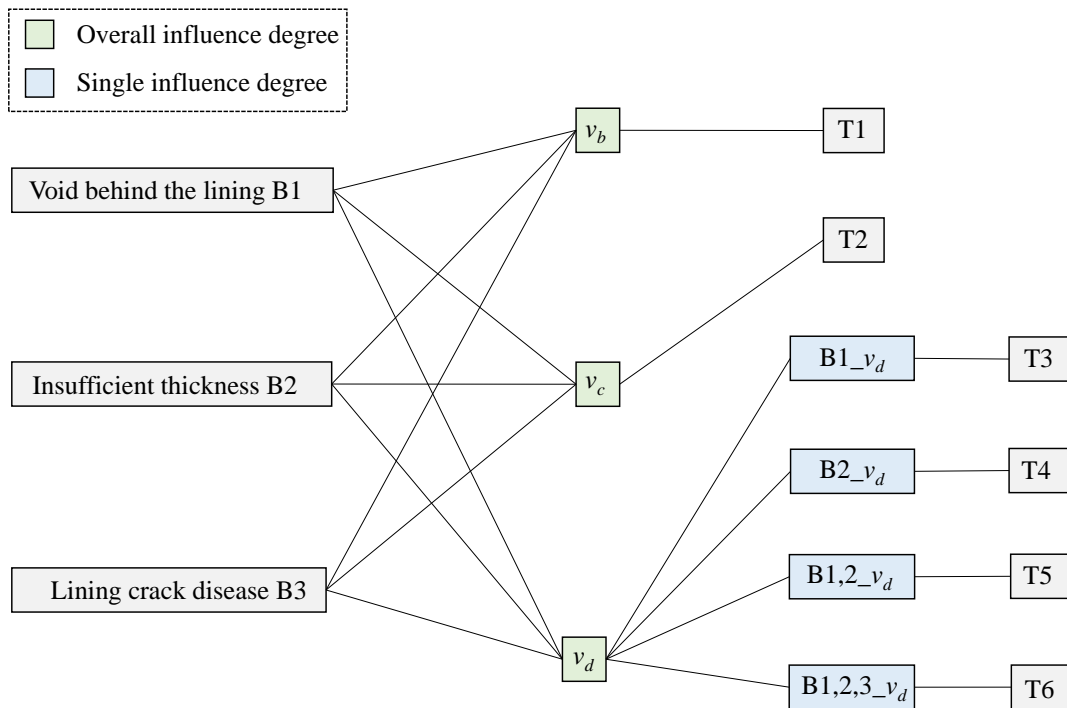


Fig. 7.7 Principles of reinforcement design of lining structure with typical quality defects and disease.

7.7 Conclusions

In this chapter, the reinforcement design of the defective and diseased lining structure was carried out. At first, the evaluation model for the degree of influence of typical quality defects and disease on the health of lining structures was established. Then, to conduct a reasonable reinforcement design, this chapter reviewed the research status of reinforcement methods for tunnel structures. Finally, according to the established FCE model, the reinforcement design of the defective and diseased lining structure was provided. The conclusions of this chapter can be listed as follows:

- (1) The order of index weight affecting the health of the lining is as follows: crack develop state, crack width and crack length, void longitudinal length, void circumferential range, degree of defect, defect longitudinal length, crack depth degree, crack pattern, void spatial location, defect circumferential range, defect spatial location, and void radial height.
- (2) In the established model, the degree of influence of typical quality defects and disease

on the health status of lining structures is divided into four levels. To provide a safe reinforcement design, this model considers the lower limit of the corresponding level. Combined with the specific case, the degree of influence under the corresponding index parameters is determined.

- (3) The reinforcement methods, including the backfill method, bolting reinforcement, inner surface reinforcement, and FRP method, of tunnel linings were reviewed. It is noted that different reinforcement methods have a different scope of application. The application conditions and remarks were also summarized.
- (4) Combining the established FCE model, the reinforcement design of the defective and diseased lining structure was given. The process of reinforcement design for defective and diseased lining structures was summarized.
- (5) The evaluation index system affecting the health of linings should be modified according to the actual conditions of the tunnel. The irregularity of defects is not fully considered in the established model, so in order to obtain more reasonable evaluation results, it is necessary to fully consider the irregularity of defects in future evaluation models. Furthermore, the evaluation results are greatly affected by the weight and membership degree of each index. Therefore, the determination of weight and membership degree should be based on more investigations and analysis to optimize the evaluation results. Furthermore, the reinforcement design can be flexibly adjusted according to the actual characteristics of the tunnel and the specific parameters of detected defects and diseases.

References

- Ali OAM, Ali AY, Sumait BS. Comparison between the effects of different types of membership functions on fuzzy logic controller performance. *International Journal of Emerging Engineering Research and Technology*, 2015, 3, 76-83.
- Deng T, Zhang SL, Yao JM, Huang M. Research on Optimized Tunnel Cavity Reinforcement Scheme Considering the Earthquake Action. *Chinese Journal of Underground Space and Engineering*, 2013, 9(3), 640-645, 696.
- Dong ZJ, Guo SC, Xu HY, Zhou P, Zhao QC. Treatments defects of secondary lining thickness of an expressway tunnel. *Engineering Journal of Wuhan University*, 2017, 50(6), 957-962. <https://doi.org/10.14188/j.1671-8844.2017-06-024>

- Fan YJ, Gong L, Wang LC, Zhang ZX, Lu F, Liu SQ, Qiu WG. Remediation Technology for the Long Segment and Large-scale Cavity behind Vault Linings of an Operating Railway Tunnel. *Railway Standard Design*, 2020, 64(11), 116-121, 135.
- Fang K, Hu Y, Cui CL, Guo J. Fuzzy Comprehensive Evaluation of Equipment Support Capability Based on AHP-Entropy Weight Method. *Journal of Information Engineering University*, 2021, 22(5), 621-625.
- Feng G. A Study on the Structure Security of Lining-Based on the Influences of insufficient lining thickness and the voids existing at the back of lining. Master's Thesis, Beijing Jiaotong University, Beijing, 2013.
- Gao Y, Xia JJ, Geng JY, Zhou J, Zhu YQ. Study on the Evaluation System of Freezing Damage of Railway Tunnel in Cold Region Based on Fuzzy Comprehensive Evaluation Method. *Railway Standard Design*, 2018, 62(7), 124-129.
- Gong YP. Study on the tunnel structure safety under the impact of the lining thickness deficiency. Master's Thesis, Beijing Jiaotong University, Beijing, 2019.
- Guan BS. Focus of maintenance and management of tunnel engineering [M]. Beijing: China Communications Press, 2004.
- Guo HP, Wang YH, An YC, Zhang JK. Cause Analysis and Renovation of Railway Tunnel Lining Cavity. *Tunnel Construction*, 2020, 40(S1), 444-453.
- Han W, Jiang YJ, Luan HJ, Liu JK, Wu XL, Du YT. Fracture evolution and failure mechanism of rock-like materials containing cross-flaws under the shearing effect. *Theoretical and Applied Fracture Mechanics*, 2020, 110, 102815.
- Han W, Jiang YJ, Zhang XP, Koga D, Gao Y. Quantitative assessment on the reinforcing behavior of the CFRP-PCM method on tunnel linings. *Geomechanics and Engineering*, 2021a, 25(2), 123-134. <https://doi.org/10.12989/gae.2021.25.2.123>.
- Han W, Jiang YJ, Li NB, Wang G, Luan HJ, Liu CZ. Failure behavior and reinforcing design of degraded tunnel linings based on the three-dimensional numerical evaluation. *Engineering Failure Analysis*, 2021b, 129, 105677. <https://doi.org/10.1016/j.engfailanal.2021.105677>
- Hara T. Corrugate Fiber Reinforced Plastic Sheet in Repairing Tunnel Linings. *Journal of Civil Engineering and Architecture*, 2015, 9, 684-690. <https://doi.org/10.17265/1934-7359/2015.06.006>
- He C, Li ZW, She J, Wang B. Research on Indoor Model Test About Effect of Combined

- Reinforcing on Structure Bearing Capacity of Defect and Disease Tunnel. *Highway*, 2007, (3), 195-201.
- He XQ. *Multivariate Statistical Analysis*. China Renmin University Press, 2004.
- He ZY, Zhong HW, Chen ZH. Safety Evaluation and Finite Element Analysis of Tunnel Lining with Cracks. *Tunnel Construction*, 2019, 39(S2), 69-77.
- Higashi Y, Li B, Jiang YJ. Analytical Evaluation of Tunnel Reinforcement Effect by PCM Shotcrete Method Using FRP Grid. *Journal of Society of Materials Science, Japan*, 2014, 63(6), 451-458. <https://doi.org/10.2472/jsms.63.451>
- Hong P, Liu PJ. Application of Analytic Hierarchy Process in Comprehensive Assessment for Health Condition of Railway Tunnels in Operation. *Modern Tunneling Technology*, 2011, 48(1), 28-32.
- Hu Q, Zhou B, Wang F, Niu Z. Structural safety assessment technology of long highway tunnel based on fuzzy analytic hierarchy process. *Journal of Natural Disasters*, 2018, 27(4), 41-49. <https://doi.org/10.13577/j.jnd.2018.0406-en>
- Japan Ministry of Land, Infrastructure, Transport and Tourism, Road tunnel periodic inspection procedure, 2018.
- Jiang HL, Fan HB. Cause Analysis and Treatment Study of Insufficient Secondary Lining Thickness of Highway Tunnel. *Urban Roads Bridges & Flood Control*, 2016, (4), 113-116. <https://doi.org/10.16799/j.cnki.csdqyfh.2016.04.035>
- Jiang W, Yang L, Shi Q, Zhang MJ, Zhang JM, Shang YJ. Adaptability evaluation of shield tunneling based on analytic hierarchy process and fuzzy synthetic evaluation method. *Science Technology and Engineering*, 2021, 21(1), 358-365.
- Jiang YJ, Wang XS, Li B, Higashi Y, Taniguchi K, Ishida K. Estimation of reinforcing effects of FRP-PCM method on degraded tunnel linings. *Soils and Foundations*, 2017, 57(3), 327-340. <https://doi.org/10.1016/j.sandf.2017.05.002>
- Keller T, Schaumann E, Vallée T. Flexural behavior of a hybrid FRP and lightweight concrete sandwich bridge deck. *Composites Part A: Applied Science and Manufacturing*, 2007, 38(3), 879-889. <https://doi.org/10.1016/j.compositesa.2006.07.007>
- Lai J, Qiu J, Fan H, Chen J, Hu Z, Zhang Q, Wang J. Structural Safety Assessment of Existing Multiarch Tunnel: A Case Study. *Advances in Materials Science and Engineering*, 2017, 2017, 1697041. <https://doi.org/10.1155/2017/1697041>

- Lei D. Mitigation of Voids Behind a Tunnel Liner. *Soils Engineering and Foundation*, 2020, 34(2), 117-120.
- Li SY. *Engineering fuzzy mathematics with applications*. Harbin Institute of Technology Press, Harbin, 2004.
- Li SH, Zhang Y, Han SS. Safety inspection system and comprehensive evaluation method for concrete structure of gas pipeline tunnel based on fuzzy mathematics. *Advances in Mechanical Engineering*, 2021, 13(9), 1-14.
<https://doi.org/10.1177/16878140211046098>
- Li YJ, Xu HJ, Zhang Y, Yao JJ. Application of Carbon Fiber Cloth in Reinforcement of Metro Tunnel Disease. *Applied Mechanics and Materials*, 2013, 353-356, 1525-1528.
<https://doi.org/10.4028/www.scientific.net/AMM.353-356.1525>
- Liu C, Zhang DL, Zhang SL. Characteristics and treatment measures of lining damage: A case study on a mountain tunnel. *Engineering Failure Analysis*, 2021, 128, 105595.
<https://doi.org/10.1016/j.engfailanal.2021.105595>
- Liu D, Shang Q, Li M, Zuo JP, Gao Y, Xu F. Cracking behaviour of tunnel lining under bias pressure strengthened using FRP Grid-PCM method. *Tunnelling and Underground Space Technology*, 2022, 123, 104436.
<https://doi.org/10.1016/j.tust.2022.104436>
- Liu HL, Lu HQ, Li HW, Song H. Applition of new method based on fuzzy comprehensive assessment for stability of landslide. *Journal of PLA University of Science and Technology (Natural Science Edition)*, 2013, 14(1), 84-88.
- Liu SH, Shi Y, Sun R, Yang JS. Damage behavior and maintenance design of tunnel lining based on numerical evaluation. *Engineering Failure Analysis*, 2020, 109, 104209.
<https://doi.org/10.1016/j.engfailanal.2019.104209>
- Luo X. *Study of Diagnosis Method and System for Health Condition of Highway Tunnel*. Ph.D. Thesis, Tongji University, Shanghai, 2007.
- Ministry of Railways of the PRC, Code for design of railway tunnel, TB10003-2001, 2001.
- Ministry of Railways of the PRC. *Technical Specification of Maintenance for Highway Tunnel*, JTG H12-2003, 2003.
- Ministry of Railways of the PRC. *Provisional Regulations on the Evaluation of Safety Classification for Railway Operation Tunnel Lining*, 2004. (in Chinese)

- Nie ZY. Study on the failure mechanism and control techniques of the voids behind tunnel lining. Master's Thesis, Central South University, Changsha, 2013.
- Ren R. Research on the geometric characteristics and deterioration mechanism of high-speed railway tunnel cavities. Master's Thesis, Beijing University of Civil Engineering and Architecture, Beijing, 2018. (in Chinese)
- Saaty TL. The Analytic Hierarchy Process, McGraw-Hill, 1980.
- Schnerch D, Dawood M, Rizkalla S, Sumner E. Proposed design guidelines for strengthening of steel bridges with FRP materials. *Construction and Building Materials*, 2007, 21(5), 1001-1010.
<https://doi.org/10.1016/j.conbuildmat.2006.03.003>
- Sheng SY, Qi ZG, Chen YF, Li XT, Yang XQ. Analysis of the Influence of Partial Thickness of the Secondary Lining on Tunnel Structure Safety. *Journal of Lanzhou Jiaotong University*, 2020, 39(6), 32-36.
<https://doi.org/10.3969/j.issn.1001-4373.2020.06.006>
- Stallings JM, Tedesco JW, EI-Mihilmy M, McCauley M. Field Performance of FRP Bridge Repairs. *Journal of Bridge Engineering*, 2000, 5(2), 107-113.
[https://doi.org/10.1061/\(ASCE\)1084-0702\(2000\)5:2\(107\)](https://doi.org/10.1061/(ASCE)1084-0702(2000)5:2(107))
- The SPSSAU project (2022). SPSSAU. (Version 22.0). [Online Application Software].
- Wang B, Mo CC, He C, Yan QX. Fuzzy Synthetic Evaluation of the Long-Term Health of Tunnel Structures. *Applied Sciences*, 2017, 7(2), 203.
<https://doi.org/10.3390/app7020203>
- Wang F. Treatment of a Railway Tunnel Lining Cavity Defect. *Construction Technology*, 2014, 43, 417-420.
- Wang MN, Guo XH, Ni GB, Yu L, Tian Y. Research on the Selection of Single - tube and Double - tube for Railway Tunnel Based on AHP_Entropy Method. *Journal of Railway Engineering Society*, 2019, (11), 51-56.
- Wang XS, Wei L, Wang ZQ, Jiang YJ, Zhang LM, Meng FZ, Cong Y. Study on the Reinforcing Effects of the FRP-PCM Method on Tunnel Linings for Dynamic Strengthening. *Geofluids*, 2021, 2021, 8926423.
<https://doi.org/10.1155/2021/8926423>
- Xu ZH, Li SC, Li LP, Hou JG, Sui B, Shi SS. Risk assessment of water or mud inrush of karst tunnels based on analytic hierarchy process. *Rock and Soil Mechanics*, 2011,

- 32(6), 1757-1766.
- Yan Z, Zhu H. Study on evaluation method of fire safety of tunnel lining structure. *Deep and Underground Excavations*, 2010. [https://doi.org/10.1061/41107\(380\)39](https://doi.org/10.1061/41107(380)39)
- Yang G, Wang G, Lu W, Yan P, Chen M. Damage assessment and mitigation measures of underwater tunnel subjected to blast loads. *Tunnelling and Underground Space Technology*, 2019, 94, 103131. <https://doi.org/10.1016/j.tust.2019.103131>
- Yang YQ, Gao YT, He SH, Qi FL. Safety Evaluation of Railway Tunnel Lining By Fuzzy Pattern Recognition. *Chinese Journal of Rock Mechanics and Engineering*, 2014, 33(S2), 3903-3910.
- Ye F, He C, Xia YX. Post construction monitoring and analysis for highway tunnel lining cracks. *China Civil Engineering Journal*, 2010, 43(7), 97-104.
- Ye F, Qin N, Liang X, Ouyang AH, Qin Zhou, Su EJ. Analyses of the defects in highway tunnels in China. *Tunnelling and Underground Space Technology*, 2021, 107, 103658. <https://doi.org/10.1016/j.tust.2020.103658>
- Ye ZJ. The influence of poor contact state between tunnel lining and surrounding rock on the safety of lining structure. Ph.D. Thesis, Beijing Jiaotong University, Beijing, 2021.
- Yi ZW. Study on Structural Health Monitoring and Safety Evaluation System of Underwater Highway Tunnel. Master's Thesis, Southwest Jiaotong University, Chengdu, 2019.
- Yu L, Bai SJ, Liu XX, Chen L, Bao LS. Study on the Influence of Tunnel Lining Thickness on Bearing Capacity of Lining. *Journal of Shenyang Jianzhu University (Natural Science)*, 2017, 33(6), 1039-1047.
- Zadeh LA. Fuzzy sets, *Information and Control*, 1965, 8(3), 338-353.
- Zhang SL. Study on Health Diagnosis and Technical Condition Assessment for Tunnel Lining Structure. Ph.D. Thesis, Beijing Jiaotong University, Beijing, 2012.
- Zhang X, Wang C, Li E, Xu C. Assessment Model of Ecoenvironmental Vulnerability Based on Improved Entropy Weight Method. *The Scientific World Journal*, 2014, 2014, 797814. <https://doi.org/10.1155/2014/797814>
- Zhang Y, Yuan M, Liu C, Zhang X, Yang B, Yang J. Repairing Damaged Tunnel Lining with Small-Size Cavity in Surrounding Rocks. *Journal of Performance of Constructed Facilities*, 2021, 35(4), 06021002.

[https://doi.org/10.1061/\(ASCE\)CF.1943-5509.0001597](https://doi.org/10.1061/(ASCE)CF.1943-5509.0001597)

Zhao BJ, Kong DK, Tan ZS. Yichang—Wanzhou railway tunnel disease evaluation system based on analytic hierarchy process. *China Civil Engineering Journal*, 2017, 50(S2), 243-248.

Zheng C, Chen B, Li W, Zhang Z. Research on Risk Assessment of Complex Mountain Tunnels Based on AHP-FCE. *IOP Conference Series: Materials Science and Engineering*, 2020, 741, 012031.

<https://doi.org/10.1088/1757-899X/741/1/012031>

Zhu ZG, Geng YJ, Wu J, Zhu YQ, Wang DY, Han XM. Research on the Effect Mechanism of Cavity behind the Tunnel Lining under the Earthquake Action. *Journal of Railway Engineering Society*, 2015, (9), 79-84.

8 Summaries and prospects

8.1 Summaries

In this thesis, the influence of typical quality defects on the lining structure, including the mechanical properties, deformation characteristics, cracking distribution, safety state, failure mechanism, and dynamic response, was systematically investigated. Three defect types are mainly considered, voids, insufficient lining thickness, and compound defects, respectively. Meanwhile, the reinforcement effect of the FRP-PCM method on defective and degraded lining structures was revealed. On this basis, the reinforcement design of the lining structure was carried out. The main conclusions of this thesis were summarized in this chapter.

The fracture characteristics and cracking mechanism of lining structures with combined defects under the gradual load were concluded. The defect zone is identified as prone to cracking area, and the cracking degree of the lining corresponding to the void zone is larger than that of the insufficient thickness zone. Concerning the crack pattern, ring cracks are prone to occur on the lining outer surface corresponding to the void zone, while longitudinal cracks are prone to occur on the outer surface with insufficient thickness. The number of damaged cohesive elements, crack area, and crack volume present a positive relationship with the void range and the gradual loading level. Tensile damage is prone to occur on the outer surface of the void zone, while dominated by shear damage at the outer surface of the insufficient thickness zone. In addition, the distribution of cracking zones of TRCZ, SRCZ, SLCZ, MLCZ, and MCCZ is determined. Furthermore, the FRP-PCM method can effectively inhibit the cracking degree of the inner lining surface and the outer surface of the insufficient thickness zone. The fracture degree of the lining outer surface corresponding to the void zone can be significantly reduced with the backfill method.

The mechanical properties and failure mechanism of degraded linings with void defects and compound defects that significantly affect the lining structure were investigated, respectively. Regarding the mechanical properties, an obvious three-dimensional bending outwards phenomenon within the void-affected zone or the compound defect zone is both observed. The influence of defects on the distribution of bending moment is mainly near the defect zone and is not significant away from the defect zone. In addition, the three-

dimensional axial force exhibits a significant decreasing trend along the tangential direction within the void-affected zone. In terms of stress distribution, a significant tensile stress concentration appears on the lining outer surface of the void center and the inner surface between the double voids, while compressive stress concentration occurs at the edge of the void zone. When the voids are arranged asymmetrically, the corresponding tensile effect is more pronounced. For the lining with compound defects, a significant tensile effect occurs on the lining outer surface corresponding to the compound defect zone, while at the edge of the insufficient thickness, a compressive stress concentration generates. Regarding the failure characteristics of linings with void defects, the lining outer surface between double voids is prone to plastic shear failure, while the inner surface is prone to tensile-shear failure. In addition, tensile failure is observed within the lining outer surface corresponding to the void zone. The failure characteristics are affected by the void spatial distribution. For the lining with compound defects, failure characteristics are significantly affected by the lining deterioration degree and the ground class. The higher the deterioration degree, the more prone to tensile-shear plastic failure within the compound defect zone. Otherwise, the more likely it is for tensile failure. The lower the ground class, the more serious the failure phenomenon. In addition, the distribution of potential cracking zones of TCZ, SCZ, and TSCZ of linings with void defects and compound defects is identified, respectively. Regarding the reinforcement effect of the FRP-PCM method on degraded linings with void defects, the plastic shear failure on the lining outer surface between the double voids is inhibited significantly, and the failure rate can also be significantly reduced. For the lining with compound defects, the FRP-PCM method can effectively improve the safety state and reduce the failure rate. As the grade of FRP grids increases, the failure rate shows a non-linear decrease trend. Furthermore, the time-dependent characteristics of the lining with compound defects were discussed, and the stress, displacement, and failure rate gradually increase with time. The time-dependent reinforcement effect of the FRP-PCM method on defective linings was identified.

The dynamic response of tunnel structures with quality defects of the void and lining defect was concluded. Regarding the mechanical properties, the degree of stress concentration is affected by the defect range and shows a positive correlation. The FRP-PCM method and the backfill method can significantly optimize the mechanical properties of the lining. Concerning the physical properties, the peak acceleration and peak velocity are roughly relatively small at the crown and shoulder but large at the arch

springing and the inverted arch. The distribution of peak acceleration and velocity are significantly affected by the defect type, range, and location. Regarding the distribution of SSR, the variation of the acceleration and velocity dynamic response at the defect zone is significantly affected by the defect type. The degree of amplification or attenuation of the dynamic response varies significantly at different frequencies. For the seismic waves of strong earthquakes in the research, the acceleration or velocity dynamic response intensity at the defect zone shows a significant amplification effect near 18Hz, 40Hz, and 60Hz. The larger the void range, the more significant the amplification effect. However, for locations farther away from the defect zone, the change in the void range becomes insignificant to the change in the dynamic response. In addition, the dynamic response characteristic is related to the dynamic level. Furthermore, the dynamic response is significantly affected by the type of reinforcement methods. The backfill method is significant for optimizing the dynamic properties of linings with void defects, while for the lining defect, the FRP-PCM method is more apparent.

The reinforcement design of the defective and diseased lining was carried out. As a prerequisite, an evaluation model of the degree of influence of typical quality defects and disease on the health state of lining structures was constructed. The order of index weight affecting the health of lining structure is crack develop state, crack width and crack length, void longitudinal length, void circumferential range, degree of defect, defect longitudinal length, crack depth degree, crack pattern, void spatial location, defect circumferential range, defect spatial location and void radial height. To provide a safe reinforcement design, the lower limit of the corresponding level was considered in this model to determine the degree of membership. According to the FCE results, the degree of influence of typical quality defects and diseases on lining health can be determined. To conduct a reasonable reinforcement design, the reinforcement methods of tunnel linings were reviewed, and the application conditions and remarks were summarized. Further, based on the established FCE model, the reinforcement design of the defective and diseased lining was given. Meanwhile, the process of reinforcement design of the lining structure was summarized.

8.2 Prospects

This thesis systematically explored the influence of tunnel quality defects on the lining structure. Meanwhile, the corresponding reinforcement design was also conducted. Some

contents could be further deeply studied. Therefore, based on this thesis, it is meaningful to conduct the following work in the future:

Firstly, it is helpful to carry out model tests of lining structures with multiple defect types to more deeply clarify the failure behavior and dynamic characteristics. Meanwhile, the reinforcement behavior of the FRP-PCM method on defective linings should be further revealed combined with model tests. In addition, the evaluation index affecting tunnel health should be adjusted according to the actual characteristics of the tunnel. The evaluation results are greatly affected by the weight and membership degree, and more specific studies should be carried out. Furthermore, the reinforcement design of defective and diseased linings should be extensively studied, and flexible adjustments could be made in combination with the actual engineering.